The experimental results which were obtained during representative field tests offer for the flue gas combustion in high flares the evidence that

- in soot-free flare flames, the organically bound carbon of the flare gas is converted to carbon dioxide to at least 99%;
- in sooty flare flames, the emission factor for carbon bound in air-foreign substances and carbon bound in the gaseous state comprises a maximum of 1% of the organically bound carbon in the flare gas.

1. Introduction

1.1 The Necessity of High Flares in Refineries and Their Operation

During the operation of petroleum refineries, especially during the operating conditions of units which do not correspond to operation standards, combustible gases accumulate which must be removed without hazard to the units and without harm to the environment. For example, because of safety considerations all vessels and conduits in which combustible gases are kept under pressure, are tied-in via safety valves into a separate distribution system, namely, the flare gas network. Furthermore, gases which accumulate during startup and stoppage of units and which do not participate in the process are discharged into the flare gas network.

In some refineries, the flare gases are in part stored temporarily in gasholders and fed into the fuel gas network [1, 2]. In most refineries, however, the flare gases are led directly into a flue gas combustion unit, namely, the flare [3].

Flare gases accumulate:

- during startup and stoppage of units. This operating condition is predictable and can be taken into consideration in the heat requirement plan;
- during operating trouble with controllable operating conditions (unit continues to operate) as, for example, the leakage of safety valves, which are tied-in into the flare gas network, or during the pressure drop in parts of the plant;
- during operating breakdown with uncontrollable operating conditions (unit must be shut down) as, for example, during power or cooling water failure.

Depending on the causes of the gas accumulation or the extent of the operating trouble, a situation arises where several hundred to several hundred thousand cubic meters of flare gas must be burned for a short time without endangering the units. Since the most diversified process units are tied-in into the flare gas network, the flare gases show quite variable compositions.

The variety of gases and vapors, which reaches the flare as a mixture of steadily varying composition, extends from a hydrogen-rich gas coming from the reforming units to liquefied gases. The varying gas composition and the gas amount fluctuating strongly with time require a combustion unit which has a considerable range of control. In addition, it is required, as a rule, that the combustion proceed soot-free, at least within load ranges corresponding to the gas accumulation, brought about by operating trouble with controllable operating conditions and by the startup and stoppage of units.

High flares are generally used as the flue gas combustion units for flare gases, since only the high flares have the necessary range of control for the safety of the units. Ground flares whose range of control is considerably smaller are of minor importance. Out of 32 refineries in the German Federal Republic, 5 have ground flares in addition to high flares. Altogether, there are 60 high flares and 11 ground flares in operation [3].

A high flare system shown schematically in Fig. 1-1, according to reference [7], generally consists of the water ~~plunge~~ seal, the 50 to 100-meter high flare pipe, and the burner designated as the flare ~~head~~ tip.

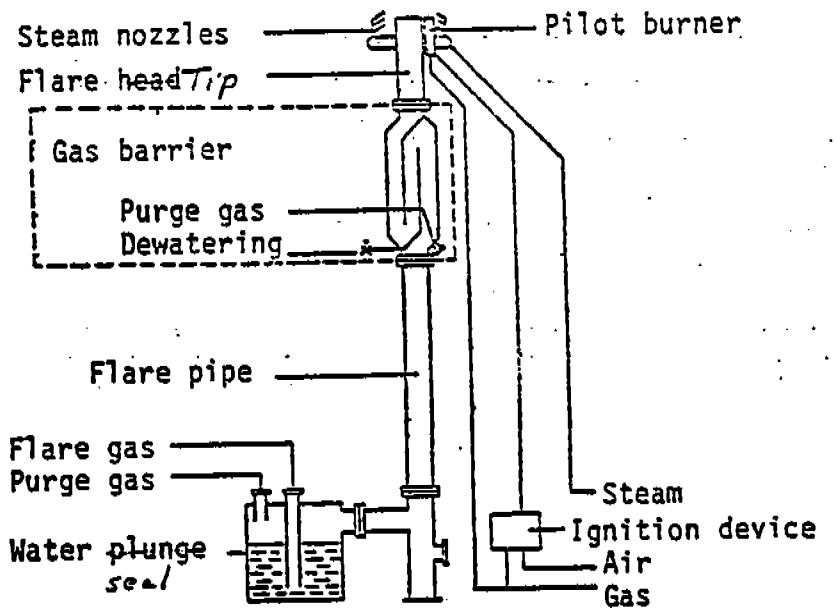

Fig. 1-1 ~~High~~-Flare System (schematically)
Elevated

Water ~~plunges~~ seals are provided in order to protect the flare gas network from air influx. The inflow of air into the flare pipe with a nonburning flame is prevented by purging with inert gas or steam [4, 5]. In some flares the purge gas demand is reduced by the incorporation of gas barriers below the flare head [6].

The flare head is designed for the maximum amount of accumulated gases during emergency shutdowns. As a result, the flare head is considerably overdimensioned for the amount of gases with which it is usually charged.

The flare gas exiting from the cylindrical pipe of the flare head expands as a free jet into the atmosphere and sucks in the air necessary for combustion. The gas-air mixture is ignited by the pilot flames which are fed by a separate gas network. The pilot flames are usually ignited with a climbing flame [8].

In order to increase the air suction and to improve the mixing of the air with the gas jet, steam is usually added as a "driving medium" to the flare gas at the flare head. The steam addition is performed semiautomatically by the operating staff in the control room, from which the flame can be observed directly or via television cameras. As a rule, the steam addition is increased until the flare flame is soot-free.

In addition to being dependent on the steam addition, the combustion also depends on the flare gas mass flow, the flare gas composition, the atmospheric influences--especially the wind--and on the flare head design. The latter should control primarily the steam/gas ratio necessary for soot elimination, which indicates how many kg steam are added per kg flare gas.

The effect of these operating parameters on the combustion is discussed below in connection with the experimental results.

At this point the following should be recorded:

The flare head design is set in the plant. The gas mass flow, gas composition, and atmospheric influences are subject to constant changes, unpredictable in time. The flaring, therefore, can only be influenced by the steam mass flow. However, even the steam mass flow may only be varied within specified limits and may exert both a positive or a negative effect on the combustion, for example, by quenching the flame. Moreover, the steam addition cannot be controlled automatically, since suitable flare gas fluxmeters, whose metered quantity could be applied as the controlled variable for the steam addition, are not available at the present time [9].

Therefore, given the insufficiently defined conditions, it is impossible to run the "flaring" process with firmly set, optimal operating data. The constantly fluctuating and, especially, unpredictable changes lead to a case where the conditions do not correspond to operation standards.

It should also be noted that the operation of flares is not limited to refineries. Flares are used in the petroleum industry beginning with oil fields, transportation, and refining of crude oil in petroleum refineries and petrochemical plants to the storage and distribution of the refined products. Furthermore, flares are also required in other chemical industries, the steel industry [10], and in coal gasification [11].

7. Summary of the Experimental Results and Conclusions

Figures 7-1 (a-d) show the local burnout degree for carbon bound in air-foreign substances and carbon bound in the gaseous state as a function of the investigated operating parameters, namely, the flare gas mass flow m_G, the flare gas density ϱ_G°, the steam/gas ratio m_D/m_G, and the wind u_Q.

In addition, all local burnout degrees measured at the flame end and downstream from the flame end are shown as a function of one operating parameter in each of the Figures. Furthermore, the local burnout degrees which are equal to and higher than 0.99 are assembled in the shaded bands, and only those that are smaller than 0.99 are shown separately.

In the experiments, the local burnout degree was determined in a total of 1298 measurement points at the flame end and downstream from the flame end. As a result, the local burnout degree was found to be equal to or higher than 0.99 in 1294 measurement points. Only in four cases, a local burnout degree at the flame end was found to be smaller than 0.99. In one case, this was attributed to an excessive steam addition (it is marked in the Figures as a triangle). For the remaining three cases (marked by +), no correlation with the operating parameters was found.

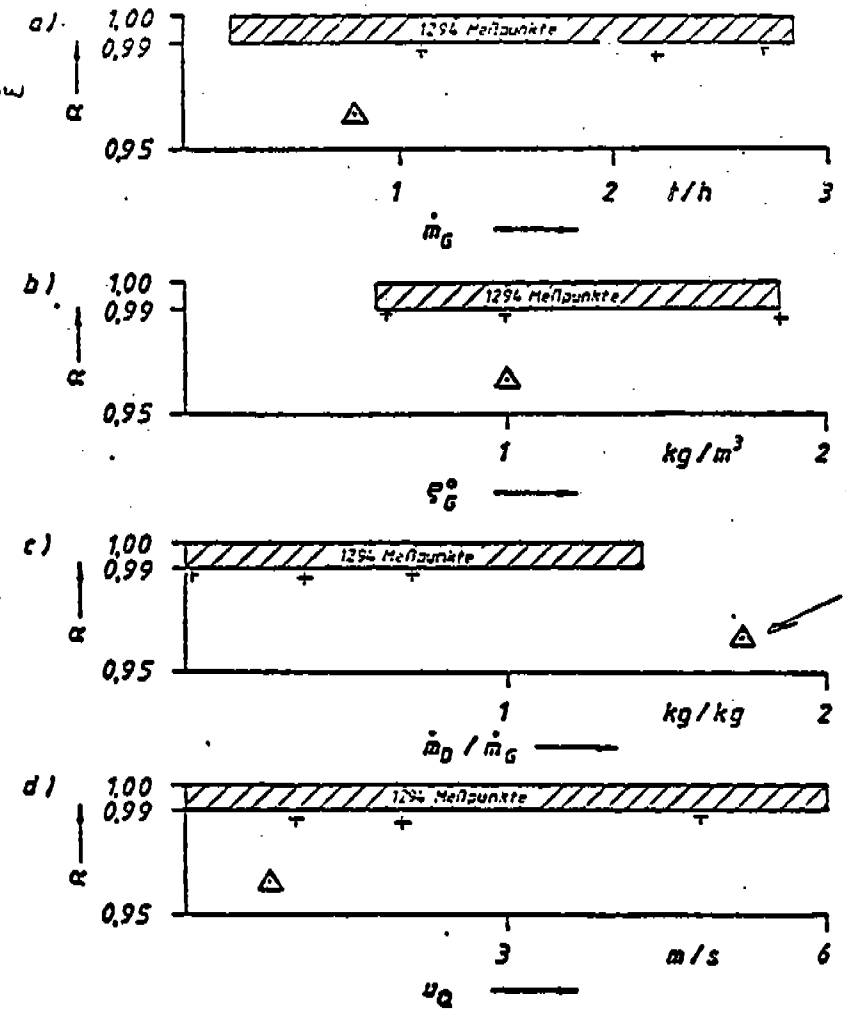

Fig. 7-1:

Local burnout degree as a function of the investigated operating conditions.

The local burnout degree was determined at 42 gas mass flows with 23 different flare gas densities. For the case of soot-free flare flames, no correlation was found between the degree of conversion and the flare gas mass flow or the flare gas composition.

For 114 tested steam/gas ratios, the minimum degree of conversion dropped to values below 0.99 only at a steam/gas ratio, which corresponded to almost a 10-fold amount required to eliminate the soot. Also, in the case of sooty flare flames, the maximum emission factor is less than 0.01 for carbon bound in air-foreign substances and carbon bound in the gaseous state.

The wind velocity during the experiments was up to 6 m/s. In this range, no unburned fuel was discharged at the flame end.

The experimental results which were obtained during representative field tests offer for the flue gas combustion in high flares the evidence that

- In soot-free flare flames, the organically bound carbon of the flare gas is converted to carbon dioxide to at least 99%;
- the emission factor for carbon bound in air-foreign substances and carbon bound in the gaseous state, independent of the optical flame picture (soot containing or soot-free), comprises a maximum of 1% of the organically bound carbon in the flare gas;
- the mass concentration of the organically bound carbon at the flame end is less than 50 mg/m^3, even in the case of sooty flare flames;
- the bulk of the organically bound carbon at the flame end consists of methane and acetylene;
- the nitrogen oxide emission of flare flames, referred to the heat unit, is low.

It is, therefore, recommended that the proposal of the air specification, allowing to proceed with a "conversion degree" of 75% during flue gas combustion in high flares, be so modified that a conversion degree of 99% could be considered in the future.

List of Frequently Used Symbols

A	Fläche	surface
D	Dampf	steam
d_o	Fackelkopfdurchmesser	flare head diameter
E	Emissionsfaktor	emission factor
g	Erdbeschleunigung	gravitational acceleration
H	Heizwert	calorific (heat) value
I	Massenstromdichte	mass flow density
k	Isentropenexponent	isentropic exponent
L	Flammenlänge, Luftvolumen	flame length, air folume
l	Luftbedarf für stöchiometrische Verbrennung	air requirement for stoichiometric combustion
M	Molmasse	molecular (mass weight)
m	Masse	mass
MV	Molvolumen	molecular volume
p	Druck	pressure
Q	Wärme	heat
R	Gaskonstante	gas constant
r	Radius	radius
T	Temperatur	temperature
t	Zeit	time
Tp	Taupunkt	dew point
U	Umsatzgrad	degree of conversion
u	Geschwindigkeit	velocity (rate)
V	Abgasvolumen	flue gas volume
v	Abgasvolumen bei stöchiometrischer Verbrennung	flue gas volume at stoichiometric combustion
w	Massenanteil	mass (weight) fraction
x	Molenbruch	mole fraction
x,y,z	kartesische Koordinaten	Cartesian coordinates
Θ,Ψ	Verhältnis	ratio
α	örtlicher Ausbrandgrad	local burnout degree
δ	Wiederauffindrate	rate of retrieval
λ	Luftzahl	air number
$\varkappa$	Volumenanteil	volume fraction
ϱ	Massenkonzentration	mass concentration
ϱ^o	Normdichte	standard density
φ	Luftfeuchte	air humidity

List of Frequently Used Indexes

a	Umgebung, adsorbiert	environment, adsorbed
aus	aus dem Reaktor ausgetragen	discharged from the reactor
B	bei Betriebsbedingungen	at operating conditions
C	Kohlenstoff	carbon
D	Dampf	steam
ein	dem Reaktor zugeführt	supplied to the reactor
G	Fackelgas	flare gas
ga	gasförmig	gaseous
H	Wasserstoff	hydrogen
kal	bei Kalibrierbedingungen	at calibrated conditions
L	Luft	air
o	oberer (Heizwert)	upper (heat value)
Q	Queranströmung, Wind	relative cross (lateral) flow, wind
sie	trocken	dry
u	unverbrannt, unterer (Heizwert) . .	unburned, lower (heat value)
v	verbrannt	burned
w	wasserfeucht	water moist
WM	Windmaschine	fan (blower)
(D)	Dampf	steam
(L)	Luft	air
(R)	Reaktion	reaction
.	auf die Zeiteinheit bezogen	referred to a unit of time
o	bei Normbedingungen, trocken . . .	at standard conditions, dry
^	Augenblickswert	instantaneous value

List of Figures

List of Figures (cont'd.)

List of Figures (cont'd.)

List of Figures (cont'd.)

List of Tables

Bibliography

/1/ F. Schwarz, E. Bauer
Erdöl-Erdgas-Zeitschrift, 93, 91/92 (1977)

/2/ A. F. Orlicek
Erdöl und Kohle, Erdgas, Petrochemie, 19 (11), 824/829 (1966)

/3/ W. Hansen
"Systemanalyse zum Fackelgeschehen," DGMK Forschungsbericht Nr. 135-01 (1978)

/4/ H. W. Huss
Hydroc. Process., 43 (5), 179/182 (1964)

/5/ R. D. Reed
The oil and gas J., February 14, 91/92 (1972)

/6/ H. Glamm
"Anordnung und Betrieb von Notabblasesystemen"
Haus der Technik - Vortragsveröffentlichungen, H. 199 S. 15 - 28

/7/ K. Hess, R. Stickel
Verfahrenstechnik, 3 (7), 282/287 (1969)

/8/ L. Unterstenhöfer, N. Rao
Gaswärme, 15 (7), 219/223 (1966)

/9/ K. Haber
"Durchfluß- und Massenermittlung der den Fackeln zugeführten Gase", DGMK Forschungsbericht Nr. 135-03 (1978)

/10/ J. F. Straitz, III
"Flaring for Gaseous Control in the Petroleum Industry"
Annual Meeting of the Airpollution Control Association 1978,
Paper-No. 78-38.3

/11/ A. Heller
Schriftenreihe des Vereins für Wasser-, Boden- und Lufthygiene,
16 (1960); entnommen aus Technik der Luftreinhaltung S. 341,
Otto Krauskopf Verlag, 1972

/12/ Günther, R.
"Verbrennung und Feuerungen" Springer Verlag, 1974

/13/ J. D. Hajek, E. E. Ludwig
Petro/Chem Engineer, June 1960, 31/38

/14/ API RP 521 "Guide for Pressure Relief and Depressuring Systems",
American Petroleum Institute, 1969

Bibliography (cont'd.)

/15/ S. H. Tan
Hydroc. Process., 46, 172/176 (1967)

/16/ K. Hess, R. Stickel
Chem. Ing. Techn., 39 (5/6), 334/340 (1967)

/17/ R. Becker, K. Hess, A. Stöckel
Chem. Ing. Techn., 47 (1), 33 (1975)

/18/ K. G. Karbacher
Canadian Aeronautics and Space Journal, January 62, 1/6

/19/ Ismants Reba
"Applications of the Coanda Effekt" Fundstelle nicht bekannt

/20/ T. A. Brzustowski
Prog. Energy Combust. Sci., 2, 129/141 (1976)

/21/ W. Lauderback
Hydroc. Process., 51 (1), 127/128 (1972)

/22/ R. Becker
"Fackelbrenner für rauchlose und geräuscharme Verbrennung"
KTI - Firmenschrift, Petrotechnik GmbH, Hamburg 1976

/23/ o. V.
"New concepts in flaring" National Airoil Burner Comp., Firmenschrift 1976

/24/ o. V.
"John Zink flare tips help improve atmosphere in Welsh Valley"
J. Inst. Fuel, 36, 203 (1973)

/25/ o. V.
"The anti-Pollutant smokeless flare" Flaregas Engineering Ltd. Firmenschrift 1976

/26/ Bundes-Immissionsschutzgesetz - BImSchG vom 15. März 1974; Bundesgesetzblatt, Teil I, 721/743 (1974)

/27/ 9. Verordnung zur Durchführung des BImSchG (Grundsätze des Genehmigungsverfahrens) vom 18. Februar 1977 (9. BImSchV); Bundesgesetzblatt, Teil 1, 274/278 (1977)

/28/ 11. Verordnung zur Durchführung des BImSchG (Emissionserklärungsverordnung) vom 20. Dezember 1978 (11. BImSchV); Bundesgesetzblatt, Teil 1, 2027/2036 (1979)

Bibliography (cont'd.)

/29/ K. Michaelis
Gesundheits-Ingenieur, 96 (10), 281/287 (1975)

/30/ Private Mitteilung der Oberrheinischen Mineralöl-Werke an die Landesanstalt für Umweltschutz, Baden-Württemberg

/31/ Technische Anleitung zur Reinhaltung der Luft vom 28. Aug. 1974 (TA-Luft), Erste allgemeine Verwaltungsvorschrift zum BImSchG, Gemeinsames Ministerialblatt, 25 (24), 426/452 (1974)

/32/ R. Becker
"Ausbrandmessungen an Fackelflammen", Technische Informationen der Endress und Hauser GmbH & Co, 32, 23/25 (1974)

/33/ R. Günther, B. Lenze
"Gutachten über den Umsetzungsgrad des Fackelgases in den Hochfackeln der Oberrheinischen Mineralöl-Werke GmbH in Karlsruhe" 1972

/34/ Technische Richtlinie zur Luftreinhaltung in Mineralölraffinerien und petrochemischen Anlagen zur Kohlenwasserstoffherstellung (Raffinerie-Richtlinie), Rd Erl. d. Ministers für Arbeit, Gesundheit und Soziales (Nordrhein-Westfalen) - III B 4/III B 6 - 8856.4 (III Nr. 13/1975) v. 14.4.1975

/35/ P. Brüdern
Erdöl und Kohle, Erdgas, Petrochemie, 15 (4), 289/291 (1962)

/36/ Y. W. Lee
"Der Verbrennungsverlauf in auftriebsbehafteten Flammen mit und ohne Windeinfluß", Dissertation, Universität Karlsruhe 1977

/37/ Y. W. Lee
Gaswärme Internat., 27 (1), 13/19 (1978)

/38/ G. R. Kent
Hydroc. Process. and Petroleum Refiner, 43 (8), 121/125 (1964)

/39/ R. D. Reed
Chem. Eng. Progr., 64 (6), 53/57 (1968)

/40/ L. Heitner
Hydroc. Process., 49 (11), 209/212 (1970)

Bibliography (cont'd.)

/41/ T. A. Brzustowski
Comb. Sci. Technol., 6, 313/319 (1973)

/42/ T. A. Brzustowski, H. F. Sullivan
2-nd Europ. Symp. for Comb., Sept. 5 (1975), 739/744

/43/ T. A. Brzustowski, E. C. Sommer
Proceedings of Refining, API 53, 865/893 (1973)

/44/ T. A. Brzustowski et al.
The American Society of Mechanical Engineers, 75 HT 4 1/7

/45/ R. Schwanecke
Luftverunreinigung 1974, 49/55

/46/ J. Grumer et al.
"Hydrogen Flare Stack Diffusion Flames" Dept. of the Interior, Bureau of Mines (1970), Report of Investigation 7457

/47/ J. F. Straitz
Hydroc. Process., 56 (10), 131/135 (1977)

/48/ Mitteilung des Umweltbundesamtes an die Landesanstalt für Umweltschutz, Baden-Württemberg

/49/ R. M. Fristrom, A. A. Westenberg
"Flame Structure", McGraw-Hill, 1965

/50/ H. Reichardt
"Gesetzmäßigkeiten der freien Turbulenz" VDI-Forschungsheft 414 (1942)

/51/ R. Günther
Archiv für Eisenhüttenwesen, 39 (7), 515/519 (1968)

/52/ B. Lenze
Gaswärme Internat., 20 (12), 451/457 (1971)

/53/ K. H. Homann
Comb. Flame, 11, 265/269 (1967)

Bibliography (cont'd.)

/54/ L. Glassman
"Combustion", Academic Press, 1977, S. 55

/55/ K. H. Homann, H. G. Wagner
11-th Symp. (int.) on Comb. 1966, The Combustion Institute 1967, pp 371-379

/56/ J. Lahaye, G. Prado
"Mechanisms of Carbon Black Formation" in
P. L. Walker, P. A. Thrower "Chemistry and Physics of Carbon", Vol. 14, 167/294 (1978)

/57/ E. R. Place, F. J. Weinberg
11-th Symp. (int.) on Comb. 1966, The Combustion Institute 1967, pp. 245-255

/58/ B. L. Wersborg, J. B. Howard, G. C. Williams
14-th Symp. (int.) on Comb. 1972, The Combustion Institute 1973, pp. 929-938

/59/ T. W. Lester, L. K. Wittig.
16-th Symp. (int.) on Comb. 1976, The Combustion Institute 1977, pp. 671-680

/60/ C. P. Fenimore, G. W. Jones
J. Phys. Chem., 71 (3), 593/597 (1967)

/61/ F. J. Wright
15-th Symp. (int.) on Comb. 1974, The Combustion Institute 1975, pp. 1449-1459

/62/ L. Kurylko, R. H. Essenhigh
14-th Symp. (int.) on Comb. 1972, The Combustion Institute 1973, pp. 1375-1386

/63/ Janaf, Thermodynamic Tables, 1971

/64/ Landolt-Börnstein, II Band, 4. Teil, Springer-Verlag 1961

/65/ E. Fitzer, W. Fritz
"Technische Chemie" Springer-Verlag 1975

/66/ T. Miyauchi, Y. Mori, A. Imamura
16-th Symp. (int.) on Comb. 1976, The Combustion Institute 1977, pp. 1073-1081

Bibliography (cont'd.)

/67/ H. Cremer
Chem. Ing. Techn., 44 (1+2), 8/15 (1972)

/68/ Ya. B. Zeldovich
Acta Physecochem. USSR 21, 577 aus /54/

/69/ C. P. Fenimore
13-th Symp. (int.) on Comb. 1970, The Combustion Institute 1971, pp. 373-379

/70/ F. Bachmeier, K. H. Eberius, Th. Just
Combust. Sci. Technol., 7, 77/84 (1973)

/71/ B. S. Haynes, D. Iverach, N. Y. Kirov
15-th Symp. (int.) on Comb. 1974, The Combustion Institute 1975, pp. 1103-1112

/72/ J. N. Mulvihill, L. P. Phillips
15-th Symp. (int.) on Comb. 1974, The Combustion Institute 1975, pp 1113-1122

/73/ E. L. Merryman, A. Levy
15-th Symp. (int.) on Comb. 1974, The Combustion Institute 1975, pp. 1073-1083

/74/ D. Shore
"Towards quieter flaring" A paper presented at the 74-th meeting of the American Institute of Chemical Engineers, March 1973

/75/ J. Hengstenberg, B. Sturm, O. Winkler
"Messen und Regeln in der Chemischen Techn." Springer-Verlag 1964

/76/ B. Baule
"Die Mathematik des Naturforschers und Ingenieurs"
Bd. 2, S. Hirzel-Verlag, Leipzig 1959

/77/ Aspirationspsychrometer-Tafeln
Herausgeber: Verlag Friedrich Vieweg u. Sohn, Braunschweig 1976

/78/ H. A. Becker, S. Yamazaki
16-th Symp. (int.) on Comb. 1976, The Combustion Institute 1977, pp. 681-691

/79/ K. Hein
Comb. Sci. Technol. 5, 195/206 (1972)

Bibliography (cont'd.)

/80/ Jahresbericht 1973 der Abteilung Strahlenschutz und Sicherheit der Gesellschaft für Kernforschung mbH, Karlsruhe

/81/ F. L. Dryer
16-th Symp. (int.) on Comb. 1976, The Combustion Institute
1977, pp. 279-295

/82/ C. T. Bowman
15-th Symp. (int.) on Comb. 1974, The Combustion Institute
1975, pp. 869-881

/83/ K. Hess
"Flammenlänge und Flammenstabilität" Dissertation T.H. Karlsruhe
1964, entnommen aus /12/

/84/ Gmelins Handbuch der anorganischen Chemie, System-Nr. 4 Stickstoff
8. Auflage 1936, S. 748ff.
Verlag Chemie

/85/ J. A. Fay, D. H. Lewis
16-th Symp. (int.) on Comb. 1976, The Combustion Institute
1977, pp. 1397-1405

/86/ A. G. Gaydon, H. G. Wolfhard
"Flames, their structure, radiation and temperature" Chapman and Hall 1970

/87/ 1. BImSchV. vom 5.2.79 (BGBl I S. 165)

/88/ Hommel
"Handbuch der gefährlichen Güter" Springer-Verlag 1973,

/89/ P. A. Leighton
"Photochemistry of Air Pollution" Chapter 10, Academic Press, New York, 1961

/90/ W.M. Bufalini
Environ. Sci. Technol., 10, 908/912 (1976)

/91/ H. Wagner
VDI-Berichte Nr. 146, 5/9 (1970)

/92/ U. Schurath
VDI-Berichte Nr. 270, 13/18 (1977)

Bibliography (cont'd.)

/93/ G. von Nieding, H. M. Wagner
VDI-Berichte Nr. 247, 55/58 (1974)

/94/ R. Zahn
VDI-Berichte Nr. 247, 74/76 (1974)

/95/ N. Peters
VDI-Berichte Nr. 346, 285/292 (1979)

/96/ L. Lützke
VDI-Berichte Nr. 247, 9/16 (1974)

/97/ E. Fitzer, D. Siegel
Chem. Ing. Techn., 47 (13), 571 (1975)

/98/ D. Siegel
"Stickstoffoxidemission industrieller Feuerungsanlagen in Abhängigkeit von den Betriebsbedingungen" Diplomarbeit am Institut für Chemische Technik der Universität Karlsruhe, 1973

/99/ H. Kruppe
"Über die Bildung von Stickoxiden bei Verbrennungsprozessen"
Dissertation TH Aachen 1970

/100/ H. D. Winkler, D. Weizel
Wasser, Luft und Betrieb, 16 (7), 213/215 (1972)

/101/ B.G. Newmann,
"The deflexion of plan jets by adjacent boundaries - Coanda effect"
in G.V. Lachmann "Boundary layer and flow control" Vol.1, p. 232,
Pergamon Press, 1961

/102/ R.C. Milliken
J. Phys.Chem., 66, 794 (1962)

The present investigation was conducted over the period from Summer 1975 to Spring 1979 at the State Institution for Environmental Protection Baden-Württemberg, Institute for Air Pollution-, Labor- and Radiation Protection, Department of Air Purity Control.

The plant tests were carried out during the period from Winter 1977 to Summer 1978 at the Oberrheinische Mineralöl-Werke GmbH in Karlsruhe. We are indebted to the management for making available to us the testing premises, the installations for the test flare and the flare gas.

We also wish to thank Flaregas Engineering Limited, West Drayton, Middlesex, England, for their willingness to make a flare head available for the tests.

Special thanks are due to the following gentlemen:

Prof. Dr.-Ing. R. Günther, professor of combustion engineering at the Engler-Bunte-Institute of the University of Karlsruhe, Prof. Dr. rer. nat. K. Hedden, professor of chemistry and engineering of gas, petroleum and coal at the Engler-Bunte Institute of the University of Karlsruhe, Dr. R. Becker (BASF, Ludwigshafen) and Dr. W. Zeiss (OMW, Karlsruhe) for their valuable suggestions relating to the tests performed.

The project on which this report is based has been supported financially by the Federal Minister of the Interior.

I am sincerely grateful to Prof. Dr. rer. nat. K. Hedden for his kind and unstinting support and for the critical examination of my work and also for acting as the official chief reviewer.

To Prof. Dr.-Ing. R. Günther I am obliged for valuable suggestions and for acting as associate reviewer.

To the President of the State Institution for Environmental Protection, Dr. H. Prassler, to the Director of the Institute for Air Pollution-, Labor- and Radiation Protection, Mr. W. Morgenstern, and to the Head of the Department of Air Purity Control, Dr. W. Obländer, I express my thanks for proposing the subject, for the assignment of the testing facilities and for the release of the test data.

I wish to thank all my colleagues, particularly Mr. R. Walenda, for their support during the field tests and for their ready cooperation.

1.2. State of Development of Elevated Flare Heads

There is no generally valid relation between the refinery capacity and the number of installations connected to the flaring-system nor is there any connection with the selection or the design of the flaring system [3].

The dimensioning of the flare head is limited by the flame stability which results from flash-back, lift-off or extinction of the flame. In order to operate the combustion at a stable operating point at which the flame burns steadily at a site close to the burner, the flow velocity of the gas-air mixture at the point of stabilization must be equal to the flame velocity [12 (p. 173 ff.)]. In the literature [15, 38] it is sometimes assumed in estimating the lift-off velocity that the lift-off occurs when the velocity of the fuel jet as it leaves the burner amounts to about one fifth the speed of sound.

$$u_o = 0.2\sqrt{\frac{\varkappa R T}{M}} \qquad \text{G 1-1}$$

(The symbols employed in G 1-1 are explained in the Appendix, p. 11-1)

Some authors [13, 14] point out that flares with flame holders can be operated even at flare gas velocities higher than those estimated according to G 1-1. Hess and Stickel [16] show that partially premixed flames stabilize anew at some distance from the flare mouth at exit velocities above those

corresponding to a stable operating point, which results in a considerable enlargement of the control range.

The flare heads of various manufacturers differ in the design and in the arrangement of steam input units.

Becker [17] divides the flare heads fed with flare gas from low-pressure networks into those with air-admixing before and those with air-admixing after the exit of the gas. The different flare head designs are shown schematically in Fig. 1-2.

When the air is admixed after the exit of the gas (Fig. 1-2a), the steam is introduced into the gas jet through a ring of steam nozzles. On the way between nozzle and gas jet the steam, in accordance with the law of free jets aspirates a portion of the combustion air. Since the pilot burner is arranged on the same plane, not only the air aspiration and the mixing of the gas with steam and air but also the ignition and stabilization of the flame must take place in this plane. Depending on the load range, these tasks cannot be fulfilled at the same time. The flame then stabilizes itself away from the flare mouth in the range of lower flow velocities, which even at slight load fluctuations leads to pulsating unstable flames.

Flare burners with air-admixing before the exit of the gas (Fig. 1-2b) are designed like Bunsen burners without a mixing tube. The air aspiration, mixing and combustion occur in critical load ranges on separate planes. For the air aspiration, the Coanda effect is utilized in most cases [18, 19].

a. Air-admixing after the exit of the gas

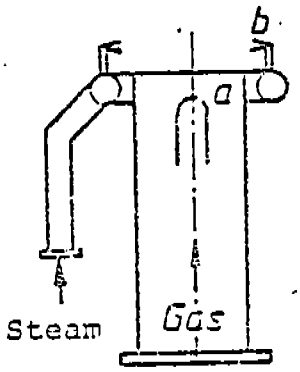

1.a internal steam nozzle
1.b external steam nozzle in one plane

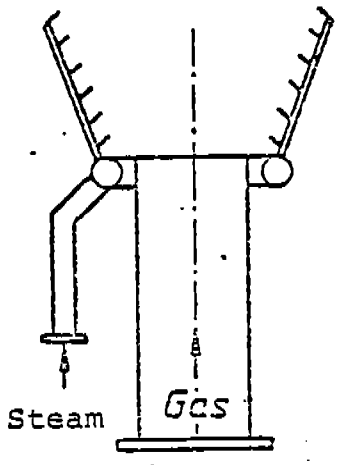

2. external steam nozzles in several planes

b. Air-admixing before the exit of the gas

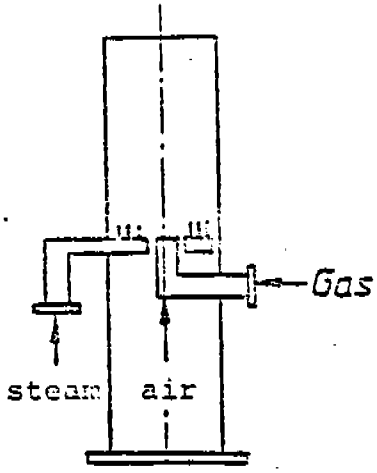

3. internal steam- and gas nozzles (Bunsen system)

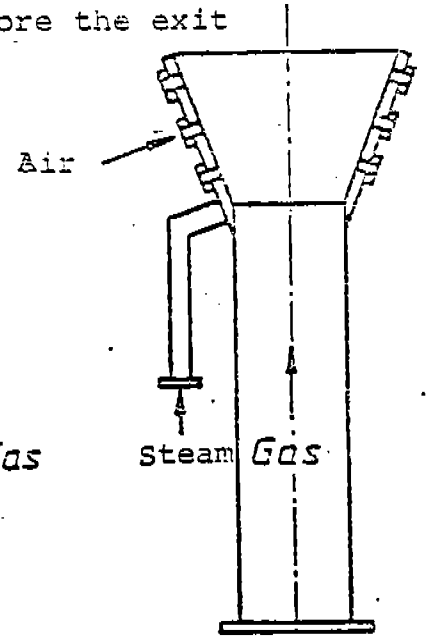

4. annular gap injectors (wall jet)

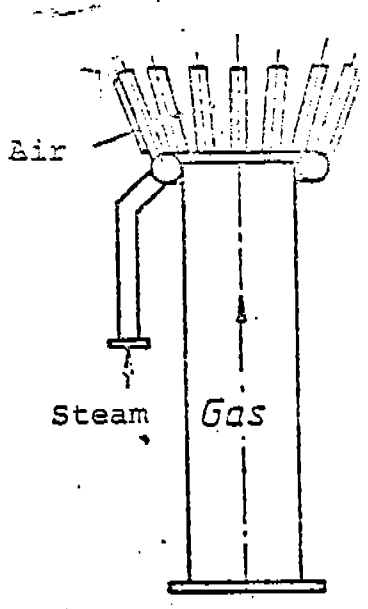

5. injector rods (wall jet)

Fig. 1-2: Different designs of elevated flare heads (with minor changes according to [17])

By the Coanda effect, the following is meant: A gas jet issuing from an opening expands as a rule in the form of a free jet. However, with the proper shaping of the surfaces adjacent to the exit opening the gas jet is deflected and hugs the adjacent walls. Close to the walls, the pressure is lower than in the vicinity and for fixed conditions upstream of the exit opening, the mass flow through the exit opening increases and, in addition, the volume of aspirated ambient air is also increased.[101].

The flare heads with air-admixing before the exit of the gas are for the most part expanded upwardly like a funnel. The aspiration of air and the mixing take place inside the cone. The partially premixed fuel-air-steam mixture is ignited by the pilot flame burning outside the cone. In addition to flame stability, this arrangement has the advantage that in load ranges comprising the accumulation of gas due to operating difficulties under controllable operating conditions the flare flame does not burn as a diffusion flame but as a partially premixed flame. The inner zones are admixed with air before the ignition. Premixed flames have a lesser tendency toward soot formation and, therefore, perhaps also less of a tendency toward the emission of unburned fuel than diffusion flames. In the event of a sudden drop-off of the flare-gas mass flow, the fuel-air-steam mixture is fully premixed.

A compilation of the conventional flare heads is found in Brzustowski [20]. A horizontally arranged "elevated flare" with

water injection for soot-free combustion is described by Lauderback [21]. Individual features of flare heads are found in the company prospectuses [22-25].

2. THE SIGNIFICANCE OF ELEVATED FLARES AS EMISSION SOURCES FOR AIR POLLUTANTS AND OBJECTIVE OF THE PRESENT INVESTIGATION

The flaring of excess gas is associated with the emission of nonatmospheric substances whose qualification and quantification has thus far not been clarified in a satisfactory manner. In the following, nonatmospheric substances are understood to be carbon monoxide, organic compounds, soot and nitrogen oxides, but not carbon dioxide and water.

People living near elevated flares usually feel molested by the noise caused by the addition of steam and by the light coming from the flare flames. Molestations by soot or smells hardly exist [3]. This is explained by the fact that with elevated flares soot and nonatmospheric substances are emitted at a great height. The elevated flare acquires significance as an emission source for nonatmospheric substances in the new creation of refinery capacities by the authorization procedure according to § 4 BImSchG and for existing installations in the emission declaration according to § 27 BImSchG [26]. In both cases, the applicant or operator of the installation must report and substantiate where, of what kind and in what quantities nonatmospheric substances are emitted during the operation of the installations (cf. 9th BImSchV [27] and 11th BImSchV [18]). These data form the basis for decisions concerning the operating permit and the conditions under which the installations can be operated.

On Lines 4 and 5 of Table 2-1 are shown the estimated values for 2 petroleum refineries of the losses of the crude oil

throughput dissipated via the flare and the emissions possibly associated with them. Line 6 shows the losses and possible emissions of all the refineries in the Federal Republic of Germany. To this end, their annual capacity was taken from Ref.[3] and the losses and emissions were calculated on the assumption that they are comparable to those of Refinery 1.

Table 2 - 1: Estimated values of the crude oil throughput lost by combustion in the flares

	Crude oil throughput	Loss		To the flare		Emi... U=	...on at ...1-99 %
	10^3 t/a	%	10^3 t/a	%	10^3 t/a	1[illegible]	10^3 t/a
Refinery 1 [29]	8900	0,33	29	45	13	[illegible]	[illegible]
Refinery 2 [30]	7000	0,2	14	50	7	1	0,07
∑Refinery (BRD)	153860 /3/	0,2	308	50	154	3[illegible]	1,54

U = degree of conversion

The table shall be explained briefly by taking Ref as an example. The estimated loss of the crude oil thr is of the order of 0.2%. At a capacity of 7 million t/ this amounts to a loss of 14,000 t/year. Of this, abou burned in the flare so that the annual flare load is ap mately 7000 tons. According to TA-Luft No. 3.27.1.1. m in calculating the emissions of organic gases and vapor maximum of 75% can be figured as the degree of conversi the off-gas combustion in the elevated flare. With thi

the resulting emission of organic gases and vapors amounts to 1800 t/year which is emitted via the elevated flare. This 75% degree of conversion is, however, not supported by experimental studies. This figure is also contradicted by studies on model flares [32] and by theoretical calculations [33] which lead to the result that the degree of conversion for the off-gas combustion in the elevated flare must be figured at the least at 99%. According to this figure, the resulting emission would be 70 t/year.

If we now extrapolate this figure, for example, to the refinery capacity in the Karlsruhe area, that is, to the refineries Oberrh. Mineralölwerke, Esso and Mobil Oil, Wörth, we obtain at a crude oil capacity of 18.5 million t/year an emission of organic gases and vapors of 4600 t/year at a conversion rate of 75% and of 180 t/year at a conversion rate of 99%. These two figures which differ by a factor of 25 make it clear that the elevated flare as an emission source may, depending on the conversion formula, be of considerable importance, for example, in calculating the air pollution load.

The specification of a conversion degree of 75% for the off-gas combustion in elevated flares has also led to the fact that in some refineries the construction of ground-level flares - in addition to the elevated flare - has been ordered in which a conversion degree of 95% may be figured for the off-gas combustion [31].

According to the Refinery Guideline No. 1.1.8 [34], "elevated flares may be used only in an emergency. For operating difficulties during which an installation continues to operate (controllable operating conditions) and also for the starting up and shutting down of installations, ground-level flares or equivalent devices are to be used."

Summarizing, it can be said that the discussion dealing with the criteria governing the operation of elevated flares concerning the emission of nonatmospheric substances has lacked proven arguments because only contradictory and inadequate findings have been available concerning the degree of conversion of flare gas in elevated flares and the pollutants emitted during flaring, even in the case of soot-free combustion. This has made it difficult to arrive at an estimate of the emissions occurring in the operation of refineries and at an objective evaluation of the conditions necessary for the operation.

For this reason, it has been the objective of this investigation to determine by experiment the degree of conversion of flare gas in refinery elevated flares and, more particularly, to obtain data on the emission of nonatmospheric gases and vapors during flaring.

In order to obtain representative test results, the operating conditions of the experimental flare had to be comparable with those of elevated flares integrated into the refinery operation. An operating condition corresponding to that of an emergency

shut-down was excluded. With the experimental flare system selected, it was impossible to simulate this state of operation both for reasons of safety and also because of a lack of gas. The frequency of this state of operation is very low and is also excluded in the specifications of the TA-Luft (= technical guidance for the maintenance of clean air).

The tests were, therefore, restricted to those states of operation in which the accumulation of flare gas can be traced to the starting up and shutting down of installations and also to those operating difficulties in which the installation continues to operate. For these states of operation, sufficient steam for a soot-free combustion was to be available.

3. LITERATURE SURVEY

The literature with the emphasis on "elevated flares" concerns itself mainly with measures for reducing the incidence of flare gas and increasing the operational safety of elevated flares.

Thus, in recent years, the gas volumes fed to the elevated flare have been considerably reduced. This has been achieved by storing the gas accumulating in the flare gas network intermediately in gasometers or by feeding them directly into the heating-gas network [1, 2, 3, 5]. Measures taken at the equipment level such as, for example, refitting of fixed roof- to floating roof-tanks and the improved design of valves have also led to a reduction of the incidence of flare gas [29]. For the safer operation of elevated flares, not only the aforementioned measures to prevent ingress of air into the flare system [4-6] but also the length of the flare flames [37-42] and their heat radiation [38, 43, 44] are of importance since they determine the distance of the elevated flare from the process installations.

Only very few studies are known which deal with the degree of conversion of the flare gas in elevated flares. In some of these studies, the knowledge gained with tube burners was applied to flare burners. However, the studies on tube burners were carried out with objectives other than the emission of nonatmospheric substances.

GRUMER et al. [46], in a study of the stability of hydrogen flames at flare burners also examined the effect of the wind on the discharge of unburned jet substance. The burner had

a diameter of 9.2 cm. The velocity of the hydrogen jet was 0.28 and 3.5 m/s and that of the wind 7.6 and 11.9 m/s, resp. In spite of the large velocity ratio of the gas- and wind-jet, they were unable to measure any discharge of hydrogen.

GUENTHER and LENZE [33], in dealing with the emission from refinery elevated flares, start from the supposition that unburned gas can be emitted by the detachment of batches at the edge of the jet. They assume that the burnout of detached eddies amounts to only 50%. From the eddy diameter and the frequency of detachment they estimate that as a result of batch detachment a maximum of 1% of the gas throughput is discharged unburned. They arrive at the conclusion that the burnout must be figured at the least at 99%.

LANDERBACK [21] fails to report any conversion degrees for the horizontally arranged flare with water injection into the flame for the suppression of soot even though it would be relatively simple to make such measurements with this flare.

It is difficult to judge whether the injection of water along the flame promotes the combustion or whether farther downstream the fuel pyrolysis is increasingly prevented so that unburned material is emitted in gaseous form.

SCHWANECKE [45] believes that "in the operation of elevated flares the formation of nitrogen oxides at the flame surface takes place to a larger extent than in a combustion muffle because the dwell time in the flame required for splitting the nitrogen oxides into nitrogen and oxygen cannot be maintained".

Because of the large temperature dependence of their rate

of formation, the formation of nitrogen oxides is tied to high temperatures. However, high temperatures are present in the core of the flame and not at the "flame surface". Moreover, in the case of flare flames the flame surface is in contact with the cold atmosphere and not with the hot surroundings of the combustion chamber. For this reason alone it is to be expected that because of the lower temperatures smaller amounts of nitrogen oxides are formed in the flare flames than in flames burning in a combustion chamber.

BECKER [32] made measurements on model flares in the wind tunnel. With natural gas as the fuel, he reports at wind velocities between 5 and 10 m/s burnout values of 99.8 to 99.9%.

BRZUSTOWSKI [20] starts from the supposition that even with a steam/gas ratio sufficient for a soot-free combustion it cannot be assumed that the combustion is complete. When the flare is operated under controllable operating conditions, he suspects a source for unburned gas at the end of the flame and also above and in the lee of the flare mouth. He himself calls his statements in the chapter "Air Contaminations by Flares" a "little speculative" since accurate measurements inside and outside the combustion field of the flare flames are lacking.

LEE [37] assumes that under the influence of the wind the cross section of the jet becomes horseshoe-shaped since the outer jet substance possesses a smaller impulse than the inner one. He calculates which segments are blown away at right angles to the flame axis to such an extent that they are no longer in contact with the rest of the jet. The calculation shows

that the largest amount of jet substance is carried away within the first one-sixth of the jet path. The amount carried away is greatly dependent upon the wind and is calculated for a flare diameter of 50 cm at 0.4% at a slight breeze (1 m/s) while with a strong wind (5 m/s) the carry-away may increase up to 12%. Since the burnout begins from the outside, the substance separated from the flame by the wind consists predominantly of off-gas.

STRAITZ [47] reports that in the combustion of natural gas in flares with diameters between 5.1 and 25 cm a conversion degree of more than 99% is attained even without an addition of steam. A dependence of the degree of conversion on the nominal width of the flare head could not be detected.

With a small steam addition, the degree of conversion and the temperature at the end of the flame were increased. With increasing steam addition, both reached a maximum and then dropped off again, which was caused by a quenching of the flame. With natural gas, the maximum occurred at a steam/gas ratio of 1 kg/kg. Measurements with sooty flames of other fuel gases showed conversions of 75%. With the addition of steam it was again possible to achieve a conversion of more than 99%, which dropped off again with excessive steam additions.

According to STRAITZ himself, the validity of his data is difficult to quantify. Uncertainties are caused by the flickering of the flame, the effect of the wind and also by dead time and mixing in the sampling lines. Furthermore, prolonged sampling would be necessary to support the statements.

From another publication by STRAITZ [10] which describes

the experimental setup and procedure and also reports a few test results, the following can be inferred:

Because of the experimental arrangement chosen, only the vertical edge of the flame was accessible. In the tests, neither the flow velocity of the off-gas nor its carbon dioxide volume portion was measured. Therefore, nothing definite can be said concerning the degree of conversion or the local burnout. Moreover, some of the data from the table "Typical results of tests relating to the emission from flares (without steam)" contained in [10] contradict the statement made by STRAITZ in [47] according to which a degree of conversion of more than 99% was attained. He reports, for example, with natural gas as the fuel, a maximum volume portion of hydrocarbons in the off-gas of 5.2% at an oxygen volume portion of 11%. This would correspond to a conversion degree of less than 50%.

According to the TA-Luft [31] No. 3.27.1.1.m, "the emissions of organic gases and vapors in a refinery without further petrochemical processing should as a rule not exceed 0.04% of the mass of crude oil processed; for this, at the most 75% can be figured as the degree of conversion for the off-gas combustion in the elevated flares unless some special proof makes the application of higher degrees of conversion appear permissible".

Accordingly, in calculations of the emissions of organic gases and vapors from the percentage lost by combustion via the elevated flares, an emission factor [28] of at least 25% must be taken into account. Since emissions of soot are not mentioned, it must be assumed that the flare flame should as a

rule burn free of soot.

According to the opinion of the parties involved in the drafts of the TA-Luft (§ 51 BImSchG), the tests on model flares cannot be directly extrapolated to elevated flares. As a justification it is adduced that the model flares were operated under optimal combustion conditions and that these do not correspond, according to experience, to those encountered in the practical operation of refineries. In addition, the burnout degrees in the case of elevated flares must on the whole be rated as less satisfactory than those of ground-level flares (95%) since the combustion does not take place in a combustion chamber but in an open flame in a manner largely uncontrollable. In addition, the combustion process is at least in part associated with the discharge of partially unburned or burned substance, which is intensified by large load fluctuations and changing gas composition.

In this, the parties involved were aware of the fact that the postulate of a soot-free combustion refers only to the range of a 0-25% flare load, that is, to the controllable operating conditions at which an adequate steam mass flow is available for a soot-free combustion [48].

4. GENERAL

4.1. Description of the Combustion Process [12,49]

Fig. 4-1 shows by the example of the photograph of a flare flame which burned without steam addition that in turbulent free-jet flames there is no closed combustion front, but that a distinction can be made between a large number of separate and incoherent zones. This can be explained by the fact that in the flow field no individual molecules are transported but tight associations of molecules - so-called cells or batches - in which the combustion has already progressed to a greater or lesser extent.

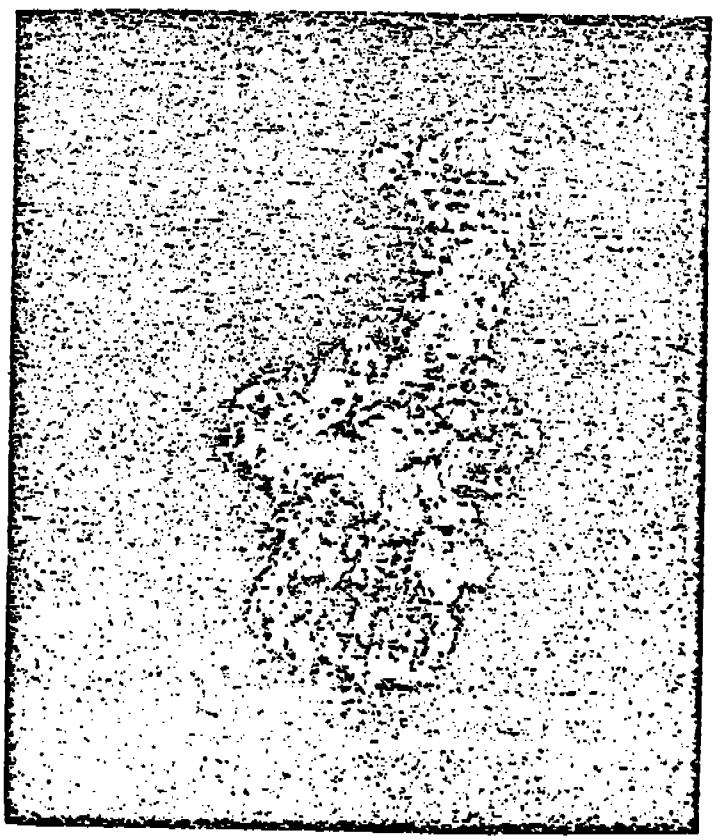

Fig. 4-1 : Photograph of a flare flame burning without steam addition.

During the combustion, the fuel components are converted by chemical reaction with atmospheric oxygen to carbon dioxide and water.

$$C_m H_n + \left(m + \frac{n}{4}\right) O_2 \longrightarrow m\,CO_2 + \frac{n}{2}\,H_2O$$

The reaction does, however, not take place in one step but by way of a large number of intermediate products which can be considered as secondary fuels. The oxidation reactions can proceed only when the required energy of activation is available and the reaction partners have been mixed with each other. As far as the flames are concerned, a basic distinction has in this case to be made between macroscopic mixing where molecular associations participate in the mixing process and molecular mixing where individual molecules take over the mixing process. The oxidation reactions can, however, proceed only when the reaction partners have been mixed on a molecular scale.

4.1.1. Flow and Mixing in Freely Burning Diffusion Flames [12]

Macroscopically, the flow- and reaction-field of the flare flame is determined by the forces of inertia and buoyancy. The mixing necessary for the reaction is brought about by exchange processes between the fuel jet and the medium surrounding the jet, in which case the velocity-, temperature- and material gradients control the exchange processes. Because of the turbulent state, the flow velocity, temperature and composition of the mixture vary randomly around a mean value. For the velocity, for example, the

momentary value $\hat{u}$ can be perceived as the sum of the chronological mean value u and the momentary difference $\hat{u}$ between u and $\hat{u}$. $\hat{u}$ has also been designated as the fluctuation variable and the mean square deviation of the fluctuation variable from the mean value $\sqrt{\overline{\hat{u}^2}}$ as the mean fluctuation variable. The chronological mean values differ from one location to the next.

For the mathematical description of flow and mixing, the impulse transfer equation by REICHARDT [50] is frequently used. He determined from measurements that in the case of free turbulence the velocity profiles related to the axial values can be represented by error functions. In order to derive this behavior of turbulent flow from the impulse equation and, more precisely, for a flow which is steady and frictionless and in which there exist no pressure differences, he postulated that the flow of x-impulse (x-direction of flow prior to the entrance into the region of turbulent mixing), which flows off in the transverse direction y, is proportional to the impulse gradient in the transverse direction. The proportionality factor, the transfer quantity Λ, is a length which is independent of the y-direction but which may be a function of the longitudinal direction x. The error functions are solutions of the defining equation for the impulse when, for example, for the round free jet the transfer quantity Λ is made equal to $\Lambda = \frac{1}{2} c_i^2 \cdot x$. The dimensionless transfer factor c_i is considered as constant. The same applies to the distributions of material and heat. The numerical values of the transfer factors are determined from measured values. The numerical values of the transfer factors for material and heat are equal. Impulse is exchanged more slowly than heat and

material. The most important factors of influence are the Reynolds number and the density ratio between jet and environment. The exchange decreases with increasing Reynolds number and increasing density ratio.

LEE [36] expands Reichardt's equation by including the buoyancy forces for whose description he introduces a dimensionless buoyancy number. The latter is dependent upon the transfer factor, the flow path, the Froude-number based on the jet origin and on the density difference between gas-air-jet and surroundings, based on the density of the gas jet at its point of origin.

In free-jet flames, the combustion lags considerably behind the mixing. This is taken into account by the state of segregation [51] which depends on the interaction between macroscopic and molecular mixing and which must be determined empirically. According to LENZE [52], the segregation is proportional to the eddy factor and conversely proportional to the fluctuation variable.

This flow-mechanical model for the mixing and combustion process in flames affected by buoyancy reproduces their length fairly accurately, in which case the flame length can be taken as a measure of the path necessary for the molecular mixing of fuel and oxidant.

4.1.2. Reaction Mechanisms of Partial Reactions Involved in Combustion

It is customary to divide flames into premixed flames and diffusion flames. In premixed flames, HOMANN [53] distinguishes between the blue oxidation zone and the yellow pyrolysis zone.

Some authors, for example, GLASSMAN [54] make a further subdivision into a post-reaction zone in which a large portion of the previously formed carbon monoxide and hydrogen is reacted to carbon dioxide and water.

In contrast to premixed flames, diffusion flames cannot be separated into different zones. In the following analysis, it is assumed that in regions where the molecular mixing of fuel and oxidant predominates, oxidation zones are present. They can be found primarily at the boundary surfaces of the batches of fuel and oxidant. Regions in which there is no molecular mixing of fuel and oxidant, but in which the temperature is sufficient for the pyrolysis of the fuel, are considered to be pyrolysis zones. In this case, pyrolysis zones may be formed either due to the fact that in the fuel batches only heat has been transported but no oxidant, or else due to the fact that the fuel batch has become mixed with combustion products instead of with oxidant.

It can be imagined that the diffusion flame consists of a multiplicity of small premixed flames in which the optical properties of the pyrolysis zones mask those of the oxidation zones. This has been justified by the fact that in the combustion in premixed flames and in diffusion flames the same intermediate products are formed. Thus, for example, HOMANN and WAGNER [55] were able to detect in the oxidation zone of premixed methane flames polycyclic aromatic hydrocarbons which are looked upon as nucleus-formers for soot. However, the formation of soot can be

observed only in the pyrolysis zone. Moreover, the properties of soot formed in flames are hardly dependent on the type of flame [56].

(The above notion that the diffusion flame is composed of many small premixed flames is expedient for the explanations below but represents the true conditions only with reservations. In premixed flames, fuel and air are mixed prior to ignition and the combustion takes place in the reaction zone whose location is determined by the equilibrium between flow- and flame velocity. In the diffusion flame, on the other hand, the molecular mixing is achieved by diffusion at the boundary surface between fuel and air and the reaction proceeds at the point to which fuel and oxidant diffuse at the stoichiometric ratio.)

In the oxidation zone, a portion of the fuel is burned to carbon monoxide and hydrogen while the other portion is reacted to carbon-containing intermediate products (R 4-1). Since in the oxidation zone there is already a formation of water and carbon dioxide (R 4-2 and R 4-3), oxygen continues to be consumed so that the formation of hydrocarbon radicals according to R 4-4 may be larger than their oxidation:

$$C_mH_n + y\,O_2 \longrightarrow 2y\,CO + \frac{n}{2}H_2 + (m - 2y)\,C \qquad \text{R 4-1}$$

$$H_2 + OH \longrightarrow H_2O + H \qquad \text{R 4-2}$$

$$CO + OH \longrightarrow CO_2 + H \qquad \text{R 4-3}$$

$$C_xH_y + OH \longrightarrow H_2O + C_xH_{y-1} \qquad \text{R 4-4.}$$

In hydrogen-containing flames, the autodissociation of hydrogen can be considered as the starting reaction for the formation of hydroxyl radicals:

$$H_2 + M \longrightarrow 2H + M \qquad \text{R 4-5}$$

$$H + O_2 \longrightarrow OH + O \qquad \text{R 4-6}$$

$$O + H_2 \longrightarrow OH + H \qquad \text{R 4-7.}$$

In aliphatic hydrocarbon flames, acetylene is always formed as a stable intermediate product. HOMANN and WAGNER [55] assume that, for example, in methane flames, acetylene is formed by the recombination of methyl radicals via ethane and ethene:

$$2CH_3 \longrightarrow C_2H_6 \longrightarrow C_2H_4 \longrightarrow C_2H_2 \qquad \text{R 4-8.}$$

Acetylene is considered the smallest molecule in the reaction sequence leading to the formation of soot-nuclei according to a radical mechanism. Only when in the oxidation zone fuel and air are mixed sufficiently on a molecular scale is it possible to reduce the formation of acetylene, for example, by reaction of the methyl radicals with oxygen:

$$CH_3 + O_2 \longrightarrow CH_3OO \longrightarrow CH_2O + OH \qquad \text{R 4-9.}$$

Besides, excess oxygen may also cause a rupture of the chain in the polymerization reactions of hydrocarbon radicals of higher C-number, for example, with the formation of oxidized

products such as aldehydes:

$$R-CH_3 + O_2 \rightarrow R-CH_3OO \rightarrow R-CH_2O + OH \qquad \text{R 4-10.}$$

Flaring without steam-addition is generally accompanied by the emission of soot, since the formation of soot particles predominates over their combustion. The fact that also in soot-free flames carbon particles are formed as intermediate products can be recognized by the luminosity of the flame. The yellow color of the flame is due to the fact that, at the temperatures present in flames, the eye perceives the continuous radiation of a black body as yellow.

We designate as soot particles of high carbon content whose composition can be rendered approximately by the summation formula C_8H. The particle diameter generally ranges between 10 and 50 nm. Each particle consists of approximately 10^4 crystallites. A crystallite is formed by 5 to 10 layers of carbon atoms comparable to those in graphite. Each layer comprises approximately 100 carbon atoms [54].

The formation of soot can be divided into the formation of soot nuclei and the particle growth with subsequent particle-particle coagulation. The most important step is the formation of soot nuclei which proceeds in the pyrolysis zone at temperatures between 500 and 800°C and for which several hypotheses are under discussion [56], for example, the formation of soot nuclei via radicals [55] or via ions [57].

According to investigations by WEINBERG et al. [57], the formation of soot increases with increasing ion intensity. The ion concentration reaches its maximum at the end of the oxidation zone and drops off sharply in the pyrolysis zone. The formation of ions does in this case not seem to be temperature-related since the temperatures at the end of the oxidation zone and the beginning of the pyrolysis zone are comparable. It is, therefore, assumed that the ions are formed by proton transfer reactions between ions and molecules:

$$RH^+ + CH_2O \longrightarrow CH_3O^+ + R \qquad \text{R 4-11.}$$

For this reaction, the formation of CHO^+ by chemi-ionization according to R 4-12 is considered to be the primary step:

$$CH + O \longrightarrow CHO^+ + e^- \qquad \text{R 4-12.}$$

For the formation of soot nuclei, the ion of an unsaturated hydrocarbon adds other ions or molecules and forms a cluster which by dehydration and polymerization grows into a stable particle with a high C/H-ratio. Investigations by WERSBORG [58] show, however, that in flames without an electric field approximately 70% fewer ions are formed than in flames with an electric field.

A radical mechanism for the formation of soot nuclei which is sketched in Table 4-1 has been suggested by HOMANN and WAGNER [55].

Table 4-1: Formation of soot according to a radical mechanism [55]

Acetylene	radical reactions with C_2H and C_2H_3 →	polyacetylenes polyacetylene radicals
Addition of a radical →	chain branching	addition of C_2H_2 and polyacetylenes, cyclization →
	polycyclic aromatic hydrocarbons ↓	
→	reactive, partly cyclic hydrocarbons, hydrogen-rich	addition of polyacetylenes →
→	small soot particles (reactive)	addition of small soot particles and polyacetylenes → inactivation
→	large soot particles	→
→	agglomeration of large soot particles to soot, slow growth by heterogeneous decomposition of acetylene and polyacetylenes	

By the addition of radicals to acetylene, polyacetylenes are formed in the reaction zone which cyclize to polycyclic aromatic hydrocarbons (PCAK). While PCAK without side chains are considered to be final products, hydrogen-rich cyclic hydrocarbons continue to add acetylene and form small reactive soot particles at the transition from the oxidation zone to the pyrolysis zone. Simultaneously with the addition and decomposition of polyacetylenes and with the addition of other soot particles to form large soot particles, the particles are deactivated. The large soot particles agglomerate into soot.

One shortcoming of this mechanism is that it cannot explain why soot nuclei are formed only at the beginning of the pyrolysis zone, that is, discontinuously, even though later on enough polyacetylenes are still present.

LESTER and WITTIG [59] conclude from their experimental data that radical as well as ion reactions lead to soot nuclei, with the ionic mechanism prevailing in weakly fatty mixtures.

The combustion of soot particles already formed proceeds as a heterogeneous reaction at the surface of the soot. According to MILLIKAN [102], soot is oxidized rather by hydroxyl radicals (R 4-13) than by carbon dioxide (R 4-30) or water (R 4-31) even when the latter are present at a concentration many times higher. FENIMORE and JONES [60] show that soot is disintegrated substantially more rapidly by hydroxyl radicals than by oxygen. According to their test results, soot is hardly oxidized at temperatures

below 1200 K even at an oxygen partial pressure of 0.21 bar.

WRIGHT [61] concludes from his experiments that oxygen atoms play an important role in the oxidation of soot (R 4-14 a,b,c) and that carbon dioxide is already formed at the surface of the soot and not by the gas-phase reaction of carbon monoxide with oxygen atoms (R 4-32).

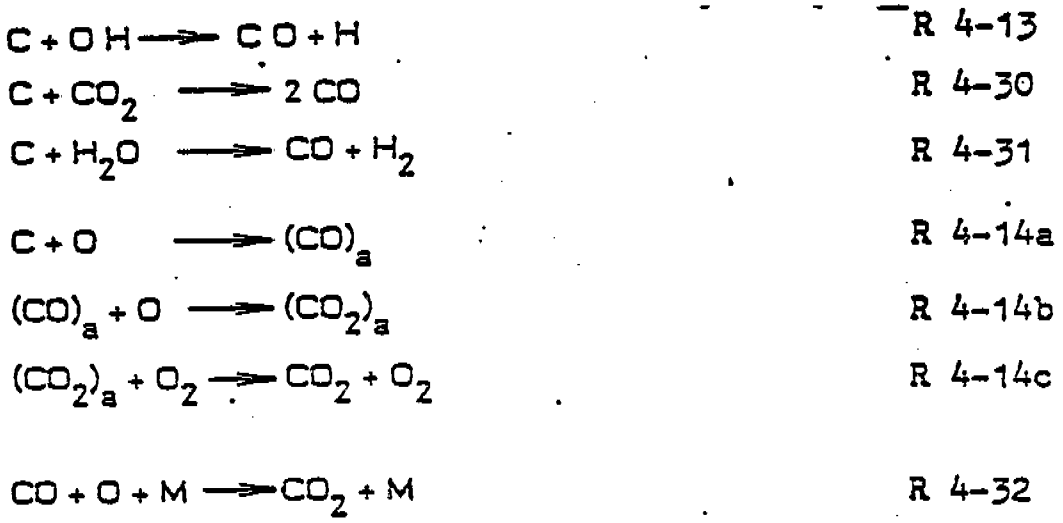

According to the results of WRIGHT's tests, in the temperature range between 500 and 900 K the reaction is restricted to the external surface of the soot. In contrast to this, KURYLKO and ESSENHIGH [62] concluded from their experimental data that the internal as well as the external surface of the soot is affected by the reaction, with the reaction site being dependent on the temperature. At approximately 800 K, the reaction at the external surface is so slow that the particles may lose up to 80% of their weight without any significant change at their external

surface. At temperatures above 1250 K, however, the weight loss could be readily correlated with the decrease of the external surface.

4.2. Preliminary Thermodynamic and Kinetic Analyses

The tendency of the hydrocarbons toward decomposition into carbon and hydrogen and the tendency of the reaction products carbon monoxide, carbon dioxide and water to be formed from the elements can be read from the standard free enthalpies of formation ΔG_f° of the components.

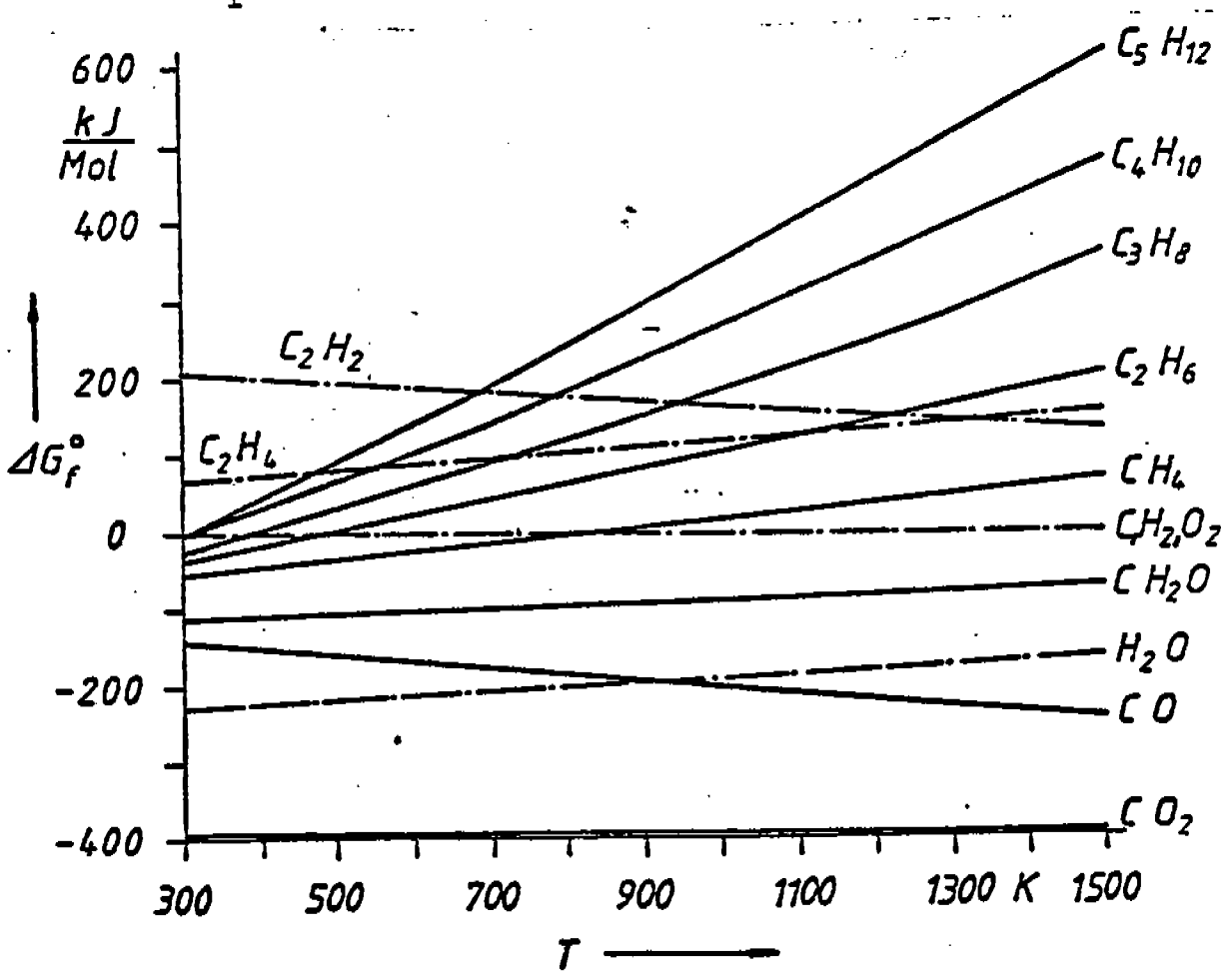

Fig. 4-2 : Standard free enthalpy of formation as a function of the temperature.

Fig. 4-2 shows the standard free enthalpies of formation as a function of the temperature for some of the components. Negative numerical values signify that the component is stable. The values of the standard free enthalpy of formation are found in the literature in tabular form [63,64].

It is evident from the diagram that

- all saturated hydrocarbons become unstable upon heating and decompose into their elements carbon and hydrogen,
- the stability of the paraffins decreases with increasing temperature more rapidly than that of the olefins,
- only acetylene becomes more stable with increasing temperature,
- in the group of the paraffins, methane is much more stable than ethane, propane, etc.,
- carbon dioxide and water are more stable than the hydrocarbons in question.

The maximum degree of conversion of a reaction partner which is thermodynamically possible in a reaction under specified experimental conditions can be calculated from the equilibrium constant. In Fig. 4-3, the common logarithm of the equilibrium constant K_p is shown as a function of the temperature for various summary reactions. A large numerical value of K_p signifies that the equilibrium of the respective reaction lies far on the right-hand side. The values for K_p were for each of the reactions indicated on the diagram calculated from the standard free enthalpies

of formation. It is evident from the diagram that the thermodynamic equilibrium lies far on the side of the desired reaction products.

In order to obtain an idea of the number of the parts by volume of gases alien to air contained in the off-gas, for example, after the stoichiometric combustion of methane with air

$$CH_4 + 2\,O_2 \rightleftharpoons CO_2 + 2\,H_2O \qquad \text{R 4-15,}$$

we calculated the equilibrium composition of the off-gas according to G 4-1 [65]

$$\sum_i \nu_i \log \left(\frac{x_i^{ein} + \frac{\nu_i}{|\nu_k|}\, x_k^{ein}\, U_{k,Gl}}{1 + \frac{\sum_i \nu_i}{|\nu_k|}\, x_k^{ein}\, U_{k,Gl}} \right) = \log K_a - \sum_i (\nu_i \log f_i)_{Gl} - \left(\sum_i \nu_i\right) \log P \qquad \text{G 4-1}$$

In G 4-1:

K_a = equilibrium constant

f_1 = fugacity coefficients

P = total pressure

ν_i = molar number of component i

ν_k = molar number of leading component

$x_{i,k}$ = mole fractions of initial mixture

The calculation shows that at a temperature of 1500 K an equilibrium degree of conversion higher than 0.999 is attained. This degree of conversion corresponds to a methane volume portion of ca. 4 ppb.

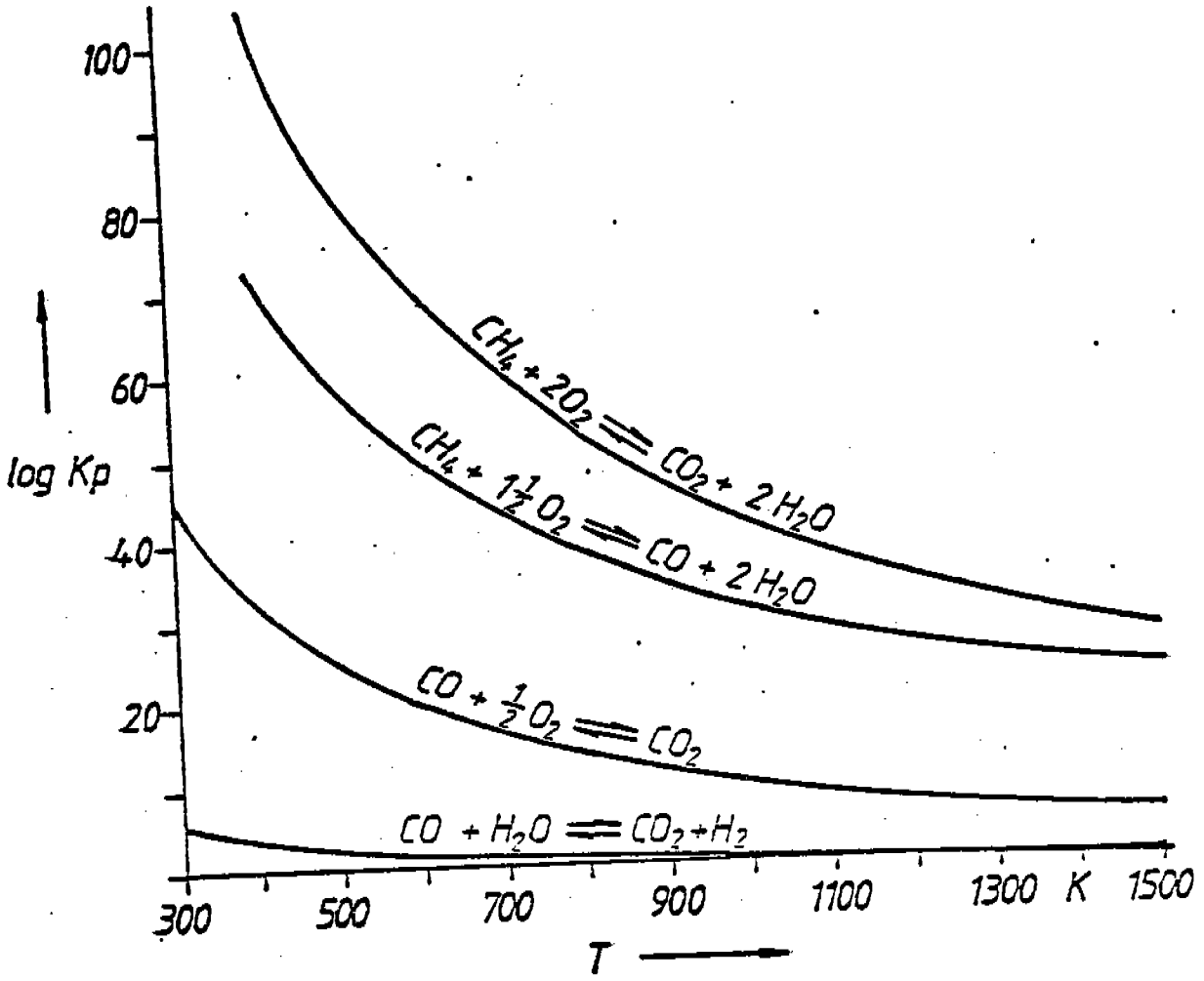

Fig. 4-3 : Equilibrium constants as a function of the temperature.

The thermodynamic equilibrium between carbon dioxide and carbon monoxide

$$CO_2 \longrightarrow CO + \tfrac{1}{2} O_2 \qquad \text{R 4-16}$$

also lies in the off-gas at temperatures lower than 1000 K completely on the carbon dioxide side. The carbon monoxide volume portion in the off-gas at temperatures below 1000 K amounts to less than 2 ppm.

This upward estimate shows that from the standpoint of thermodynamics conversion degrees higher than 0.99 are possible.

However, thermodynamics does not allow any conclusions concerning the intermediate products, the reaction rate and the reaction mechanism. These are so complex in the case of flames that a unified presentation is impossible. While rate constants for many of the partial reactions involved in the reactions can be found in the literature [49,66], calculations for the reaction sequences are available only for the oxidation of methane in an ideal homogeneous mixture with air and oxygen.

CREMER [67], for example, uses for the calculation of the methane-air-oxidation the model of a reaction mechanism which comprises 25 elementary reactions for the methane oxidation and 19 elementary reactions for the simultaneously occurring formation of nitrogen oxides. For a starting temperature of 1200 K and a pressure of 8 bar and with nitrogen as an inert component, the methane portion has after only ca. 380 µs dropped by a factor of 10^{-10}. His calculations with nitrogen as a reaction partner show that the formation of nitrogen oxides impedes the progress of the reaction. A total of 20 components, 8 of them radicals, participate in the simultaneous reactions.

This preliminary reasoning shows that from the thermodynamic standpoint a complete conversion is possible and that with homogeneous mixing and sufficient temperature the reaction rates are such as to permit the velocity of the reaction sequence to be

determined by mixing processes. The emission of unburned fuel from flare flames must, therefore, be caused by a macroscopic lack of oxygen, high segregation or the quenching of the reaction partners below the reaction temperature.

4.3. Formation of Nitrogen Oxides in Flames

The complicated processes leading to the formation of nitrogen oxides in flames have thus far prevented the development of a unified theory. However, from numerous investigations the relationships are at least qualitatively quite well known. It appears that in the case of fuels which do not contain any nitrogen compounds, basically 3 processes are involved.

Process 1 : Formation of thermal NO

Process 2 : Formation of prompt NO

Process 3 : Transformation of the resulting NO into NO_2

In the formation of thermal NO according to the so-called Zeldovich-mechanism [68], atmospheric oxygen and nitrogen react to form nitrogen monoxide:

$$N_2 + O_2 \longrightarrow 2\,NO \qquad \text{R 4-17}$$

$$N_2 + O \xrightarrow{(k_1)} NO + N \qquad \text{R 4-18}$$

$$N + O_2 \longrightarrow NO + O \qquad \text{R 4-19.}$$

In this case, R 4-18 as the slowest reaction is rate-determining and is, owing to the strong temperature-dependence of the rate

constant (k_1) tied to high temperatures [95].

According to FENIMORE [69], nitrogen monoxide is formed in hydrocarbon flames not only according to the Zeldovich-mechanism. He postulates that in the reaction zone hydrocarbon radicals react with atmospheric nitrogen by way of the intermediate stages HCN, CN, OCN to NO. He called the NO formed in this manner "prompt NO". The formation of prompt NO has been confirmed by the experiments of BACHMEIER et al. [70]:

$$CH + N_2 \longrightarrow HCN + N \qquad \text{R 4-20}$$

$$C_2 + N_2 \longrightarrow 2\,CN \qquad \text{R 4-21.}$$

In flames, the equilibrium between CN-radicals and HCN establishes itself very quickly [71]:

$$CN + H_2 \rightleftharpoons HCN + H \qquad \text{R 4-22}$$

$$CN + H_2O \rightleftharpoons HCN + OH \qquad \text{R 4-23.}$$

In zones which are not excessively rich in fuel, the resulting CN-radicals react immediately further to form NO [72]:

$$CN + O_2 \longrightarrow OCN + O \qquad \text{R 4-24}$$

$$OCN + O \longrightarrow CO + NO \qquad \text{R 4-25.}$$

However, the prompt NO formed in the reaction zone accounts for only a small portion of the nitrogen monoxide formed in the

region downstream of the flame where the Zeldovich-mechanism controls the nitrogen oxide formation.

The oxidation of the nitrogen monoxide formed in flames to nitrogen dioxide occurs for the most part only in the atmosphere:

$$2\,NO + O_2 \longrightarrow 2\,NO_2 \qquad \text{R 4-26.}$$

In Fig. 4-4, the equilibrium concentration of nitrogen dioxide (calculated according to G 4-1) has been plotted against the temperature for an initial nitrogen monoxide volume portion of 0.1% in mixtures with an oxygen volume portion of 1 and 20% respectively. The slope of the curves shows that the oxidation of nitrogen monoxide to nitrogen dioxide increases with decreasing temperature.

The rate of oxidation also increases with decreasing temperature [84] (p. 766). However, under the conditions normally present in the atmosphere, the oxidation reaction R 4-26 proceeds very slowly. Thus, for example, for a nitrogen monoxide volume portion of 1 ppm in a mixture with air at 20°C, the half-time amounts to 56 hours. (The half-time value was calculated according to Eq. 3b in [84] (p. 768).

On the other hand, investigations by MERRYMAN and LEVY [73] show that nitrogen dioxide is already formed in the oxidation zone of flames and is again consumed in the near downstream region of

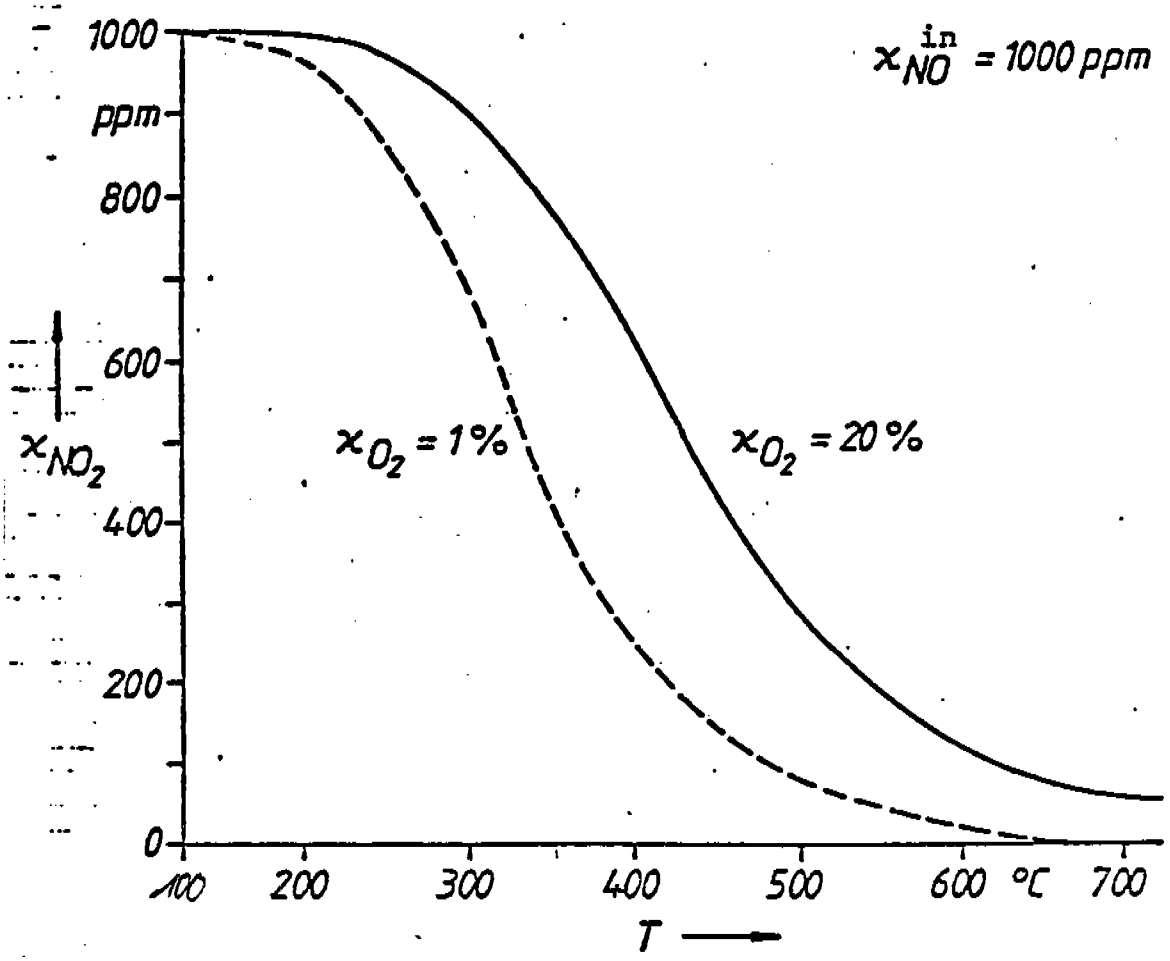

Fig. 4-4 : Equilibrium concentration of nitrogen dioxide as a function of the temperature for a nitrogen monoxide volume portion of 0.1% in mixture with oxygen volume portions of 20 and 1%, resp.

the flame with the formation of nitrogen monoxide. For this they postulate the reaction sequence R 4-27 to R 4-29:

$$\begin{matrix} NH \\ CH \end{matrix} + O_2 \longrightarrow NO + \,?$$ R 4-27,

$$NO + HO_2 \longrightarrow NO_2 + OH$$ R 4-28,

$$NO_2 + O \longrightarrow NO + O_2$$ R 4-29.

5. EXPERIMENTAL PART

5.1. Planning and Scope of the Experiments

The degree of conversion of flare gas during the combustion in elevated flares is impossible to determine on an elevated flare integrated into the refinery operation. It cannot be done because of the difficulties of sample-taking and also for reasons of safety. For the experiments a flare head was, therefore, installed on the plant premises of the Oberrheinische Mineraloel-Werke (OMW) Karlsruhe, and connected to their flare gas network. The mouth of the flare head was situated 5 m above the ground. The probes for taking samples were mounted on a movable construction crane. We tried to simulate the wind effect by means of a blower.

The determining considerations for the selection of the flare head were the following:

According to the objective of the investigation, the tests were to cover a load range in which the formation of flare gas is conditioned by operating difficulties with controllable operating conditions and by the starting up and shutting down of installations. For these operating conditions, an adequate supply of steam for a soot-free combustion was to be available. The stipulation of a soot-free combustion was to apply to maximally 25% of the rated load of the flare head [48].

Of the flare heads forming part of the refinery operation no data were known concerning their diameter, rated load, frequent operating loads and maximum load for a soot-free combustion. Only for one elevated flare was a part of the data available,

that is, the rated load with 82 t/h at a flare gas standard density of 0.74 kg/m^3 and the diameter with 0.6 m [33]. However, a flare head with such a capacity is not suitable for an experimental operation because the flare gas mass flow even for small partial loads is not available on call in the running operation of the refinery.

In the case of the flare burners, a flow-mechanical similarity cannot be attained with models since the flow field of the flame is determined by the forces of inertia and updraft. Characteristic variables are the diameter of the flare head and the velocity of the flare gas at the exit from the flare head. In the Reynolds number, the diameter stands in the numerator and in the Froude number in the denominator. The velocity appears in the Reynolds number in the first and in the Froude number in the second power.

The flare gas mass flow for the tests was limited by the OMW to 4 t/h. Although flares are operated almost exclusively in load ranges far below the rated load and the tests were to cover load ranges up to 25% of the rated load, higher load ranges are also of interest.

The flare head was, therefore, designed for a rated load of 10 t/h at a flare gas standard density of 0.75 kg/m^3. Furthermore, a flare head was selected in which the aspiration of air, the mixing and the combustion take place on different planes. This was based on the idea that these flare head designs correspond, particularly in the lower load ranges, to the state of the art.

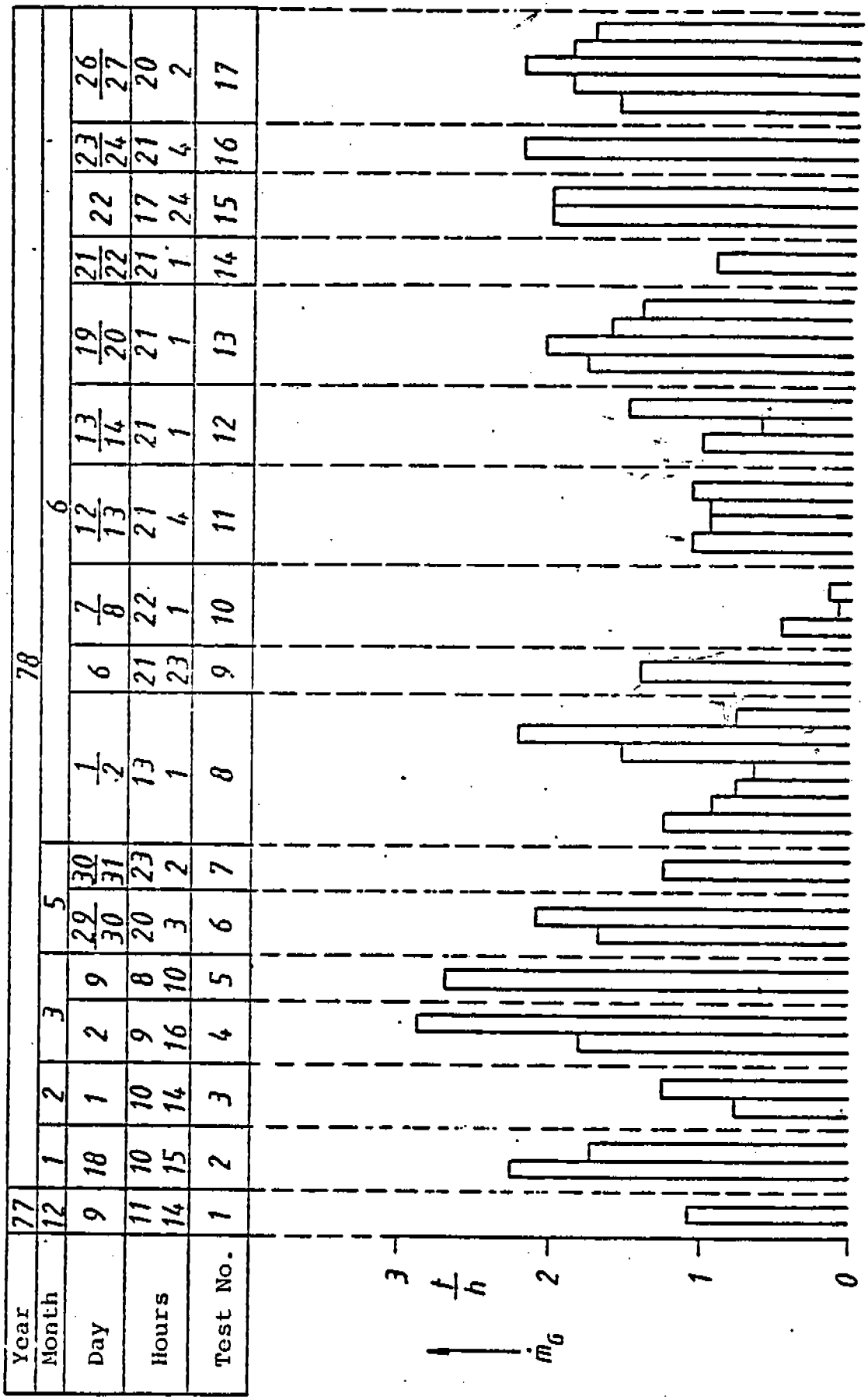

Fig. 5-1. Test Schedule

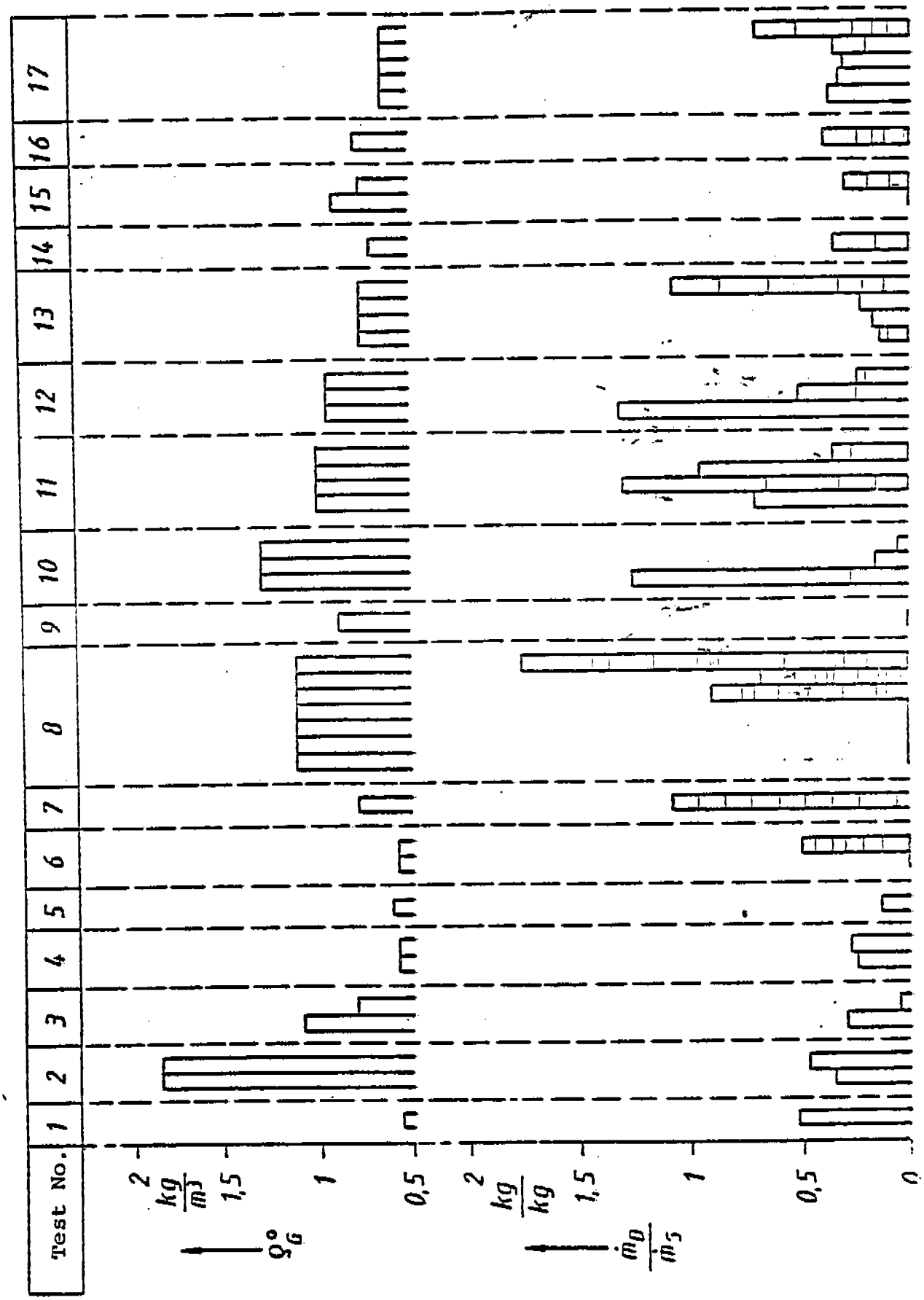

Although the flare gas composition does have an effect on the steam addition necessary for soot elimination and, therefore, on the combustion, it could be seen at the beginning of the tests that very specific gases such as occur, for example, in the petrochemical industry could not be included in the testing program since they were not available.

An overview of the scope of the tests and the operating times of the test flare for our own tests is given in Fig. 5-1. In the table at the head of Fig. 5-1, Lines 1 to 3 show the data and Line 4 the beginning and the end of the tests. On line 5, the testing days are numbered consecutively. These are the numbers to which the digits in front of the period refer in the system of numbering the tests in Sect. 6 and in Appendix 1. On the diagram, the flare gas mass flow, the flare gas standard density and the steam/gas ratio are presented in the form of bars. For the first two quantities, the height of the bar indicates their value. The bars representing the steam/gas ratio are subdivided by horizontal lines. This is to signify that at the respective flare gas mass flow several steam/gas ratios were fixed whose value is given by the height of the bar sections starting from zero.

The flare gas mass flow ranged from 0.13 to 2.9 t/h with flare gas standard densities between 0.54 and 1.86 kg/m^3. The steam/gas ratio was varied between 0 and 1.73 kg/kg.

In the tests, the flare gas mass flow was limited by the pressure drop in the test flare gas line and by the back-pressure on the main flare gas line. A limitation of the back-pressure

was, however, necessary for reasons of safety since in the event of an unexpected accumulation of gas in the flare gas network, this gas had to be burned via the main flare.

5.2. Description of the Experimental Flare System and of the Measuring Technique for Determining the Input Mass Flows

A general view of the testing area is provided by the site plan in Fig. 5-2. The test flare head together with the wind machine is shown in Fig. 5-3a and the flow diagram of the test flare system in Fig. 5-4.

The tests were carried out with a flare head of the Flare-gas Co., type FS-6-antipollutant. The nominal width of the flare head at the entrance into the cone-shaped mixing chamber amounted to 20 cm and the upper diameter of the 50 cm long core amounted to 70 cm. The mouth of the flare head, which is identical with the upper edge of the cone was situated 5 m above the ground.

The cone accommodated 6 Coanda nozzles, so-called Flarejectors® which were fed with steam in order to aspirate air. The steam temperature at TJ 121 ranged between 190 and 210°C and the steam pressure at PJ 123 between 1 and 9 bar, depending on the steam load. The dependence of the pressure at PJ 123 on the steam load is shown in Appendix 6. According to the manufacturer's data, the optimum operating pressure is of the order of 4.5 bar.

A longitudinal section through a Flarejector is shown in Fig. 5-3b. The steam exits from the annular gap at high velocity and due to the shape of the adjacent walls hugs these

walls. As a result, a suction is created above the wall jet so that air is aspirated into the cylindrical Flarejector.

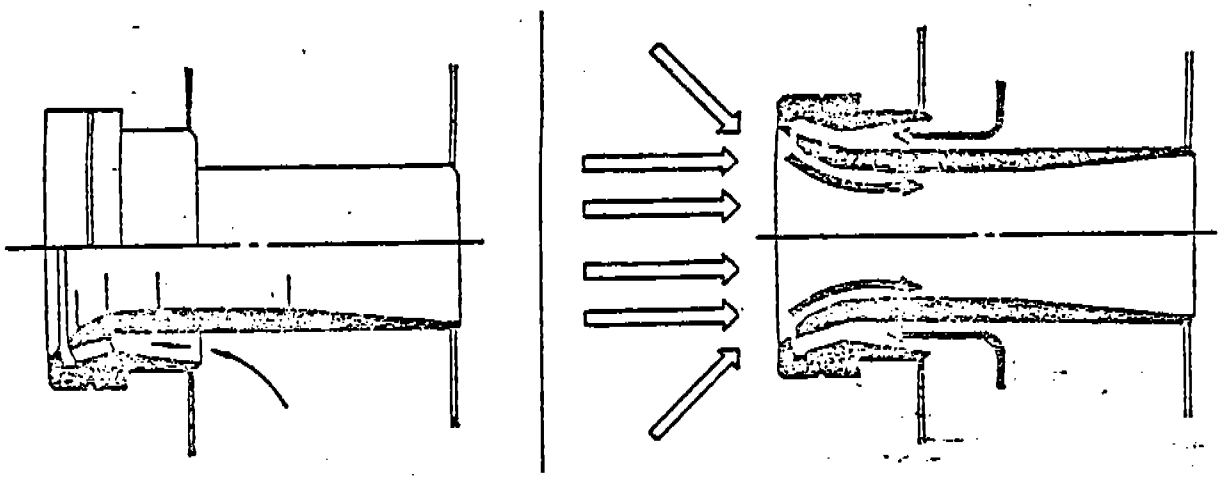

Fig. 5-3b. Section through a Flarejector© [74]

The pilot flame which was fed from a different gas network could be ignited with a Flare-Triboliter© (climbing flame ignition). During the tests, however, the pilot flame was usually lighted with a fuse since the Flare-Triboliter had to be supplied with combustion air from compressed air cylinders.

The experimental flare system was connected to the flare gas network of the OMW. To this end, the test flare gas line was tied into the flare gas network ahead of the water-trap of the main flare.

During the periods when the test flare was not burning, the test flare gas line was plugged off from the flare gas network by a contact disk.

In order to protect the flare gas line against backfire and the invasion of air during operation of the test flare,

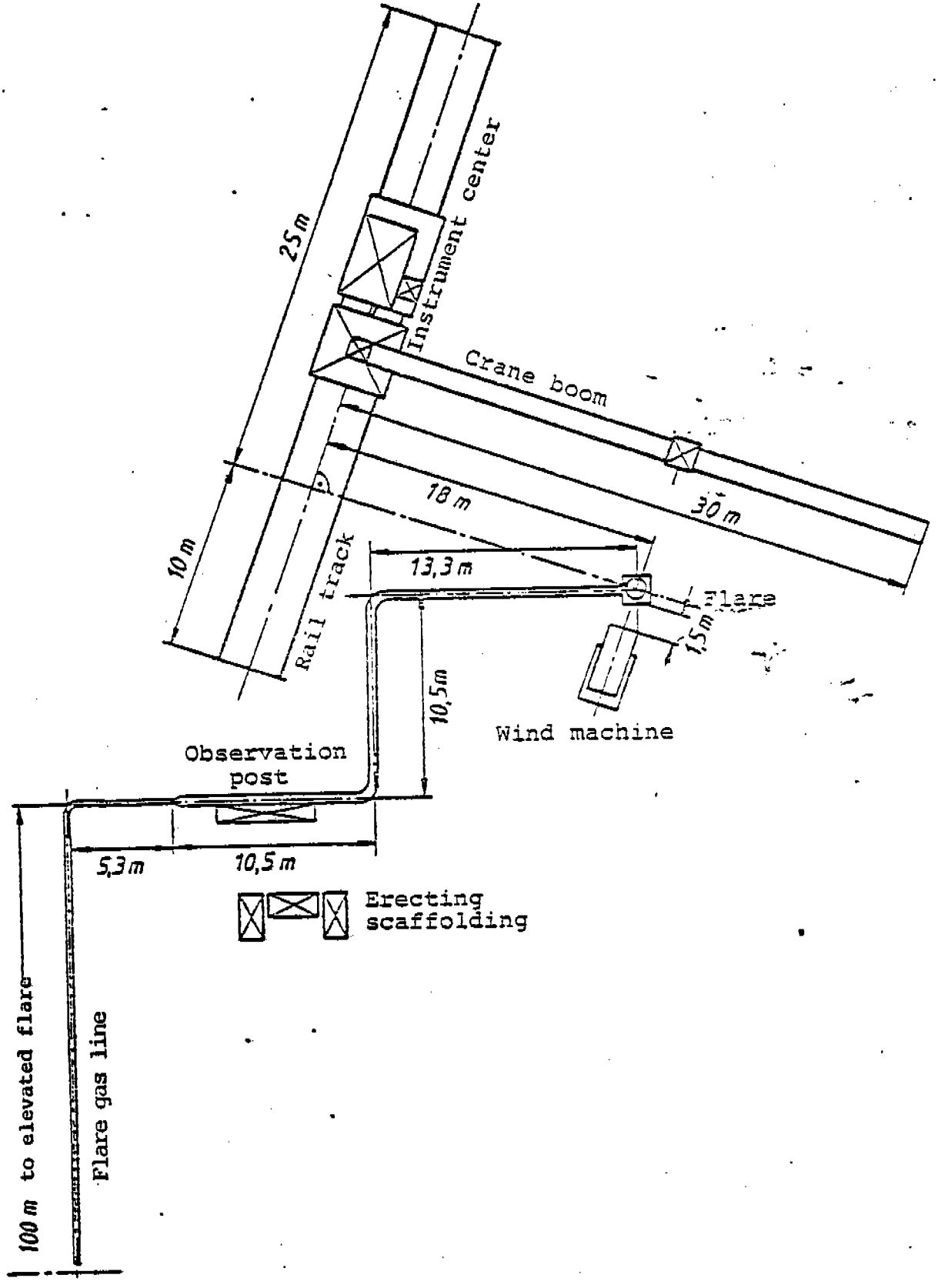

Fig. 5-2. Layout map of the testing arrangement

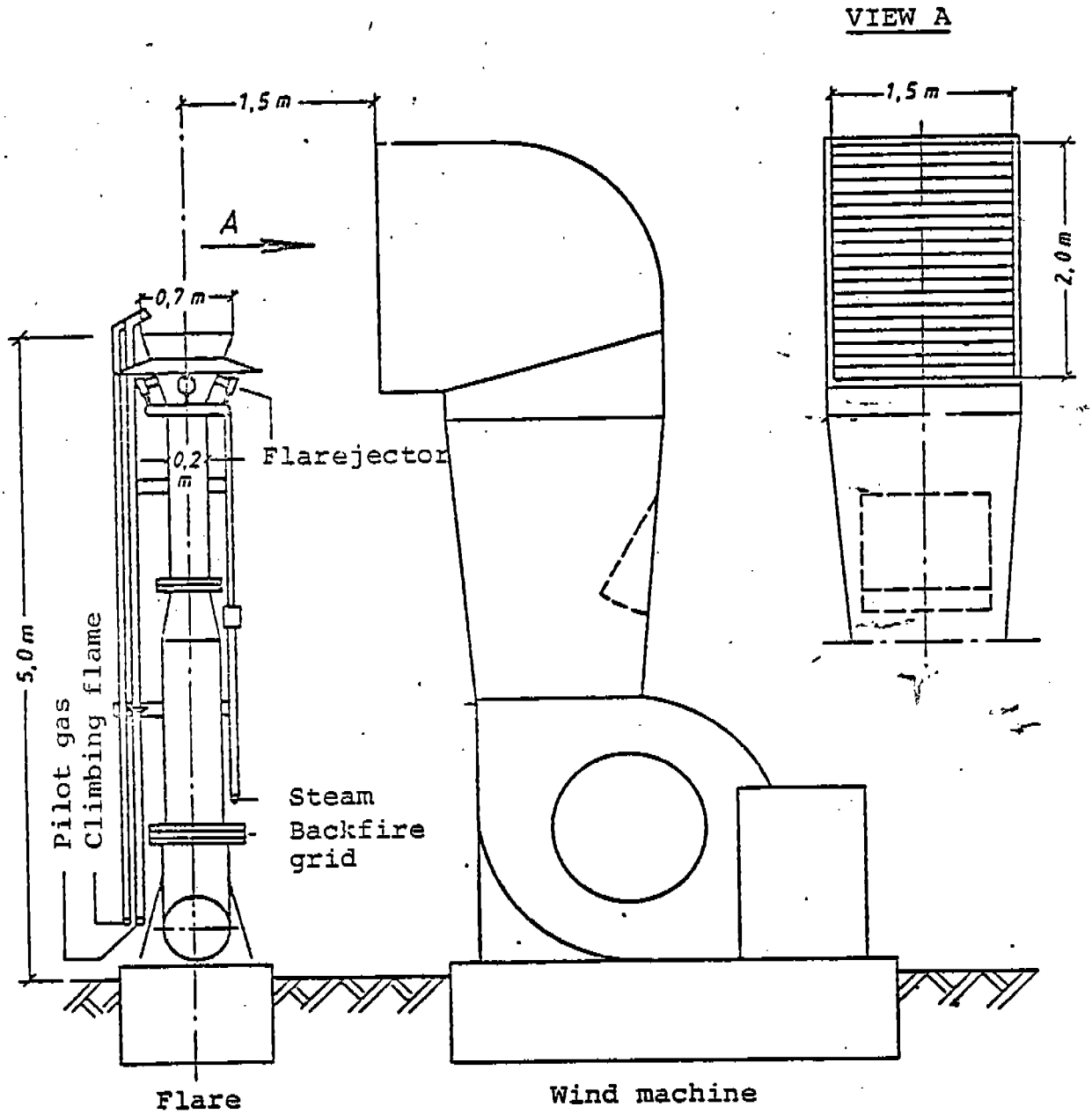

Fig. 5-3a. Test flare head and wind machine

a backfire grid was installed in the foot of the flare and a quick shut-off valve in the flare gas line. The quick shut-off valve closed automatically during operating troubles, for example, power failure, and opened via PCZ+ a steam barrier valve. The flare gas line downstream of the quick shut-off valve was then flushed with steam.

The flare gas mass flow was adjusted by way of the pressure in the main flare gas line and with the slide valve H 111. The intended regulation via the quick shut-off valve (in manual operation, a control valve) could not be realized. The poor control behavior of the valve led to a large pressure rise in the test flare gas line and to the rupture of the bursting disk in the main flare gas line.

The flare gas mass flow was measured with an AGAR flowmeter FM 700 (FQR 111). The meter was installed in the test flare gas line according to the installing instructions of the manufacturer. The flowmeter was, based on the cross section of the flare gas line at the point of installation, designed for a flare gas mass flow of up to 3.13 t/h in the measuring range 1 and of up to 8 t/h in the measuring range 2. The mass flow was determined by means of the calibration curve supplied with the instrument.

In a few tests, the flare gas mass flow was calculated from the gas velocity and the gas density. To this end, the dynamic pressure in the flare gas line was measured with a Prandtl Pitot-tube with an inclined-tube manometer (FI 111) and the static pressure with a Bourdon tube pressure gage. The flare

gas temperature was determined with a resistance thermometer PT-100 (TR 111).

The agreement between the two measuring methods was better than 10%, based on the value determined with the AGAR flowmeter. HABER reports the mean error of the AGAR flowmeter compared to the diaphragm at less than 1% [9].

For the analysis of the flare gases, samples were drawn at Q 111. The samples for the determination of the volume portions of hydrogen and hydrocarbons were taken with gas-collecting tubes which had first been filled with acidulated water.

In the gas-chromatographic analysis which was carried out in the laboratory, the components were identified via the retention times and quantified by a peak-area comparison with an external standard.

Hydrogen sulfide was determined titrimetrically according to the VDI Guideline 3486, Sheet 2. The analytical methods are described in Appendix 7.

The steam mass flow was adjusted by means of the slide valve H 121. The steam flow was measured with a standard diaphragm whose differential pressure was shown in a BARTON cell (FI 121) and recorded by hand. The diaphragm section had been laid out by OMW. The maximum measuring range amounted to 1.25 t steam/h.

For the wind simulation, a blower with an air capacity of 10^5 m^3/h was set up. The geometrical dimensions are shown in Fig. 5-3a. The delivered air volume flow could be controlled

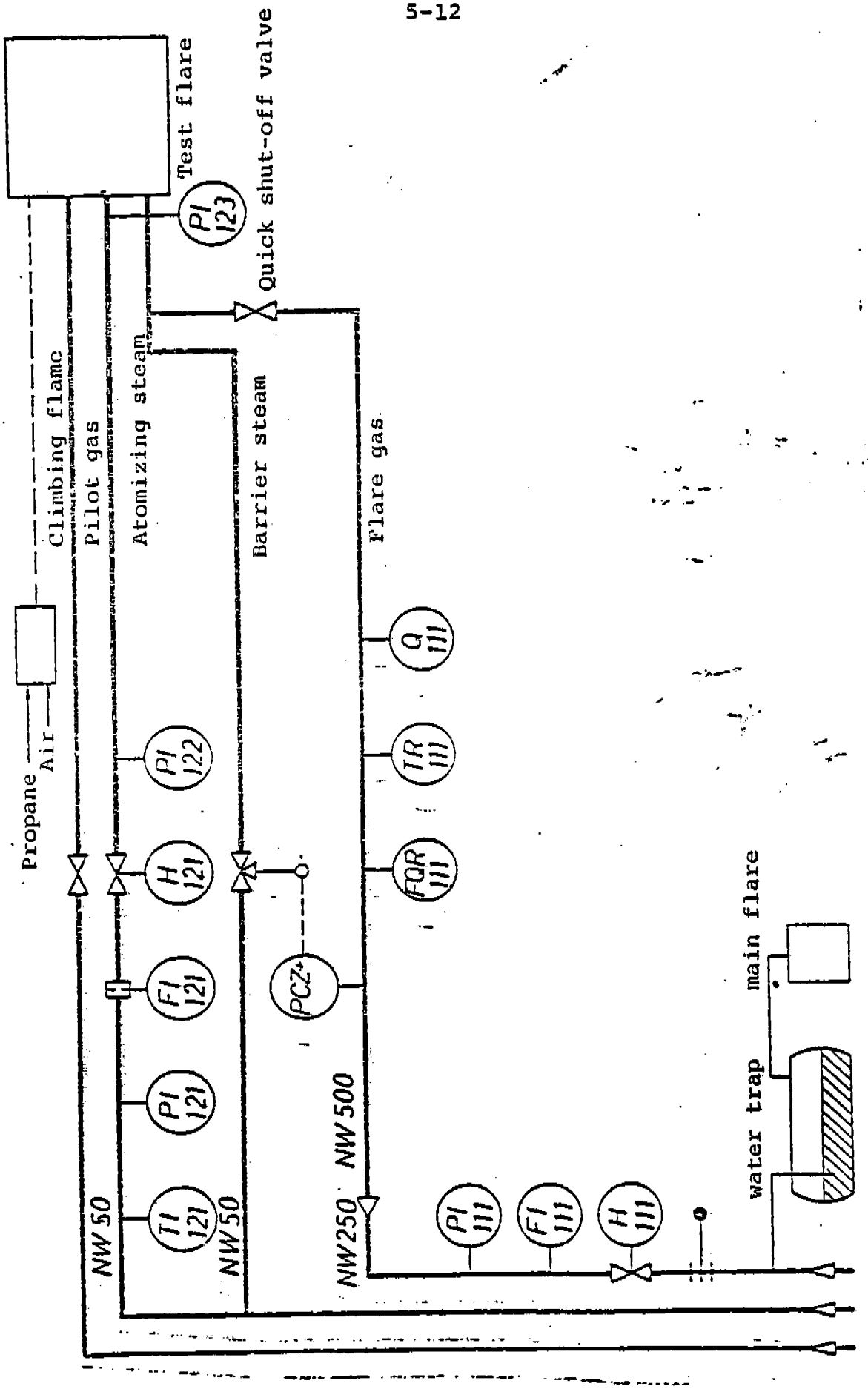

Fig. 5-4. Flow diagram of the experimental flare system

via a by-pass. The average air exit velocity was determined after the test.

To this end, the air velocity was measured for one minute with a fan-wheel anemometer at 20 points in the blower exit area which were spaced approx. 0.25 m horizontally and 0.5 m vertically. The arithmetic mean from the results of the spot measurements was taken as the mean air exit velocity.

The wind direction and the wind path were masured with a WOELFFLE recording anemometer and the air temperature and humidity were measured with an ASSMANN aspiration psychrometer at a height of 5 m above the ground.

5.3. Measuring Technique for Determining the Measuring Objects in the Off-Gas

5.3.1. Experimental Setup and Measuring Network

The experimental setup for taking samples at the end of the flame is shown schematically in Fig. 5-5.

For the sample-taking, a travelling hoisting crane on a rail-track 35 m in length was provided. The maximum hook-height of the crane could be increased from 8 m to 12.5 and 17 m above the flare mouth by the insertion of tower sections. The boom had a length of 30 m. The crane operator's cabin was installed next to the instrument center.

In order to be able to guide and to position the probes at will, the trolley was rebuilt in such a way that the steel plate could be moved vertically by means of the hoisting cable. The steel plate was supported and guided by 4 pipes 8 m in length which were in their turn guided by way of rollers at the trolley. The free height of lift of the steel plate was

5 m. The cage formed by the steel plate and the 4 pipes was on all 4 sides insulated with aluminum sheet/rock wool/aluminum sheet up to a height of 1 m.

In order to be able to rotate the measuring probes horizontally, a supporting device for a gear motor was mounted on two pipes. The rotary motion of the motor (turning speed 120°/mm) was transmitted via a spur gear and sprocket wheel to a shaft which projected 1 m from the steel plate. The gear motor was controlled from the crane operator's cabin. The turning range was 180°. Since the motor had been installed in the hot region, it was cooled with forced air. Upon overheating (80°C), the motor was turned off by a built-in thermostatic overload protector; at the same time, an acoustic signal was activated in the crane operator's cabin.

The probe holder 1 was flanged to the lower end of the shaft. The probe holder was 5 m long and 2 m high. At a maximum hook height of 8 m, samples could be drawn at levels between 0 and 5 m above the flare mouth.

The probe holder 2 had a length of 8 m and could be adjusted vertically by hand in meter distances between 0 and 3 m with reference to the lower edge of the steel plate via a swivel joint screwed to the steel plate. The sampling height could thus be chosen between 0 and 8 m above the flare mouth.

The incoming and outgoing supply- and measuring lines along the crane boom were laid for the first 5 m from the trolley in a cable conduit and from there on via 4 line carriages. Along the crane tower, the lines were braced on a wire rope.

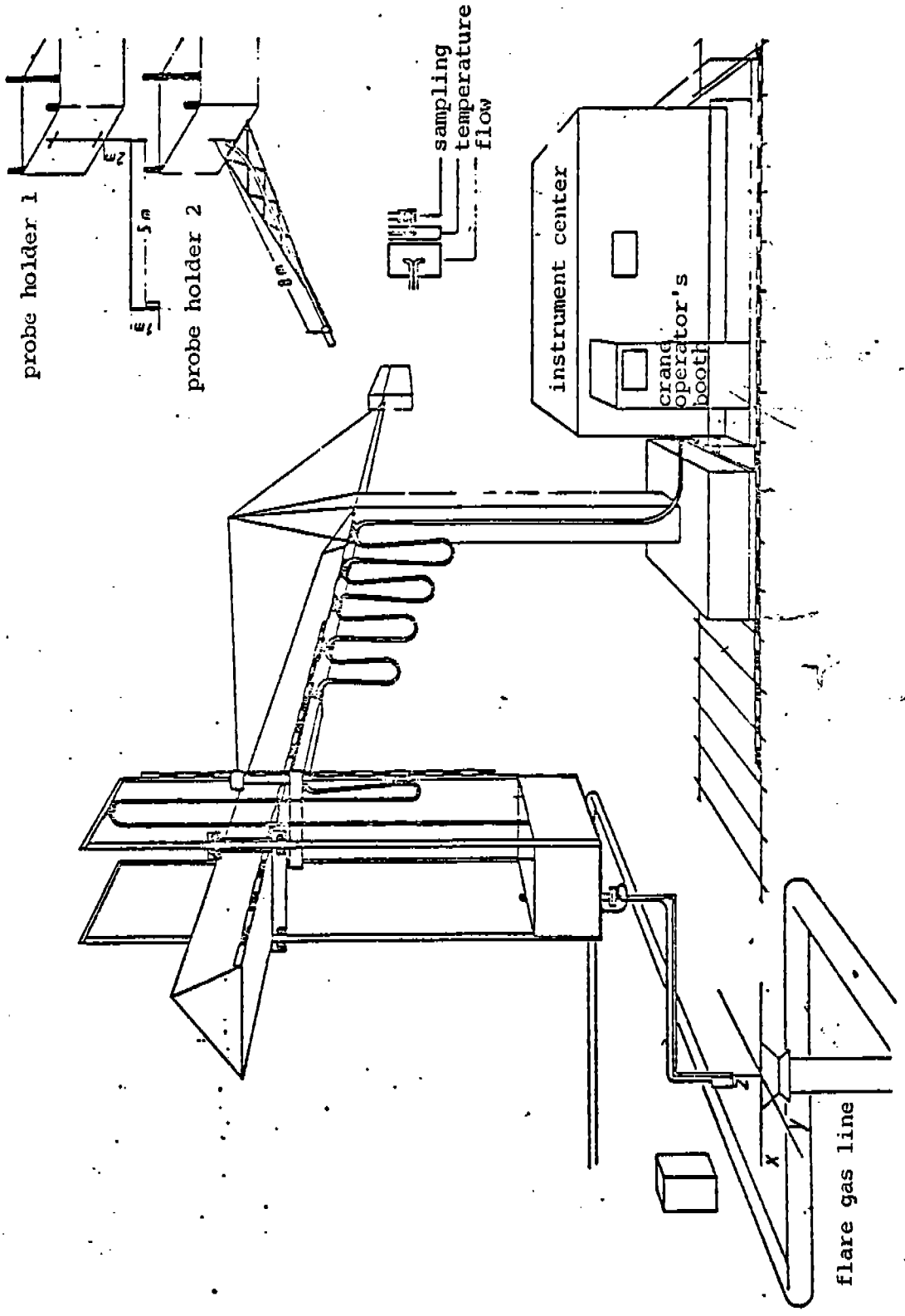

Fig. 5-5. Experimental setup for taking samples at the end of the flame.

The electrical supply lines were silicone-insulated, the leads for the thermocoupler were teflon-insulated. The maximum permissible ambient temperature amounted to 180°C.

The surface temperature of the shaft and the ambient temperature in front of the steel plate was monitored with thermocouples (chromel/alumel) and recorded in the crane operator's cabin with a 2-channel potentiometric recorder (200°C ≙ 100 sct).

The instrument center was mounted on a travelling rail car coupled to the crane. The instrument center housed the sample gas preparation, the analytical instruments, potentiometric recorders and the supply gases.

For the fixation of the measuring points, a horizontal grid system was adopted for the field surrounding the flare head. The spacing of the grid lines was 50 cm. The measuring points were situated at the points of intersection of the grid lines, with one point of intersection placed at the center of the flare head. The measuring height was related to the flare head mouth.

The approach to a measuring point was guided by color markings at 0.25 m distances on the rail track, the crane boom and on one of the pipes between the cage and the crane trolley. The meter markings were provided with numbers. The correlation between measuring point and marker value for the different probe positions was determined by plumbing the sampling orifice on the center of the flare head. For the setting of the crane boom at right angles to the rail track a marker was provided on the turntable. The space coordinate parallel to the crane

track was designated x, the one at right angles to it y, and the height z. The origin of the coordinates lay at the center of the flare mouth.

In the initial tests, the position reached via the markings was measured in addition with 2 theodolites. The discrepancies between the positions reached via the markings and those calculated goniometrically were on the average less than ±5 cm so that after three trials the theodolite measurements were dispensed with.

5.3.2. Sampling, Gas Analysis and Calibration of the Gas Analyzers

The flow diagram for the taking of samples at the end of the flame is shown in Fig. 5-6.

The off-gas to be analyzed was aspirated at Q 200 by way of an alloy steel probe (S 210) ($\emptyset_i$ = 14 mm). The sampling gas inlet was expanded to 30 mm and filled over a length of 5 cm with quartz wool in order to separate any soot (A 210). In order to keep the quartz wool from being sucked into the sampling gas line an alloy steel screen was inserted at the point of reduction. The transition from the alloy steel line to the flexible heatable teflon line (S 211 to S 213) occurred in the case of the probe holder 1 underneath the steel plate and in the case of probe holder 2 in the cage. S 211 was 10 m in length and S 212 and S 213, 40 m each.

The sampling probe was not cooled since during sampling the sampling gas was cooled more rapidly than if it had remained in the off-gas stream. In addition, for the determination of the

degree of conversion the samples had to be drawn in a temperature region in which, had they remained in the off-gas stream, a further reaction would not have been likely.

The gas to be analyzed was aspirated with blower P 210 which under the testing conditons transported a volume flow of 60 l/min.

The temperature of the sampling gas in the sampling line was measured at TR 210 to TR 213 with thermocouples (chromel/alumel). During the tests, the temperature of the sampling gas at TR 210 ranged between 60 and 100°C. At TR 211 to TR 213 this temperature was raised to between 120 and 140°C by TRC 211 to TRC 213 (temperature of the teflon wall, installed by the plant engineers for controlling the heating).

Before entering the blower P 210, the sampling gas passed through the quartz wool filter A 211 which was heated to 130°C. The filter housing was made of glass. Its length was 10 cm and its diameter 2.5 cm. On the pressure side of the blower, the sampling gas stream was divided.

One partial gas stream of 9 l/m corresponding to an approach velocity of 6 m/s passed over the sensor of the dew-point hygrometer (QR 216). The partial gas stream was adjusted with the hose clamp H 216 and monitored with the flowmeter FI 216. In accordance with the manufacturer's recommendations, the sensor was mounted inside a cylinder which was thermostated with water at a temperature of 40°C.

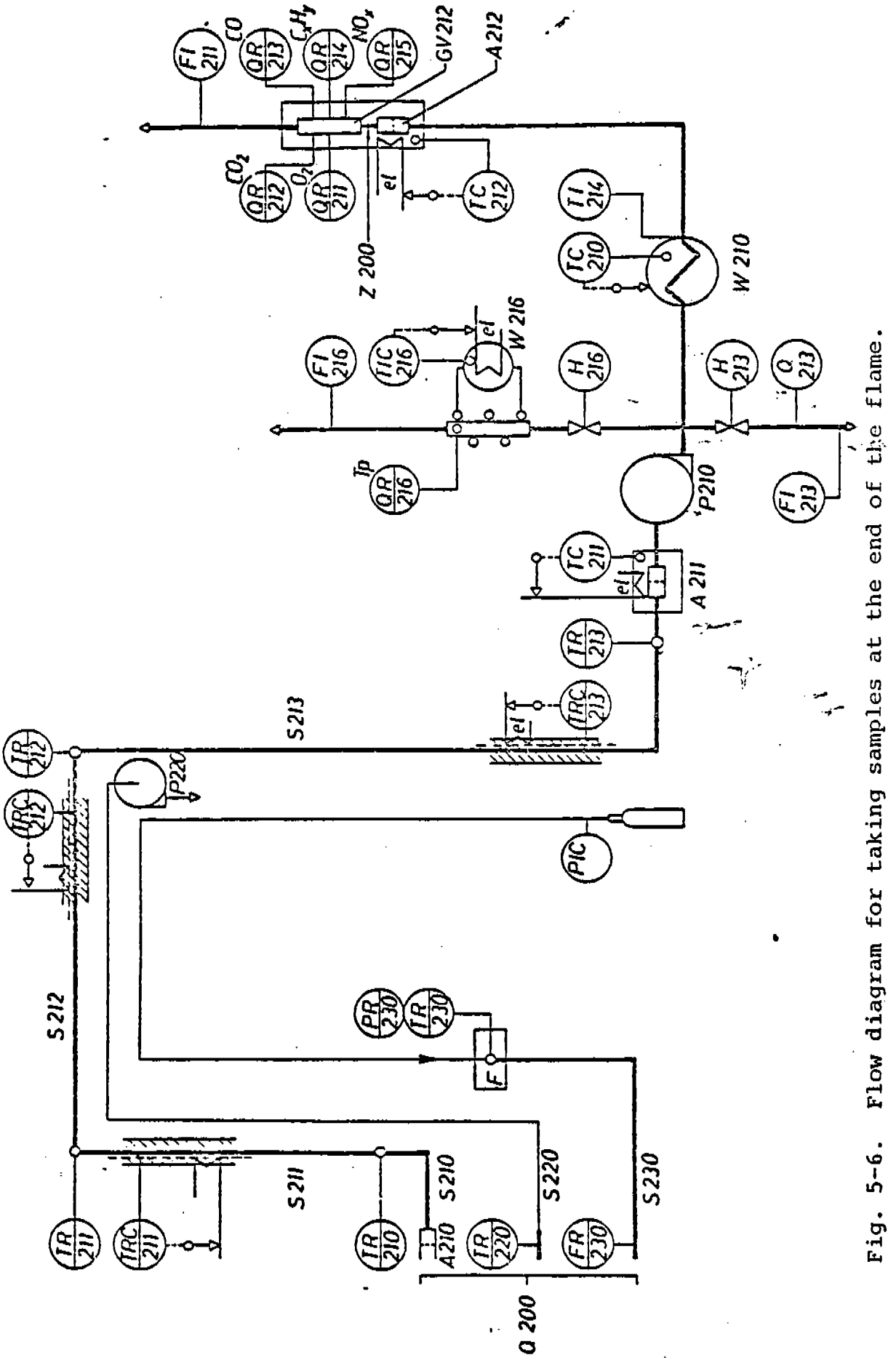

Fig. 5-6. Flow diagram for taking samples at the end of the flame.

Another partial gas stream of 10 l/min was dehydrated to a dew point of 10°C in the measuring gas cooler W 210; the remaining residual gas stream was vented into the atmosphere via the water trap FI 213.

In the dehydrated measuring gas stream, after its passage through the quartz glass A 212 and the measuring gas distributor GV 212, the following measuring objects were determined with continuously recording gas analyzers:

Oxygen (QR 211)

Carbon dioxide (QR 212)

Carbon monoxide (QR 213)

Sum total of ionizable organic compounds (QR 214)

Sum total of nitrogen monoxide and nitrogen dioxide (QR 215)

The measuring gas flow not needed for the gas analysis was vented into the atmosphere via the water trap FI 211.

Filter housing A 212 consisted of glass. Its length amounted to 5 cm and its diameter to 2.5 cm. The gas distributor was made of teflon. It had a length of 10 cm and a diameter of 2.5 cm. The exit ports to the autosuctioning gas analyzers were set into the cylinder jacket. The filter housing and the sampling gas distributor were thermostated at 80°C.

The gas analyzers with the measuring-object-specific sampling gas preparations were housed in an analytical cabinet. The sample gas lines between the gas distributor and the analyzers were made of teflon ($\emptyset_i$ = 4 mm). The flow diagram of the gas analysis downstream of the measuring gas distributor GV 212 is shown in Appendix 9. The measuring principles and the measuring

ranges of the gas analyzers, together with the test gases used for their calibration are listed in Table 5-1.

The gas analyzers were calibrated before, during and after the tests with test gases from compressed gas cylinders. To this end the test gases were switched via solenoid valves into the system upstream of the measuring-object-specific sampling gas preparations. The test gases were always supplied in excess and the residual gas stream which was not needed was discharged into the atmosphere via a water trap. The test gases with analysis certificate were obtained partly from Messer Griesheim and partly from L'Air Liquide.

Individual organic components in the off-gas were determined by spot tests. For this purpose, gas samples were drawn at Q 213 with evacuated gas-collecting tubes. These samples were analyzed by gas chromatography (cf. Appendix 7).

The soot content of the off-gas was determined at Q 200 with a STROEHLEIN type head filter probe. As the filtering medium, glass-fiber cartridges were used whose specifications together with their preparation are described in Appendix 7.

The off-gas temperature at Q 200 was measured with a suction-thermocouple (TR 220) (chromel/alumel). The gas flow velocity at the thermocouple was 7 m/s. The suction blower P 220 was installed in the crane tower. The reference junction was kept in ice water.

The off-gas velocity at Q 200 was determined with a "Stack-Gas-Velocity-Meter", Model EGSM-1 D 5 KX of the Teledyne Hastings-Raydist Co. (FR 230). The measuring principle is a combination

Table 5-1. Gas analyzers used in the test for analyzing the off-gas components.

Measuring object	Measuring variable	Measuring value	Measuring ranges		Test gases used for calibration		Manufacturer Type
				χ in %		χ in %	
Sum total of ionizable organic compounds	Variation of the electrical conductivity of a hydrogen flame due to ionization of organic compounds	χ_{CH_4}	1	$0\text{-}10^{-3}$			
			2	$0\text{-}10^{-2}$	C_3H_8 in air	$30 \cdot 10^{-4}$	IPM/RS 5
			3	$0\text{-}10^{-1}$			
			4	0-1	C_3H_8 in air	0.3	IMP/RS 5
CO	Absorption of IR radiation	χ_{CO}	1	0-1	CO in N_2	0.7	
			2	0-10	CO in N_2	4.0	Maihak/ Unor 5 N
CO_2		χ_{CO_2}	1	0-10	CO_2 in N_2	4.0	
O_2	Pressure differential during joint conduction of two gases with different O_2-content in a magnetic field.	χ_{O_2}	1	0-10	O_2 in N_2	0.0	Siemens Oxymat 2
			2	0-21	O_2 in N_2	14.0	
$NO + NO_2$ NO_x	Light emission by the reaction $NO + O_3 \rightarrow NO_2 + O_2 + h \cdot \nu$ (chemiluminescence)	χ_{NO_x}	1	$0\text{-}10 \cdot 10^{-4}$			Thermo Elektron 10 A
			2	$0\text{-}25 \cdot 10^{-4}$			
			3	$0\text{-}10 \cdot 10^{-3}$	NO in N_2	$80 \cdot 10^{-4}$	
			4	$0\text{-}25 \cdot 10^{-3}$	NO in N_2	$105 \cdot 10^{-4}$	
H_2O	Capacitance change during dew formation on measuring receiver	Dew point	1	-15° - $35^{\circ}C$	Endress and Hauser/ hygrometer system-recorder		
			2	35° - $135^{\circ}C$			

of Pitot tube and hot-wire anemometer. Under calibration conditions, the measuring range extended to 8 m/s (cf. Appendix 8). The flow probe (S-tube) was mounted inside a flow tube 13 cm in diameter and 30 cm in length. The flow tube could be aligned manually in the main flow direction. The flow probe and the measuring bridge were connected by 2 alloy steel tubes ($\emptyset_i$ = 8 mm). In the case of the probe holder 1, the flexible transition below the cage was made of teflon. The measuring bridge was housed in a sheet metal box in the cage. The pressure (PR 230) and the temperature (TR 230) were measured at the inlet to the measuring bridge.

5.3.3. Calibration of the Measuring System

For the calibration of the thermocouple TR 220, the solidification curves of antimony (630.5°C), zinc (419.6°C), lead (327.4°C) and tin (231.9°C) were recorded. An additional calibration point was determined by the boiling temperature of water. At the reference junction, ice water was used. The measuring value for 700°C was set at 100 scale divisions on the potentiometric recorder.

The calibration curves for the thermocoupler TR 210 to TR 213 were determined by the temperatures of ice water and boiling water.

The arrangement for measuring the flow velocity was calibrated volumetrically. To this end, the flow tube was lengthened upstream by 1 m and air from a blower was made to flow through it. The air volume was measured with a gas volume counter and the time was determined with a stopwatch. The velocity was

calculated from the air volume flow and the cross section of the flow tube. Good agreement could be noted between the calibration curve determined in this manner and the calibration curve of the manufacturer.

The gas metering arrangement was calibrated with test gas mixtures which were prepared dynamically. To this end, a constant flow of the measuring object was produced by way of microdiaphragms and injected into a constant flow of carrier gas. As the measuring objects we used carbon dioxide, ethene and propene and as the carrier gas, synthetic air. The specified volume concentration for carbon dioxide was 99.9%, for ethene 99.7% and for propene 99%. A change in concentration was brought about by varying the pressure of the measuring object upstream of the diaphragm, the diameter of the diaphragm orifice and the flow of the carrier gas.

The test gases prepared in this manner were introduced at Q 200 and Z 200 and fed into the gas analyzers. The test gas was always prepared in excess and the residual gas stream was discharged into the atmosphere via a water trap.

In Fig. 5-7, the test values of the gas analyzers after the introduction of the test material at Q 200 has been plotted against the corresponding values obtained after the introduction at Z 200. It can be seen that the measured values are in good agreement so that any adsorption in the sampling gas line can be neglected.

In order to be able to make a statement as to how the nearly 100 m long sampling line may affect the measurement of organically bound carbon at QR 214 compared to a direct

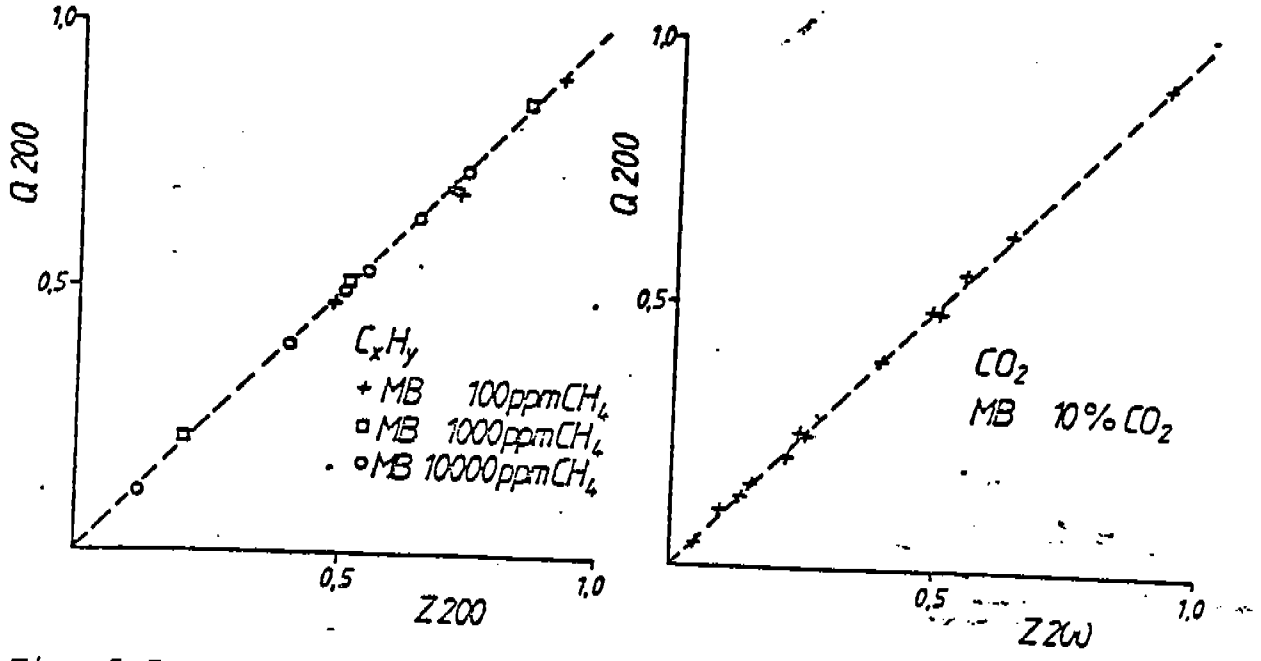

Fig. 5-7. Comparison of the test values of the gas analyzers for carbon dioxide and organically bound carbon with the measuring object being introduced at the sampling orifice and at the sampling gas distributor.

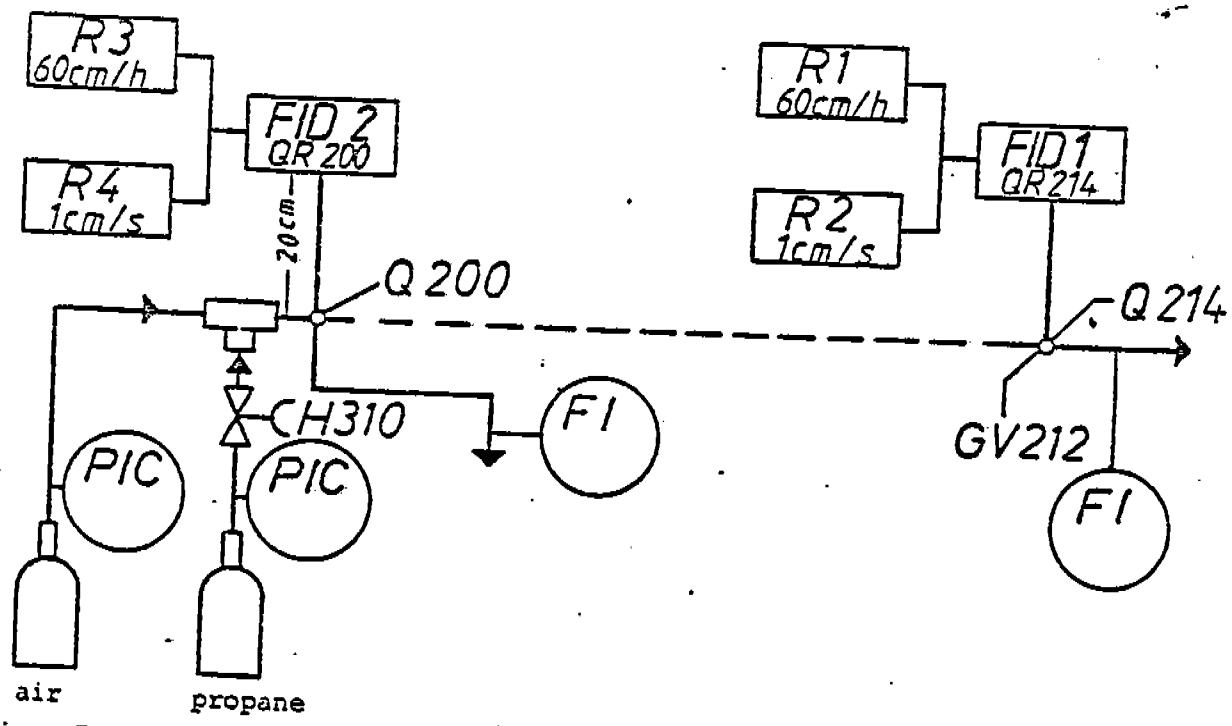

Fig. 5-8. Flow diagram for the testing arrangement for determining the behavior in time of the sample gas line.

measurement at QR 200, we studied the behavior in time of the measuring arrangement.

The testing arrangement is sketched in Fig. 5-8.

In the carrier flow of synthetic air, propane was apportioned via the rocker-arm valve H 310. The concentration of organically bound carbon in the test material was measured at Q 200 with the FID 2 whose sample gas line was 20 cm long and at Q 124 with the FID 1 which was reached after traversing a sample gas line approximately 100 m in length.

The FID 2 had first been matched with the FID 1, that is, with the same length of sampling line, the same output signal was obtained for the same input signal. The test data were recorded on 2 potentiometric line recorders each of whose chart speed amounted to 60 cm/h and 1 cm/s, resp. In the following, the signal of the FID 2 was adopted as the input signal at Q 200. At first, different concentrations of propane were introduced at Q 200 in the manner of a jump function. A jump function means the following:

At a point in time t=0, the concentration of a marker substance jumps from zero to the value ρ_i^{in} and retains this value for all times t>0.

The measuring signal at QR 124 always attained the value at QR 200. The 90%-dead time which is here defined as the time difference between the 90%-value at QR 200 and that at QR 214 was found to be t = 20 s.

Because of the large fluctuations in flames, a concentration change at Q 200 is approximated by a needle-point function

rather than by a jump function. In the case of an input signal according to a needle-point function, at the time t = 0 a specified amount of a marker substance is introduced into the test material in the shortest possible time Δt_0.

When the marker substance is introduced in the manner of a needle-point function, the quantity m_i is found to be:

$$m_i^{in} = \varrho_i^{in} \cdot \dot{V} \cdot \Delta t_o \qquad \text{G 5-1}$$

The quantity charged must after an infinitely long time have again left the sampling line so that the amount added can be determined from G 5-2:

$$m_i^{in} = \dot{V} \int_0^{\infty} \varrho_i^{out} \, dt \qquad \text{G 5-2}$$

The volume which at Q 200 was sucked into the sample gas line amounted to 1 l/s.

In order to approximate a needle-point function, the time span (jump duration) during which the valve H 310 was open was varied between 5 seconds and 1 second. The amount of organically bound carbon which was introduced at Q 200 and received at Q 214 was determined by graphic integration of the area underneath the input and output signal (R2 and R4), resp. The limits of integration were given by the departure of the measuring signal from the zero line. The results have been summarized in Table 5-2.

Column 1 shows the test value which would have resulted if the marker substance had been added in the manner of a jump function. Column 2 shows the duration of the jump. Column 3

shows the quotient formed from the amount detected at Q 214 and the amount added at Q 200. Column 4 shows the same for the maximum deflection of the recorders R1 and R3.

Table 5-2. Comparison between added (Q 200) and detected (Q 214) amount of organically bound carbon.

$\chi^{max}_{CH_4}$	t	$\frac{m_{Q214}}{m_{Q200}}$	$\frac{h^{max}_{Q214}}{h^{max}_{Q200}}$	$\chi^{max}_{CH_4}$	t	$\frac{m_{Q214}}{m_{Q200}}$	$\frac{h^{max}_{Q214}}{h^{max}_{Q200}}$
ppm	s			ppm	s		
2100	5	1,10	1,00	880	2	1,00	0,74
	3	1,10	0,87		1	1,01	0,55
	2	1,06	0,79	75	5	1,03	0,99
	1	1,09	0,50		3	1,07	0,94
880	5	1,00	0,95		2	1,05	0,82
	3	0,96	0,88		1	1,05	0,63

The quotient in Column 3 is close to 1 irrespective of the amount added. This proves that no loss of volume has occurred as a result of the long sampling line. The quantitative determination must, however, be done planimetrically because, as shown in Column 4, the analysis of the height produces errors of up to 50%. The quotient in Column 3 happens to be for the most part larger than 1. During the attenuation of the measuring signal when the latter approached the zero line asymptomatically, the difference between the two was small so that an accurate

planimetration was no longer possible.

It is also important to know what amount of organically bound carbon must be drawn in at Q 200 in order to be still recognized at Q 214 (R1). In order to determine this amount, the duration of the jump - at different concentrations - was shortened to intervals of less than 1 second. The amount added was determined from the area underneath the output signal at Q 214 (R2).

In Fig. 5-9, the maximum deflection of the recorder 1 has been plotted against the amount of organically bound carbon, added at Q 200. The parameter is the measuring range of the FID 1 which was 10 and 100 ppm, resp.

Recorder R1 had a recording width of 25 cm which corresponded to 100 scale divisions. The background noise in both measuring regions was less than 1 scale division so that a deflection at R1 of 2.5 scale divisions could be recognized as a test value. The amount of organically bound carbon which must be aspirated at QR 200 in order to produce a deflection at QR 214 can be determined from the point of intersection of the compensating straight line with the ordinate value of 2.5 scale divisions. It amounted to 1.5 mg C for the 10 ppm methane and to 8 mg C for the 100 ppm methane measuring range.

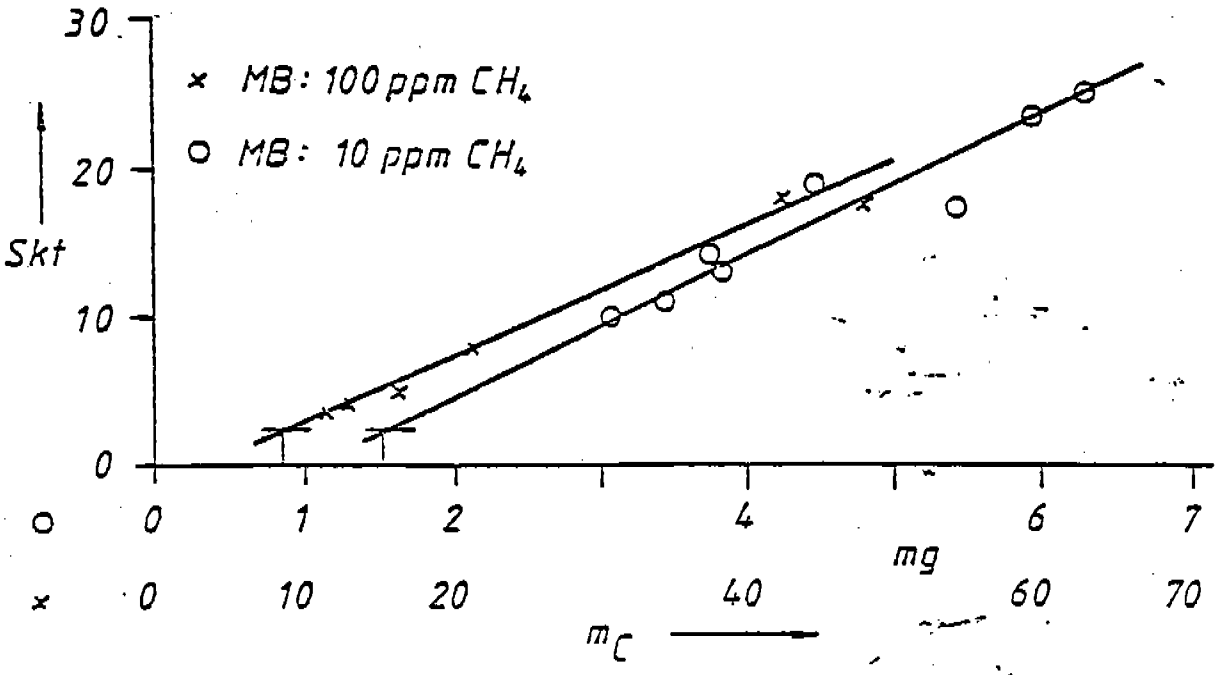

Fig. 5-9. Maximum test value as a function of the aspirated amount of organically bound carbon.

5.4. General Data on Experimental Procedures and Evaluation of Recording Charts

Prior to the beginning of the tests, the test flare system was flushed for ca. 12 hours with inert gas and cleared for testing only when the oxygen volume portion in the test-flare gas-line was smaller than 1.5%. After igniting the pilot flame, the disk plug was pulled and flare gas was called in.

The measuring system was turned on about 2 hours before the tests were started so that steady conditions existed when the measurements were begun. In order to test the tightness of the gas sampling line, the line was sealed off at Q 200 and the volume flow delivered by the blower P 210 was checked on the pressure side with a gas volumeter for steadiness.

The measuring points were found with the aid of the markings. The measuring height was in most instances adjusted in accordance with the end of the flame which was determined by observation from the crane tower. The measuring time - as a rule 3 minutes per measuring point - was noted on the temperature recording chart with an event-marker giving the number of the measuring point, the measuring height and the pressure reading of the BARTON-cell. The clock time was marked on all the recording charts and recorded at irregular intervals. The chart speed in all the potentiometric recorders was 60 cm/h.

The communication between the instrument center, the crane operator's cabin and the metering point at the flare gas input line was by two-way telephone and communication with

6. EXPERIMENTAL RESULTS AND DISCUSSION

In the following sections, the experimental results are frequently presented in exemplary form in figures and tables. The measured data are listed in Appendix 1 which is divided into Sheet 1, 2 and 3.

Sheet 1 contains first the day of the test, with the test days being numbered consecutively. On the left side of the sheet the flare gas is described in terms of the volume portions of the flare gas components. The standard density, mean molecular weight and the carbon- and hydrogen-portions of the flare gas are listed on the right side.

Sheet 2 contains the flare gas- and steam mass-flow and the values measured at the point of sampling in tabular form.

On Line 1, the measuring point is marked by the serial number between the event-markings (cf. Section 5.4).

The Lines 2 to 4 contain the flare-gas flow $\dot{m}_G$, the steam mass flow $\dot{m}_D$ and the steam/gas ratio $\Psi_{D,G}$ in kg steam per kg flare gas. The space coordinates x, y and z of the measuring point have been entered on the Lines 5 to 7. The origin of the coordinates is the center of the circular exit area of the flare head. On the Lines 2 to 7, a value is shown only when the latter has changed in relation to the value shown in the preceding column. The Lines 8 to 15 describe the combustion off-gas. The off-gas composition is listed on the lines 8 to 12. The volume portions of the measuring objects,

oxygen, carbon dioxide, carbon monoxide, organically bound carbon (reported as methane) and nitrogen oxides (reported as nitrogen monoxide) relate to test material dehydrated to a dew point of 10°C. The volume portion of nitrogen is not shown. In calculating the latter, it is necessary to consider that in accordance with the adjusted dew point the volume portion of water in the test material amounted to 1.2%. The dew point of the off-gas is shown on Line 13, the off-gas temperature on Line 14 and the flow velocity--based on the calibration conditions (Appendix B)--on Line 15. In the case of flames burning in a cross-flow, the flow velocities were not measured so that for these tests no value is reported on Line 15.

On Sheet 3 are listed the components of the organically bound carbon in the off-gas.

6.1. Description of the Flare Flame as a Tubular Reactor and Definition of the Degree of Conversion and of the Emission Factor for Nonatmospheric Gases

In the waste-gas combustion, the aim is a complete oxidation of the combustible flare-gas components. The desired reactions can be described summarily by the reaction equations R 6-1 to R 6-5:

$$C_mH_n + \left(\frac{m}{2} + \frac{n}{4}\right) O_2 \longrightarrow mCO + \frac{n}{2} H_2O \qquad \text{R 6-1,}$$

$$CO + \frac{1}{2} O_2 \longrightarrow CO_2 \qquad \text{R 6-2,}$$

$$C + O_2 \longrightarrow CO_2 \qquad \text{R 6-3,}$$

$$H_2 + \frac{1}{2} O_2 \longrightarrow H_2O \qquad \text{R 6-4,}$$

$$H_2S + \frac{3}{2} O_2 \longrightarrow SO_2 + H_2O \qquad \text{R 6-5.}$$

An undesirable side reaction is the formation of nitrogen oxides by the fixation of atmospheric nitrogen according to

$$N_2 + O_2 \longrightarrow 2NO \qquad R\ 4\text{-}17.$$

As described in Sect. 4.1, the processes are in reality much more complicated because, owing to the temperatures in flames, radicals are involved in the reactions.

In the combustion of hydrocarbons, intermediate products in the form of hydrogen, carbon monoxide, aldehydes as well as unsaturated hydrocarbons and, particularly, acetylenes occur. Acetylenes are capable of binding hydrocarbon radicals. In this process new radicals are formed and ultimately - via the polyacetylenes and cyclic compounds - soot particles.

For the calculation of the degree of conversion from the measured data the flare flame is considered as tubular reactor with a steady mode of operation (Fig. 6-1). The reaction space - the flame - is geometrically described by a truncated cone. The reaction partners contained in the flare gas enter through the flare tube into the reaction space. The reaction partner atmospheric oxygen is in part admixed at the reactor entrance and in part aspirated via the lateral surface of the reactor (jacket of the truncated cone). In the reactions are formed both the desired reaction products carbon dioxide and water as well as relatively stable but undesirable intermediate products such as carbon monoxide, hydrocarbons, oxygen-

containing hydrocarbon compounds, hydrogen and soot. The latter may be reacted further to carbon dioxide and water or else be discharged from the reactor as undesirable reaction products. This means that the discharge flowing out of the reactor is a mixture consisting of the reaction products and unreacted reaction partners. The composition of the reaction mass, as well as its temperature and flow velocity, varies from place to place. The differences exist both in the axial as well as radial direction.

Of the components of the reaction mass, carbon monoxide, organically bound carbon and soot are classified as environmental pollutants. They are in the following also referred to as "non-atmospheric gases". Furthermore, the term "organically bound carbon" stands for the carbon present in the form of organic compounds which can be ionized in a hydrogen flame. Considered as unreacted is carbon which is present at the reactor exit bound as carbon monoxide, organically bound or as soot. On the assumption that the flare gas is free of carbon monoxide, which was the case with the flare gases used in the tests, the degree of conversion can be calculated according to Equation G 6-1:

$$U = \frac{\dot{m}_C^{ein}(C_mH_n) - \dot{m}_C^{aus}(C_xH_y, CO, Ruß)}{\dot{m}_C^{ein}(C_mH_n)} \qquad G\ 6\text{-}1.$$

For the organically bound carbon at the reactor entrance, the designation C (C_mH_n) was chosen since at that point the individual components are known from the flare gas analysis. At the reactor exit, however, the organically bound carbon was measured as a sum, for the most part without knowing the individual components. For this reason, the organically bound carbon at the reactor exit has been designated by $C(C_xH_y)$. For calculations, it is necessary, on the basis of the calibration, to equate C_xH_y with CH_4.

The carbon bound as carbon monoxide or carbon dioxide has been designated by C(CO) and $C(CO_2)$, respectively.

Since it was impossible to measure the mass concentration of the soot continuously, it is impossible to calculate its mass flow like that of the gaseous components. For this reason, the following restrictions become necessary:

- A prediction concerning the degree of conversion of flare gas in the combustion in elevated flares is possible only in the case of soot-free flames.
- In the case of sooty flames, only the indication of the emission for gases extraneous to air - in the following usually designated only as emission factor - is possible.

The emission factor E_{ga} is defined by Equation G6-2:

$$E_{ga} = \frac{\dot{m}_C^{aus}(CO, C_xH_y)}{\dot{m}_C^{ein}(C_mH_n)} \qquad \text{G 6-2.}$$

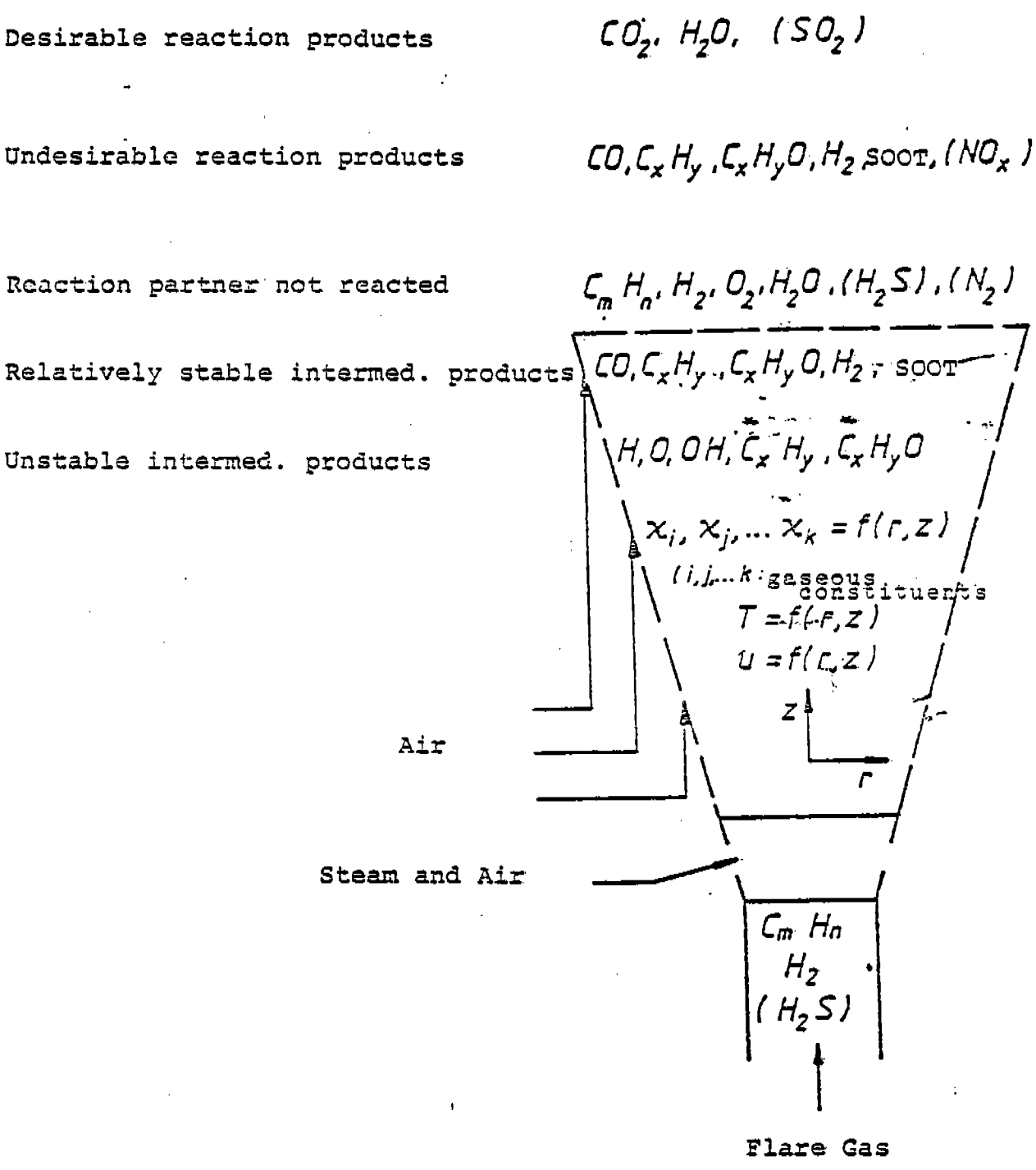

Fig. 6-1: Flare flame as a tubular reactor (schematic)

6.2. Degree of Conversion in Soot-Free Flare Flames in the Absence of Wind

Emission Factor of Sooty Flare Flames in the Absence of Wind

The determination of the degree of conversion and of the emission factor requires a steady mode of operation of the flame. The angle between the flame- and the flare-head axis is greatly affected by the wind. The wind, however, is subject to strong and short-term fluctuations with respect to direction as well as to velocity. A steady mode of operation is, therefore, most likely to exist in calm weather. In the following, calmness means wind velocities up to 1m/s. Furthermore, when there is a wind - also referred to as a cross draft - the exit plane of the reactor is inclined toward the horizontal. This makes it difficult to find suitable measuring points since the measuring plane cannot be determined in advance. Because of these two reasons, the determination of the degree of conversion according to G 6-1 and that of emission factor according to G 6-2 was restricted to flare flames without cross draft.

6.2.1. Test Evaluation and Estimate of Errors

For the calculation of the degree of conversion and of the emission factor the following measured variables were available:

at the reactor entrance

- flare gas mass flow $\dot{m}_G$
- analysis of the flare gas $\chi_{C_mH_n}$

at the reactor exit

- volume portions of carbon monoxide and organically bound carbon (based on methane) is the off-gas which has been dehydrated to a dew point of 10°C χ_i
- flow velocity of the moist off-gas, based on the calibration conditions u_{kal}
- temperature of the off-gas T_B

From this we first calculated the following quantities:

for the reactor entrance

- mass flow of organically bound carbon

$$\dot{m}_C^{ein}(C_mH_n) = \frac{\dot{m}_G}{\varrho_G^o} \sum \frac{\chi_{C_mH_n} \cdot \varrho_{C_mH_n}^o \cdot M_C \cdot a}{M_{C_mH_n}} \qquad G\ 6\text{-}3$$

ϱ_G^o : standard density of the flare gas

$\varrho_{C_mH_n}^o$: standard density of the hydrocarbon C_mH_n

M : molar mass

a : C - number of the hydrocarbon C_mH_n

for the reactor exit

- mass concentration of carbon bound organically and as carbon monoxide in the standard cubic meter of dry off-gas

$$\varrho_C^{(i)} = \frac{\chi_i (1 + \chi_{H_2O})\ \varrho_i^o\ M_C}{M_i} \qquad G\ 6\text{-}4$$

χ_{H_2O} : volume portion of water corresponding to a dew point of 10°C (0.012)

ϱ_i^o : standard density of the component i

i : CO, CH_4

- flow velocity of the off-gas under standard conditions u_o. The calculation of the flow velocity u_o from u_{kal} is described in Appendix 8.

Deviations of the air pressure from the standard pressure are neglected.

With these quantities it is possible to calculate the degree of conversion and the emission factor:

$$U = \frac{\dot{m}_C^{in}\ (C_mH_n) - \dot{m}_C^{out}\ (C_xH_y, CO, Ruß)}{\dot{m}_C^{in}\ (C_mH_n)}$$

$$E_{ga} = \frac{\dot{m}_C^{out}\ (C_xH_y, CO)}{\dot{m}_C^{in}\ (C_mH_n)}$$

The mass flow through a reactor cross section is determined by integration of the mass flow density across the reactor cross section. The mass flow density is given by the product of mass concentration times flow velocity. The mass flow density at the distance r from the axis is to be designated by J(r). The mass flowing through the circular area with radius r_a per unit time is then calculated by the specific integral:

$$\dot{m}_i = \pi \int_0^{r_a^2} J_i(r) \cdot d(r^2) = \pi \int_0^{r_a^2} \varrho_i(r) \cdot u_i(r) \cdot d(r^2) \qquad G\ 6\text{-}5.$$

The integral was determined graphically. To this end, the mass flow density was plotted against the square of the radius and the area underneath the curve was determined with a planimeter.

The mass flow thus becomes:

$$\dot{m}_i = \pi r_a^2 \frac{J_v \cdot A_i}{A_{i,v}} \qquad G\ 6\text{-}6.$$

J_v : mass flow density for the reference area

A_i : planimeter value for the unknown area

$A_{i,v}$: planimeter value for the reference area

The radius of the reference area was not equal to that of the unknown area. Since the reactor is not bounded by walls at

the exit, the reactor boundary r_a was specified by a carbon monoxide volume portion of 0.1%.

The relative errors afflicting the particular derived quantities result according to the law of error propagation [76] from the errors of the measured variables. For this, the following values were estimated:

- volume portion C_mH_n in the flare gas : 3%
- flare gas mass flow $\dot{m}_G$: 4%
- volume portion of the off-gas component χ_i : 2%
- off-gas temperature T_B : 2%
- dew point T_p : 2%
- flow velocity u_{kal} : 2%

Concerning the measuring error caused by tilting of the flow tube with respect to the principal flow direction, no statement can be made. In drawing up the balance sheet of the reactor in Sect. 6.2.2 an attempt will be made to arrive at a statement. For the time being, this error is assumed to be negligible.

For the errors of the derived quantities we then obtain the following estimated values:

- mass flow of organically bound carbon $\dot{m}_C^{in}$: 8%
- mass concentration of the off-gas component ρ_i : 2%
- flow velocity u_o : 5%
- mass flow of carbon bound in gaseous form and non-atmospheric gases $\dot{m}_C^{out}$: 6%
- degree of conversion U, emission factor E_{ga} : 10%

6.2.2. Results of Measurement and Balance Sheet of the Flare Flame

The distributions of the measured components in a secant with a sooty flare flame burning in a calm atmosphere are shown in Figs. 6-2a and 6-2b. The flare gas mass flow amounted to 1.78 t/h and the flare gas standard density to 0.75 kg/m^3. No steam was added. The measuring height was 8 m above the flare mouth, the observed length of the flame was of the order of 10 m.

In the diagrams, the volume portions of carbon dioxide, carbon monoxide, organically bound carbon (reported as methane) and oxygen, as well as the temperature and the flow velocity, were plotted against the radius.

It can be seen that the distributions drop off on both sides from the assumed flame axis toward the edge of the flame; as expected, the oxygen volume portion varies in the opposite direction. The distributions have the shape of a Gaussian bell-curve as expected on the basis of law of free jets. However, the distributions also show that the assumption of a steady mode of operation has not been met. Thus, the distributions in the right-hand portion of the diagram do not drop off steadily but rise again between the measuring point at r = 1 m and that at r = 1.5 m. This rise can only be explained by the fact that because of the springing up of a light breeze the flame had been deflected. Moreover, the

distributions are not symmetrical to the apex. All the components have at the measuring point with r = 0.5 m to the right of the apex higher values than on the left. From this one must conclude that the flame axis in the x-y-plane was not located at r = 0 m.

It is worth noting that already in a measuring plane 2 m upstream from the visible end of the flame the volume portion - averaged over the measuring time - of carbon monoxide and organically bound carbon (reported as methane) in the presumed flame axis amounted to only 0.67 and 0.28%, respectively. At a volume ratio $\Psi_C(CO_2, CO, C_xH_y)$ = 1:0.16:0.07, this corresponds to a local burnout degree of α' = 0.88. Local burnout is defined in Sect. 6.3.

As an example of the distributions of the measured components toward the end of the flame, this flame was selected because at the end of the visible flame the volume portion of carbon monoxide lay, even in the extreme values, below the limit of detection of 0.01%. Organically bound carbon was at that point detectable only for brief periods of time. This is shown in Appendix 10 on a section of the recording strip of the flame ionization detector. The peak-like appearance of the hydrocarbons is due to the fact that there is no closed combustion front but that separate zones can be distinguished in which the combustion has already progressed to a greater or lesser extent. What this means is that the

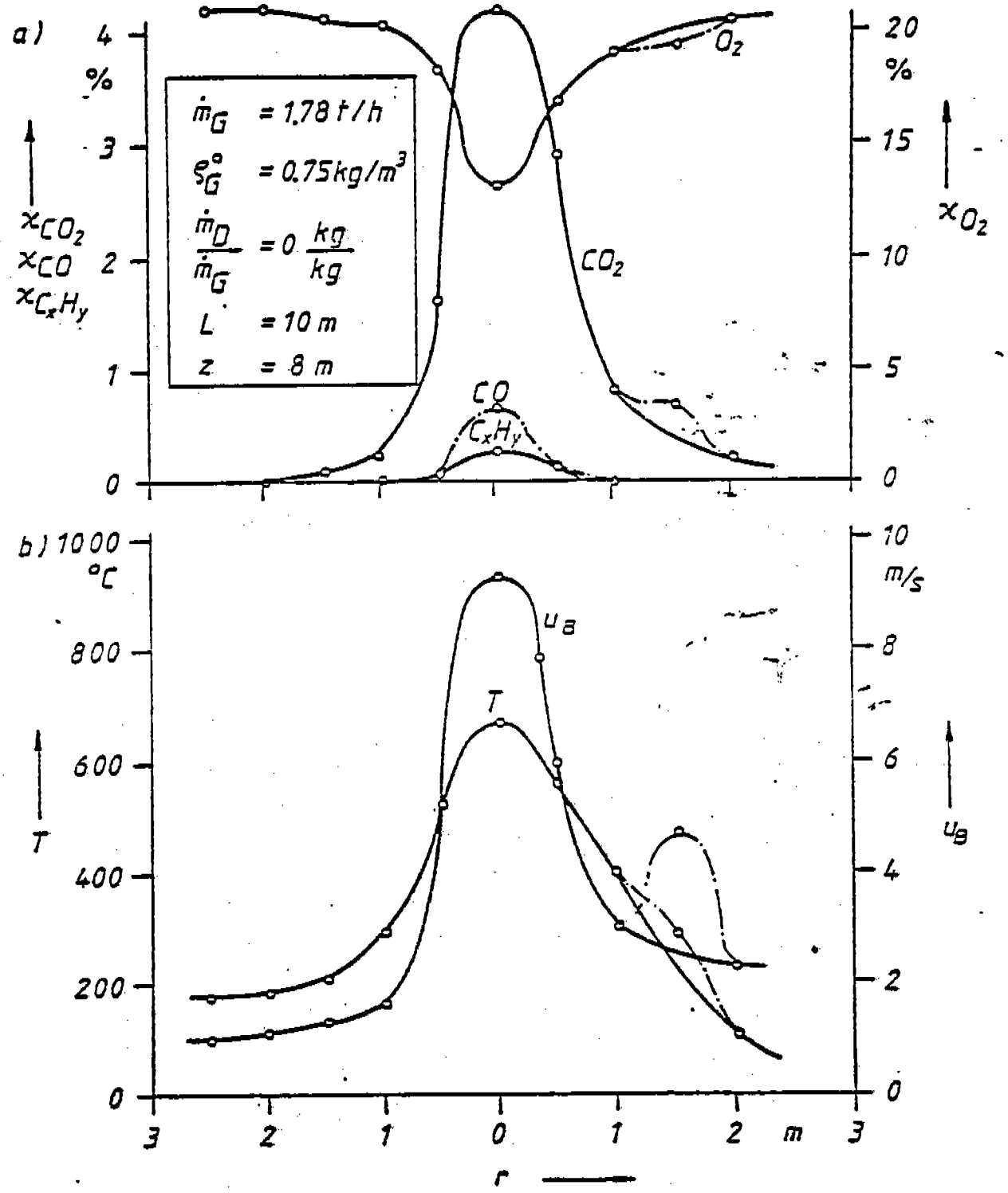

Fig. 6 - 2 : Distribution of the measured components in a secant of a flare flame burning in a calm atmosphere

Test No. 13.011-.020

measuring material flowing past the sampling point contains next to burned also unburned material in rapid variation.

Table 6-1 lists the degree of conversion of the emission factor for flare flames in a calm atmosphere together with their operating conditions and balance sheet data (cf. below). In this table, each flame is correlated with one of the columns 3 to 7. As shown by a comparison between the incoming and outgoing mass flows of carbon bound in gaseous form and non-atmospheric gases (Lines 5, 7, 8), in soot-free flare flames a degree of conversion of over 0.99 is attained (Line 9). Even in the case of a sooty flame (Flame 4), the emission factor for carbon bound in gaseous form and non-atmospheric gases lies surprisingly enough below 1% of the incoming mass flow of organically bound carbon.

In Sect. 6.8. an explanation is given for the low mass concentration of carbon bound in gaseous form and non-atmospheric gases at the end of the flame.

In order to verify the statements concerning the degree of conversion and the emission factor, the material balance sheets were drawn up for carbon and water.

The carbon balance can be written in the form of Equation G 6 - 7:

$$\dot{m}_C^{in}\ (C_mH_n) = \dot{m}_C^{out}(CO_2) + \dot{m}_C^{out}(CO) + \dot{m}_C^{out}\ (C_xH_y) + \dot{m}_C^{out}\ (\text{Soot}) \quad \text{G 6-7.}$$

Table 6.1.: Operating Conditions, Degree of Conversion and Emission Factor as well as Balance Sheet Data for Flare Flames Burning in a Calm Atmosphere

1	2		3 a	3 b	4 a	4 b	5 a	5 b	6 a	6 b	7 a	7 b
1	Test No.		11.001-.035		11.066-.070		11.093-.105		14.017-.021		14.020-.031	
2	Flame No.		1		2		2		4		5	
3	$\dot{m}_G$	kg/h	1100		940		940		940		940	
4	ψ_{DG}	kg/kg	0.60		0.32		1.20		0		0.34	
5	Flame picture		soot-free		soot-free		soot-free		sooty		soot-free	
6	$\dot{m}_C^{in}$ (C_mH_n)	kg/h	825		705		705		705		705	
7	$\dot{m}_C^{out}$ (CO)	kg/h	/		/		/		/		/	
8	$\dot{m}_C^{out}$ (C_xH_x)	kg/h	< 1		< 1		< 1		< 1		< 1	
9	U		> 0.99		> 0.99		> 0.99				> 0.99	
10	E_{ga}								< 0,01			
11	$\dot{m}_C^{out}$ (CO_2)	kg/h	560	825	240	705	305	705	70		305	705
12	$\delta_C = \frac{\dot{m}_C^{out}}{\dot{m}_C^{in}}$		0.68	1	0.34	1	0.55	1	0.24		0.54	1
13	$f = \frac{1}{\delta_C}$		1.476		2.975		1.03		(2.975)		1.046	
14	$\delta_{H_2O} = \frac{\dot{m}_{H2O}^{out}}{\dot{m}_{H2O}^{in}}$		0.00	1.05	0.52	1.14	0.60	1.08	0.38		0.80	1.22
15	χ_{O_2}(calc.)	%	10.6	19.3	17.1	19.5	10.6	19.7			17.0	19.3
16	χ_{O_2}(det.)	%	19.8		19.9		19.8				19.5	

a uncorrected values b values corrected by factor from Line 13

Since, as mentioned already in Sect. 6.1., it was not possible to measure the mass concentration of soot like that of the gaseous components, the drawing up of balance sheets must be restricted to soot-free flare flames.

In drawing up the balance sheet for water it is necessary to consider in addition to the steam mass flow (D) and the mass flow (R) of the water formed in the combustion also the mass flow (L) of the water introduced by the moisture in the air. The water balance is, therefore, as follows:

$$\dot{m}^{in}_{H_2O} = \dot{m}^{in}_{H_2O}(D) + \dot{m}^{in}_{H_2O}(R) + \dot{m}^{in}_{H_2O}(L) = \dot{m}^{out}_{H_2O} \qquad G\ 6\text{-}8.$$

The mass flow of the water introduced by the moisture in the air is given by the product of the volume flow of the input air L^{in} and its water mass concentration ρ_{H_2O}. The air volume flow L^{in} results from the measured off-gas volume flow $\dot{V}^{out}$ and the air- and off-gas volume flow at Stoichiometric combustion. The latter can be determined by the combustion calculation [12]:

$$\dot{L}_o^{in} = \dot{V}_o^{out} + \dot{l}_o - \dot{v}_o \qquad \text{G 6-9.}$$

$\dot{L}_o^{in}$: air volume flow under standard conditions

$\dot{V}_o$: off-gas volume flow under standard conditions

$\dot{l}_o$: air volume flow for stoichiometric combustion under standard conditions

$\dot{v}_o$: off-gas volume flow at stoichiometric combustion under standard conditions

For drawing up the balance sheet, the following items were available (cf. also 6.2.1.):

<u>at the reactor entrance</u>

- volume portions of the hydrocarbons in the flare gas $\chi_{C_mH_n}$
- volume portion of free hydrogen in the flare gas χ_{H_2}
- flare gas mass flow $\dot{m}_G$
- steam mass flow $\dot{m}_D$
- temperature of the dry and wet thermometer of the Assman aspiration psychrometer

<u>at the reactor exit</u>

- volume portions of carbon dioxide, carbon monoxide and organically bound carbon (based on methane) χ_i
- dew point of the off-gas T_p
- off-gas temperature T_B
- flow velocity of the off-gas u_{kal}

From these, the following quantities were calculated:

for the reactor entrance

- mass flow of organically bound carbon $\dot{m}_C^{in}\ (C_mH_n)$ nach G 6 - 3
- mass flow of hydrogen $\dot{m}_{H_2}^{in}$

$$\dot{m}_{H_2}^{in} = \dot{m}_{H_2}^{in}\ (C_mH_n) + \dot{m}_{H_2}^{in}\ (H_2) \qquad \text{G 6-10}$$

$$\text{with } \dot{m}_{H_2}^{in}\ (C_mH_n) = \frac{\dot{m}_G}{\varrho_G^0} \sum \frac{x_{C_mH_n} \cdot \varrho^0_{C_mH_n} \cdot M_{H_2} \cdot \frac{n}{2}}{M_{C_mH_n}} \qquad \text{G 6-11}$$

n: number of hydrogen atoms in the hydrocarbon C_mH_n

and with

$$\dot{m}_{H_2}^{in}\ (H_2) = \frac{\dot{m}_G}{\varrho_G^0}\ x_{H_2} \cdot \varrho^0_{H_2} \qquad \text{G 6-12}$$

- mass flow of water produced during the combustion

$$\dot{m}_{H_2O}^{in}\ (R) = \dot{m}_{H_2}^{in} \frac{M_{H_2O}}{M_{H_2}} \qquad \text{G 6-13}$$

- mass concentration of water in the ambient air $\rho^L_{H_2O}$. These values have been tabulated as a function of the psychometric temperature differences and of the temperature of the wet thermometer [77].

for the reactor exit

- mass concentration of carbon bound in the form of carbon dioxide, carbon monoxide and organically $\varrho_{OC}(i)$ according to G 6 - 4.

- mass concentration of water ρ_{oH_2O}. These values have been tabulated as a function of the dew point [75].
- flow velocity u_o (see Appendix 8)

With the data determined in this manner one then obtains the following quantities:

$$\dot{m}^{out}_{H_2O} = \pi \int_0^{r_a^2} J_{H_2O}(r) \cdot d(r^2) = \pi \int_0^{r_a^2} \rho_{oH_2O}(r) \cdot u_o(r) \cdot d(r^2) \quad G\ 6-14$$

with $r_a = r(\chi_{CO_2} = 0{,}1\ \%)$

$$\dot{V}^{out}_o = \pi \int_0^{r_a^2} u_o(r) \cdot d(r^2) \quad G\ 6-15$$

with $r_a = r(\chi_{CO_2} = 0{,}1\ \%)$

$$\dot{m}^{out}_C(i) = \pi \int_0^{r_a^2} J_C(i)(r) \cdot d(r^2) \quad G\ 6-16$$

with $r_a = r(\chi_{CO_2} = 0{,}1\ \%)$

$$\dot{m}^{in}_{H_2O}(L) = \dot{L}^{in}_o \cdot \rho^L_{H_2O} \quad G\ 6-17.$$

Balance sheet data which for reasons of clarity have been omitted in Table 6 - 1 are shown in Appendix 2.

In Column a of Lines 12 and 14 of Table 6 - 1 are listed the retrieval rates from the carbon- and water balance sheets. The retrieval rate is defined as the quotient of outgoing and incoming mass flow. The retrieval rate for carbon shows in the case of Flame 1 with 68% the highest value. Considering the estimated

error of ± 8% for the incoming and of ± 6% for the outgoing carbon mass flow, there remains a deficit of ca. 20%. On the basis of the results of the calibration of the total measuring system (cf. 5.3.3.), an incorrect measurement of the components at the end of the flame of this order of magnitude can be ruled out. Nor can the deficit in the case of Flame 1 be attributed to the fluctuation of the flame or to the position of the measuring points in secants which were not diameters.

Figure 6 - 3 shows for Flame 1 the mass flow density profiles of the carbon bound as carbon dioxide in 4 flame diameters. At the measuring points no carbon monoxide and only sporadically organically bound carbon was measured. Since the median, the apex and the variance of the Gaussian mass flow density profiles are comparable, it can be assumed that the measuring point did indeed lie on the reactor diameters. However, as shown by the distributions on the left-hand side of the diagram, also in this test some deflection of the flames had occurred.

Since with all the flames the retrieval rate for water is higher than that for carbon and since the calculated mass flow of the water introduced by the moisture in the air depends on the off-gas volume flow, it was natural to check whether the deficits could be attributed to an incorrect measurement of the flow velocity. To this end, the outgoing carbon mass flow was equated to the incoming flow. The resulting factor (Line 13 of Table 6 - 1) was used to multiply the measured off-gas volume

flow. With this corrected off-gas volume flow, the mass flow of the water introduced by the moisture in the air was calculated anew. If one now forms the quotient of the outgoing and the incoming water mass flow, the resulting retrieval in the case of Flame 1 amounts to 105%. This deviation lies within the limits of error and must be considered as satisfactory for field tests.

The balance sheets for Flame 1 shown with a steady mode of operation of the flame and with the measuring points located on diameters the retrieval rate - disregarding measuring errors - is of the order of 70%. The deficit must be attributed to a low reading in the flow measurements which is caused by the tilt of the flow tube with respect to the principal flow direction outside the flame axis.

Because of the unusually long duration of calmness and due to the relatively large steam/gas ratio, the burning stability of Flame 1 was exceptionally good. These optimal conditions did not exist in the case of Flames 2 to 5 so that in contrast to Flame 1 only a traverse could be surveyed. Moreover, since the flame fluttered slightly to and fro owing to the fluctuating wind, the measuring points along the traverse did not always lie on a diameter. Since, however, the value of the measuring object drops off sharply from the flame axis toward the edge of the flame, even slight departures from the diameter lead to low readings of the outgoing mass flows.

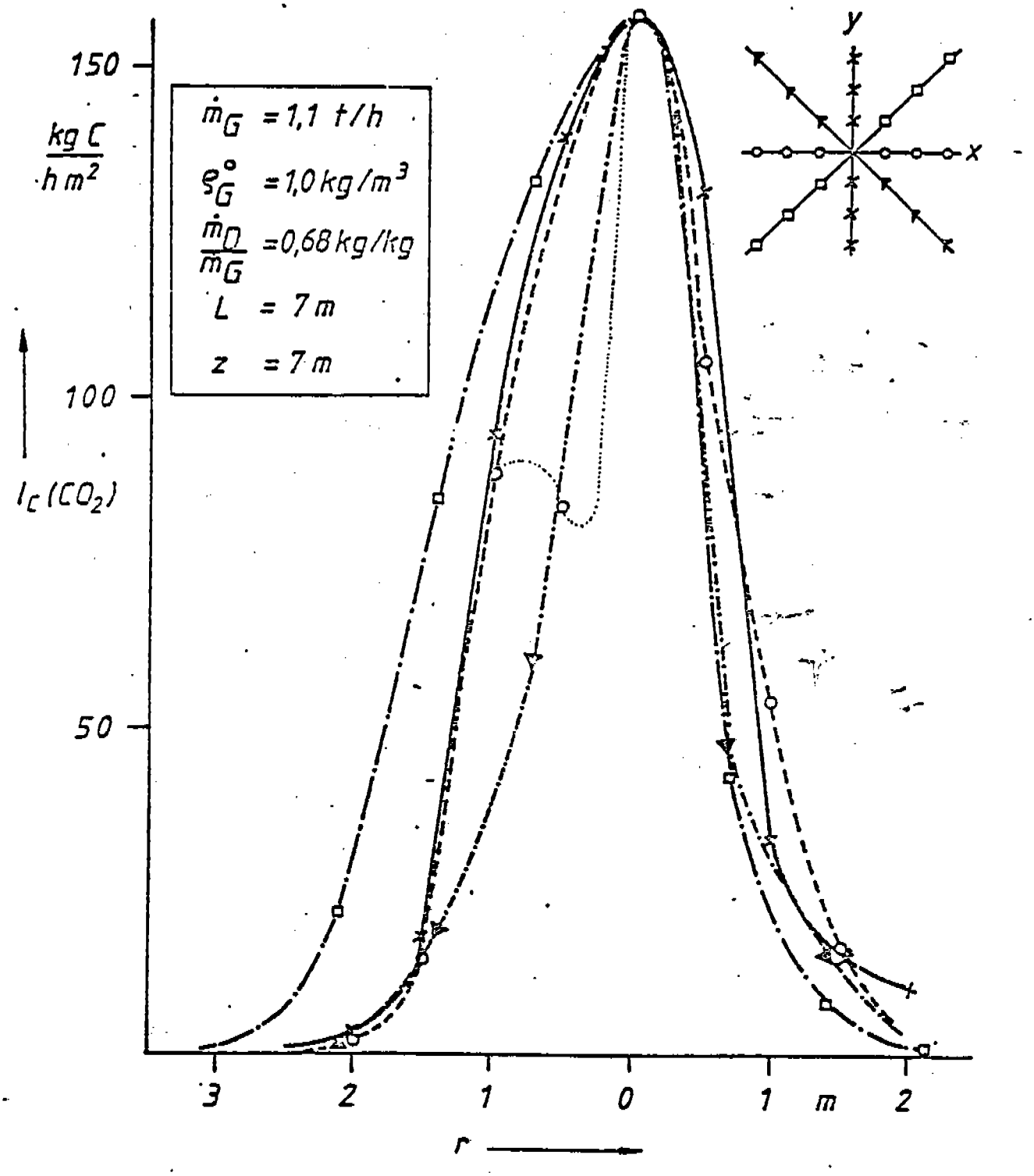

Fig. 6 - 3: Distribution of the mass flow density of the carbon bound as carbon dioxide in 4 diameters of a flare flame burning in a calm atmosphere
Test 11.011-.035

The larger deficit in the carbon balance in the case of sooty Flame 4 compared to the soot-free flames must also be attributed to the aforementioned causes and cannot be explained by a high soot emission, because then improbable soot mass concentrations would have to occur in the off-gas. To this end, the following estimate was made.

The outgoing carbon mass flow was corrected with factor 2.975 from Flame 2 and the then still remaining carbon mass flow was assessed as soot emission. In that case, the corrected off-gas volume flow shows a carbon mass concentration of approximately 1 g/m^3 for Flame 4 at an oxygen volume portion of around 19%. This estimated soot mass concentration is higher than the one measured by Becker [78] in the flame axes of the turbulent diffusion flames.

Becker examined the variation of the soot mass concentration along the flame axis of vertically burning turbulent diffusion flames. For the taking of samples he used a water-cooled probe with a filter connected downstream. He reports for propane flames a maximum soot mass concentration of 0.8 g per standard cubic meter which was found toward the end of the first half of the flame. The fact that the soot mass concentration measured by him along the axis of propane flames are low in comparison with the results of the measurements by Hein [79] he explains by the fact that the flame studied by Hein burned horizontally inside a combustion chamber. The burning characteristics of

the flames are, therefore, not comparable since in combustion chambers there exists a back flow. Hein reports soot mass concentrations of around 7 g per standard cubic meter.

However, since the soot formed in the flame reacts further, the results of the measurements by Becker and Hein are in any event not comparable with the soot mass concentration estimated here. Nevertheless, the comparison does show that the assesment of the deficit in the carbon balance remaining after the correction as soot emission gives a soot mass concentration in the off-gas which is much too high. After conversion to an air number of 1, it is of the order of 10 g per standard cubic meter.

Furthermore, the estimated soot mass concentration is by 1 g per standard cubic meter out of line with the results of the experimental determination of the soot mass concentration in the off-gas of a very sooty flare flame. In this case, soot mass concentrations of between 20 and 80 mg per standard cubic meter were found (cf. Sect. 6.7.). Consequently, also in the case of Flame 4 the deficit must be largely attributed to the location of the measuring points in a secant which was not a diameter.

A check of the off-gas volume via the oxygen volume portion by a combustion calculation can give a correct description of the conditions only as far as the tendency is concerned. Because of the large size of the oxygen volume portion of between 19 and 20% at the end of the flame, its effect on the off-gas volume

flow is considerable. The calculated oxygen volume portions χ are listed in the a-columns of Line 15 of Table 6 - 1 for the measured off-gas volume flow and in the b-column for the corrected off-gas volume flow. Line 16 shows the oxygen volume portion obtained by measurement and averaged across the reactor exit according to G 6 - 18.

$$\chi_{O_2} = \frac{\pi \int_0^{r_a^2} J'_{O_2}(r) \cdot d(r^2)}{\pi \int_0^{r_a^2} u(r) \cdot d(r^2)} \qquad \text{G 6-18}$$

$$J' = \chi_{O_2}(r) \cdot u(r)$$

$$r_a = r(\chi_{CO_2} = 0{,}1\ \%)$$

The oxygen volume portion increases for all the flames in the order of: χ_{O_2} (uncorrected), χ_{O_2} (corrected, χ_{O_2} (measured). The discrepancies between the corrected and the measured oxygen volume portion even lie within the estimated error of 2%. This comparison which is to be appraised only with respect to the tendency also shows that the correction of the off-gas volume flow applied here is justified.

If in the case of the outgoing mass flows allowance is made for the errors caused by the tilt of the flow tube with

respect to the principal flow direction and by the location of the measuring points outside of diameters, then the degrees of conversion or emission listed on Lines 9 and 10 of Table 6 - 1 are in fact corroborated by the material balances of carbon and water. Therefore, as far as the off-gas combustion in elevated flares is concerned, the following statements can be made:

- In soot-free flare flames without a cross draft, the organically bound carbon of the flare gas is converted to carbon dioxide at a rate of at least 99%.
- In the case of sooty flare flames without a cross draft the emission factor for carbon bound in gaseous form and non-atmospheric gases amounts maximally to 1% of the incoming mass flow of organically bound carbon.

The results of the tests for the determination of the degree of conversion in soot-free flare flames burning in a calm atmosphere confirm the assertion of Günther and Lenze [33] that in the case of flare flames without the detachment of balls the burnout at the end of the flame is complete.

Brzustowski's supposition [20] that even in the case of soot-free flare flames unburned fuel is still present at the end of the flame has been invalidated by our test results.

6.3. Definition of the Local Degree of Burnout and of the Minimum Degree of Conversion and Maximum Emission Factor

The results of the tests for the determination of the degree of conversion in flare flames without a cross draft showed that

even in a calm atmosphere a steady mode of operation of the flare flame exists only conditionally since the position of the flame is greatly affected by wind. As a consequence, the arrangement of the measuring points on flame diameters was subject to the vagaries of the wind's behavior. The fluctuations of the wind increase with increasing wind force.

An example of this is given in Fig. 6 - 4 which shows the temperature distribution in a horizontal plane across a flare flame operating in a cross draft. The plane was situated ca. 1 m upstream of the end of the flame. The operating conditions are specified on the diagram. $\theta_{G,Q}$ stands for the ratio of the area-related impulse-forces of the gas jet and the wind. The impulse-force of the gas jet was calculated from the average velocity of the fuel jet - based on the entrance to the mixing chamber of the flare head - and from the average density of the combustion gases at a mean temperature of 900°C. The standard density of the combustion gases was set equal to that of air.

On the diagram, the temperature has been plotted against the space coordinate x; the space coordinate y is the parameter. In spite of the large ratio $\theta_{G,Q} \approx 20$, the temperature maximum is found not, as expected, at x = 0m, y = 0m but at x = -2m, y = 0m. This corresponds to a deflection of the flame by 20° from the vertical. The diagram further shows that on the line with y = 2m, a low was present instead of the maximum. This can only be explained by the fact that the wind was not constant

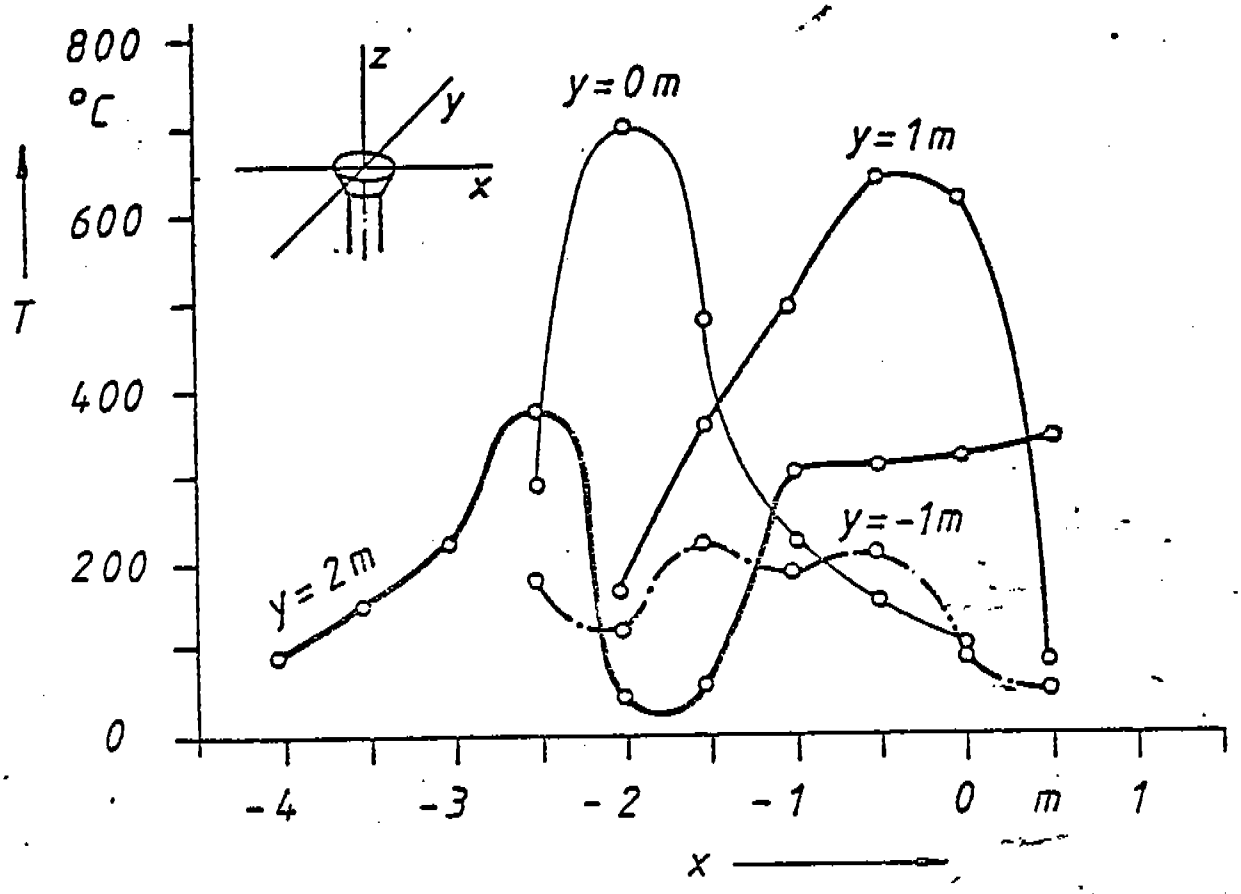

$\dot{m}_G = 1{,}26\ t/h$, $\varrho^{\circ}_G = 0{,}81\ kg/m^3$, $\dot{m}_D/\dot{m}_G = 0{,}06\ kg/kg$

$u_Q = 1{,}5\ m/s$, $\theta_{G,Q} \approx 20$, $L = 6\ m$, $z = 5\ m$

Fig. 6 - 4: Distribution of the temperature in a horizontal plane of measurement in the case of a flare flame burning in a slight cross draft
Test 03.040-.094

during the surveying of the line. As a result, the position of the flame was changed.

Under these conditions, the determination of the degree of conversion according to G 6 - 1 is not feasible with the experimental arrangement chosen when the flare flame burns in a cross

draft. The reasons for this lie, however, not only in the unsteady mode of operation of the flame but also in the difficulties in fixing the reactor exit plane and in measuring the off-gas velocity in the principal flow direction.

According to the objective of this investigation, the operating conditions of the test flare should be comparable to the operating conditions of elevated flares integrated into the refinery operation. However, elevated flares burn for the most part under the influence of wind. This is confirmed by Fig. 6 - 5 which shows the distribution of the wind velocity at different heights in the Karlsruhe area [30]. What is worth noting particularly is the increase of the frequency maxima of 1-2 m/s at the 20 m level to ca. 6 m/s at the 100 m level and also the large decrease of the weak breezes and calms with increasing height.

In order to be able to make a statement concerning the degree of conversion and the emission factor also in the case of flames burning in a cross draft we resorted to the local degree of burnout [12].

The local degree of burnout indicates which portion of the carbon present at a point exists there in burned form. The value is normalized with the total carbon present at the same point both as burned C_v and unburned C_u:

$$\alpha = \frac{\varrho_C(C_v)}{\varrho_C(C_v) + \varrho_C(C_u)} \quad .$$

Since the soot mass concentration could not be measured like that of the gaseous components, in the case of sooty flare flames only the carbon portions bound in gaseous form are available for the calculation of the local degree of burnout. Therefore, the term local burnout is always understood to mean the local degree of burnout related to the carbon bound in gaseous form. It is further stipulated that:

- the carbon portion present in bound form as carbon dioxide is considered as burned.
- the carbon portion bound as carbon monoxide is at measuring points located upstream of the end of the flame considered as an intermediate stage of the fuel oxidation to carbon dioxide and one half each is added to the burned and to the unburned carbon portion. At measuring points at or downstream of the end of the flame the carbon portion bound as carbon monoxide is added exclusively to the unburned material.
- the organically bound carbon portion is always classified as unburned irrespective of the location of the measuring point.

The local degree of burnout is, therefore, defined by G 6 - 20 and G 6 21 as follows:

- for measuring points at and downstream of the end of the flame

$$\alpha = \frac{\varrho_C (CO_2)}{\varrho_C (CO_2) + \varrho_C (CO) + \varrho_C (C_x H_y)} \qquad \text{G 6-20,}$$

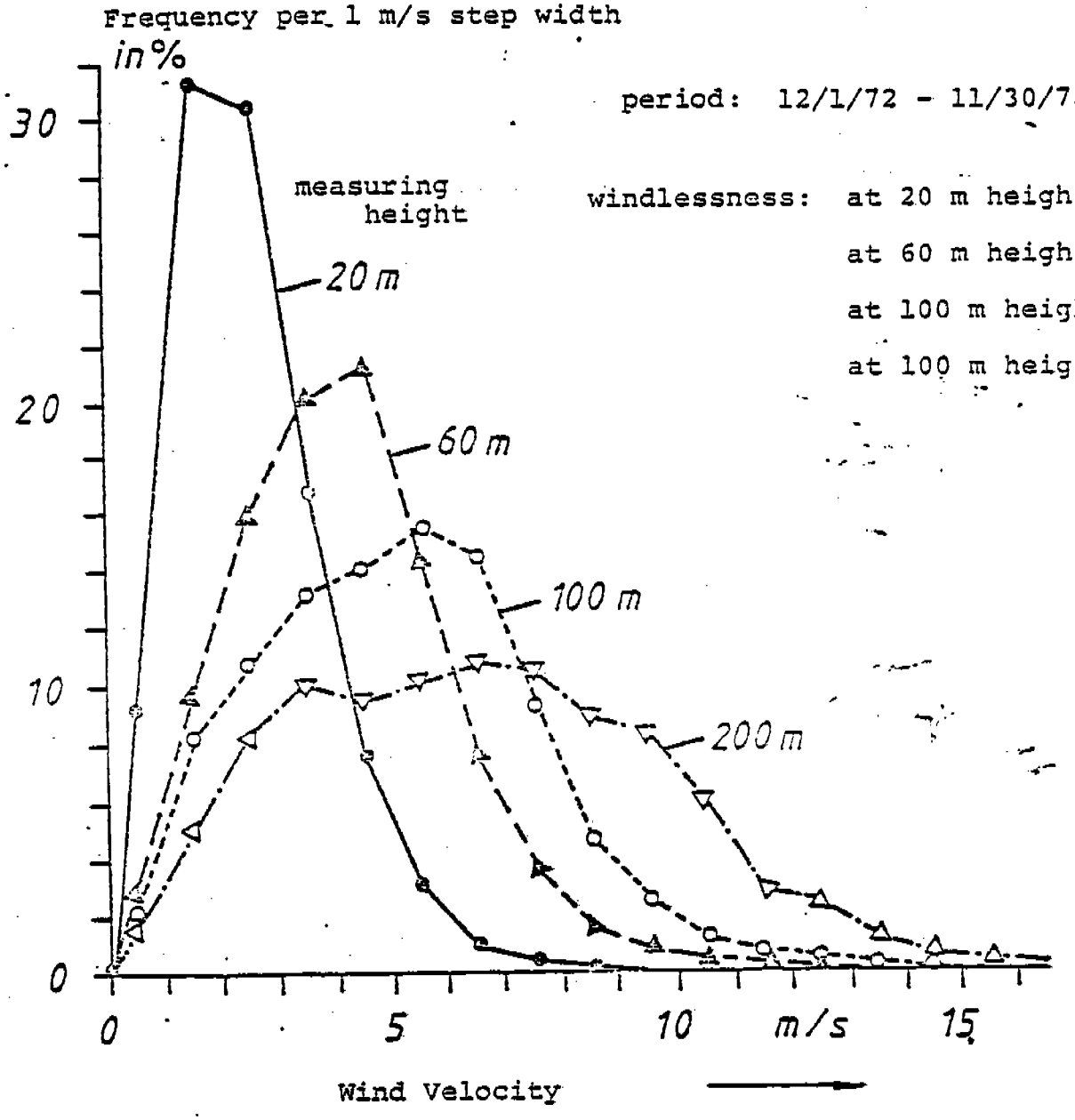

Fig. 6 - 5: Distribution of wind velocity at different heights [80]

- for measuring points upstream of the end of the flame

$$\alpha' = \frac{\varrho_C(CO_2) + \frac{1}{2}\varrho_C(CO)}{\varrho_C(CO_2) + \varrho_C(CO) + \varrho_C(C_xH_y)} \qquad G\ 6\text{-}21.$$

The smallest local degree of burnout α_{min} at a measuring point of the measuring plane at the end of the flame is linked to:

- the maximum degree of conversion U_{min} in the case of soot-free flare flames by

$$U_{min} = \alpha_{min} \qquad G\ 6\text{-}22,$$

- the maximum emission factor for carbon bound in gaseous and non-atmospheric gases in the case of sooty flare flames by

$$E_{ga,max} = 1 - \alpha_{min} \qquad G\ 6\text{-}23.$$

6.3.1. Effect of the Mass Concentration of Unburned Carbon at the End of the Flame on the Local Degree of Burnout

The minimum degree of conversion and the maximum emission factor cannot be verified by drawing up material balance sheets. For this reason it is estimated what effect an incorrect measurement of the organically bound carbon at the end of the flame can have on the minimum degree of conversion and on the maximum emission factor.

To this end we calculated for a flare gas with a standard density of 1 kg/m^3, whose carbon portion is of the order of 0.8 kg carbon per kg flare gas, the mass concentration of organically bound carbon in the off-gas as a function of the degree of conversion at three different oxygen volume portions. The method of computation is described in Appendix 3; the results are shown in Fig. 6 - 6.

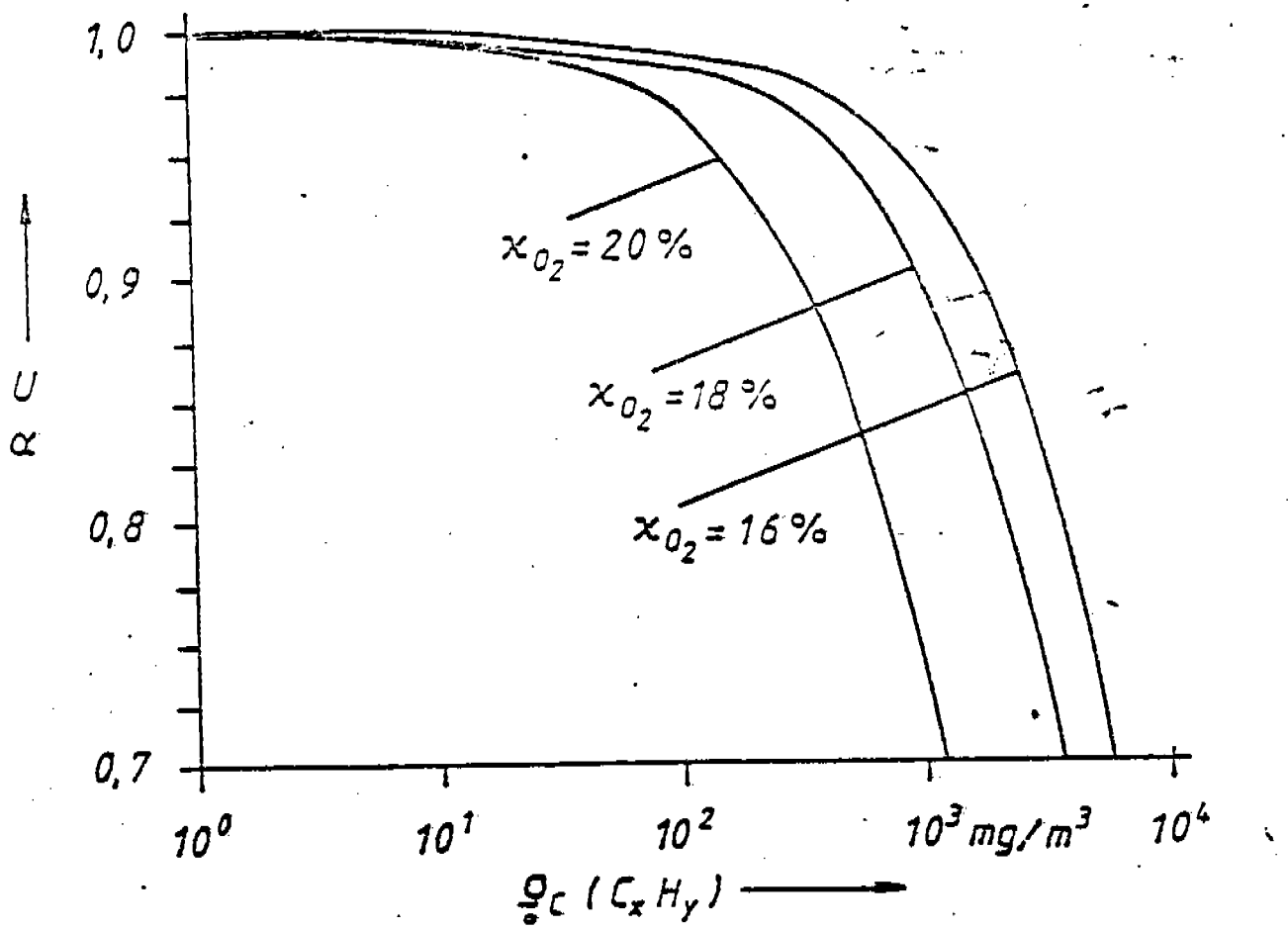

Fig. 6 - 6: Degree of conversion and local degree of burnout as a function of the mass concentration of organically bound carbon with different oxygen volume portions

In Fig. 6 - 6, the degree of burnout has been plotted against the mass concentration of the organically bound carbon in the off-gas at an oxygen volume portion of 16, 18 and 20%. It can be seen that the slope of the curve is very flat at a high degree of burnout. Therefore, at a burnout degree of around 0.99, an incorrect measurement of the organically bound carbon by, for example, 10% has hardly any effect on the prediction of the degree of conversion.

6.4. Minimum Degree of Conversion in Soot-Free Flare Flames and Maximum Emission Factor in the Case of Sooty Flare Flames Burning under Windy Conditions

6.4.1. Effect of the Wind on the Combustion

If the length of the flame is considered a measure of the path necessary for the aspiration of air and for the mixing of fuel and air, then the combustion can be graphically described by the flame length.

The length of up-draft flames burning under the influence of a cross wind has been calculated and explained by Lee [36]. Lee's calculations show that with a given flare-head diameter and mass flow the length of the flame first decreases and then again increases with increasing wind velocity. He explains this by saying that with increasing wind velocity the air penetrates farther into the substance of the jet and that the aspiration of air is improved as a result. At high wind velocities, however, the jet is already deflected at the flare head to such a degree

that the wind direction and the flame axis become nearly parallel. Due to the low relative velocity between the jet substance and the surrounding medium the impulse exchange is reduced, which results in longer flames. Since at the edge of the jet the ratio of jet and wind forces is smaller than at the center of the jet, the jet cross section assumes the shape of a horseshoe. This means that at the edge of the jet certain portions can be deflected vertically to the jet axis to such a degree that they are no longer in contact with the jet, which may lead to an emission of unburned fuel.

Brzustowski [20] supposes that in the case of flare flames burning in a cross draft unburned material is discharged on the side turned toward the wind.

6.4.2. Experimental Procedure and Presentation of the Test Results

In the tests for determining the local degree of burnout in flare flames burning in a cross draft no secants, as in the test described in Sect. 6.2., but planes were surveyed. The measuring planes were applied horizontally and vertically at the end of the flame. The boundary of the measuring field was specified by a carbon dioxide volume portion of 0.1% in the off-gas.

In Figs. 6 -7 to 6 - 10 and also in Appendix 4, the test results are presented in the following manner: The centers of the circles arranged in the measuring plane indicate the coordinates of the respective measuring point in the x/y-plane and the y/z-plane, respectively. The third space coordinate is

shown on the diagrams together with the operating conditions. The sector angle of the filled-in circle segment is a measure of the quantity presented. The reference values indicated by a sector angle of 0 to 360° are shown in the illustrations.

6.4.3. Local Degree of Burnout in Flare Flames Burning in a Cross Draft

Figs. 6-7a and 6-8a show for 2 different operating conditions the distributions of the carbon dioxide volume portion in a horizontal measuring plane above the flare flame burning in a cross draft. The average wind velocity in the tests shown in Figs. 6-7 and 6-8 was of the order of 1.2 and 2 m/s, respectively.

In the draft direction of the wind, the volume portion of carbon dioxide drops off more slowly at the edge of the flame than in the flame axis. Although one could easily attribute these horseshoe-shaped distributions to the causes described above, this can be done only with reservations. These distributions could also have been brought about by a slight turning of the wind. Since the measuring of the wind direction only had a resolution of about 30°, an unequivocal correlation is not possible. The temperature distributions shown in Appendix 4 likewise do not permit any sure conclusion in this direction.

The distributions of the local burnout degrees for the two flames are shown in Figs. 6-7b and 6-8b. In the illustrations, a sector angle of 0° is assigned to a local burnout degree of 1

and a sector angle of 360° to a local burnout degree of 0.975. To measuring points in the measuring plane which lie outside the measuring field a local burnout degree of 1 would have to be assigned.

It can be seen that the local burnout at all measuring points is almost complete. At the edge of the flame, a slight drop of the local burnout degree can occasionally be noted. However, no general relationship can be derived from the test results.

The distribution of the local burnout degrees at the end of a flame burning in a strong wind is shown in Fig. 6-9. The ratio of the area-related impulse forces of gas jet and wind $\vartheta_{G,Q}$ amounted to approximately 3.8. The measuring plane was applied vertically in order to pick up also non-atmospheric gases discharged in the lee of the flare head. In this test, a discharge of material at the flare head could be observed.

It can be seen that even in the case of a flame burning in a strong cross wind the local burnout degree at the end of the flame is nearly complete. Also at the flame edge in the lee no discharge of unburned gaseous material could be measured ($z = 0$ m and $z = 1$ m) so that the observed material discharge consisted of carbon dioxide and water vapor.

This result has also been confirmed by Test 08.001 to 47 (cf. Fig. 6-10).

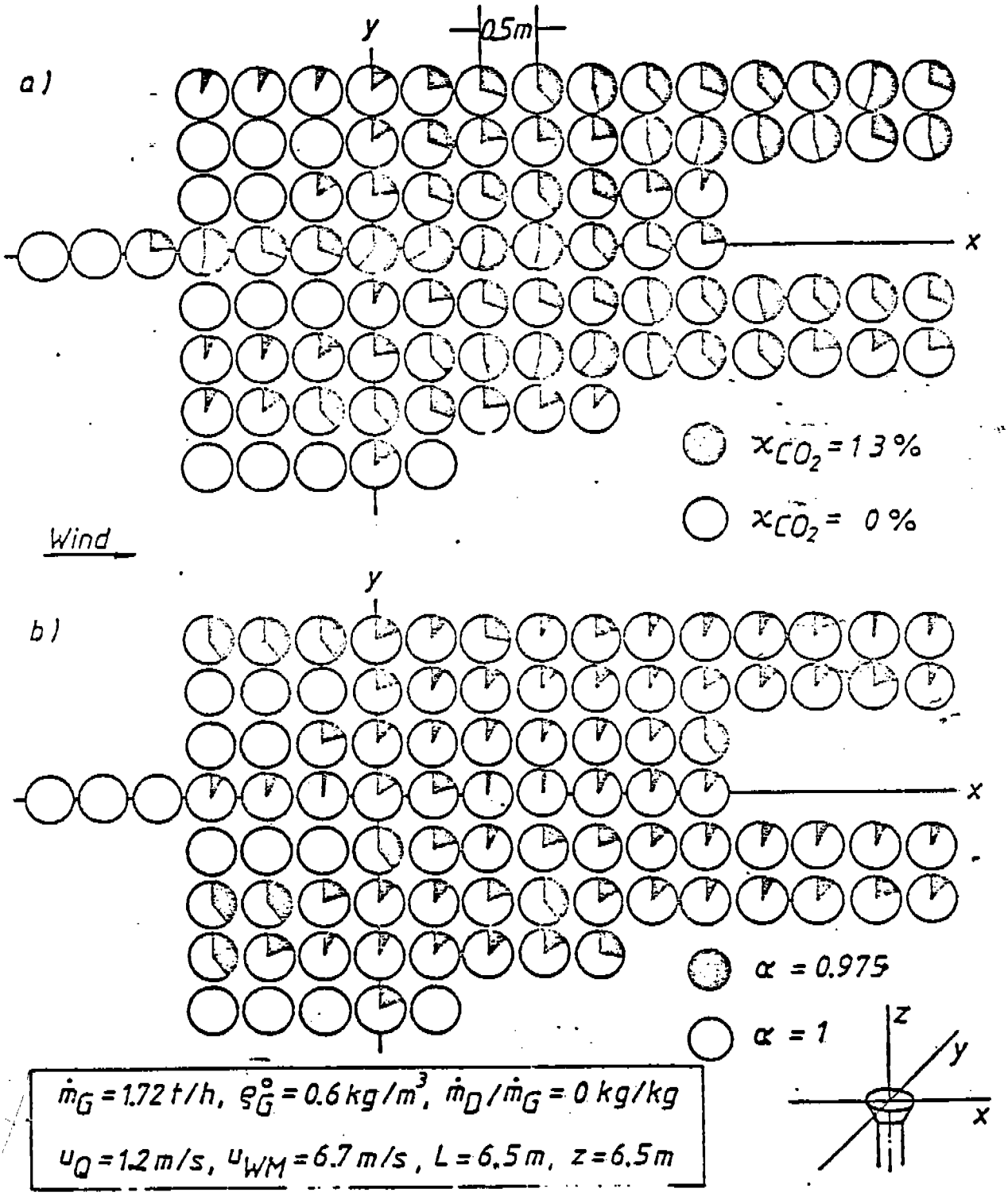

Fig. 6 - 7: Distribution of the volume portions of carbon dioxide and the local burnout degrees in a horizontal plane across a flare flame burning in a cross draft
Test 06.101-.143

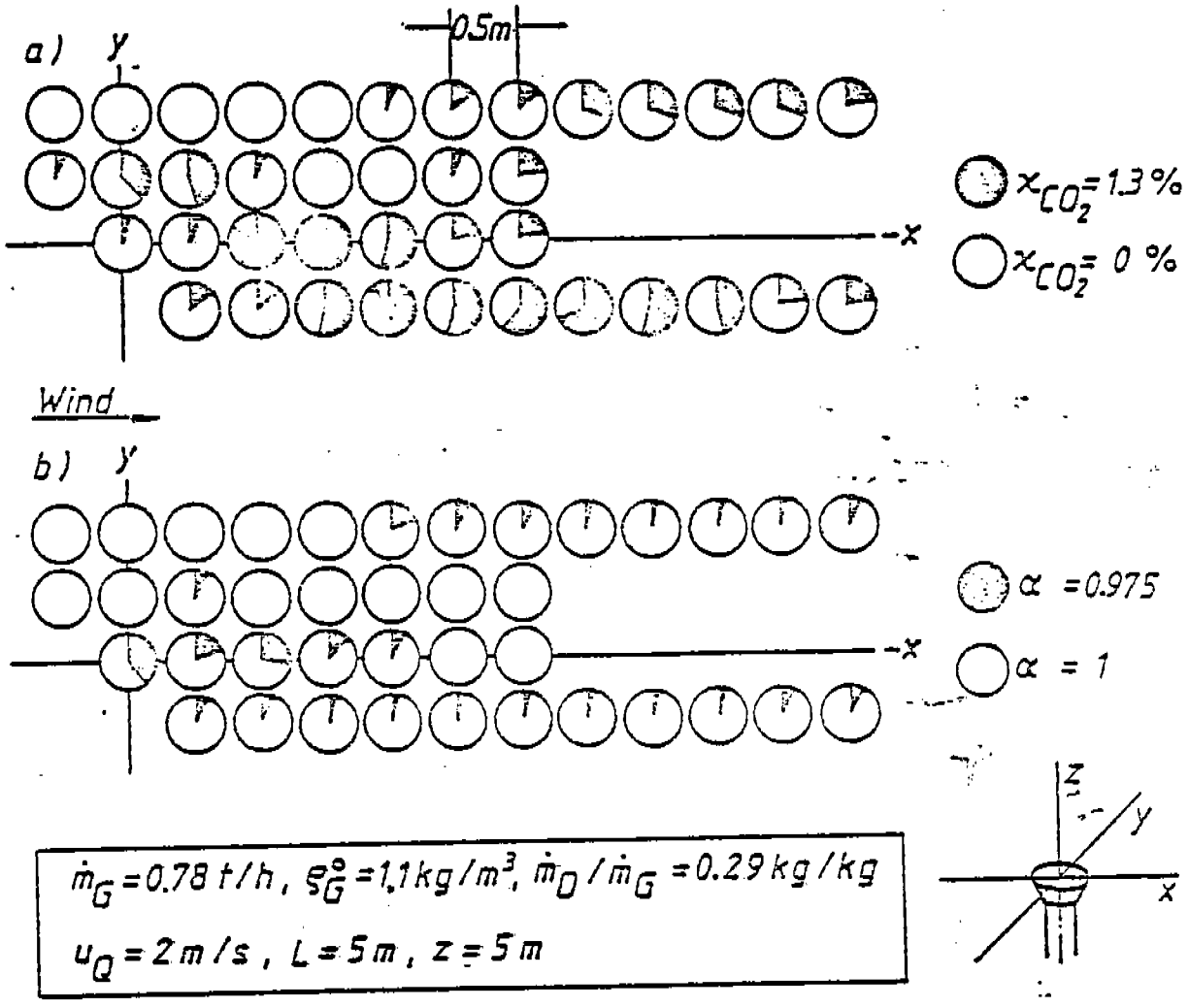

Fig. 6 - 8: Distribution of the volume portions of carbon dioxide and the local burnout degree in a horizontal plane across a flare flame burning in a cross draft
Test 03.001-.039

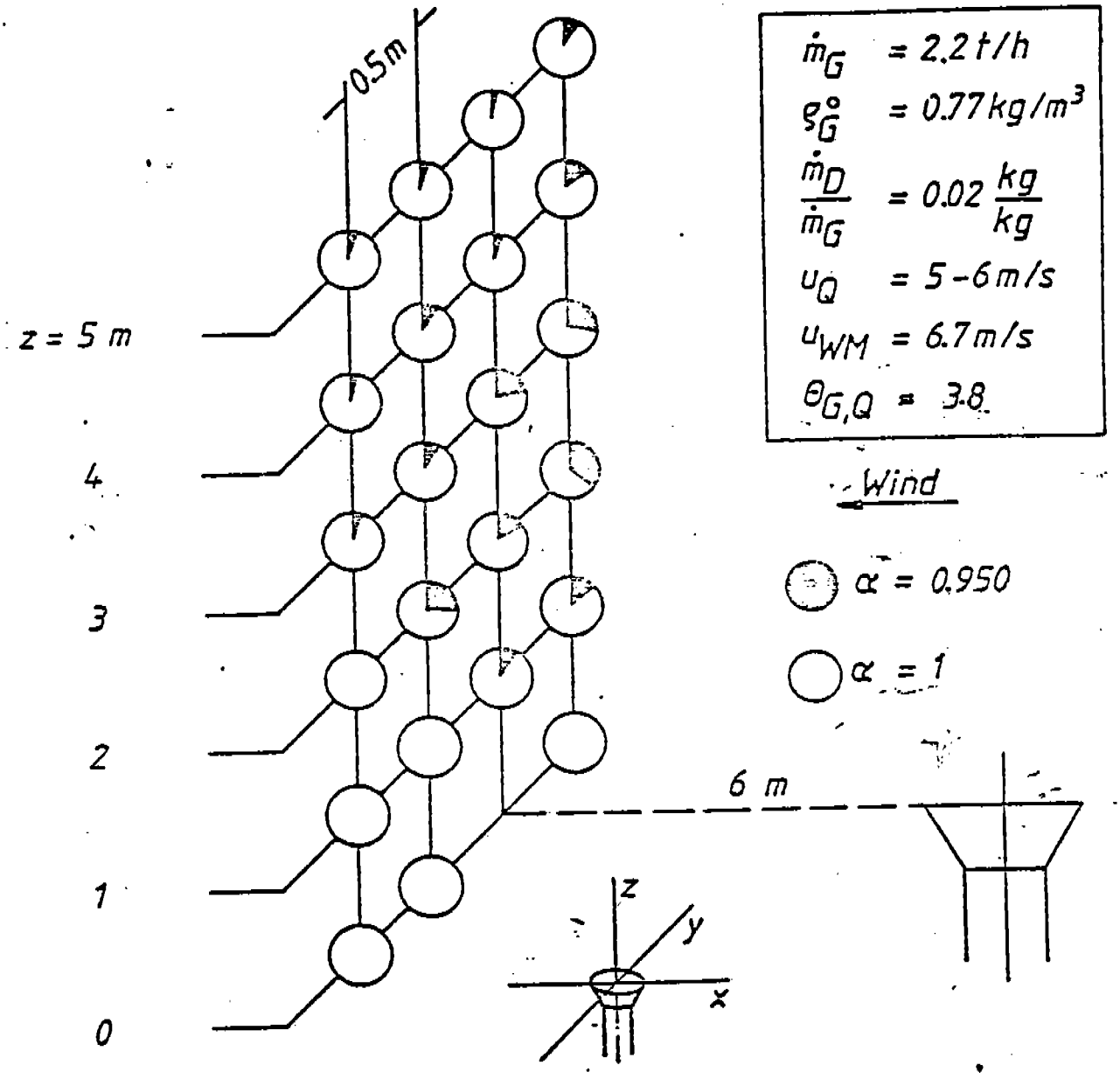

Fig. 6 - 9: Distribution of the local burnout degrees in a vertical plane at the end of a flare flame burning in a strong cross wind
Test 16.001-.027

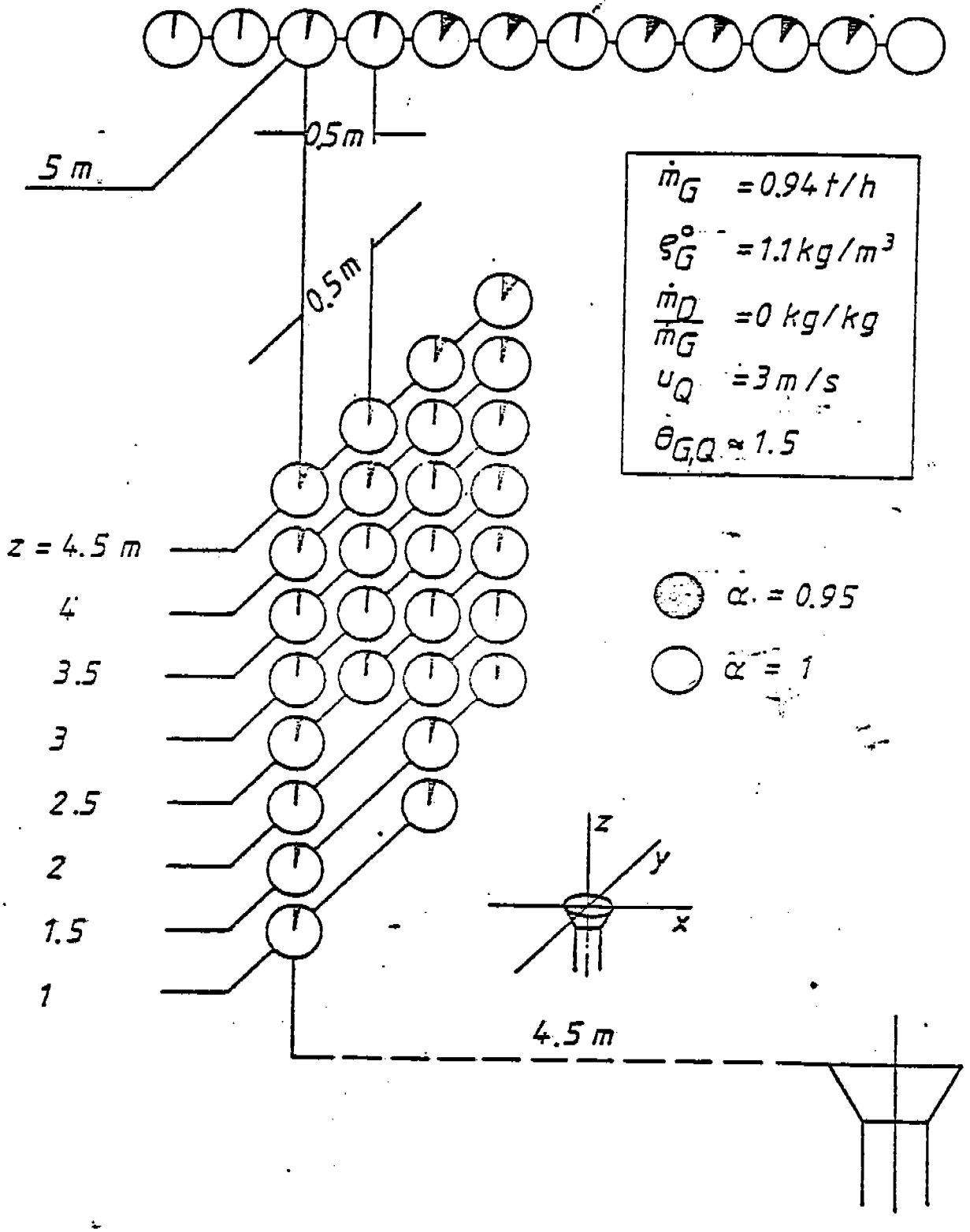

Fig. 6 -10: Distribution of the local burnout degrees in a vertical plane at the end of a flare flame burning in a cross draft
Test 08.001-.047

These test results agree with those reported by Grumer [46] who was unable to measure any discharge of unburned fuel with flare flames operated with hydrogen as the fuel gas in a cross draft.

In the case of flare flames burning in a cross draft, Brzustowski [20] suspects unburned material above the flare head. In order to be able to pass judgement on this conjecture, the measuring in the case of a flare flame burning in a cross draft was done in a plane extending through the axis of the flare flame and through the axis of the flare head (Fig. 6-11). In the measuring plane, the measuring points lay on grid lines of 2, 3, 4 and 5 m above the flare mouth. The distance of the vertical grid lines was Δx=1 m. The measuring points were located at the points of intersection of the grid lines.

In Figs. 6-11a to d, the local burnout degree has been plotted above the space coordinate x. The diagrams differ from each other with respect to the height coordinate z. The wind drift ran parallel to the x-axis. If we compare at the heights of z = 3 m and z = 4 m the local burnout degree of the windward (cross-hatched) edge of the flame with the one in the lee, we recognize that in the lee the local burnout is complete while on the windward side some unburned material is discharged. The discharge increases as we move upstream. The local burnout degree α at the measuring point .064 was found to be α = 0.76 and at the measuring point .063, α = 0.97. The volume portions of the carbon-containing off-gas component and the off-gas temperatures amounted to:

- at the measuring point .064 (z = 3 m, x = 0 m)

χ_{CO_2} = 0.2 % χ_{CO} = 0.05 % $\chi_{C_xH_y}$ = 145 ppm T = 80° C

- at the measuring point .063 (z = 4 m, x = -1 m)

χ_{CO_2} = 0.1 % χ_{CO} 0.01 % $\chi_{C_xH_y}$ = 25 ppm T = 140° C.

The presence of carbon monoxide and carbon dioxide at the measuring point .064 leads to the conclusion that the mixture of materials discharged at that point had been quenched after the ignition. Furthermore, it must be assumed that the C-containing components measured at the measuring point .063 had already been discharged above the flare head and had been driven by the wind toward the flame.

The discharge of unburned material above the flare head must be attributed to the fact that the impulse force in the z-direction of particular cells is sufficient to detach them from the flame. Cells detached in this manner are, however, quenched very quickly below the reaction temperature. They move into a region where owing to the cross wind there is a constant flow of cold air so that their heat of combustion is not sufficient to maintain the temperature necessary for the progress of the reaction.

These cells are, however, driven by the wind toward the flame where they burn out. This assertion is based on the

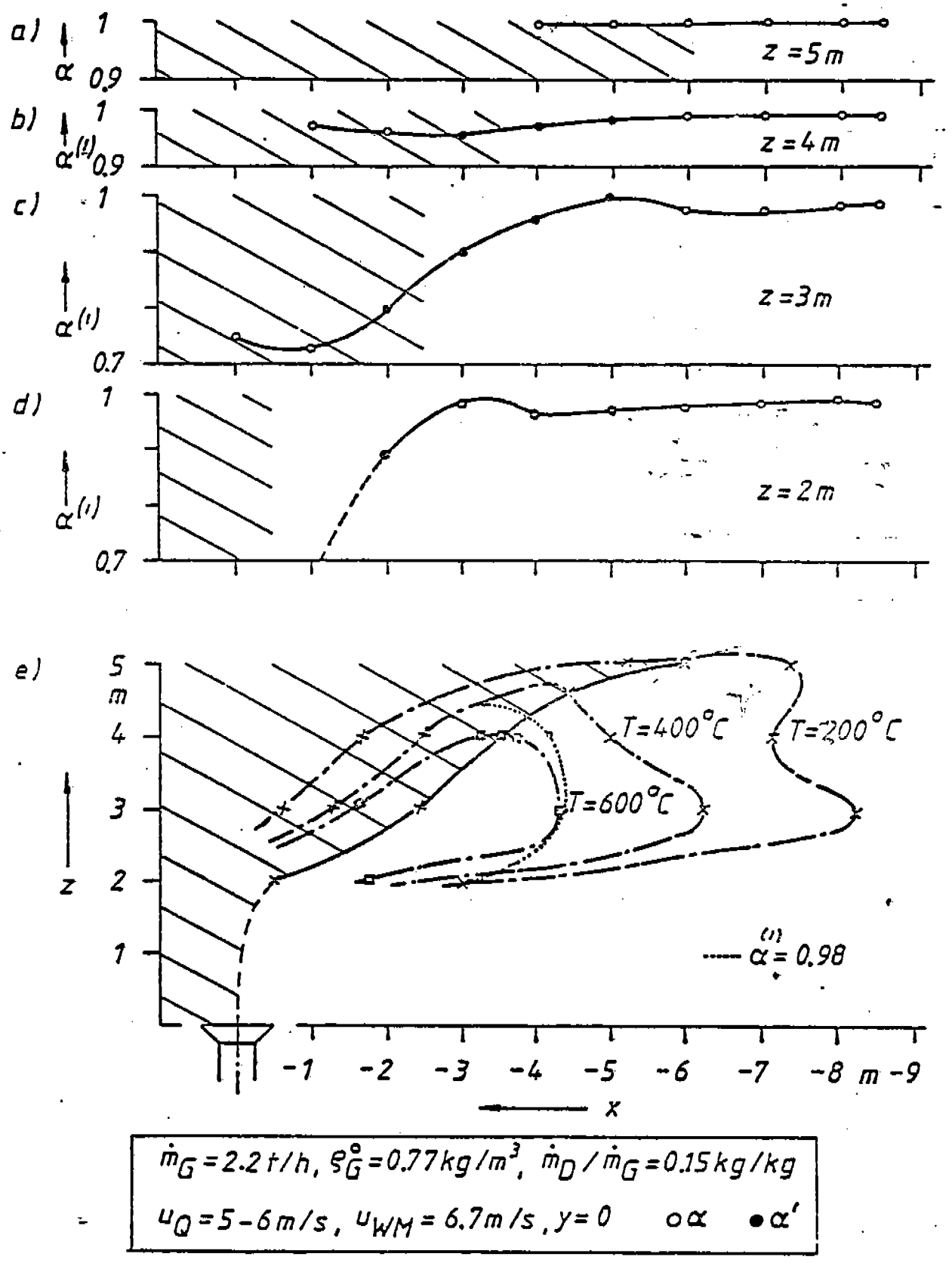

$\dot{m}_G = 2.2\ t/h$, $\varrho_G^0 = 0.77\ kg/m^3$, $\dot{m}_D / \dot{m}_G = 0.15\ kg/kg$

$u_Q = 5-6\ m/s$, $u_{WM} = 6.7\ m/s$, $y = 0$ $\quad o\,\alpha \quad \bullet\,\alpha'$

Fig. 6 - 11: Local burnout degree in and at the edge of a flare flame burning in a cross draft and its flame axis and isotherms of 200, 400 and 600°C.
Test 16.049-.089

fact that the local burnout degree at the flame edge in the lee is complete and that even at a height of z = 5 m no unburned material could be detected in the off-gas.

Fig. 6-11e shows the course of the flame axis and that of the isotherms of 600, 400 and 200°C in the measuring plane. The flame axis was determined as the connecting line of the temperature maxima in the measuring plane. The diagram shows that the course of the flame axis is determined by three forces. In the initial region of the flame, the inertial forces predominate; after that, the effect of the wind produces at first a strong deflection of the flame axis, which toward the end of the flame is weakened by the effect of the up-draft. The dotted line shows the local burnout degree of 0.98. Furthermore, the isotherms above the flame axis lie closer to it than in the region below the axis. This can be attributed to the fact that in the region below the flame axis there is a flow of hot off-gases while in the region above the flame axis the flow consists mainly of fresh air.

In order to determine the local burnout at the end of the flame in very gusty wind, the sampling locations were kept constant for a longer period of time. In Fig. 6-12, the test results have been plotted against the temperature for three measuring points. Departing from the usual procedure, the diagram does not show values averaged over the measuring time but momentary values instead. It can be seen that the local burnout degree calculated from the maximum momentary values is subject to

large fluctuations and shows no dependence on the temperature. This must be attributed to the mode of emission of the organically bound carbon. The volume portion of organically bound carbon shows, in distinction from that of carbon dioxide and carbon monoxide, no dependence on the temperature. The decrease of the carbon dioxide volume portion with decreasing temperature is based on a dilution of the off-gas. The diagram also shows that carbon monoxide is present only at off-gas temperatures above ca. 400°C.

In contrast to the burnout degrees calculated from the maximum momentary values, the local burnout degree averaged over the measuring time was at all three measuring points higher than 0.99.

The test results obtained with flare flames burning under the influence of wind can be summarized as follows:

In flare flames burning in a cross draft, the local burnout degree at the end of the flame is greater than 0.99. Therefore, in soot-free flames a conversion degree higher than 0.99 is attained even in the presence of a cross draft and in sooty flames the emission factor becomes smaller than 0.01. The results obtained with soot-free flare flames agree with those obtained by Becker [32] with model flares in the wind-tunnel. Brzustowski's supposition [20] that in flare flames burning in a cross-draft unburned material is discharged above the flare head has been confirmed by our results. However, organically

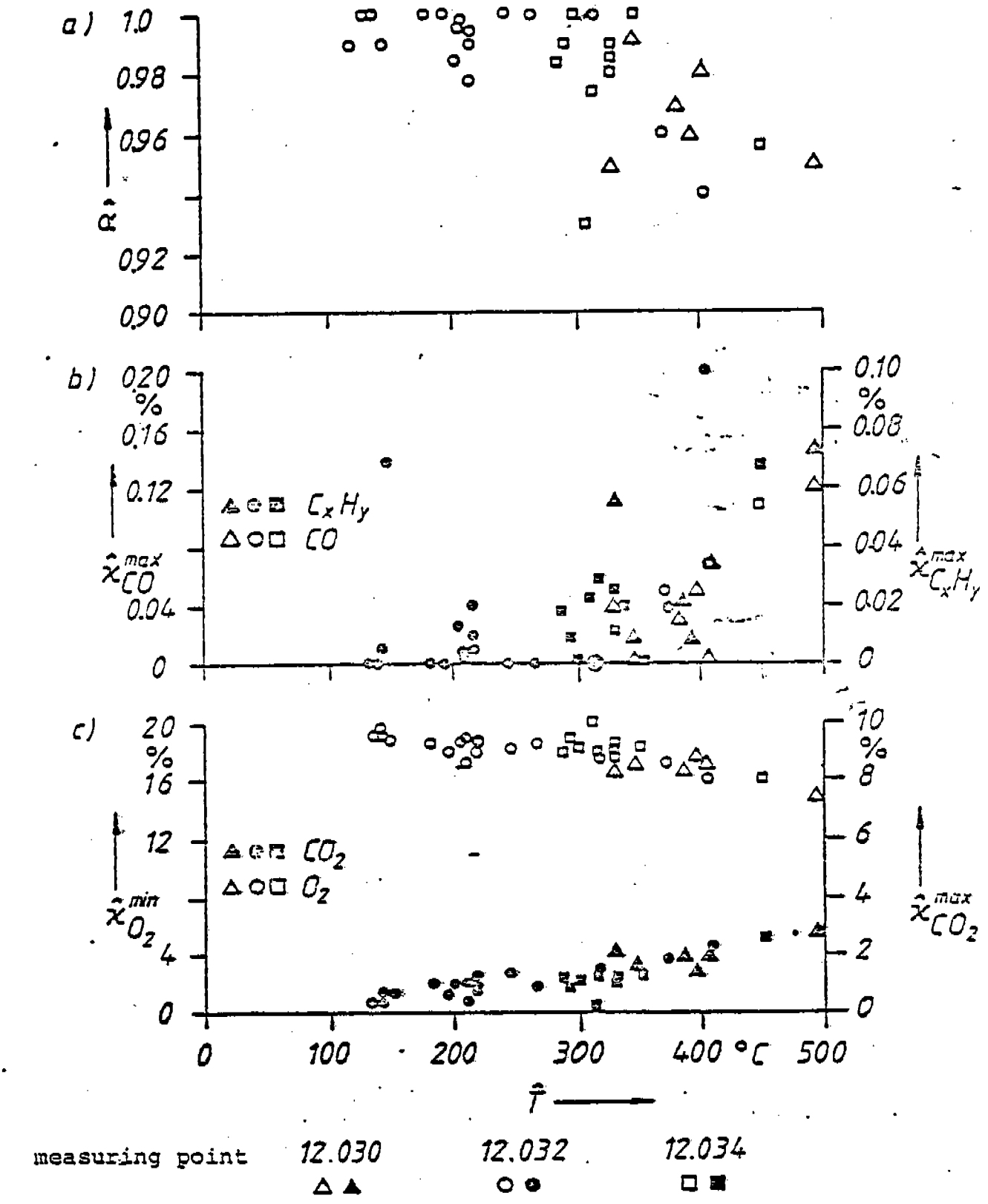

Fig. 6 - 12: Momentary values of measuring components and the local burnout degree in gusty wind calculated from these values Test 12.030-.034

bound carbon discharged above the flare head cannot be counted as having been emitted unburned since it is driven toward the flame and burned. Similarly, no unburned material could be measured in the discharge at the flare-head edge on the lee side. Lee's conclusion [36] that the substance separated from the flame by wind consists predominantly of off-gas has thus been confirmed.

6.5. Effect of the Steam/Gas Ratio on the Degree of Conversion

6.5.1. Effect of the Steam Addition on the Optical Flame Picture and on the Combustion

In flaring, the addition of steam is the only operating variable by which the combustion can be controlled. The effect of steam addition on the flame picture and the flame length is comparable to the admixture of air in a Bunsen flame.

Without the addition of steam, the flare flame is very sooty. It burns as a diffusion flame without premixing. The combustion extends over a wide region which is defined by molecular mixing of fuel with air. The time required for combustion is determined by the molecular mixing of the fuel with air. Because of the soot eddies which form in the flame and because of the relatively low flame temperature, the flame appears optically orange which can be attributed to radiant soot particles.

With the addition of steam, air is introduced into the gas jet before the ignition as a result of the aspiration of air associated with the steam injection and with increasing steam addition the flare flame burns more and more like a diffusion flame with premixing. At the same time, molecular mixing is enhanced by the addition of steam. The color of the flame always changes from orange toward yellow and at the end of the flame no soot formation can be observed any longer. Although soot particles are still formed in the flame - which can be recognized by the yellow color of the flame - the soot formed in the flame is reacted to carbon dioxide and water before it reaches the end of the flame .

If the steam addition is increased further, a double flame with a blue inner cone and a yellow outer cone can be observed. The time required for the combustion is determined for the fully premixed portion of the fuel-air mixture which reacts in a thin layer along the surface of the blue inner cone by the time required for the ignition and reaction. The length of the inner cone is determined by the ratio of the flow velocity to the flame velocity. The mixture flowing between the inner and the outer cone consists mostly of carbon monoxide, hydrogen, carbon dioxide, water and nitrogen; the hydrocarbons are reacted in the premixed flame [12] (p. 98).

If the steam addition is increased still more, the yellow outer cone changes into the blue inner cone and the flame burns as a fully premixed flame. (In spite of the blue light of the flame which is attributable to the glowing of CH- and C_2-radicals, in the following a nonluminous flame is understood to be a flame which consists only of the blue "inner cone"). The length of the flame is greatly reduced during the transition from the sooty to the nonluminous flame.

When after the establishment of a nonluminous flame still more steam is added, no substantial change in the optical flame picture can at first be recognized. Only with a very large increase of the steam addition is it possible to observe inside the blue cone a white cone which consists of water vapor with droplets of condensate. The end of the blue flame becomes slightly reddish, which can be attributed to soot particles.

Steam or water is added not only during the flaring of gases; for example, water is sometimes added to reduce the formation of nitrogen oxides or for the soot-free combustion of high-boiling oils [81]. In spite of the frequent application of water in combustion, the resulting effect cannot be explained in detail. In a survey article - "water addition for practical combustion systems - concepts and applications" - DRYER [81] distinguishes between physical and chemical effects.

Physical Effects. In the combustion of water-oil emulsions, physical effects appear to be of major importance. With fine dispersion of the water droplets, the latter are occluded in the oil. Upon heating, the enclosed droplets vaporize more quickly than the enveloping oil. The result is a "second atomization" or "micro-explosion" in which many smaller droplets are formed which have a shorter combustion time. This effect in the combustion of droplets which results in an enlargement of the boundary surface between fuel and air can be compared in the burning of gases in flare flames with the breaking up of the fuel balls by steam-air-injection.

Chemical Effects. The flame velocity of laminar hydrogen flames is slowed down by the addition of water and that of stoichiometric methane- and butane-air flames by the addition of steam. There is no logical explanation for this delaying action by water or steam on the flame velocity. The assumption that the addition of water favors the recombination of hydrogen and molecular oxygen and thus reduces the chain branching according to R 4-6

$$H + O_2 \longrightarrow O + OH \qquad \text{R 4-6,}$$

has not been confirmed by kinetic calculations of the methane oxidation which show that the reaction rate of the total reaction is hardly affected by the addition of water. With a 10% substitution of oxygen or nitrogen by water, the oxygen-atom concentration decreases in both cases by approx. 20%, while the concentration of hydroxyl radicals increases by approx. 30% [82]. The flame velocity of carbon monoxide-air flames, on the other hand, is catalyzed by moisture. The catalysis of carbon monoxide oxidation by water can be explained by R4-3 which is considered to be the principal reaction in the oxidation of carbon monoxide to carbon dioxide [54] (p. 36).

$$CO + OH \longrightarrow CO_2 + H \qquad \text{R 4-3}$$

$$CO + O \longrightarrow CO_2 \qquad \text{R 6-6}$$

$$CO + O_2 \longrightarrow CO_2 + O \qquad \text{R 6-7}$$

It has been mentioned in Sect. 4.1.2. that hydroxyl radicals are involved in the oxidation of soot particles. As long as little oxygen is present in fuel-rich zones, few hydroxyl radicals are formed according to R 4-6 and R 4-7 so that the reaction of hydrogen atoms with water (R 6-8) is the richest source of hydroxyl radicals:

$$H_2 + O \longrightarrow OH + H \qquad \text{R 4-7}$$

$$H + H_2O \longrightarrow H_2 + OH \qquad \text{R 6-8.}$$

Furthermore, hydroxyl radicals are said to have an effect on the formation factors of soot nuclei so that at high concentrations of hydroxyl radicals fewer soot particles are formed [81].

6.5.2. Effect of the Steam/Gas-Ratio on the Flame Length and Comparison of Observed and Calculated Flame Lengths

The effect of the addition of steam on the flame length is shown in Figs. 6-13 where the flame lengths observed by night have been plotted against the steam/gas-ratio. The optical impression of the flame is depicted on the diagram for Flame 1.

It can be seen that as a result of the steam addition the flame is shortened by up to 50%. The reduction of the flame length can be explained by the transition from the turbulent diffusion flame via the diffusion flame with premixing to the fully premixed flame.

Double flames or fully premixed flames are of little significance in flaring. The interest in estimating the length of flare flames is, therefore, limited to diffusion flames, in which case it is above all the maximum possible flame length under full load which is of interest because of the heat radiation.

In Table 6-2, the flame lengths observed in our own tests are compared with those which were calculated according to formulae proposed in the literature with emphasis on "elevated flares" for estimating the length of flare flames. The operating data of the flare are shown on Lines 2 to 9.

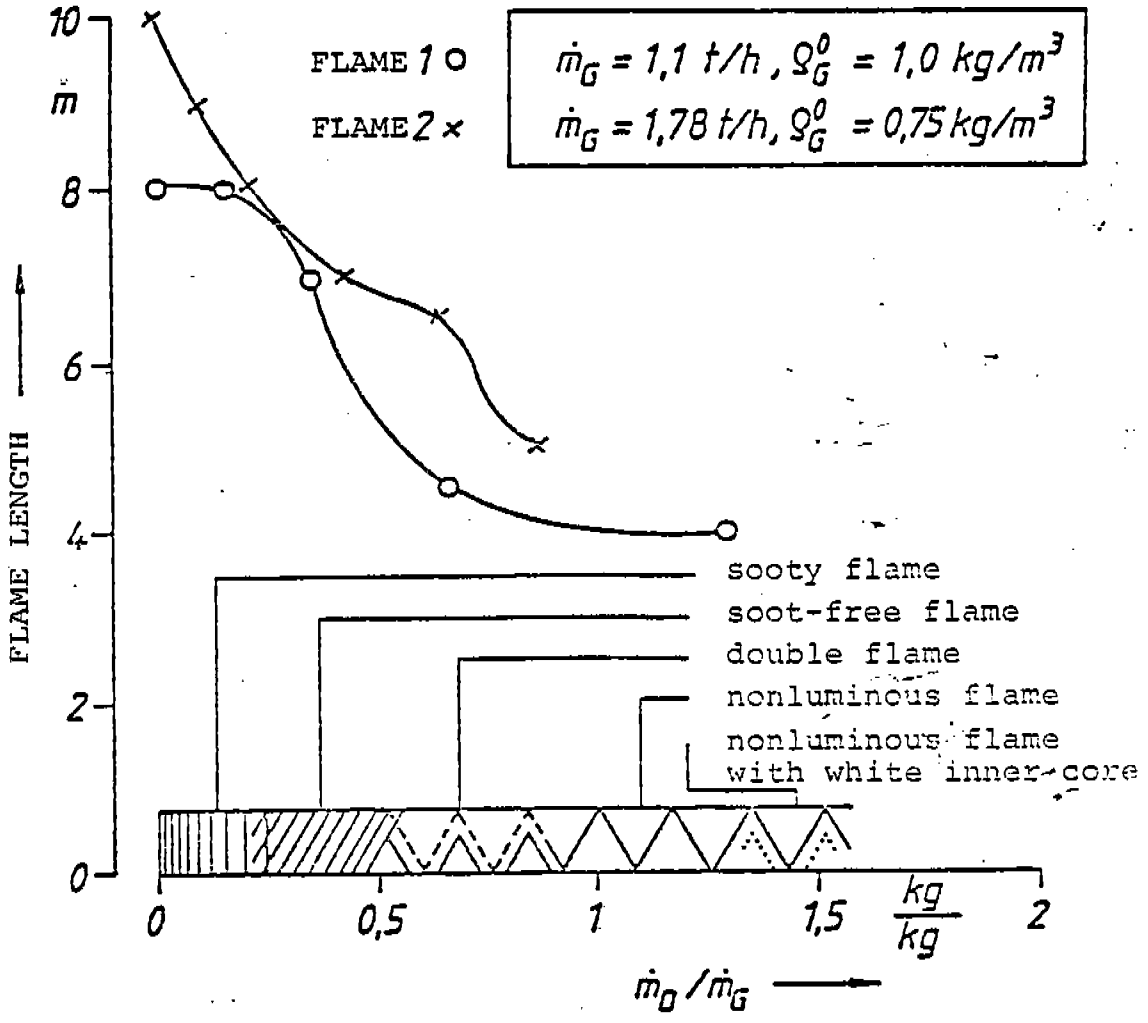

Fig. 6-13. Observed flame lengths as a function of the steam/gas ratio.
Tests 11 and 13

Line 10 shows the lengths of flames observed in our own tests which burned without steam addition and in the absence of wind.

The flame length on Line 11 results from a proposal by KENT [38] (1964) according to which it is 100 times the

diameter of the flare head. Formulas which give the flame length as a multiple of the diameter of the burner are common for estimating the length of flow-controlled flames.

On Line 12, the flame lengths calculated according to a proposal by REED [39] (1968) according to G 6-24 are entered. REED fails to give an explanation of the method of calculation suggested by him.

$$L = 5{,}7 \cdot 10^{-3} \frac{\dot{Q}_o}{d^2} \qquad \text{G 6-24}$$

$$\dot{Q}_o = H_o \cdot \dot{m}_G \qquad \text{in GJ/h}$$

d: flare-head diameter in m

L: flame length in m

The relation G 6-25 which gives the flame length only as a function of the incoming heat flow was determined by HEITNER [40] (1970) by regression analysis. He took the required data from the API-Reprint 521 [14] which lists the flame lengths observed at different heat flows.

$$L = 1{,}188 \sqrt{\dot{Q}_u} \qquad \text{G 6-25}$$

$$\dot{Q}_u = H_u \cdot \dot{m}_G \qquad \text{in GJ/h}$$

L: flame length in m

Lee [36] (1977) calculates the length of up-draft flames by expanding known formulas for the spreading of impulse and material in free-jet flames by including up-draft forces (and wind forces). His calculations showed that for city-gas

as the fuel and for Froude numbers smaller than 10^3 the length of flare flames can be calculated according to G 6-26:

$$\frac{L}{d_o} = 16{,}8\ Fr_o^{0{,}2} = 16{,}8 \left(\frac{u_o^2}{g \cdot d_o}\right)^{0{,}2} \qquad \text{G 6-26.}$$

u_o: flow velocity of the flare gas at the flare head in m/s

G: gravitation constant

d_o: flare-head diameter in m

L: flame length in m

The flame lengths calculated with G 6-26 are shown on Line 14.

In comparing the flame lengths, we are struck by the fact that those on Line 11 are always longer than those observed. On the other hand, good agreement can be noted between the observed flame lengths and those calculated according to G 6-24 to G 6-26. The flame lengths calculated according to Lee [36] come closest to those observed.

The reason why the observed flame lengths and those calculated by LEE [36] are comparable is that the composition of the flare gases used here is similar to that of city-gas in which the volume portion of hydrogen is of the order of 44% and that of methane of 22% [12] (p. 16). The transfer factors which describe the exchange of impulse and material and which enter into LEE's calculations thus become comparable.

Formulas like those proposed by KENT[38] which give the flame length as a multiple of the flare diameter are bound to

give flames which are too long since they neglect the effect of the up-draft.

Table 6-2: Observed and calculated flame lengths

1	Test No.		13.001-.020	14.017-.021	11.142-.147
2	$\dot{m}_G$	kg/h	1780	940	1100
3	ϱ^o_G	kg/m^3	0.75	0.72	1.0
4	u_o	m/s	21	11.5	9.8
5	Fr_o		22?	68	48
6	H_u	kJ/kg	31700	30130	42170
7	H_o	kJ/kg	35650	34100	47050
8	$\dot{Q}_u$	GJ/h	56.37	28.32	46.39
9	$\dot{Q}_o$	GJ/h	63.47	32.10	51.75
10	L*	m	10.5	8	8.5
11	L /38/	m	20	20	20
12	L /39/	m	9	4.5	7.4
13	L /40/	m	8.9	6.3	8.1
14	L /36/	m	10	8	7.5

L: flame length extending from the entrance of the flare tube into the mixing chamber
(see Fig. 5-3a, p.5-9)

The length of the flare flames is still affected by the forces of the up-draft even in operation under full load. For example, for a flare head which is integrated into the refinery operation and whose design data are known (d_o = 0.6 m, $\dot{V}_{max}$ = 110,000 m^3/h at a flare-gas standard density of 0.74 kg/m^3) the Froude number with 2,000 lies even under full load still in a range in which the effect of the up-draft on the combustion cannot be neglected. According to investigations by HESS [83], with Froude numbers smaller than 10^5, the effect of the up-draft on the flame length has to be taken into account.

6.5.3. Examples of the Effect of Steam Addition on the Degree of Local Burnout

The dependence of the degree of local burnout on the steam addition is shown in Fig. 6-14. In this test, the steam/gas-ratio was varied between 0 and 1.1 kg/kg. Samples were withdrawn at heights of 3 and 4 m above the flare mouth.

At a height of 3 m, the degree of local burnout increases from 0.94 in the case of a very sooty flame with increasing steam addition to 1. At the same time, the flame becomes soot-free. In this test, the carbon monoxide was counted at one half each as burned and unburned material, resp., since the sampling site was located upstream of the flame end. At a steam/gas ratio of 0.6 kg/kg, a flame length of 4 m was observed.

At a measuring height of 4 m, no carbon monoxide could be measured in the off-gas at any steam/gas ratio. The degree of local burnout increases with increasing steam addition

and about 0.5 m upstream of the flame end already reaches values of around 0.99.

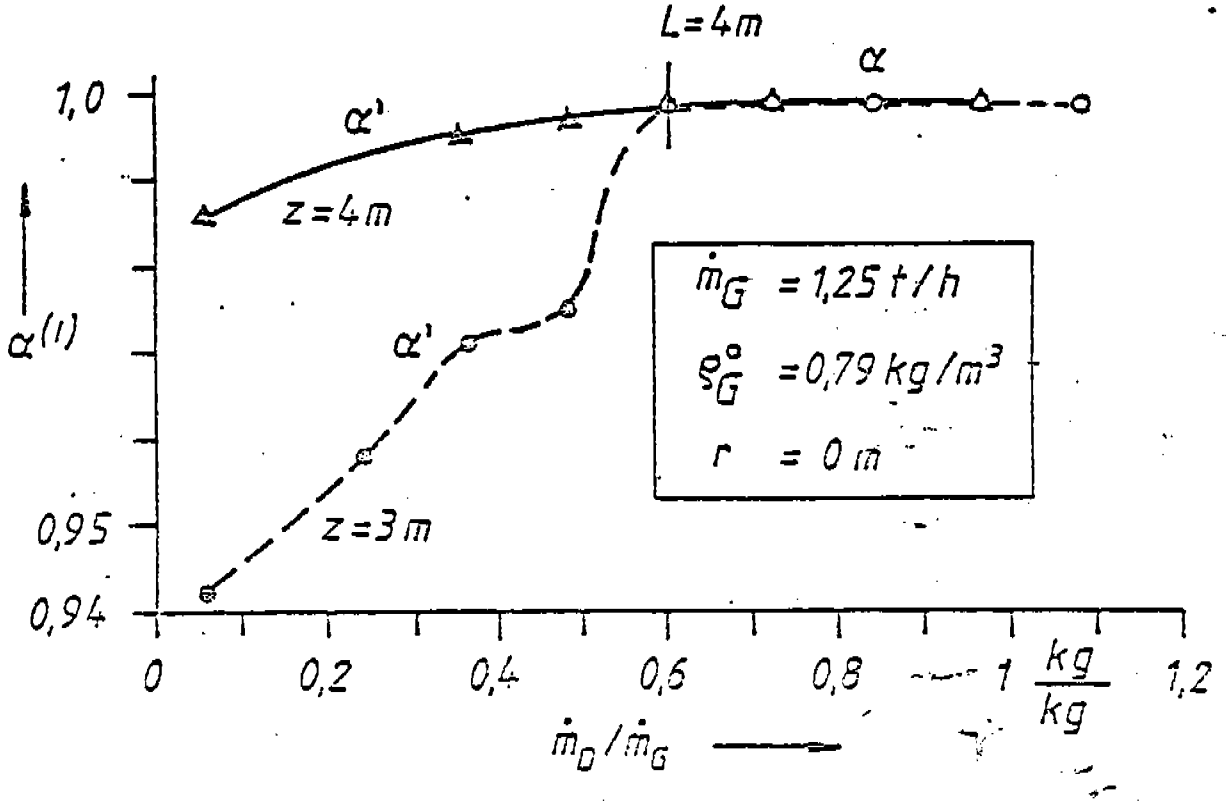

Fig. 6-14: Degree of local burnout as a function of the steam/gas ratio
Test 07.055-.077

The reason for the improved combustion in flare flames with steam addition has thus far been seen both in the fact that the steam addition has a favorable effect on the equilibrium of the heterogeneous water-gas reaction (R 6-9) [45]

$$C + H_2O \longrightarrow CO + H_2 \qquad \text{R 6-9,}$$

and also in the fact that the jet impulse is enhanced by the steam addition and that the gas jet aspirates more air [17]. On the other hand, the results of our own tests reported in the following permit the conclusion that it is above all the molecular mixing which is promoted by the steam addition.

Table 6-3 shows the oxygen volume portions which were measured at and above the flare mouth at different steam/gas ratios. It can be seen that without steam addition, oxygen is present at the flare mouth and that the oxygen decreases even with increasing steam addition. This can be explained by the fact that because of improved molecular mixing more oxygen is consumed.

Table 6-3. Oxygen volume portions at and above the flare mouth at different steam/gas ratios

Test		16.091-.095				17.047-.051		
$\dot{m}_G$	t/h	2,2				1,72		
$\frac{\dot{m}_D}{\dot{m}_G}$	$\frac{kg}{kg}$	0		0,11		0	0,17	0,35
z	m	0	1	0	1	0,5	0,5	0,5
χ_{O_2}	%	8,2	12	5,3	6	6,8	3,8	2,4

The large oxygen volume portion shows that in flare flames, molecular mixing lags considerably behind macroscopic mixing already at the beginning of the flame. According to LENZE [52], the segregation which describes the difference between the mixture and the burnout is proportional to the

size of the vortex and indirectly proportional to the rate of fluctuation.

Without steam addition, fuel and oxidant drift downstream in separate cells and the mixing is determined solely by the exchange variables of impulse and material. With steam addition, on the other hand, the inclination of the steam-air jet toward the fuel jet causes the break-up of the fuel cells so that the molecular mixing of fuel with air and steam is promoted. As a consequence, the number of zones in which a reaction is possible, if the activation energy is available, is enlarged.

Aside from the comminution of the fuel balls, the steam addition also raises the flow velocity of the fuel-air off-gas jet.

Fig. 6-15 shows the flow velocity under operating conditions in the flame axis as a function of the steam/gas ratio for 2 fixed measuring points. The flow velocity increases with increasing steam addition.

(The drop-off of the velocity at steam/gas ratios between 0.1 and 0.2 kg/kg cannot be clearly explained. During the tests it was observed that at these steam/gas ratios two vortex paths rotating in opposite directions are sometimes formed in the flame, such as can also be observed in flue gas plumes).

Since the degree of turbulance is largely independent of the Reynolds number, the fluctuation variable increases with increasing velocity; impulse- and material exchange are accelerated. This promotes molecular mixing and reduces the

segregation so that the zones of possible reactions are increased.

Due to the improved molecular mixing with steam addition, the heat generation takes place in a smaller flame volume which - also because of the change in the radiant intermediate products - leads to a hotter flame.

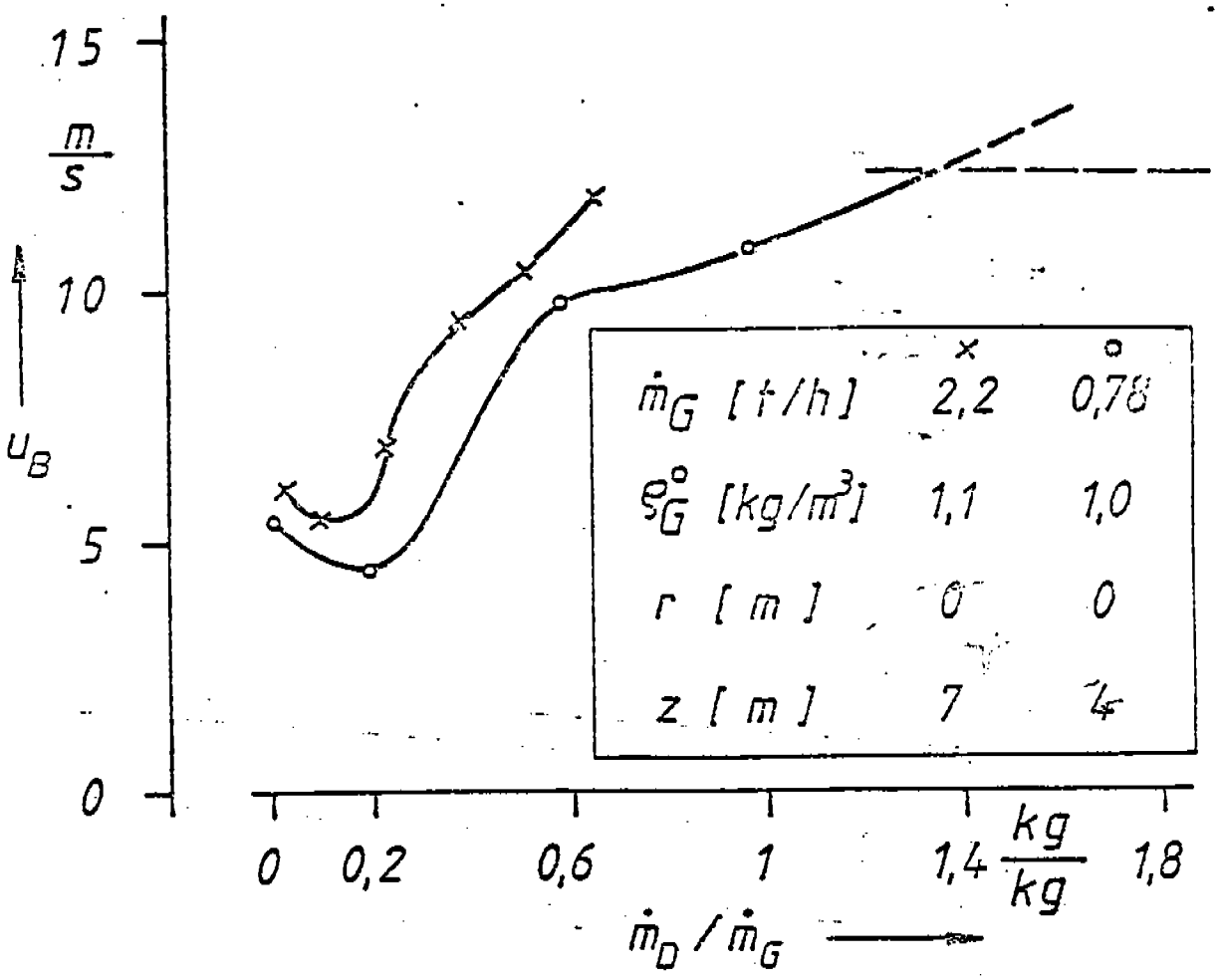

Fig. 6-15. Effect of steam/gas ratio on off-gas velocity.
Tests 08.127-.132 and 08.167-.172

Fig. 6-16 shows the temperature downstream (and upstream) of the end of the flame. The steam/gas ratio is the parameter.

The end of the flame which is marked on the diagram by L was identified by a local burnout degree of 0.98.

It can be seen that because of the improved molecular mixing due to the steam addition, the flame becomes hotter. Therefore, in the zones of possible reaction the required energy of activation is more likely to be available than in the case of flames without steam addition in which possible reaction zones do not occur until farther downstream where, however, due to the large volumes of ballast-air the temperature drops off more and more.

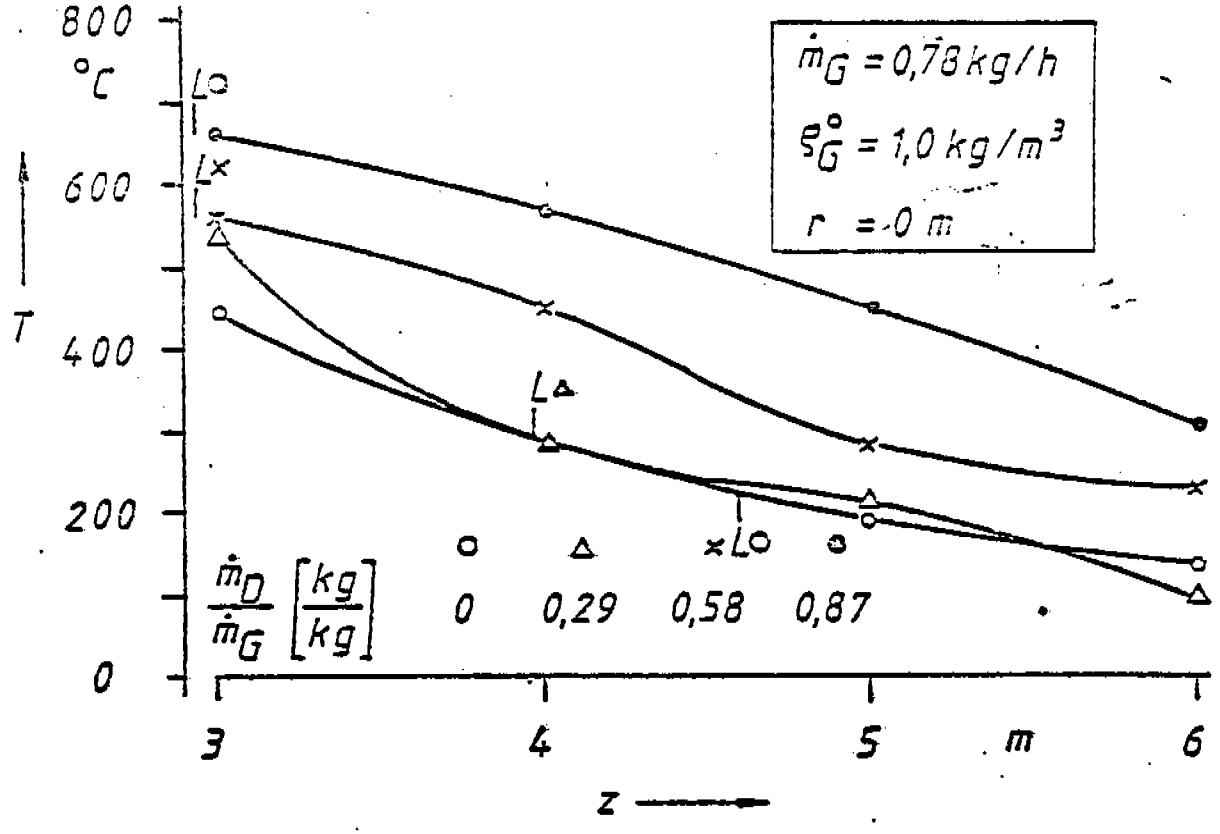

Fig. 6-16. Temperature downstream (and upstream) of the end of flame L as a function of the steam/gas ratio. Test 08.133-.151

This has also been confirmed by the results of the tests in which the components and also the temperatures at different steam/gas ratios were measured along the axis of the flame.

Of this, Fig. 6-17 shows the volume portions of oxygen and the temperatures. These have been plotted on the diagram against the measuring height. The steam/gas ratio is the parameter. At a steam/gas ratio of 0.17 kg/kg, the flare flame burned with slightly sooty peaks; at 0.38 kg/kg the flame was soot-free, and at 0.52 kg/kg almost nonluminous. The place where the local burnout degree amounted to $a' = 0.99$ is marked by ▽. The absolute values of the oxygen volume portions must be examined critically since no cooled sampling probes were used so that a further reaction of the gas mixture and, therefore, an oxygen consumption in a segment of the sampling line cannot be ruled out. The sample-gas temperature at TR 120 amounted in these tests to 160°C max. (cf. Fig. 5-6).

A comparison of the oxygen volume portions and of the temperatures shows that at the steam/gas ratio of 0.17 kg/kg the oxygen volume portion is the largest and the temperature the lowest. In the almost nonluminous flame, on the other hand, the oxygen volume portions are only near the flare mouth and toward the end of the flame higher than in the soot-free flame.

In the almost nonluminous flame, the temperature maximum is likewise reached only farther downstream than in the other two flames which implies a longer preheating zone since more air and steam must be heated along with the rest. But then

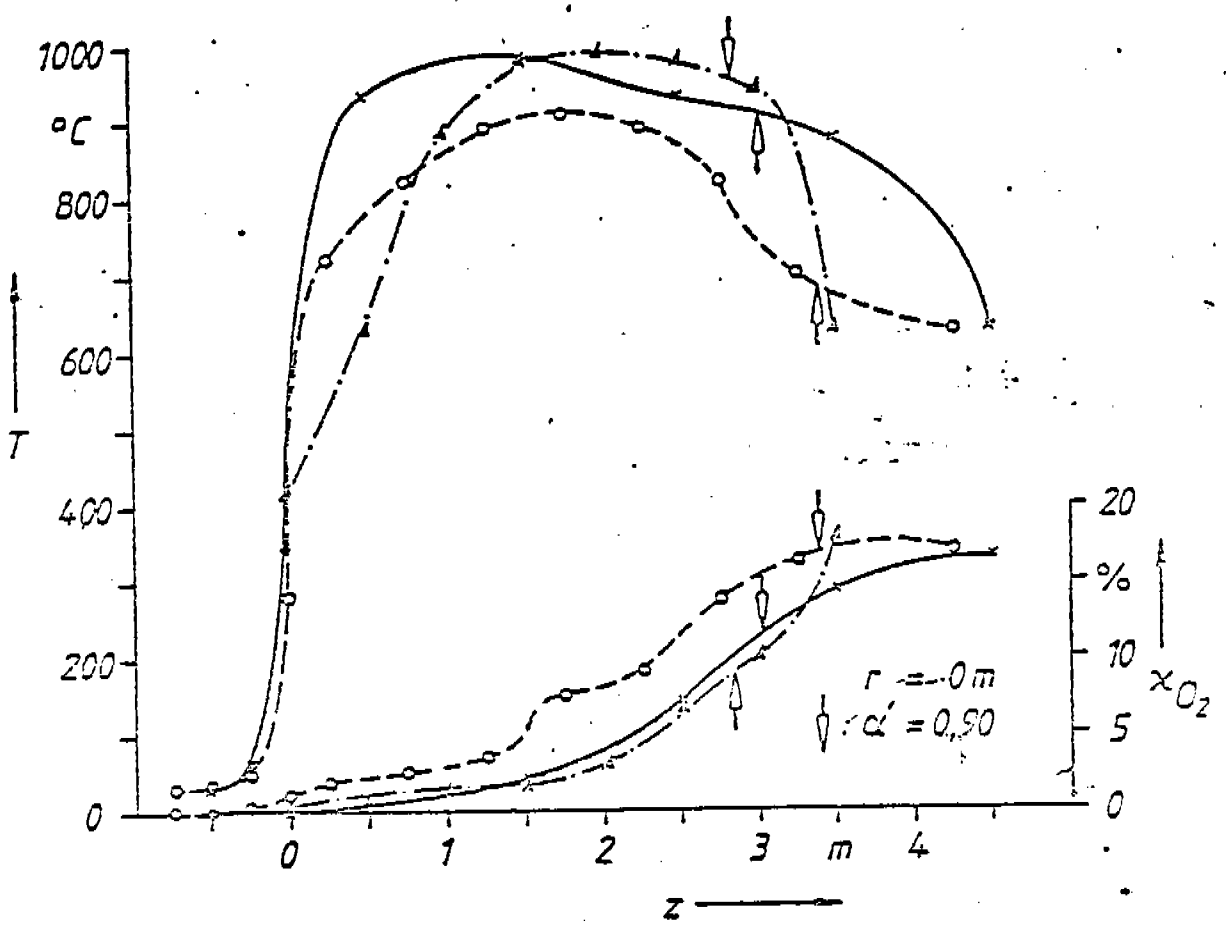

	$\dot{m}_G$ [t/h]	$\dot{m}_D / \dot{m}_G$ [kg/kg]	
o	1,72	0,71	slightly sooty peaks
x	1,57	0,38	soot-free
Δ	1,72	0,52	almost nonluminous

Fig. 6-17. Temperature and oxygen volume portion along the flame axis at different steam/gas ratios.
Test 17.002-.046

the mixing is so efficient that the heat generation due to the reaction and the losses due to radiation and heating of the aspirated air balance each other, which leads to a temperature plateau. Although in the soot-free flame the temperature maximum is reached farther upstream, the heat losses predominate in that case and the temperature drops off. In the flame with slightly sooty peaks, macroscopic mixing predominates over molecular mixing to such an extent that only a relatively low flame temperature is attained.

These test results lead to the conclusion that it is above all the molecular mixing process which is improved by the steam addition. Furthermore, the effect of the steam addition on the course of the chemical reactions is probably slight in comparison with its mechanical and dynamic contributions toward better combustion. Even without steam addition and at low steam/gas ratios which are not sufficient to make the flame soot-free, oxygen is present in the macroscopic mixture. Therefore, the formation of hydroxyl radicals is not limited to the reaction of hydrogen atoms with water (R 6-8) but is also possible according to R 4-6 and R 4-7:

$$H + O_2 \longrightarrow O + OH \qquad \text{R 4-6}$$

$$H_2 + O \longrightarrow OH + H \qquad \text{R 4-7}$$

$$H + H_2O \longrightarrow H_2 + OH \qquad \text{R 6-8.}$$

To investigate the effect of large steam/gas ratios on the emission of unburned fuel by quenching of the flare flame

we increased the steam/gas ratio up to 1.73 kg/kg.

In Fig. 6-18a, the local burnout degree and the temperature, and in Fig. 6-18b, the volume portions of carbon monoxide, carbon dioxide and those of the organically bound carbon have been plotted against the steam/gas ratio. The sampling point was situated in the flame axis which at steam/gas ratios higher than 0.19 kg/kg coincided with the flare axis. The measuring height was 4 m and the flame length observed at a steam/gas ratio of 0.84 kg/kg was 4 m.

The degree of local burnout and the temperature first increase with the steam/gas ratio. A complete burnout is achieved. With further steam addition, the local burnout degree drops off again. As shown by a comparison of the volume portions of carbon monoxide and organically bound carbon, increased amounts of organically bound carbon are discharged due to the quenching of the flame.

Figs. 6-19a and 6-19b show the effect of large steam additions on the temperature and on the volume portions of organically bound carbon and carbon monoxide downstream of the end of the flame. As evident from the diagrams, at large steam/gas ratios the temperature decreases with increasing steam addition while the discharge of unburned material increases. The discharge of unburned material is, even at large steam/gas ratios, restricted to a narrow region around the flame axis (cf. Test 11.107-.11.118).

The increasing steam addition not only promotes molecular mixing but also introduces more steam and air into the flame.

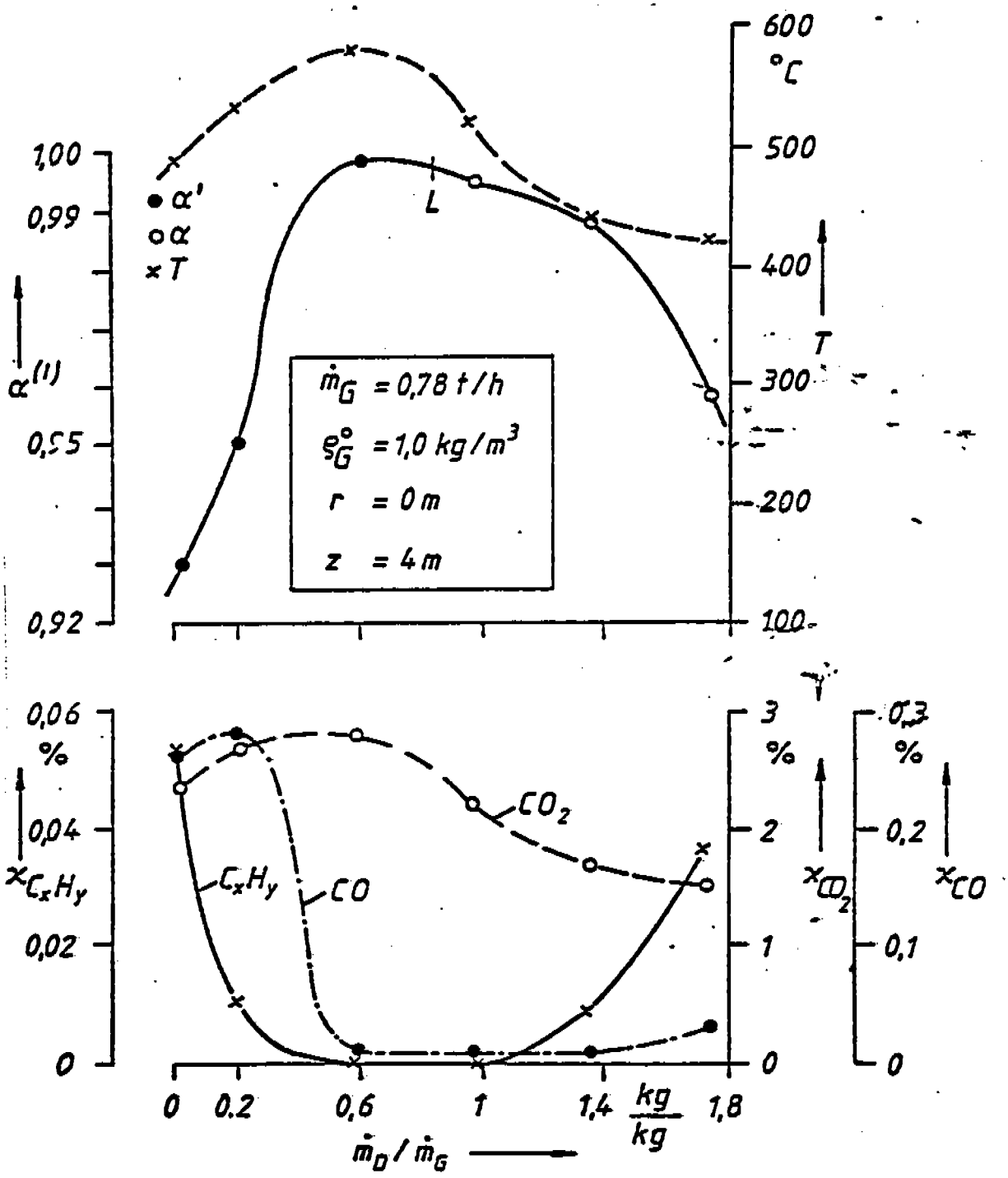

Fig. 6-18. Effect of large steam/gas ratios
a) on the local burnout degree and the temperature
b) on the volume portions of organically bound carbon, carbon monoxide and carbon dioxide
Test 08.167-.172

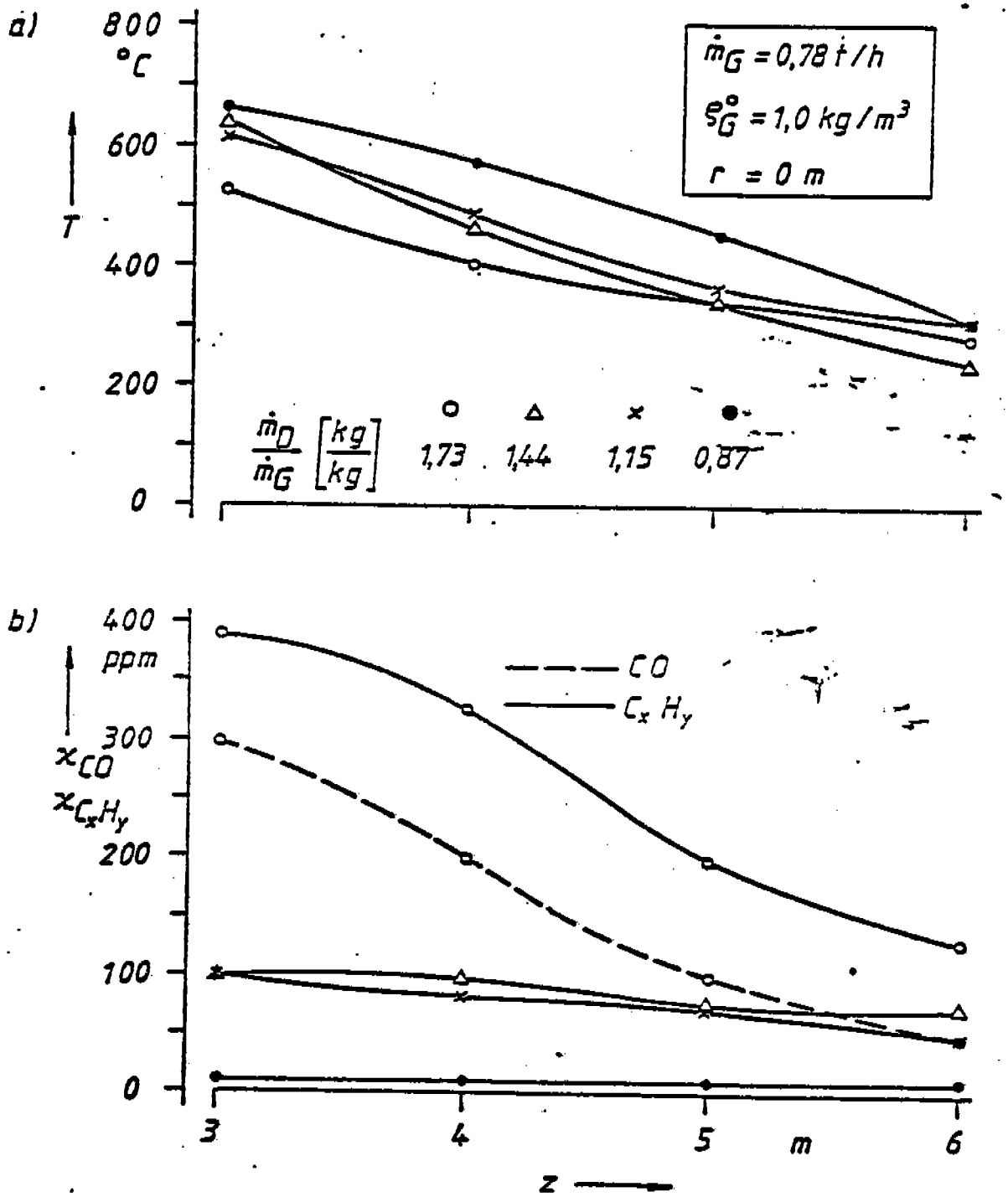

Fig. 6-19. Effect of large steam additions on the temperature and on the volume portions of organically bound carbon and carbon monoxide downstream of the end of the flame.
Test 08.148-.166

Air and steam which after adequate mixing are present beyond the measure necessary for stoichiometric combustion reduce the flame temperature since they have to be heated up with the rest. Therefore, the probability that in zones of molecular mixing the required energy of activation is available, is reduced. Added to this is the fact that particular zones may even be diluted below the ignition limit.

A discharge of unburned fuel caused by a quenching of the flare flame has also been reported by STRAITZ [47] who does not, however, cite any figures. Our own test results show that even with an excessive steam addition the drop in the degree of conversion is less than 5%.

However, steam/gas ratios many times higher than necessary to make the flame soot-free rarely occur in the operation of a flare.

6.5.4. Burnout of Detached Balls

The high degree of segregation in flare flames may lead to situations where fuel drifts downstream in balls which are not ready for reaction until near the end of the flame where they can still be ignited. Due to heat generated during the combustion, the ball receives an additional lifting force which may cause the ball to detach itself from the flame and to burn independently.

Observation has shown that the detachment of balls occurs very irregularly and that sometimes the entire end of the flame

is detached. The frequency of ball separation increases with increasing steam addition.

In the tests, the ball separation was observed from the crane operator's cabin. As soon as a ball hit the sampling orifice, which happened about 100 times during the almost 100 hours of testing, this event was reported to the instrument center and noted on the recording strip of the FID. During these events, no organically bound carbon was measured, not even in the small measuring ranges (measuring range down to 10 ppm CH_4 and 100 ppm CH_4, respectively).

However, these test results do not permit the conclusion that no organically bound carbon is emitted by detached balls. Because of the geometry of the sampling probe, it was impossible to capture an entire ball but always only a portion of it. It can, therefore, not be ruled out that the captured amount of organically bound carbon was too small to be recognized.

For this reason, it is first estimated whether, during the passage of a still unignited ball through the sampling aperture, this event could have been recognized on the recording strip of the FID. To this end, the following assumptions are made.

The original fuel volume of a spherical ball is supposed to amount to 2200 and 60 cm^3, respectively, with a proportion of organically bound carbon of 0.8 kg C/m^3. The ball is heated to 600°C without a reaction and as a result, a volume of 7035 or 190 cm^3 and a diameter of 23 or 7 cm, respectively, is obtained.

The mass concentration of organically bound carbon in this ball is calculated at 250 g C/m^3. At a velocity of 6 m/s, the ball is for a period of maximally 0.038 or 0.012 s in the area of the sampling aperture. At a suction capacity of 1 l/s, 38 or 12 ml is taken from the ball as a sample in which are contained 9.5 or 3 mg C, respectively. This amount is offered at Q 200 (cf. Fig. 5 - 6) in a kind of needle function.

In Sect. 5.3.3., it had been shown that amounts of 8.5 mg C in a measuring range of 100 ppm CH_4 and amounts of 1.5 mg-C in a measuring range of 10 ppm CH_4 were still recognized.

A comparison shows that a ball which had not yet been ignited could, depending on ball size and measuring range, just barely be recognized. However, the amount of organically bound carbon in a ball decreases very rapidly after the ignition so that balls in which the ignition had already set in were unable to produce a measuring signal.

Detached balls do not always burn out completely. This can be recognized by the fact that they tend toward soot formation. The combustion is presumably broken off because the ball has become mixed with too much air and has, therefore, been cooled below the ignition temperature.

On the assumption that the large balls burn out only by one half and that the separation frequency is 1/s, we obtain an emission flow of 4 m^3/h of unburned material. At a flare gas throughput of 1000 m^3/h, this would result in a lowering of the degree of conversion by 0.004.

The above-assumed fuel volume of 2200 and 60 cm^3 were estimated from the observed diameters of detached and burning - that is, mixed with air - balls which ranged between 0.3 and 1 m. To this end, we made use of the relation G 6 - 27 reported by Fay and Lewis /85/ for the maximum diameter of burning balls as a function of the original fuel volume.

$$d_{max} = 7.7\, V^{1/3} \qquad G\ 6\text{-}27$$

d_{max} : maximum diameter in cm

V : original fuel volume in cm^3

They studied the size and burning time of methane - ethane- and propane balls which were enclosed in a soap bubble before being ignited.

The results of the tests by Fay and Lewis /85/ can be applied to the ball separation from flare flames only with qualifications. The balls used in their tests were ignited at room temperature and without initial impulse. This means that the exchange variables for these balls and for those from flare flames are different.

6.6. Effect of the Flare Gas Composition on the Degree of Local Burnout

6.6.1. Effect of the Flare Gas Composition on the Combustion

The composition of the flare gases varies very widely, ranging from hydrogen-rich gas all the way to liquid petroleum

gases. The effect of the gas composition on the combustion can be recognized by the tendency toward soot formation of the flame.

The C/H ratio is usually chosen as a measure of the tendency toward soot formation. However, in addition to this, the molecular structure and the state of mixing of the flame are also of significance. In diffusion flames, the tendency toward soot formation in the case of the paraffins increases slightly with increasing C-number while in the case of the olefins it decreases with increasing C-number. Unsaturated hydrocarbons tend more toward soot formation than saturated ones, and branched hydrocarbons more than straight-chained ones [86].

In Sect. 4.1.2. it had been shown that even in the case of methane the fuel oxidation proceeds by way of a large number of intermediate products and that unsaturated hydrocarbon radicals are soot precursors. The combustion of hydrocarbons with higher C-numbers becomes more complicated because of the instability of the higher alkyl radicals and the large scattering of the secondary products.

According to Fristrom and Westenberg [49], in oxygen-rich flames saturated hydrocarbons are broken down according to R 6 - 11:

$$C_mH_{2n+2} + OH \rightarrow H_2O + C_mH_{2n+1} \rightarrow C_{m-1}H_{2n-2} + CH_3 \qquad R\ 6\text{-}10$$

$$C_mH_{2n+2} + H \rightarrow H_2 + C_mH_{2n+1} \rightarrow C_{m-1}H_{2n-2} + CH_3 \qquad R\ 6\text{-}11.$$

The radicals formed by splitting off one hydrogen atom split off one methyl radical with the formation of an olefin.

The reaction sequence according to R 6 - 11 can also proceed without an oxidant. When the reaction starts as in R 6 - 10, no molecualr mixing with oxygen need any longer be present after the splitting off of the hydrogen atom. When oxygen and hydrocarbons are not mixed molecularly, the synthesis of polyacetylenes is more likely with hydrocarbons of large C-number than with methane where such a synthesis is only possible after recombination of methyl radicals.

6.6.2. Example of the Effect of the Flare Gas Composition on the Local Degree of Burnout

The testing chart (Fig. 5 - 1) showed that for the tests usually flare gases with standard densities between 0.5 and 1.2 kg/m^3 were available. Furthermore, a high proportion of hydrogen and a low proportion of unsaturated hydrocarbons was typical for all the flare gases (cf. Appendix 1, Sheet 1).

Although the tendency toward soot formation is related to the fuel composition, the test results obtained thus far showed that the degree of conversion in soot-free flare flames and the emission factor in the case of sooty flames (see Sect. 6.1., p. 6-5) does not depend on the composition of the flare gas. This has also been confirmed by the test results with the heaviest flare gas used. In this test, the standard density of the flare gas amounted to 1.86 kg/m^3, with the C_3+ portion accounting for more than 65%.

The local degree of burnout in a horizontal measuring plane with this flare gas is shown in Fig. 6 - 20. The flare gas mass flow was of the order of 2.2 t/h and the steam/gas ratio necessary to get rid of the soot was 0.37 kg/kg. The measuring height was by day adjusted optically to match the end of the flame. The consequence was that the measuring plane was situated upstream of the analytical end of the flame. The analytical end of the flame is called by Lee [36] the place where there is a carbon monoxide volume portion of 0.1%. In this test, the maximum carbon monoxide volume portion amounted to 0.21% at a temperature of 555°C.

On the illustration, the local degree of burnout is presented in the form described in Sect. 6.4.2. It can be seen that the local burnout degree was only at a few measuring points smaller than 0.99, which was mainly due to the carbon monoxide volume portion. Because of the still relatively high temperature of the combustion gases it can be assumed that the carbon monoxide is still reacted to carbon dioxide downstream of the measuring plane. In that case, a local burnout degree higher than 0.99 is obtained for all the measuring points.

As shown by the test results, the flare gas composition in the range studied here has no effect on the degree of conversion in soot-free flare flames and on the emission factor for carbon bound in gaseous form and non-atmospheric gases in the case of sooty flare flames. The flare gas composition

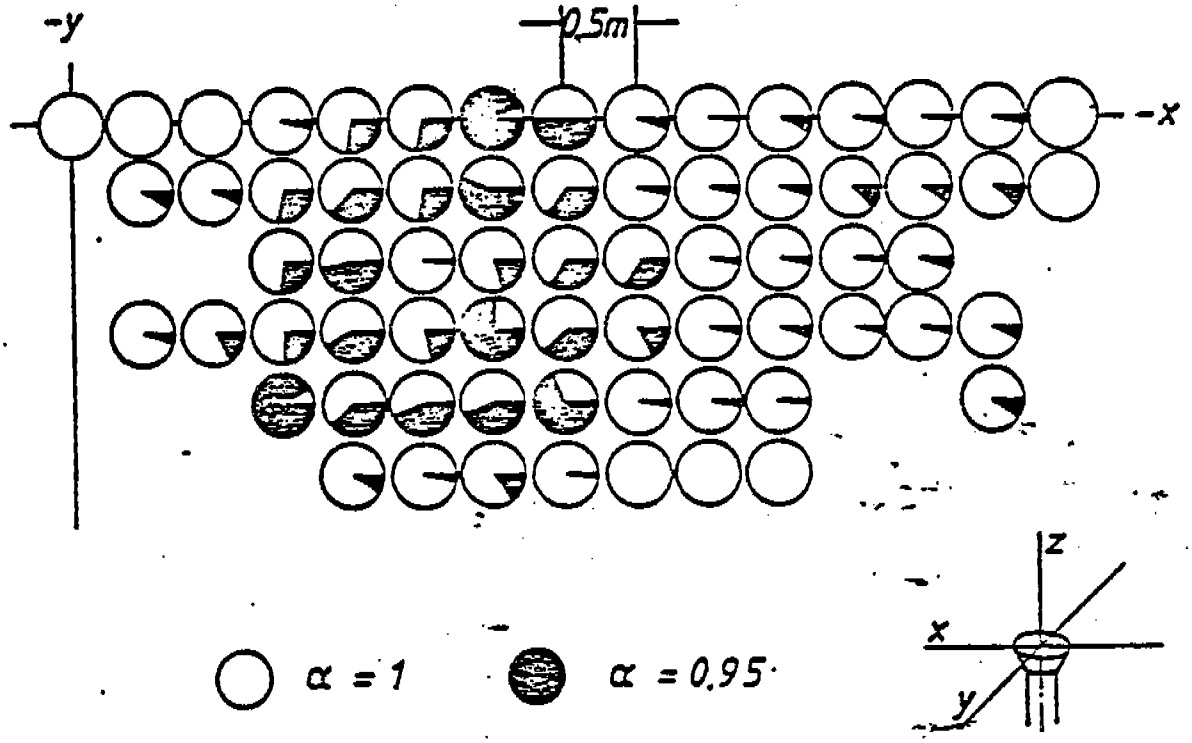

$\dot{m}_G = 2.2\ t/h$, $\varrho_G^\circ = 1.86\ kg/m^3$, $\dot{m}_D/\dot{m}_G = 0.37\ kg/kg$

$u_Q = 2 - 2.5\ m/s$, $L = 6\ m$, $z = 5\ m$

Fig. 6 - 20: Distribution of the local burnout degree in a horizontal plane in the case of a flare flame burning with heavy flare gas in a cross draft Test 02.001-.086

is, however, a critical factor in determining the steam addition necessary to eliminate the soot.

Thus, for example, with the same flare gas mass flow, but with a standard density of 1.1 kg/m^3 (see Test 08.130-.131) the flame was already soot-free at a steam/gas ratio of 0.2 kg/kg while at a flare gas standard density of 1.86 kg/m^3 a steam/gas ratio of 0.37 k/kg was necessary for eliminating the soot.

The volume of combustion air required per standard m^3 of flare gas, the C/H ratio and the tendency toward soot formation increase with increasing gas density. Because of the larger number of intermediate products with increasing C-number of the fuel, a more intensive molecular mixing is necessary for its degradation than in the case of methane because the intermediate products formed during the combustion can be burned further only after molecular mixing with the oxidant. At the same mass flow, the flow velocity and therefore the fluctuation variable becomes smaller with increasing gas density so that the molecular mixing becomes poorer. As a consequence, the molecular mixing necessary for soot-free combustion must be further promoted. This is accomplished by increasing the steam addition.

6.7. Emission Factor for Soot in the Case of Sooty Flare Flames

With elevated flares it can be noted that in the flaring of gases whose output could not be anticipated the flame is, after the start-up, at first sooty until the steam necessary for soot-free combustion is added. The addition of steam is not automatic, but is controlled manually from the control room.

Although the specification of a safe emission factor would be desirable, this is not possible. The optical impression of the sooty flame cannot be judged objectively as, for example, the smoke plume of coal-fired installations according to Ringelmann [87].

In the experiments with the test flare it was found that depending on the angle of view and the distance of the observer the same flame can be rated from sooty to very strongly sooty.

The impression conveyed by a sooty flare flame depends on the soot mass concentration, the size and distribution of the particles in the soot plume, the background and also the layer thickness. It is, moreover, intensified with increasing distance of the observer from the flame. Since the layer thickness of the soot plume of flare flames, even at a favorable angle of view, is of the order of several meters, it is very easy to gain the impression that the flame is very sooty.

In the tests, a determination was made of the soot mass concentration in the off-gas of a sooty flame (cf. Appendix 7, A.7-3). The flare gas mass flow amounted to 1.9 t/h and the flare gas standard density to 1.0 kg/m^3. No steam was added.

As the point of sampling we chose the streamer which was optically most sooty. Therefore, because of the fluctuation of the flame due to cross drafts, the point of sampling had to be changed several times. The suction rate was adjusted as closely as possible to the off-gas velocity in order to at least approach isokinetic sampling.

The test results have been summarized in Table 6-4. Line 1 shows the sample number and Line 2 the duration of sampling. Lines 3 to 5 contain the values of the temperature and of the volume portions of carbon dioxide and oxygen, all averaged over the sampling time. The carbon monoxide volume portion in the

Table 6 - 4: Soot mass concentration in the off-gas of a sooty flare flame
Test 15 R

Sample number		1	2	3	4
Δt	min	36	12	19	25
T	°C	105	80	160	170
χ_{CO_2}	%	0.4	0.3	0.5	0.5
χ_{O_2}	%	20.3	20.4	19.8	19.9
ϱ_{soot}	mg/m^3	68	23	30	81

off-gas was, even in the maximum values, below the detection limit of 0.01% and organically bound carbon could be measured only sporadically. The soot mass concentrations are listed on Line 6.

There is a surprisingly small mass concentration of soot with values between 20 and 80 mg/m^3. In this case, however, it is necessary to consider also the high oxygen volume portion and the dilution resulting from it. An estimate of the soot mass concentration in stoichiometric combustion via the oxygen volume portion leads to soot mass concentrations between 400 mg and 1.6 g/m^3. The large scattering of the soot mass concentration is presumably due to the fluctuation of the flame.

The local burnout degree defined by G 6-27

$$\alpha = \frac{\rho_C(CO_2)}{\rho_C(CO_2) + \rho_C(CO) + \rho_C(C_xH_y) + \rho_{soot}} \qquad G\ 6\text{-}27,$$

gives values between 0.97 and 0.98 which would correspond to an emission factor for soot of 0.03. ($\rho_C(CO)$ and $\rho_C(C_xH_y)$ were practically equal to zero.)

However, it should be pointed out once more that it is impossible to specify an emission factor for soot in flare flames and that the values cited here should be accepted for orientation and not as binding. Added to this is the fact that the sooting of the flare flame in the event flare gas is produced as a result of controllable operating difficulties in the refinery should be confined to the start-up of the flare flame. The length of time during which the flare flame is sooty is, therefore, short in comparison with the total time during which the flame burns soot-free.

6.8. Mass Concentration of Nonatmospheric Gases at the End of the Flame

In installations emitting nonatmospheric substances, the lawmaker limits not their mass flow but their mass concentration.

According to TA-Luft Nr. 3.2.1.2., "Installations destined to eliminate completely or partially other waste products by combustion," Pt. e,"the emissions of carbon in the combustible

organic substances must not exceed 50 mg/m^3 (f), based on a volume content of oxygen of 11%."

Basing the mass concentration on an oxygen volume portion of 11% is appropriate insofar as quantities of air fed into a system of the installation in order to dilute or cool the off-gas are not considered or are treated equally in the determination of the mass concentration (TA-Luft No. 2.1.3.).

In the case of flare flames, the mass concentration should not be based on a fixed oxygen volume portion since the aspirated air cannot be classified as dilution air.

Fig. 6 - 21 shows the oxygen volume portions and the mass concentrations of organically bound carbon in moist off-gas which were measured in the flame axis upstream and downstream of the end of the flame at different gas mass flows, steam/gas ratios and flare gas standard densities. The flame lengths observed at right are marked with L. It can be seen that the oxygen volume portion (upper half of diagram) at the end of the flame lies far above 11%, irrespective of the operating conditions of the flare. The diagram further shows that the mass concentration of organically bound carbon (lower half of diagram) has even without steam addition - and, therefore, with a sooty flame - dropped at the end of the flame to values smaller than 50 mg/m^3.

In the case of sooty flames, the low mass concentration of hydrocarbons at the end of the flame may be due to their conversion to soot and/or to their sorption on soot. Nor can in

this regard a reliable statement be made on the basis of the known literature.

It can, however, be assumed that the fuel portion which is neither oxidized nor converted into soot is small. The formation of soot takes place in the pyrolysis zone at temperatures between 600 and 900°C. Yet this temperature is characteristic for flare flames (cf. Fig. 6 - 17). Added to this is the fact that the dwell time of the gases in this temperature range is around one second so that with poor molecular mixing a conversion to soot is more probable than a sorption on soot.

The low mass concentrations of organically bound carbon at the end of sooty flames measured in our own tests are in contradiction with those measured by Straitz [10] who reports for hydrocarbons volume portions between 200 ppm and 5.2% without naming a reference hydrocarbon. Since he used mainly natural gas in his experiments, it must be assumed that the volume portions relate to methane. However, because of his sampling device and the high temperatures which ranged between 600 and 1000°C, it can be conjectured that he drew his samples not at the end of but inside the flame. This supposition is based on the fact that, for example, at high volume portions of hydrocarbons the volume portions of oxygen ranged between 11 and 15% and those of carbon monoxide always above 100 ppm, the maximum measuring range of the gas analyzer used by Straitz for this purpose. These measurements are also in contradiction with the assertion made by Straitz [47] to the effect that in

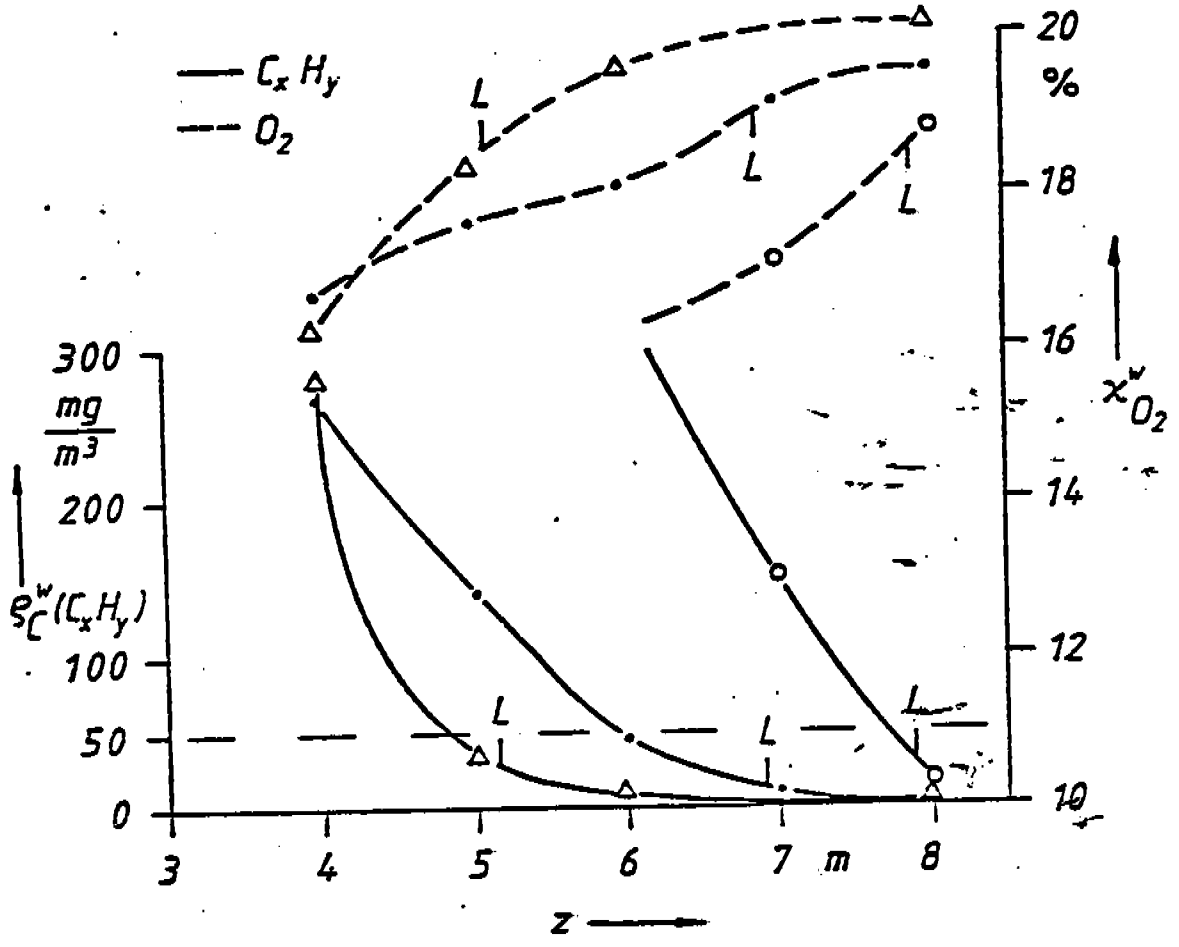

		o	•	△
$\dot{m}_G$	[t/h]	1.1	1.5	2.1
ϱ^o_G	[kg/m³]	1.0	1.1	0.6
$\dot{m}_D/\dot{m}_G$	[kg/kg]	0	0.15	0.29

Fig. 6 - 21: Oxygen volume portion and mass concentration of organically bound carbon upstream and downstream of the end of the flame
Test 06.171-.174, 08.058-.062, 11.142-.145

natural gas flames a conversion of 99% is attained even without steam addition. It has already been shown in Sect. 3 that on the basis of the components measured it is doubtful whether with the test arrangement chosen by Straitz it is possible at all to say something about the degree of conversion.

In our own tests, carbon monoxide could be detected at the end of the flame only at the maximum momentary values with volume portions larger than 100 ppm. As shown in Fig. 6 - 12, only at temperatures above 400°C had the carbon monoxide, even at the extreme values, not yet been completely reacted to carbon dioxide.

Hydrogen is of no significance as an environmental pollutant. For this reason, the hydrogen volume portion was determined only in a few samples. In three off-gas samples drawn approximately 1 m upstream of the end of the flame, the ratios of the volume portions of hydrogen to hydrocarbons amounted to 3 21:1, 3 32:1 and 1 69:1. The volume portions of the individual hydrocarbons were in this case recalculated for methane (Test 16). In another off-gas sample, only hydrogen could be detected with a volume portion of 0.25% (Test 17). These test results are in harmony with the observation that toward the end of the flame it is primarily hydrogen and carbon monoxide which burn out [12].

Hydrogen sulfide and sulfur oxides were not analytically determined in the off-gas. No hydrogen sulfide odor could be noticed in the off-gas. In the literature, an odor threshold

value of, for example, 0.01 ppm has been reported for hydrogen sulfide /88/. It can, therefore, be assumed that hydrogen sulfide is completely reacted to sulfur dioxide/sulfur trioxide whose emission can be calculated from the volume portion of hydrogen sulfide in the flare gas.

6.9. Chemical Composition of the Organically Bound Carbon at the End of the Flame

The organic components differ in significance as far as the environment is concerned. Aliphatic hydrocarbons are of interest mainly when they participate in photochemical oxidation processes. Alkanes and alkines are not classified as photochemically reactive [90]. Alkenes and aldehydes, on the other hand, are determining factors in the formation of photooxidants [89] so that they are of greater significance as pollutants than the alkanes and alkines.

In Figs. 6-22 a to c, the ratios of the volume portions of the hydrocarbons in the off-gas are compared with those in the flare gas. The volume portion of the hydrocarbons determined by gas-chromatography was based on the methane portion of the same sample:

$$\psi_{C_mH_n,CH_4} = \frac{\chi_{C_mH_n}}{\chi_{CH_4}} \qquad \text{G 6-28.}$$

The concentration ratios in the off-gas are represented by the cross-hatched bars and those in the flare gas by the white bars. The operating conditions are also shown in the diagrams.

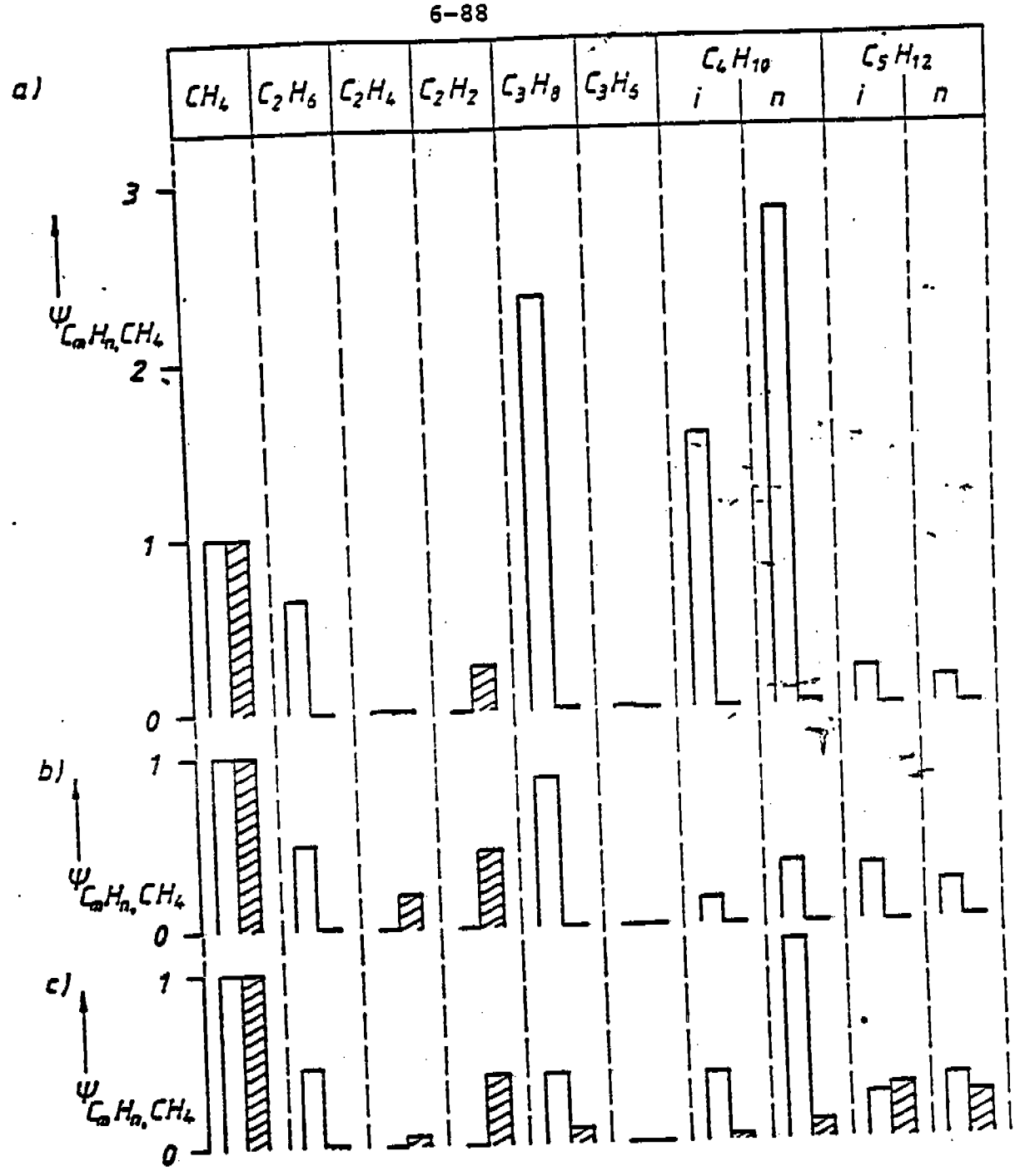

		a	b	c
$\dot{m}_G$	[t/h]	2.2	0.94	0.75
ϱ^o_G	[kg/m³]	1.86	1.0	1.1
$\dot{m}_D/\dot{m}_G$	[kg/kg]	0.37	0	0.24

flare gas

off-gas

Fig. 6 - 22: Volume portion ratios of hydrocarbons in the flare gas and in the off-gas
Test 2, 11, 12

It can be seen that irrespective of the operating conditions methane accounts for the major portion of the hydrocarbons identified previously by a sum. The higher hydrocarbons have been destroyed almost completely. Acetylene which was not [illegible] in the flare gas and which is formed during [illegible] shows next to methane the largest [illegible] are present only in [illegible] flames.

[illegible]

radical which decomposes into a methyl radical and ethene. The methyl radical forms with molecular hydrogen methane and one hydrogen atom. Methyl radicals are also formed in the reaction with hydrogen or oxygen (see R 6 -17 to R 6 - 19 below). Mean temperatures in flare flames are relatively low (see Fig. 6 - 17), substantially higher temporarily so that acetylene is

It can be seen that irrespective of the operating conditions methane accounts for the major portion of the hydrocarbons identified previously by a sum. The higher hydrocarbons have been destroyed almost completely. Acetylene which was not present in the flare gas and which is formed during the combustion, shows next to methane the largest volume portion. Olefins are present only in trace amounts in the off-gases of flare flames.

The large methane volume portion ratio in the off-gas can be attributed to the fact that up to temperatures of approximately 1650°C methane is thermodynamically more stable than the other hydrocarbons; only at still higher temperatures does acetylene become more stable than methane (cf. Fig.4-2, p.4-13). The formation of methane from a saturated C_3+ hydrocarbon can be imagined as occurring by way of the following reaction sequences R 6 - 12 and R 6 - 13:

$$C_mH_{2n+2} + M \longrightarrow HM + C_mH_{2n+1} \longrightarrow C_{m-1}H_{2n-2} + CH_3 \qquad \text{R 6-12,}$$

$M = H, OH, O$

$$CH_3 + H_2 \longrightarrow CH_4 + H \qquad \text{R 6-13.}$$

The saturated hydrocarbon reacts, for example, in the case of propane as the fuel, with a hydrogen atom, hydroxyl radical or oxygen atom with the release of a hydrogen atom to a propyl

radical which decomposes into a methyl radical and ethene. The methyl radical forms with molecular hydrogen methane and one hydrogen atom. Methyl radicals are also formed in the reaction of ethene with hydrogen or oxygen (see R 6 -17 to R 6 - 19 below).

Although the mean temperatures in flare flames are relatively low (max. 1000°C, cf. Fig. 6 - 17), substantially higher temperatures occur in the reaction zones temporarily so that the formation of acetylene is also plausible. Acetylene is already at temperatures above 1090°C more stable than ethene so that the ethene formed in R 6 - 12 can react further to acetylene. Acetylene can, according to Homann and Wagner [55] also be formed from methyl radicals via the intermediates ethane and ethene.

Alkenes are also formed in the flare flame. This is shown in Figs. 6 - 23a and 6 - 23b by the example of two samples which were drawn at a height of 0.5 m (a) and 1 m (b), respectively, above the flare mouth. In the two diagrams, the volume portion ratios of hydrocarbons in the flare flame are compared with those in the flare gas. The volume portions were again based on the methane volume portion of the same sample. Those test results show that in the flame the volume portions of the alkenes (in this case ethene and propene) are larger than that of acetylene.

According to Wagner [91], acetylene is broken down only by oxygen, while ethene is broken down by oxygen and by hydrogen.

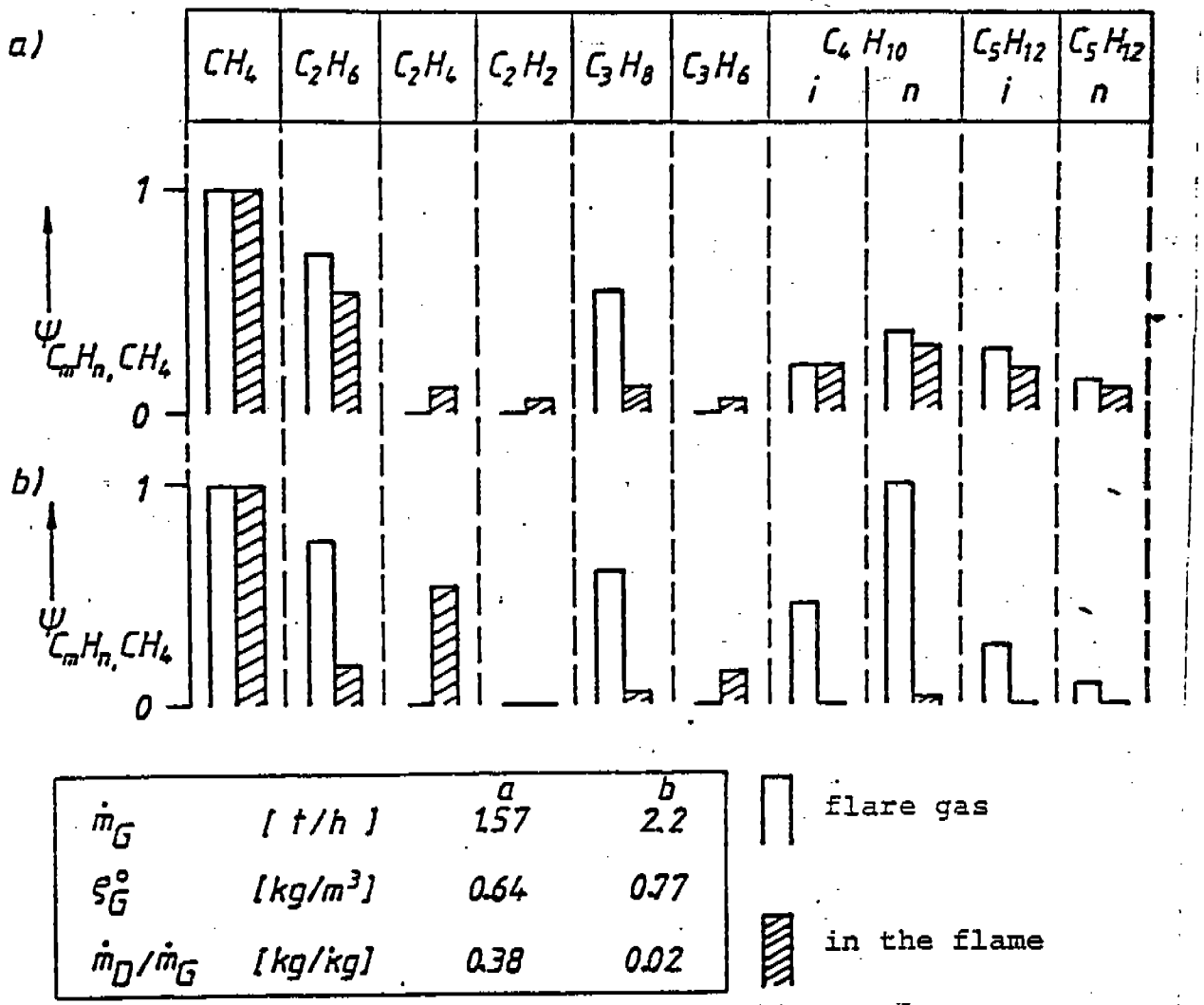

		a	b
$\dot{m}_G$	[t/h]	1.57	2.2
ϱ_G°	[kg/m³]	0.64	0.77
$\dot{m}_D/\dot{m}_G$	[kg/kg]	0.38	0.02

flare gas

in the flame

Fig. 6 - 23: Volume portion ratios of hydrocarbons in the flare gas and in the flame
Test 16, 17

The reaction of acetylene with hydrogen atoms does not lead to the cracking of the C-C triple bond. Only hydrogen atoms are consumed (R 6 - 14 and R 6 -15):

$$C_2H_2 + H \longrightarrow C_2H_3 \qquad \text{R 6-14,}$$

$$C_2H_3 + H \longrightarrow C_2H_2 + H_2 \qquad \text{R 6-15.}$$

When, however, acetylene reacts with oxygen atoms, the C-C triple bond is opened up. The oxygen atom is added at the multiple bond and a ketene is formed which by splitting off carbon monoxide forms a methylene radical (R 6 - 16):

$$C_2H_2 + O \longrightarrow H_2C_2O \longrightarrow CO + CH_2. \qquad \text{R 6-16.}$$

In the reaction of ethene with a hydrogen atom, an addition product is formed first (R 6 - 17) which then, after a further reaction with a hydrogen atom, decomposes into two methyl radicals (R 6 - 18):

$$C_2H_4 + H \longrightarrow C_2H_5 \qquad \text{R 6-17,}$$

$$C_2H_5 + H \longrightarrow 2CH_3. \qquad \text{R 6-18.}$$

Ethene reacts with one oxygen atom via the intermediate ethene oxide to one methyl- and one formyl radical (R 6 - 19):

$$C_2H_4 + O \longrightarrow C_2H_4O \longrightarrow CH_3 + HCO \qquad \text{R 6-19.}$$

The methyl radical forms with oxygen formaldehyde (R 6 -20 and R 6 - 21):

$$CH_3 + O \longrightarrow H_2CO + H \qquad \text{R 6-20,}$$

$$CH_3 + O_2 \longrightarrow H_2CO + OH. \qquad \text{R 6-21.}$$

The formaldehyde is broken down by hydroxyl radicals via the intermediate formyl radical to carbon monoxide and water (R 6 - 22 and R 6 - 23) [54] (p. 52):

$$H_2CO + OH \longrightarrow HCO + H_2O \qquad \text{R 6-22,}$$

$$HCO + OH \longrightarrow CO + H_2O \qquad \text{R 6-23.}$$

In the tests, formaldehyde was not determined separately. However, smelling tests in the off-gas allow the conclusion that the proportion of aldehyde in the off-gas was small. The pungent odor of the aldehydes which is noticeable even at concentrations below 5 mg/m^3 [88] occurred only in very weak form.

The formaldehyde portion in the off-gas was, however, included in the sum total of the organically bound carbon measured. This is mentioned specifically because the flame ionization detector used in the analysis of individual organic components did not - even after replacing the separating column with an empty teflon tube - respond to formaldehyde. However, in the flame ionization detector used for the off-gas analysis

formaldehyde is also indicated. There is a linear relationship between the measured values and the formaldehyde portion in the test material [100].

6.10. Effect of Rapid Load Fluctuations on the Burnout Degree

Because of the uncontrollable gas accumulation, the throughput in elevated flares fluctuates strongly even over short periods of time. This state of operation could not, as intended, be simulated by the opening and closing of the quick-shut-off valve (cf. Fig. 5 ÷ 4) because this resulted in the rupture of the safety disk in the main flare gas line.

However, because of operating difficulties in the plant, large and rapid load fluctuations did occur in some of the tests.

In the event of load fluctuations, the test program under way was, whenever possible, continued while the place of sampling was changed in accordance with the flame geometry. In none of the tests were we able to detect an effect of the load fluctuations on the local burnout degree.

Furthermore, as described earlier, we determined in the tests the local burnout degree also under operating conditions of the test flare which in actual flare operation are hardly encountered over longer periods of time. This applies most of all to the flaring of gases produced during operating difficulties yet with the operating conditions controllable. Due to the broad scope of our tests, we therefore also investigated states of operation which occur transiently in the

case of rapid load fluctuations such as, for example, sooty flames or flames burning with an excessive steam addition.

6.11. Nitrogen Oxide Emission from Flare Flames

The oxides of nitrogen of which here only nitrogen monoxide and nitrogen dioxide are of interest, also constitute a group of air pollutants whose emission has to be watched in evaluating a combustion plant.

In the atmosphere near the ground, the formation of ozone is due exclusively to the photolysis of the nitrogen dioxide [92]. Also when acting directly on the human and plant organism, nitrogen dioxide is more harmful than nitrogen monoxide [93, 94]. Nevertheless, the two nitrogen oxides cannot be considered separately since the nitrogen monoxide is oxidized in the atmosphere to nitrogen dioxide, in which case the reaction in question is very slow unless a photochemical reaction mechanism is involved.

In the following, the term nitrogen oxides is always understood to mean the sum total of nitrogen monoxide and nitrogen dioxide, calculated as nitrogen monoxide.

The distribution of the nitrogen oxide volume portions at the end of the flame is shown in Fig. 6 - 24. The distribution resembles that of the other components such as can be seen, for example, by a comparison with the carbon dioxide volume portions which are also shown on the diagram.

Low nitrogen oxide volume portions were also found in the rest of the tests; the maximum nitrogen oxide volume portion at the end of the flame was of the order of 20 ppm.

Straitz [10] reports nitrogen oxide volume portions smaller than 50 ppm, but it must be considered that in his test the oxygen volume portions were smaller.

For tests verified in Sect. 6.2.2. by way of the material balance sheets, a specific nitrogen oxide emission of ca. 20 g/GJ is obtained for flare flames. This value is substantially lower than that of other industrial gas firing systems [96]. In refinery tube furnaces operated with refinery gas as the fuel, values of ca. 60 g/GJ were determined [97, 98].

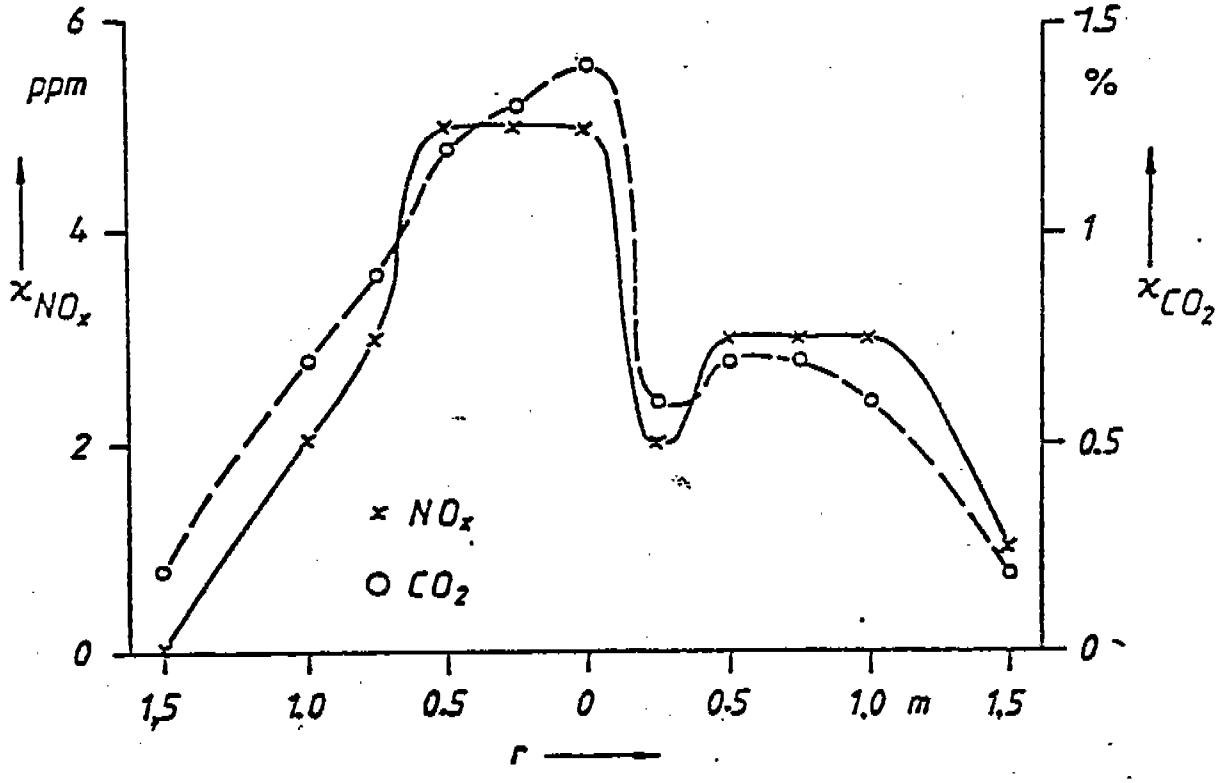

$\dot{m}_G = 1.62\ t/h \quad \varrho_G^o = 0.55\ kg/m^3$

$\dot{m}_D/\dot{m}_G = 0.15\ kg/kg \cdot L = 5m \quad z = 5m$

Fig. 6 - 24: Distribution of the volume portions of nitrogen oxides and of carbon dioxide in a secant at the end of the flame Test 01.010-.045

The small amount of nitrogen oxide formation in flare flames is due to the low flame temperature which is attributable to the large excess of air. Because of the great temperature dependence of the reaction of nitrogen oxide formation (R 4 - 17) according to the Zeldovich mechanism, the formation of the major portion of nitrogen oxides in flames is tied to high temperatures. In Fig. 6 - 17 it had been shown that the maximum temperature in flare flames is of the order of 1000°C. In this temperature range the rate of nitrogen oxide formation is, however, very small [95].

Furthermore, a comparison with the volume portions of nitrogen monoxide and nitrogen dioxide at chemical equilibrium shows that at these temperatures still no substantial nitrogen oxide formation can be expected (Fig. 6 - 25).

The low specific nitrogen oxide emission refutes the notions by Schwanecke [45] that in the combustion in elevated flares the nitrogen oxide emission is larger than in the combustion in closed combustion chambers. The dwell time necessary for the cracking of nitrogen oxides already formed is not needed in the case of flare flames; because of the low temperature of the flare flame far fewer nitrogen oxides are formed than in flames burning inside a combustion muffle.

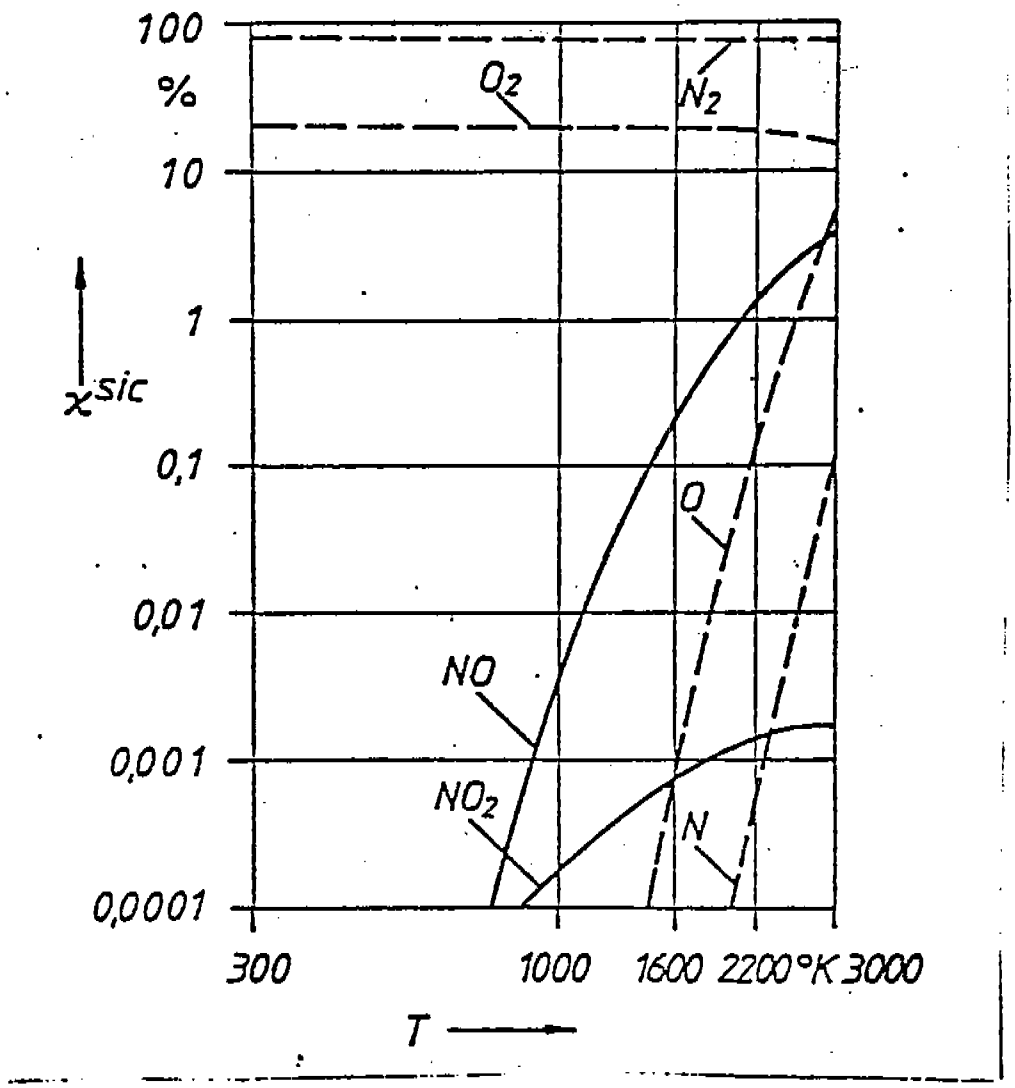

Fig. 6 - 25: Volume portions of nitrogen oxides at chemical equilibrium [99]

7. Summary of the Experimental Results and Conclusions

Figures 7-1 (a-d) show the local burnout degree for carbon bound in air-foreign substances and carbon bound in the gaseous state as a function of the investigated operating parameters, namely, the flare gas mass flow m_G, the flare gas density ϱ_G^o, the steam/gas ratio m_D/m_G, and the wind u_Q.

In addition, all local burnout degrees measured at the flame end and downstream from the flame end are shown as a function of one operating parameter in each of the Figures. Furthermore, the local burnout degrees which are equal to and higher than 0.99 are assembled in the shaded bands, and only those that are smaller than 0.99 are shown separately.

In the experiments, the local burnout degree was determined in a total of 1298 measurement points at the flame end and downstream from the flame end. As a result, the local burnout degree was found to be equal to or higher than 0.99 in 1294 measurement points. Only in four cases, a local burnout degree at the flame end was found to be smaller than 0.99. In one case, this was attributed to an excessive steam addition (it is marked in the Figures as a triangle). For the remaining three cases (marked by +), no correlation with the operating parameters was found.

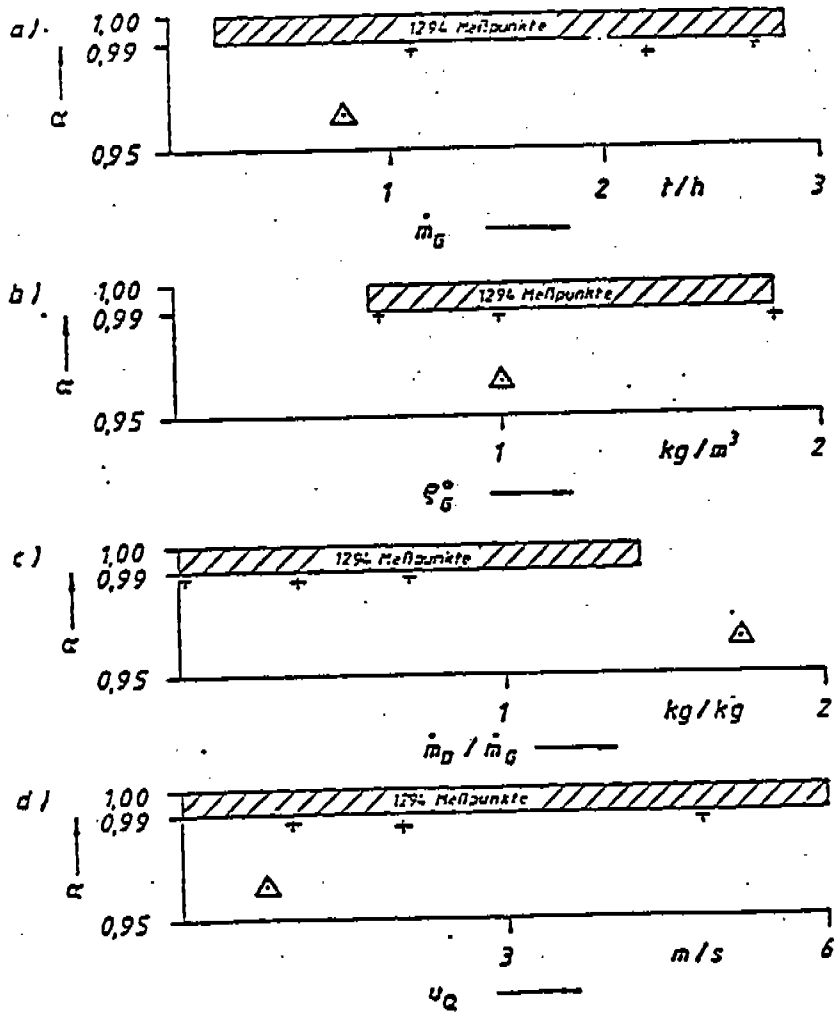

Fig. 7-1:

Local burnout degree as a function of the investigated operating conditions.

The local burnout degree was determined at 42 gas mass flows with 23 different flare gas densities. For the case of soot-free flare flames, no correlation was found between the degree of conversion and the flare gas mass flow or the flare gas composition.

For 114 tested steam/gas ratios, the minimum degree of conversion dropped to values below 0.99 only at a steam/gas ratio, which corresponded to almost a 10-fold amount required to eliminate the soot. Also, in the case of sooty flare flames, the maximum emission factor is less than 0.01 for carbon bound in air-foreign substances and carbon bound in the gaseous state.

The wind velocity during the experiments was up to 6 m/s. In this range, no unburned fuel was discharged at the flame end.

The experimental results which were obtained during representative field tests offer for the flue gas combustion in high flares the evidence that

- In soot-free flare flames, the organically bound carbon of the flare gas is converted to carbon dioxide to at least 99%;
- the emission factor for carbon bound in air-foreign substances and carbon bound in the gaseous state, independent of the optical flame picture (soot containing or soot-free), comprises a maximum of 1% of the organically bound carbon in the flare gas;
- the mass concentration of the organically bound carbon at the flame end is less than 50 mg/m^3, even in the case of sooty flare flames;
- the bulk of the organically bound carbon at the flame end consists of methane and acetylene;
- the nitrogen oxide emission of flare flames, referred to the heat unit, is low.

It is, therefore, recommended that the proposal of the air specification, allowing to proceed with a "conversion degree" of 75% during flue gas combustion in high flares, be so modified that a conversion degree of 99% could be considered in the future.

Bibliography

/1/ F. Schwarz, E. Bauer
Erdöl-Erdgas-Zeitschrift, 93, 91/92 (1977)

/2/ A. F. Orlicek
Erdöl und Kohle, Erdgas, Petrochemie, 19 (11), 824/829 (1966)

/3/ W. Hansen
"Systemanalyse zum Fackelgeschehen," DGMK-Forschungsbericht Nr. 135-01 (1978)

/4/ H. W. Huss
Hydroc. Process., 43 (5), 179/182 (1964)

/5/ R. D. Reed
The oil and gas J., - February 14, 91/92 (1972)

/6/ H. Glomm
"Anordnung und Betrieb von Notabblasesystemen"
Haus der Technik - Vortragsveröffentlichungen, H. 199 S. 18 - 28

/7/ K. Hess, R. Stickel
Verfahrenstechnik, 3 (7), 282/287 (1969)

/8/ L. Untersteinhöfer, N. Rao
Gaswärme, 15 (7), 219/223 (1966)

/9/ K. Haber
"Durchfluß- und Massenermittlung der den Fackeln zugeführten Gase", DGMK Forschungsbericht Nr. 135-03 (1978)

/10/ J. F. Straitz, III
"Flaring for Gaseous Control in the Petroleum Industry"
Annual Meeting of the Airpollution Control Association 1978, Paper-No. 78-58.8

/11/ A. Heller
Schriftenreihe des Vereins für Wasser-, Boden- und Lufthygiene, 16 (1960); entnommen aus: Technik der Luftreinhaltung S. 341, Otto Krauskopf Verlag, 1972

/12/ Günther, R.
"Verbrennung und Feuerungen" Springer Verlag, 1974

/13/ J. D. Hajek, E. E. Ludwig
Petro/Chem Engineer, June 1960, 31/38

/14/ API RP 521 "Guide for Pressure Relief and Depressuring Systems", American Petroleum Institute, 1969

Bibliography (cont'd.)

/15/ S. H. Tan
Hydroc. Process., 46, 172/176 (1967)

/16/ K. Hess, R. Stickel
Chem. Ing. Techn., 39 (5/6), 334/340 (1967)

/17/ R. Becker, K. Hess, A. Stöckel
Chem. Ing. Techn., 47 (1), 33 (1975)

/18/ K. G. Korbacher
Canadian Aeronautics and Space Journal, January 62, 1/6

/19/ Ismants Reba
"Applications of the Coanda Effekt" Fundstelle nicht bekannt

/20/ T. A. Brzustowski
Prog. Energy Combust. Sci., 2, 129/141 (1976)

/21/ W. Lauderback
Hydroc. Process., 51 (1), 127/128 (1972)

/22/ R. Becker
"Fackelbrenner für rauchlose und geräuscharme Verbrennung"
KTI - Firmenschrift, Petrotechnik GmbH, Hamburg 1976

/23/ o. V.
"New concepts in flaring" National Airoil Burner Comp.,
Firmenschrift 1976

/24/ o. V.
"John Zink flare tips help improve atmosphere in Welsh Valley"
J. Inst. Fuel, 36, 203 (1973)

/25/ o. V.
"The anti-Pollutant smokeless flare" Flaregas Engineering Ltd.
Firmenschrift 1976

/26/ Bundes-Immissionsschutzgesetz - BImSchG vom 15. März 1974;
Bundesgesetzblatt, Teil I, 721/743 (1974)

/27/ 9. Verordnung zur Durchführung des BImSchG (Grundsätze des Genehmigungsverfahrens) vom 18. Februar 1977 (9. BImSchV);
Bundesgesetzblatt, Teil I, 274/278 (1977)

/28/ 11. Verordnung zur Durchführung des BImSchG (Emissionserklärungsverordnung) vom 20. Dezember 1978 (11. BImSchV);
Bundesgesetzblatt, Teil I, 2027/2036 (1978)

Bibliography (cont'd.)

/29/ K. Michaelis
Gesundheits-Ingenieur, 96 (10), 281/287 (1975)

/30/ Private Mitteilung der Oberrheinischen Mineralöl-Werke an die Landesanstalt für Umweltschutz, Baden-Württemberg

/31/ Technische Anleitung zur Reinhaltung der Luft vom 28. Aug. 1974 (TA-Luft), Erste allgemeine Verwaltungsvorschrift zum BImSchG, Gemeinsames Ministerialblatt, 25 (24), 426/452 (1974)

/32/ R. Becker
"Ausbrandmessungen an Fackelflammen", Technische Informationen der Endress und Hauser GmbH & Co, 32, 23/25 (1974)

/33/ R. Günther, B. Lenze
"Gutachten über den Umsetzungsgrad des Fackelgases in den Hochfackeln der Oberrheinischen Mineralöl-Werke GmbH in Karlsruhe" 1972

/34/ Technische Richtlinie zur Luftreinhaltung in Mineralölraffinerien und petrochemischen Anlagen zur Kohlenwasserstoffherstellung (Raffinerie-Richtlinie), Rd Erl. d. Ministers für Arbeit, Gesundheit und Soziales (Nordrhein-Westfalen) - III B 4/III B 6 - 8856.4 (III Nr. 13/1975) v. 14.4.1975

/35/ P. Brüdern
Erdöl und Kohle, Erdgas, Petrochemie, 15 (4), 289/291 (1962)

/36/ Y. W. Lee
"Der Verbrennungsverlauf in auftriebsbehafteten Flammen mit und ohne Windeinfluß", Dissertation, Universität Karlsruhe 1977

/37/ Y. W. Lee
Gaswärme Internat., 27 (1), 13/19 (1978)

/38/ G. R. Kent
Hydroc. Process. and Petroleum Refiner, 43 (8), 121/125 (1964)

/39/ R. D. Reed
Chem. Eng. Progr., 64 (6), 53/57 (1968)

/40/ L. Heitner
Hydroc. Process., 49 (11), 209/212 (1970)

Bibliography (cont'd.)

/41/ T. A. Brzustowski
Comb. Sci. Technol., 6, 313/319 (1973)

/42/ T. A. Brzustowski, H. F. Sullivan
2-nd Europ. Symp. for Comb., Sept. 5 (1975), 739/744

/43/ T. A. Brzustowski, E. C. Sommer
Proceedings of Refining, API 53, 865/893 (1973)

/44/ T. A. Brzustowski et al.
The American Society of Mechanical Engineers, 75 HT 4 1/7

/45/ R. Schwanecke
Luftverunreinigung 1974, 49/55

/46/ J. Grumer et al.
"Hydrogen Flare Stack Diffusion Flames" Dept. of the Interior, Bureau of Mines (1970), Report of Investigation 7457

/47/ J. F. Straitz
Hydroc. Process., 56 (10), 131/135 (1977)

/48/ Mitteilung des Umweltbundesamtes an die Landesanstalt für Umweltschutz, Baden-Württemberg

/49/ R. M. Fristrom, A. A. Westenberg
"Flame Structure", McGraw-Hill, 1965

/50/ H. Reichardt
"Gesetzmäßigkeiten der freien Turbulenz" VDI-Forschungsheft 414 (1942)

/51/ R. Günther
Archiv für Eisenhüttenwesen, 39 (7), 515/519 (1968)

/52/ B. Lenze
Gaswärme Internat., 20 (12), 451/457 (1971)

/53/ K. H. Homann
Comb. Flame, 11, 265/269 (1967)

Bibliography (cont'd.)

/54/ I. Glassman
"Combustion", Academic Press, 1977, S. 55

/55/ K. H. Homann, H. G. Wagner
11-th Symp. (int.) on Comb. 1966, The Combustion Institute 1967,
pp 371-379

/56/ J. Lahaye, G. Prado
"Mechanisms of Carbon Black Formation" in
P. L. Walker, P. A. Thrower "Chemistry and Physics of Carbon",
Vol. 14, 167/294 (1978)

/57/ E. R. Place, F. J. Weinberg
11-th Symp. (int.) on Comb. 1966, The Combustion Institute 1967,
pp. 245-255

/58/ B. L. Wersborg, J. B. Howard, G. C. Williams
14-th Symp. (int.) on Comb. 1972, The Combustion Institute 1973,
pp. 929-938

/59/ T. W. Lester, L. K. Wittig
16-th Symp. (int.) on Comb. 1976, The Combustion Institute 1977,
pp. 671-680

/60/ C. P. Fenimore, G. W. Jones
J. Phys. Chem., 71 (3), 593/597 (1967)

/61/ F. J. Wright
15-th Symp. (int.) on Comb. 1974, The Combustion Institute 1975,
pp. 1449-1459

/62/ L. Kurylko, R. H. Essenhigh
14-th Symp. (int.) on Comb. 1972, The Combustion Institute 1973,
pp. 1375-1386

/63/ Janaf, Thermodynamic Tables, 1971

/64/ Landolt-Börnstein, II Band, 4. Teil, Springer-Verlag 1961

/65/ E. Fitzer, W. Fritz
"Technische Chemie" Springer-Verlag 1975

/66/ T. Miyauchi, Y. Mori, A. Imamura
16-th Symp. (int.) on Comb. 1976, The Combustion Institute 1977,
pp. 1073-1081

Bibliography (cont'd.)

/67/ H. Cremer
Chem. Ing. Techn., 44 (1+2), 8/15 (1972)

/68/ Ya. B. Zeldovich
Acta Physicochem. USSR 21, 577 aus /54/

/69/ C. P. Fenimore
13-th Symp. (int.) on Comb. 1970, The Combustion Institute 1971,
pp. 373-379

/70/ F. Bachmeier, K. H. Eberius, Th. Just
Combust. Sci. Technol., 7, 77/84 (1973)

/71/ B. S. Haynes, D. Iverach, N. Y. Kirov
15-th Symp. (int.) on Comb. 1974, The Combustion Institute
1975, pp. 1103-1112

/72/ I. N. Mulvihill, L. P. Phillips
15-th Symp. (int.) on Comb. 1974, The Combustion Institute
1975, pp 1113-1122

/73/ E. L. Merryman, A. Levy
15-th Symp. (int.) on Comb. 1974, The Combustion Institute
1975, pp. 1073-1083

/74/ D. Shore
"Towards quieter flaring" A paper presented at the 74-th meeting
of the American Institute of Chemical Engineers, March 1973

/75/ J. Hengstenberg, B. Sturm, O. Winkler
"Messen und Regeln in der Chemischen Techn."
Springer-Verlag 1964

/76/ B. Baule
"Die Mathematik des Naturforschers und Ingenieurs"
Bd. 2, S. Hirzel-Verlag, Leipzig 1959

/77/ Aspirationspsychrometer-Tafeln
Herausgeber: Verlag Friedrich Vieweg u. Sohn, Braunschweig 1975

/78/ H. A. Becker, S. Yamazaki
16-th Symp. (int.) on Comb. 1976, The Combustion Institute 1977,
pp. 681-691

/79/ K. Hein
Comb. Sci. Technol. 5, 195/206 (1972)

Bibliography (cont'd.)

/80/ Jahresbericht 1973 der Abteilung Strahlenschutz und Sicherheit der Gesellschaft für Kernforschung mbH, Karlsruhe

/81/ F. L. Dryer
16-th Symp. (Int.) on Comb. 1976, The Combustion Institute 1977, pp. 279-295

/82/ C. T. Bowman
15-th Symp. (Int.) on Comb. 1974, The Combustion Institute 1975, pp. 869-881

/83/ K. Hess
"Flammenlänge und Flammenstabilität" Dissertation T.H. Karlsruhe 1964, entnommen aus /12/

/84/ Gmelins Handbuch der anorganischen Chemie, System-Nr. 4 Stickstoff 8. Auflage 1936, S. 748ff.
Verlag Chemie

/85/ J. A. Fay, D. H. Lewis
16-th Symp. (Int.) on Comb. 1976, The Combustion Institute 1977, pp. 1397-1405

/86/ A. G. Gaydon, H. G. Wolfhard
"Flames, their structure, radiation and temperature" Chapman and Hall 1970

/87/ 1. BImSchV. vom 5.2.79 (BGBl I S. 165)

/88/ Hommel
"Handbuch der gefährlichen Güter" Springer-Verlag 1973,

/89/ P. A. Leighton
"Photochemistry of Air Pollution" Chapter 10, Academic Press, New York, 1961

/90/ W.M. Bufalini
Environ. Sci. Technol., 10, 908/912 (1976)

/91/ H. Wagner
VDI-Berichte Nr. 146, 5/9 (1970)

/92/ U. Schurath
VDI-Berichte Nr. 270, 13/18 (1977)

Bibliography (cont'd.)

/93/ C. von Nieding, H. M. Wagner
VDI-Berichte Nr. 247, 55/58 (1974)

/94/ R. Zahn
VDI-Berichte Nr. 247, 74/76 (1974)

/95/ N. Peters
VDI-Berichte Nr. 346, 285/292 (1979)

/96/ L. Lützke.
VDI-Berichte Nr. 247, 9/16 (1974)

/97/ E. Fitzer, D. Siegel
Chem. Ing. Techn., 47 (13), 571 (1975)

/98/ D. Siegel
"Stickstoffoxidemission industrieller Feuerungsanlagen in Abhängigkeit von den Betriebsbedingungen" Diplomarbeit am Institut für Chemische Technik der Universität Karlsruhe, 1973

/99/ H. Kruppe
"Über die Bildung von Stickoxiden bei Verbrennungsprozessen"
Dissertation TH Aachen 1970

/100/ H. D. Winkler, D. Welzel
Wasser, Luft und Betrieb, 16 (7), 213/215 (1972)

/101/ B.G. Newmann,
"The deflexion of plan jets by adjacent boundaries - Coanda effect"
in G.V. Lachmann "Boundary layer and flow control" Vol.1, p. 232,
Pergamon Press, 1961

/102/ R.C. Milliken
J. Phys.Chem., 66, 794 (1962)

Flare gas analysis Test No. 01.010-.045

	x in %
H_2	69.3
H_2S	1.3
CH_4	8.9
C_2H_6	7.2
C_2H_4	0.04
C_2H_2	nn
C_3H_8	5.5
C_3H_6	0.06
$i\text{-}C_4H_{10}$	1.0
$n\text{-}C_4H_{10}$	1.4
$1\text{-}C_4H_8$	0.03
$i\text{-}C_5H_{12}$	1.9
$n\text{-}C_5H_{12}$	1.2
C_5-Isom.	nn
C_6H_{14}	nn
C_6H_6	nn
$C_6H_5\text{-}CH_3$	nn
$C_6H_5\text{-}C_2H_5$	nn
N_2	2.2

$\varrho_G^o = 0.55$ kg/m³

M = 12 g/mol

$\varrho_{oC} = 0.36$ kg carbon / m³ flare gas

$w_C = 0.65$ kg carbon / m³ flare gas

$\varrho_{oH} = 0.14$ kg hydrogen / m³ flare gas

$w_H = 0.25$ kg hydrogen / kg flare gas

nn: < 0.01%

Appendix 1 Sheet 2

Test No. 01

1	Consec. No.		.010	.011	.012	.013	.014	.015	.020	.021	.022	.023	.024	.025	.031	.032
2	$\dot{m}$(G)	kg/h	1620													
3	$\dot{m}$(D)	kg/h	240													
4	ψ (D,G)	kg/kg	0.15													
5	x	m	0.00	-0.25	-0.50	-0.75	-1.00	-1.50	0.00						0.25	0.50
6	y	m	0.00						0.00	0.25	0.50	0.75	1.00	1.50	0.00	
7	z	m	5.00													
8	χ(O2)	%	18.2	18.5	18.9	19.1	19.9	20.8	19.7	19.5	18.5	18.2	20.6	20.0	20.1	19.5
9	χ(CO2)	%	1.4	1.3	1.2	0.9	0.7	0.2	1.1	1.1	1.2	1.2	1.1	0.5	0.6	0.7
10	χ(CO)	%	nn	nn	nn	nn	nn	nn	nn	nn	nn	nn	nn	nn	nn	nn
11	χ(CxHy)	ppm	42	24	9	8	8	6	20	30	38	36	36	9	10	12
12	χ(NOx)	ppm	5	5	5	3	2	nh	5	5	5	5	5	3	2	3
13	Tp	°C	24.5	27.0	27.5	27.5	27.0	26.5	25.5	25.5	25.0	25.0	25.0	25.5	26.0	25.5
14	T(B)	°C	520	520	485	455	335	95	415	445	470	480	490	290	410	460
15	u(kal)	m/s														

nn: χ(CO) < 0.01%, χ(CO2) < 0.1%, χ(NOx) < 1 ppm

χ(CxHy) shown as methane equivalents

Appendix 1 Sheet 2

Test No. 01

1	Consec. No.		.033	.034	.035	.041	.042	.043	.044	.045
2	$\dot{m}$(G)	kg/h	1620							
3	$\dot{m}$(D)	kg/h	240							
4	Ψ (D,G)	kg/kg	0.15							
5	x	m	0.75	1.00	1.50	0.00				
6	y	m	0.00			-0125	-0.50	-0.75	-1.00	-1.50
7	z	m	5.00							
8	χ(O2)	%	20.0	20.1	20.8	19.1	19.6	19.3	20.1	20.5
9	χ(CO2)	%	0.7	0.6	0.2	0.7	0.5	0.3	0.2	0.1
10	χ(CO)	%	nn	nn	nn	nn	nn	nn	nn	nn
11	χ(CxHy)	ppm	13	6	6	6	6	6	6	6
12	χ(NOx)	ppm	3	3	1	3	2	2	1	nn
13	Tp	°C	25.0	25.0	25.0	24.5	25.0	24.5	24.5	25.0
14	T(B)	°C	365	300	150	335	260	195	150	80
15	u(kal)	m/s								

nn: χ(CO) < 0.01%, χ(CO2) < 0.1%, χ(NOx) < 1 ppm

χ(CxHy) shown as methane equivalents

Appendix 1 Sheet 1

Test No. . 02.001-.085

Flare gas analysis

	x in %
H_2	17.8
H_2S	0.4
CH_4	8.9
C_2H_6	5.8
C_2H_4	0.06
C_2H_2	nn
C_3H_8	21.0
C_3H_6	0.06
$i\text{-}C_4H_{10}$	14.1
$n\text{-}C_4H_{10}$	24.9
$1\text{-}C_4H_8$	0.1
$i\text{-}C_5H_{12}$	1.9
$n\text{-}C_5H_{12}$	1.2
C_5-Isom.	0.6
C_6H_{14}	0.1
C_6H_6	1.0
$C_6H_5\text{-}CH_3$	0.2
$C_6H_5\text{-}C_2H_5$	nn
N_2	1.8

$\varrho_G^o = 1.86$ kg/m^3

$M = 42$ g/mol

$\varrho_{oC} = 1.5$ kg carbon / m^3 flare gas

$w_C = 0.81$ kg carbon / kg flare gas

$\varrho_{oH} = 0.32$ kg hydrogen / m^3 flare gas

$w_H = 0.17$ kg hydrogen / kg flare gas

nn: < 0.01%

Appendix 1 Sheet 2

Test No. 02

1	Consec. No.		.001	.002	.003	.004	.005	.006	.007	.008	.009	.010	.011	.014	.015	.01
2	$\dot{m}$(G)	kg/h	2200													
3	$\dot{m}$(D)	kg/h	820													
4	ψ (D,G)	kg/kg	0.37													
5	x	m	0.0	-0.5	-1.0	-1.5	-2.0	-2.5	-3.0	-3.5	-4.0	-4.5	-5.0	-5.5	-6.0	-6.
6	y	m	0.0													
7	z	m	5.0													
8	χ(O2)	%	21.0	21.0	21.0	21.0	19.8	18.6	16.6	17.2	18.7	19.3	19.8	19.5	19.6	20.
9	χ(CO2)	%	nn	nn	nn	0.4	0.9	1.5	2.5	1.8	1.2	1.5	0.5	0.4	0.6	0.
10	χ(CO)	%	nn	nn	nn	nn	0.02	0.03	0.21	0.05	nn	nn	nn	nn	nn	n
11	χ(CxHy)	ppm	10	13	33	10	30	60	240	210	35	19	21	10	6	n
12	χ(NOx)	ppm														
13	Tp	°C	15,5	8.5	10,0	9,5	20.0	24,o	33.0	30.0	25.5	21.0	17.5	15.5	17.0	12.
14	T(D)	°C	75	45	45	50	240	380	560	575	395	295	205	175	190	0
15	u(kal)	m/s														

nn: χ(CO) < 0.01%, χ(CO2) < 0.1%, χ(NOx) < 1 ppm

χ (CxHy) shown as methane equivalents

Appendix 1 Sheet 2

Test No. 02

1	Consec. No.		.017	.034	.035	.036	.037	.038	.039	.040	.041	.042	.043	.044	.045	.0
2	$\dot{m}$(G)	kg/h	2200													
3	$\dot{m}$(D)	kg/h	820													
4	ψ (D,G)	kg/kg	0.37													
5	x	m	-7.00		-6.5	-6.0	-5.5	-5.0	-4.5	-4.0	-3.5	-3.0	-2.5	-2.0	-1.5	-1
6	y	m	0.0	0.5												
7	z	m	5.0													
8	χ(O2)	%	20.8	21.0	20.2	21.0	20.0	19.5	19.3	18.9	18.6	18.1	18.9	20.0	20.2	20
9	χ(CO2)	%	nn	nn	0.4	0.2	0.6	0.9	1.1	1.4	2.3	1.2	1.2	0.8	0.8	0
10	χ(CO)	%	nn	nn	nn	nn	nn	nn	nn	nn	0.08	0.04	0.02	0.02	0.02	
11	χ(CxHy)	ppm	5	10	25	10	40	30	25	30	30	150	70	65	30	
12	χ(NOx)	ppm														
13	Tp	°C	9.0	12.0	11.5	15.0	15.5	18.5	20.0	24.0	26.5	27.0	22.0	15.5	15.0	15
14	T(B)	°C	65	/	/	/	/	/	/	/	/	/	/	275	230	1
15	u(kal)	m/s														

nn: χ(CO) < 0.01%, χ(CO2) < 0.1%, χ(NOx) < 1 ppm

χ (CxHy) shown as methane equivalents

Appendix 1 Sheet 2

Test No. 02

1	Consec. No.		.047	.048	.049	.050	.051	.052	.053	.054	.055	.056	.057	.058	.059	.060
2	$\dot{m}$(G)	kg/h	2200													
3	$\dot{m}$(D)	kg/h	820													
4	ψ (D,G)	kg/kg	0.37													
5	x	m	-0.5	-6.0	-5.5	-5.0	-4.5	-4.0	-3.5	-3.0	-2.5	-2.0	-1.5	-6.5	-6.0	-5.5
6	y	m	0.5	1.0										1.5		
7	z	m	5.0													
8	χ(O2)	%	20.4	20.5	19.5	19.5	19.8	17.0	17.6	18.2	20.2	20.2	19.7	20.1	20.2	20.3
9	χ(CO2)	%	0.2	0.3	0.8	0.8	1.0	2.8	2.1	2.2	1.1	0.6	0.4	0.8	0.5	0.5
10	χ(CO)	%	nn	nn	nn	nn	nn	0.07	0.06	0.04	nn	0.02	nn	nn	nn	nn
11	χ(CxHy)	ppm	10	10	10	15	20	150	70	50	15	50	55	30	10	10
12	χ(NOx)	ppm														
13	Tp	°C	12.0	12.5	21.0	16.0	16.0	32.0	29.0	27.0	15.0	14.5	12.0	16.0	13.5	13.5
14	T(B)	°C	60	90	160	200	185	500	535	465	240	235	225	100	175	145
15	u(kal)	m/s														

nn: χ(CO) < 0.01%, χ(CO2) < 0.1%, χ(NOx) < 1 ppm

χ(CxHy) shown as methane equivalents

Test No. 02

1	Consec. No.		.061	.062	.063	.064	.065	.066	.067	.068	.069	.070	.071	.072	.073	.07
2	$\dot{m}$(G)	kg/h	2200													
3	$\dot{m}$(D)	kg/h	820													
4	ψ (D,G)	kg/kg	0.37													
5	x	m	-5.0	-4.5	-4.0	-3.5	-3.0	-2.5	-2.0	-1.5	-1.0	-0.5	-6.5	-4.5	-4.0	-3.
6	y	m	1.5										2.0			
7	z	m	5.0													
8	χ(O2)	%	20.5	19.9	19.1	16.7	18.0	18.1	20.4	20.0	20.1	20.9	20.2	18.3	20.3	18.
9	χ(CO2)	%	0.3	0.5	1.2	2.5	2.3	1.3	0.4	0.6	0.4	0.3	0.2	1.5	0.6	2.
10	χ(CO)	%	nn	nn	0.02	0.06	0.17	0.01	0.01	0.01	nn	nn	nn	nn	nn	0.1
11	χ(CxHy)	ppm	10	10	15	180	85	90	35	30	35	10	10	25	25	11
12	χ(NOx)	ppm														
13	Tp	°C	15.0	17.0	22.5	31.5	25.5	24.0	15.0	15.5	16.0	10.5	23.0	27.5	14.5	22.
14	T(B)	°C	90	125	285	500	460	360	240	195	245	50	35	370	190	31
15	u(kal)	m/s														

nn: χ(CO) < 0.01%, χ(CO2) < 0.1%, χ(NOx) < 1 ppm
χ (CxHy) shown as methane equivalents

Appendix 1 Sheet 2

Test No. 02

1	Consec. No.		.075	.076	.077	.078	.079	.080	.081	.082	.083	.084	.085	.086
2	$\dot{m}$(G)	kg/h	2200											
3	$\dot{m}$(D)	kg/h	820											
4	ψ (D,G)	kg/kg	0.37											
5	x	m	-3.0	-2.5	-2.0	-1.5	-5.0	-5.0	-4.5	-4.0	-3.5	-3.0	-2.5	-2.0
6	y	m	2.0					2.5						
7	z	m	5.0											
8	χ(O2)	%	17.0	17.6	19.6	20.9	19.8	21.0	21.0	21.0	20.7	20.0	20.8	20.8
9	χ(CO2)	%	2.6	2.5	1.4	0.8	0.8	nn	nn	nn	0.4	0.3	0.8	0.2
10	χ(CO)	%	0.09	0.08	0.05	0.07	nn	nn	nn	nn	nn	nn	nn	nn
11	χ(CxHy)	ppm	140	160	25	50	12	10	10	10	5	25	15	10
12	χ(NOx)	ppm												
13	Tp	°C	32.0	31.0	19.0	23.0	13.0	9.0	9.5	9.5	14.0	15.5	15.0	10.0
14	T(B)	°C	525	520	355	100	165	115	25	25	85	140	100	65
15	u(kal)	m/s												

nn: χ(CO) < 0.01%, χ(CO2) < 0.1%, χ(NOx) < 1 ppm

χ (CxHy) shown as methane equivalents

Volume portions of hydrocarbons and hydrogen in the off-gas

Test No. 02

Measuring object	x	Sample drawn at consec. No.					
	in	.006	.042	.045	.053	.065	.076
CH_4	ppm	26	32	27	23	38	110
C_2H_6	ppm	nn	7	nn	nn	nn	nn
C_2H_4	ppm	nn	nn	nn	nn	nn	9
C_2H_2	ppm	3	4	4	3	2	29
C_3H_8	ppm	1	17	nn	2	1	1
C_3H_6	ppm	nn	nn	nn	nn	nn	nn
$i\text{-}C_4H_{10}$	ppm	nn	10	nn	nn	nn	nn
$n\text{-}C_4H_{10}$	ppm	2	18	1	2	2	3
$1\text{-}C_4H_8$	ppm	nn	nn	nn	nn	nn	nn
$i\text{-}C_5H_{12}$	ppm	nn	2	nn	nn	nn	nn
$n\text{-}C_5H_{12}$	ppm	nn	nn	nn	nn	nn	nn
C_5-Isom.	ppm	nn	nn	nn	nn	nn	nn
C_6H_{14}	ppm	nn	nn	nn	nn	nn	nn

nn : < 1 ppm

Appendix 1 Sheet 1

Flare gas analysis — Test No. 03.001-.039

	x in %
H_2	43.7
H_2S	1.6
CH_4	10.5
C_2H_6	7.7
C_2H_4	0.05
C_2H_2	nn
C_3H_8	18.4
C_3H_6	0.3
i-C_4H_{10}	3.5
n-C_4H_{10}	5.4
1-C_4H_8	0.08
i-C_5H_{12}	4.3
n-C_5H_{12}	2.2
C_5-Isom.	0.8
C_6H_{14}	nn
C_6H_6	nn
C_6H_5-CH_3	nn
C_6H_5-C_2H_5	nn
N_2	nn

$\varrho_G^o = 1.12$ kg/m³

$M = 25$ g/mol

$\varrho_{oC} = 0.87$ kg carbon / m³ flare gas

$w_C = 0.78$ kg carbon / kg flare gas

$\varrho_{oH} = 0.23$ kg hydrogen / m³ flare gas

$w_H = 0.21$ kg hydrogen / kg flare gas

nn: < 0.01%

Appendix 1 Sheet 1

Flare Gas analysis Test No. 03.040-.094

	x in %
H_2	56.1
H_2S	1.5
CH_4	11.6
C_2H_6	9.0
C_2H_4	0.02
C_2H_2	nn
C_3H_8	12.8
C_3H_6	0.1
$i\text{-}C_4H_{10}$	2.0
$n\text{-}C_4H_{10}$	2.7
$1\text{-}C_4H_8$	0.06
$i\text{-}C_5H_{12}$	2.0
$n\text{-}C_5H_{12}$	1.5
C_5-Isom.	0.5
C_6H_{14}	nn
C_6H_6	nn
$C_6H_5\text{-}CH_3$	nn
$C_6H_5\text{-}C_2H_5$	nn
N_2	nn

$\varrho_G^o = 0.81$ kg/m³

$M = 18$ g/mol

$\varrho_{oC} = 0.60$ kg carbon / m³ flare gas

$w_C = 0.74$ kg carbon / kg flare gas

$\varrho_{oH} = 0.19$ kg hydrogen / m³ flare gas

$w_H = 0.23$ kg hydrogen / flare gas

nn: < 0.01%

Appendix 1 Sheet 2

Test No. 03

1	Consec. No.		.001	.002	.003	.004	.005	.006	.007	.008	.009	.010	.011	.012	.013	.01
2	$\dot{m}$(G)	kg/h	780													
3	$\dot{m}$(D)	kg/h	225													
4	Ψ (D,G)	kg/kg	0.29													
5	x	m	0.0	-0.5	-1.0	-1.5	-2.0	-2.5	-3.0	-3.0	-2.5	-2.0	-1.5	-1.0	-0.5	0.
6	y	m	0.0							0.5						
7	z	m	5.0													
8	χ(O2)	%	20.8	20.6	18.7	19.1	20.0	20.7	20.9	20.5	20.8	21.0	21.0	20.8	20.2	20.
9	χ(CO2)	%	0.1	0.1	1.1	1.3	0.7	0.3	0.3	0.3	0.1	nn	nn	0.1	0.6	0.
10	χ(CO)	%	nn	nn	nn	nn	nn	nn	nn	nn	nn	nn	nn	nn	nn	r
11	χ(CxHy)	ppm	5	5	80	45	13	nn	nn	nn	nn	nn	nn	nn	11	r
12	χ(NOx)	ppm	1	4	5	3	2	nn	nn	nn	nn	nn	nn	nn	2	
13	Tp	°C	9.0	9.0	10.0	16.5	19.0	20.5	20.5	17.5	15.0	12.0	10.0	11.0	17.5	15.
14	T(B)	°C	80	95	195	340	310	265	270	225	190	185	165	150	180	18
15	u(kal)	m/s														

nn: χ(CO) < 0.01%, χ(CO2) < 0.1%, χ(NOx) < 1 ppm
χ(CxHy) shown as methane equivalents

Appendix 1 Sheet 2

Test No, 03

1	Consec. No.		.015	.016	.017	.018	.019	.020	.021	.022	.023	.024	.025	.026	.027	.02
2	$\dot{m}$(G)	kg/h	780													
3	$\dot{m}$(D)	kg/h	225													
4	Ψ (D,G)	kg/kg	0.29													
5	x	m	0.5		0.0	-0.5	-1.0	-1.5	-2.0	-2.5	-3.0	-3.5	-4.0	-4.5	-5.0	-5.
6	y	m	0.5	1.0												
7	z	m	5.0													
8	χ(O2)	%	20.9	21.0	21.0	21.0	21.0	21.0	20.8	20.7	20.6	20.5	20.3	20.4	20.3	20.
9	χ(CO2)	%	0.1	nn	nn	nn	nn	nn	0.1	0.2	0.2	0.4	0.4	0.4	0.4	0.
10	χ(CO)	%	nn	nn	nn	nn	nn	nn	nn	nn	nn	nn	nn	nn	nn	n
11	χ(CxHy)	ppm	nn	5	5	5	5	5	5	5	5	5	5	5	5	
12	χ(NOx)	ppm	1	nn	nn	nn	nn	nn	1	1	1	1	1	1	1	
13	Tp	°C	9.0	9.0	9.0	9.5	9.5	9.5	9.5	7.0	9.0	12.0	12.0	15.0	13.5	11.
14	T(B)	°C	180	165	155	150	110	110	105	125	105	95	95	115	100	10
15	u(kal)	m/s														

nn: χ(CO) < 0.01%, χ(CO2) < 0.1%, χ(NOx) < 1 ppm
χ (CxHy) shown as methane equivalents

Appendix 1 Sheet 2

Test No. 03

1	Consec. No.		.029	.030	.031	.032	.033	.034	.035	.036	.037	.038	.039	.040	.041	.042
2	$\dot{m}$(G)	kg/h	780											1260		
3	$\dot{m}$(D)	kg/h	225											75		
4	ψ (D,G)	kg/kg	0.29											0.06		
5	x	m	-5.5	-5.0	-4.5	-4.0	-3.5	-3.0	-2.5	-2.0	-1.5	-1.0	-0.5	0.0	-0.5	-1.0
6	y	m	-0.5											0.0		
7	z	m	5.0											5.0		
8	χ(O2)	%	20.6	20.3	20.0	19.8	19.4	19.6	20.0	18.6	19.5	20.7	20.9	20.7	20.7	20.5
9	χ(CO2)	%	0.3	0.3	0.6	0.7	0.9	0.8	0.7	1.2	0.7	0.2	0.2	0.4	0.3	0.6
10	χ(CO)	%	nn	nn	nn	nn	nn	nn	nn	nn	nn	nn	nn	0.03	0.01	0.01
11	χ(CxHy)	ppm	5	5	5	5	5	5	5	10	7	5	5	225	105	55
12	χ(NOx)	ppm	1	1	2	3	4	4	3	5	5	1	1	1	1	2
13	Tp	°C	13.0	10.0	16.5	18.5	22.0	18.5	15.0	28.5	23.0	14.0	8.0	10.5	13.5	11.5
14	T(B)	°C	90	90	95	120	150	170	175	190	230	225	195	100	175	220
15	u(kal)	m/s														

nn: χ(CO) < 0.01%, χ(CO2) < 0.1%, χ(NOx) < 1 ppm

χ (CxHy) shown as methane equivalents

Appendix 1 Sheet 2

Test No. 03

1	Consec. No.		.043	.044	.045	.046	.047	.048	.049	.050	.051	.052	.053	.054	.055	.056
2	$\dot{m}$(G)	kg/h	1260													
3	$\dot{m}$(D)	kg/h	75													
4	ψ (D,G)	kg/kg	0.06													
5	x	m	-1.5	-2.0	-2.5		-2.0	-1.5	-1.0	-0.5	0.0	0.5		0.0	-0.5	-1.0
6	y	m	0.0			0.5							1.0			
7	z	m	5.0													
8	χ(O2)	%	15.9	17.1	19.8	21.0	20.3	17.7	14.9	16.8	20.5	20.8	20.9	17.1	15.6	10.1
9	χ(CO2)	%	2.7	3.0	1.6	0.2	0.5	1.7	2.9	1.9	0.5	0.2	0.4	2.5	2.6	1.2
10	χ(CO)	%	0.40	0.40	0.10	0.01	0.01	0.15	0.67	0.30	0.03	0.01	0.01	0.51	0.47	0.10
11	χ(CxHy)	ppm	1745	1820	425	10	10	770	3020	1990	10	10	nn	2435	2730	1475
12	χ(NOx)	ppm	14	14	3	nn	3	11	16	12	2	5	1	7	15	9
13	Tp	°C	32.0	34.5	36.0	36.0	36.0	35.5	36.5	36.0	36.0	36.0	36.5	37.0	36.0	36.0
14	T(B)	°C	480	710	290	95	175	445	660	575	285	105	85	620	645	495
15	u(kal)	m/s														

nn: χ(CO) < 0.01%, χ(CO2) < 0.1%, χ(NOx) < 1 ppm

χ (CxHy) shown as methane equivalents

Appendix 1 Sheet 2

Test No. 03

1	Consec.No.		0.71	.072	.073	.074	.075	.076	.077	.078	.079	.080	.081	.082	.083	.084
2	$\dot{m}$(G)	kg/h	1260													
3	$\dot{m}$(D)	kg/h	75													
4	ψ (D,G)	kg/kg	0.06													
5	x	m	-2.0	-2.5	-3.0	-3.5	-4.0		-3.5	-3.0	-2.5	-2.0	-1.5	0.0	-0.5	-1.0
6	y	m	2.0					2.5						-0.5		
7	z	m	5.0													
8	χ(O2)	%	19.1	20.3	19.8	20.8	20.8	21.0	21.0	20.5	21.0	21.0	21.0	21.0	19.5	15.7
9	χ(CO2)	%	0.2	1.6	0.7	0.3	0.1	0.1	0.1	0.3	nn	nn	nn	nn	0.8	2.9
10	χ(CO)	%	nn	0.02	0.01	nn	nn	nn	nn	nn	nn	nn	nn	nn	0.04	0.37
11	χ(CxHy)	ppm	10	420	250	10	10	10	10	10	10	10	10	10	265	1033
12	χ(NOx)	ppm	nn	10	5	1	nn	nn	nn	nn	nn	nn	nn	nn	6	25
13	Tp	°C	10.5	8.5	20.0	11.0	10.5	10.0	10.5	14.5	11.0	12.0	11.5	11.5	10.0	33.0
14	T(B)	°C	45	370	220	150	90	70	40	100	35	25	20	35	205	620
15	u(kal)	m/s														

nn: χ(CO) < 0.01%, χ(CO2) < 0.1%, χ(NOx) < 1 ppm

χ(CxHy) shown as methane equivalents

Appendix 1 Sheet 2

Test No. 03

1	Consec.No.		.057	.058	.059	.060	.061	.062	.063	.064	.065	.066	.067	.068	.069	.070
2	$\dot{m}$(G)	kg/h	1260													
3	$\dot{m}$(D)	kg/h	75													
4	ψ (D,G)	kg/kg	0.06													
5	x	m	-1.5	-2.0		-1.5	-1.0	-0.5	0.0	0.5	1.0	0.5	0.0	-0.5	-1.0	-1.5
6	y	m	1.0		1.5							2.0				
7	z	m	5.0													
8	χ(O2)	%	19.1	20.6	20.7	20.7	20.8	16.4	14.8	19.7	21.0	21.0	21.0	21.0	21.0	21.0
9	χ(CO2)	%	0.8	0.3	0.3	0.3	0.1	2.4	3.0	0.7	0.1	0.1	0.1	0.1	0.1	0.1
10	χ(CO)	%	0.07	0.01	0.01	0.02	0.09	0.41	0.62	0.16	0.10	nn	nn	nn	nn	nn
11	χ(CxHy)	ppm	530	50	20	40		2505	3510	1080	10	10	10	10	10	10
12	χ(NOx)	ppm	5	2	2	1	22	13	16	1	nn	nn	nn	nn	nn	nn
13	Tp	°C	36.0	36.0	36.0	36.0	34.5	31.5	38.0	10.0	10.0	10.0	10.0	10.0	11.0	10.5
14	T(B)	°C	360	170	140	125	105	575	670	355	105	345	320	315	310	5
15	u(kal)	m/s														

nn: χ(CO) < 0.01%, χ(CO2) < 0.1%, χ(NOx) < 1 ppm

χ (CxHy) shown as methane equivalents

Appendix 1 Sheet 2

Test No. 03

1	Consec.No.		.085	.086	.087	.088	.089	.090	.091	.092	.093	.094
2	$\dot{m}$(G)	kg/h	1260									
3	$\dot{m}$(D)	kg/h	75									
4	ψ (D,G)	kg/kg	0,06									
5	x	m	-1.5	-2.0	-2.5		-2.0	-1.5	-1.0	-0.5	0.0	0.5
6	y	m	-0.5			-1.0						
7	z	m	5.0									
8	χ(O2)	%	16.4	19.2	20.8	20.3	21.0	19.7	20.4	20.0	21.0	21.0
9	χ(CO2)	%	1.9	5.0	0.2	0.6	0.8	0.7	0.4	0.5	0.1	nn
10	χ(CO)	%	0.36	0.09	nn	0.02	nn	0.04	0.03	nn	nn	nn
11	χ(CxHy)	ppm	2265	985	230	150	nn	205	210		nn	nn
12	χ(NOx)	ppm	14	8	1	3	nn	5	3	5	nn	nn
13	Tp	°C	35,0	27.0	15.0	13.0	12.0	22.0	15.0	11.5	13.0	10.5
14	T(B)	°C	635	420	180	180	120	230	190	210	85	50
15	u(kal)	m/s										

nn: χ(CO) < 0.01%, χ(CO2) < 0.1%, χ(NOx) < 1 ppm

χ(CxHy) shown as methane equivalents

Appendix 1 Sheet 1

Flare gas analysis

Test No. 06.010-.174

	x in %
H_2	63.3
H_2S	nn
CH_4	12.3
C_2H_6	10.2
C_2H_4	0.01
C_2H_2	nn
C_3H_8	6.9
C_3H_6	0.04
i-C_4H_{10}	0.9
n-C_4H_{10}	2.3
1-C_4H_8	nn
i-C_5H_{12}	2.4
n-C_5H_{12}	1.2
C_5-Isom.	0.2
C_6H_{14}	nn
C_6H_6	nn
C_6H_5-CH_3	nn
C_6H_5-C_2H_5	nn
N_2	nn

ϱ_G^o = 0.59 kg/m³

M = 13 g/mol

ϱ_{oC} = 0.43 kg carbon / kg flare gas

w_C = 0.73 kg carbon / kg flare gas

ϱ_{oH} = 0.16 kg hydrogen / m³ Flare gas

w_H = 0.27 kg hydrogen / kg flare gas

nn: < 0.01%

Appendix 1 Sheet 2

Test No. 06

1	Consec.No.		.010	.014	.019	.023	.027	.031	.035	.040	.045	.051	.054	.055	.056	.0[illegible]0
2	$\dot{m}$(G)	kg/h	1720													
3	$\dot{m}$(D)	kg/h	0													
4	ψ (D,G)	kg/kg	0.00													
5	x	m	-3.0	-2.5	-2.0	-1.5	-1.0	-0.5	0.0	0.5	1.0	1.5	2.0	2.5	3.0	
6	y	m	0.0													0.5
7	z	m	6.5													
8	χ(O2)	%	21.0	21.0	20.5	20.2	20.6	20.8	20.2	20.0	20.3	20.2	20.6	20.8	21.0	21.0
9	χ(CO2)	%	nn	nn	0.3	0.7	0.4	0.4	0.8	0.9	0.7	0.7	0.5	0.4	0.3	0.1
10	χ(CO)	%	nn	nn	nn	nn	nn	nn	nn	nn	nn	nn	nn	nn	nn	nn
11	χ(CxHy)	ppm	nn	nn	nn	13	10	5	30	45	10	10	10	10	10	10
12	χ(NOx)	ppm	nn	nn	2	5	3	nn	5	6	5	5	3	3	2	1
13	Tp	°C	11.5	12.0	17.0	21.5	18.5	19.5	22.5	24.5	23.0	23.5	20.0	19.0	17.0	17.0
14	T(B)	°C	65	55	105	190	155	135	210	245	200	210	160	135	100	65
15	u(kal)	m/s														

nn: χ(CO) < 0.01%, χ(CO2) < 0.1%, χ(NOx) < 1 ppm

χ(CxHy) shown as methane equivalents

Appendix 1 Sheet 2

Test No. 06

1	Consec.No.		.059	.060	.061	.062	.064	.065	.066	.067	.068	.070	.071	.072	.073	.07
2	$\dot{m}$(G)	kg/h	1700													
3	$\dot{m}$(D)	kg/h	0													
4	ψ (D,G)	kg/kg	0.00													
5	x	m	2.5	2.0	1.5	1.0	0.5	0.0	-0.5	-1.0	-1.5	-1.5	-1.0	-0.5	0.0	0.
6	y	m	0.5									1.0				
7	z	m	6.5													
8	χ(O2)	%	20.9	20.9	20.8	20.9	20.9	20.9	21.0	21.0	21.0	21.0	21.0	21.0	21.0	20.
9	χ(CO2)	%	0.3	0.4	0.5	0.4	0.4	0.3	0.2	nn	nn	nn	nn	nn	0.2	0
10	χ(CO)	%	nn	nn	nn	nn	nn	nn	nn	nn	nn	nn	nn	nn	nn	
11	χ(CxHy)	ppm	<10	<10	<10	<10	<10	<10	<10	<10	<10	<10	<10	<10	<10	<
12	χ(NOx)	ppm	2	3	3	3	3	2	1	nn	nn	nn	nn	nn	nn	
13	Tp	°C	17.5	19.0	20.0	18.5	18.5	17.5	15.0	13.5	12.0	11.5	11.5	11.5	15.0	10
14	T(B)	°C	105	120	150	135	155	125	105	85	70	55	65	60	90	1
15	u(kal)	m/s														

nn: χ(CO) < 0.01%, χ(CO2) < 0.1%, χ(NOx) < 1 ppm

χ(CxHy) shown as methane equivalents

Appendix 1 Sheet 2

Test No. 06

1	Consec.No.		.075	.076	.077	.078	.079	.080	.081	.082	.083	.084	.085	.086	.087	.088
2	$\dot{m}$(G)	kg/h	1700													
3	$\dot{m}$(D)	kg/h	0													
4	$\dot{\psi}$ (D,G)	kg/kg	0.00													
5	x	m	1.0	1.5	2.0	2.5	3.0	3.5	4.0	4.5	5.0	5.0	4.5	4.0	3.5	3.0
6	y	m	1.0									1.5				
7	z	m	6.5													
8	χ(O2)	%	20.9	20.9	20.9	20.5	20.3	20.4	20.5	20.8	20.4	20.6	20.4	20.7	20.6	20.6
9	χ(CO2)	%	0.3	0.3	0.3	0.6	0.7	0.6	0.6	0.4	0.6	0.4	0.7	0.5	0.5	0.4
10	χ(CO)	%	nn	nn	nn	nn	nn	nn	nn	nn	nn	nn	nn	nn	nn	nn
11	χ(CxHy)	ppm	<10	<10	<10	<10	25	20	16	20	<10	<10	<10	<10	<10	<10
12	χ(NOx)	ppm	1	2	2	4	4	4	3	2	4	2	3	3	3	2
13	Tp	°C	18.0	18.0	18.0	21.0	22.0	20.5	20.0	19.0	20.5	20.6	20.0	18.5	18.5	18.5
14	T(B)	°C	120	120	135	170	190	175	175	150	155	125	140	140	140	140
15	u(kal)	m/s														

nn: χ(CO) < 0.01%, χ(CO2) < 0.1%, χ(NOx) < 1 ppm

χ(CxHy) shown as methane equivalents

Appendix 1 Sheet 2

Test No. 06

1	Consec.No.		.089	.090	.091	.092	.093	.094	.095	.096	.097	.099	.100	.101	.102	.103
2	$\dot{m}$(G)	kg/h	1700		2100											
3	$\dot{m}$(D)	kg/h	0													
4	ψ (D,G)	kg/kg	0.00													
5	x	m	2.5	2.0	1.5	1.0	0.5	0.0	-0.5	-1.0	-1.5	-1.5	-1.0	-0.5	0.0	0.5
6	y	m	1.5									-0.5				
7	z	m	6.5													
8	χ(O2)	%	20.4	20.7	20.8	20.8	20.8	21.0	21.0	21.0	21.0	21.0	21.0	21.0	20.8	20.6
9	χ(CO2)	%	0.5	0.6	0.5	0.4	0.3	0.2	0.1	0.1	0.1	nn	nn	nn	0.1	0.3
10	χ(CO)	%	nn	nn	nn	nn	nn	nn	nn	nn	nn	nn	nn	nn	nn	nn
11	χ(CxHy)	ppm	12	30	<10	28	<10	<10	<10	<10	<10	<10	<10	<10	<10	<10
12	χ(NOx)	ppm	3	3	3	1	1	1	1	nn	nn	nn	nn	1	2	3
13	Tp	°C	20.0	19.5	19.0	17.0	15.5	14.0	14.0	14.5	13.5	12.5	13.0	14.0	17.0	19.5
14	T(B)	°C	155	170	170	150	125	105	100	100	80	65	65	80	105	140
15	u(kal)	m/s														

nn: χ(CO) < 0.01%, χ(CO2) < 0.1%, χ(NOx) < 1 ppm

χ(CxHy) shown as methane equivalents

Appendix 1 Sheet 2

Test No. 06

1	Consec.No.		.104	.105	.106	.107	.108	.109	.110	.111	.112	.114	.115	.116	.117	.11
2	$\dot{m}$(G)	kg/h	2100													
3	$\dot{m}$(D)	kg/h	0													
4	ψ (D,G)	kg/kg	0.00													
5	x	m	1.0	1.5	2.0	2.5	3.0	3.5	4.0	4.5	5.0	5.0	4.5	4.0	3.5	3.0
6	y	m	-0.5									-1.0				
7	z	m	6.5													
8	χ(O2)	%	20.5	20.5	20.5	20.4	20.5	20.4	20.5	20.5	20.6	20.7	20.8	20.7	20.5	20.5
9	χ(CO2)	%	0.4	0.4	0.4	0.6	0.5	0.6	0.5	0.5	0.4	0.3	0.2	0.3	0.5	0.
10	χ(CO)	%	nn	nn	nn	nn	nn	nn	nn	nn	nn	nn	nn	nn	nn	n
11	χ(CxHy)	ppm	<10	20	20	20	<10	<10	<10	<10	<10	<10	<10	<10	<10	<1
12	χ(NOx)	ppm	3	3	3	4	3	4	3	3	2	2	2	2	3	
13	Tp	°C	18.8	19.0	19.0	21.0	19.0	21.0	19.5	20.0	19.0	17.0	17.0	17.5	18.5	20.
14	T(B)	°C	135	140	140	170	155	170	155	150	140	110	105	110	140	15
15	u(kal)	m/s														

nn: χ(CO) < 0.01%, χ(CO2) < 0.1%, χ(NOx) < 1 ppm

χ(CxHy) shown as methane equivalents

Appendix 1 Sheet 2

Test No. 06

1	Consec.No.		.119	.120	.121	.122	.123	.124	.125	.126	.127	.128	.129	.131	.132	.13
2	$\dot{m}$(G)	kg/h	2100													
3	$\dot{m}$(D)	kg/h	0													
4	ψ (D,G)	kg/kg	0.00													
5	x	m	2.5	2.0	1.5	1.0	0.5	0.0	-0.5	-1.0	-1.5	-1.5	-1.0	-0.5	0.0	0.
6	y	m	-1.0									-1.5				
7	z	m	6.5													
8	χ(O2)	%	20.4	20.3	20.3	20.4	20.6	20.7	20.8	21.0	21.0	21.0	20.8	20.8	20.5	20.
9	χ(CO2)	%	0.6	0.8	0.7	0.6	0.5	0.3	0.2	0.1	0.1	0.1	0.2	0.5	0.5	0.
10	χ(CO)	%	nn	nn	nn	nn	nn	nn	nn	nn	nn	nn	nn	nn	nn	r
11	χ(CxHy)	ppm	20	30	60	30	15	<10	<10	<10	<10	<10	<10	<10	<10	1
12	χ(NOx)	ppm	4	5	5	5	4	3	2	1	1	nn	2	3	3	
13	Tp	°C	22.0	23.0	22.5	22.0	19.0	17.5	15.0	14.0	13.0	14.5	16.0	20.0	19.5	20.
14	T(B)	°C	180	210	210	200	160	125	100	85	70	75	95	145	140	15
15	u(kal)	m/s														

nn: χ(CO) < 0.01%, χ(CO2) < 0.1%, χ(NOx) < 1 ppm

χ(CxHy) shown as methane equivalents

Appendix 1 Sheet 2

Test No. 06

1	Consec.No.		.135	.136	.137	.139	.140	.141	.142	.143	.171	.172	.173	.174
2	$\dot{m}$(G)	kg/h	2100								2100			
3	$\dot{m}$(D)	kg/h	0								600			
4	Ψ (D,O)	kg/kg	0.00								0.29			
5	x	m	1.0	1.5	2.0	0.5	0.0	-0.5	-1.0	-1.5	-1.0			
6	y	m	-1.5			-2.0					0.0			
7	z	m	6.5								8.0	6.0	5.0	4.0
8	χ(O2)	%	20.7	20.8	20.9	21.0	20.8	21.0	21.0	21.0	20.5	20.0	19.1	17.2
9	χ(CO2)	%	0.3	0.3	0.2	nn	0.2	nn	nn	nn	0.4	1.2	1.6	2.3
10	χ(CO)	%	nn	nn	nn	nn	nn	nn	nn	nn	nn	nn	0.01	0.21
11	χ(CxHy)	ppm	10	<10	<10	<10	<10	<10	<10	<10	<10	20	65	350
12	χ(NOx)	ppm	2	2	nn	nn	nn	nn	nn	nn	2	5	6	10
13	Tp	°C	18.0	16.5	13.0	12.0	14.0	11.5	12.0	12.0	25.0	28.0	31.0	34.0
14	T(B)	°C	125	100	60	75	55	40	35	35	245	320	435	630
15	u(kal)	m/s												

nn: χ(CO) < 0.01%, χ(CO2) < 0.1%, χ(NOx) < 1 ppm

χ (CxHy) shown as methane equivalents

Appendix 1 Sheet X

Flare gas analysis

Test No. 07.055-.077

	x in %
H_2	63.1
H_2S	nn
CH_4	10.6
C_2H_6	6.0
C_2H_4	0.01
C_2H_2	nn
C_3H_8	4.6
C_3H_6	0.1
$i\text{-}C_4H_{10}$	1.0
$n\text{-}C_4H_{10}$	6.7
$1\text{-}C_4H_8$	nn
$i\text{-}C_5H_{12}$	3.0
$n\text{-}C_5H_{12}$	3.2
C_5-Isom.	1.8
C_6H_{14}	nn
C_6H_6	nn
$C_6H_5\text{-}CH_3$	nn
$C_6H_5\text{-}C_2H_5$	nn
N_2	nn

nn: <0.01%

ϱ_G^o = 0.79 kg/m^3

M = 18 g/mol

ϱ_o^C = 0.60 $\frac{\text{kg carbon}}{\text{m}^3 \text{ Flare gas}}$

w_C = 0.80 $\frac{\text{kg carbon}}{\text{kg flare gas}}$

ϱ_o^H = 0.19 $\frac{\text{kg hydrogen}}{\text{m}^3 \text{ Flare gas}}$

w_H = 0.20 $\frac{\text{kg hydrogen}}{\text{kg flare gas}}$

Appendix 1 Sheet 2

Test No. 07

1	Consec.No.		.055	.056	.057	.059	.060	.062	.064	.066	.069	.070	.071	.074	.075	.076
2	$\dot{m}$(G)	kg/h	1250													
3	$\dot{m}$(D)	kg/h	75	450	600	750	900	1200	1350	1200	900	1050	750	600	450	300
4	ψ (D,G)	kg/kg	0.06	0.36	0.48	0.60	0.72	.096	1.08	0.96	0.72	0.84	0.60	0.48	.036	0.24
5	x	m	0.0													
6	y	m	0.0													
7	z	m	4.0						3.0							
8	χ(O2)	%	19.8	20.2	20.0	19.1	18.9	18.3	16.6	17.4	16.8	17.0	17.1	17.6	19.2	19.7
9	χ(CO2)	%	0.4	0.3	0.5	1.1	1.0	1.5	2.5	2.0	2.5	2.3	2.2	1.9	1.1	0.8
10	χ(CO)	%	nn	nn	nn	nn	nn	nn	nn	nn	nn	nn	nn	0.07	0.03	0.01
11	χ(CxHy)	ppm	55	15	15	15	10	20	17	12	15	20	25	150	180	300
12	χ(NOx)	ppm	3	1	1	3	2	2	4	4	5	4	5	5	5	4
13	Tp	°C	17.5	22.5	25.0	25.0	24.0	30.0	34.5	34.0	36.0	36.0	45.0	37.0	30.0	27.5
14	T(B)	°C	160	105	170	265	300	350	510	490	545	510	525	505	405	350
15	u(kal)	m/s														

nn: χ(CO) < 0.01%, χ(CO2) < 0.1%, χ(NOx) < 1 ppm

χ (CxHy) shown as methane equivalents

Appendix 1 Sheet 1

Flare gas analysis Test No. 08.001-.132

	x in %
H_2	55.7
H_2S	nn
CH_4	11.9
C_2H_6	5.8
C_2H_4	0.02
C_2H_2	nn
C_3H_8	4.5
C_3H_6	0.2
$i\text{-}C_4H_{10}$	1.0
$n\text{-}C_4H_{10}$	0.2
$1\text{-}C_4H_8$	0.2
$i\text{-}C_5H_{12}$	5.7
$n\text{-}C_5H_{12}$	8.1
C_5-Isom.	5.6
C_6H_{14}	1.1
C_6H_6	0.1
$C_6H_5\text{-}CH_3$	nn
$C_6H_5\text{-}C_2H_5$	nn
N_2	nn

$\varrho_G^o = 1.10$ kg/m^3

$M = 25$ g/mol

$\varrho_C^o = 0.86$ kg carbon / m^3 flare gas

$w_C = 0.78$ kg carbon / kg flare gas

$\varrho_H^o = 0.24$ kg hydrogen / m^3 flare gas

$w_H = 0.22$ kg hydrogen / kg flare gas

-

nn: < 0.01%

Flare gas analysis Test No. 08.133-.172

	x in %
H_2	50.4
H_2S	nn
CH_4	12.6
C_2H_6	6.8
C_2H_4	0.02
C_2H_2	nn
C_3H_8	18.3
C_3H_6	0.2
i-C_4H_{10}	0.4
n-C_4H_{10}	0.9
1-C_4H_8	0.1
i-C_5H_{12}	3.3
n-C_5H_{12}	4.3
C_5-Isom.	2.6
C_6H_{14}	0.3
C_6H_6	0.3
C_6H_5-CH_3	nn
C_6H_5-C_2H_5	nn
N_2	nn

ϱ_G^o = 1.0 kg/m³

M = 22 g/mol

ϱ_{oC} = 0.78 kg carbon / m³ flare gas

w_C = 0.78 kg carbon / kg flare gas

ϱ_{oH} = 0.22 kg hydrogen / m³ flare gas

w_H = 0.22 kg hydrogen / kg flare gas

nn: <0.01%

Appendix 1 Sheet 2

Test No. 08

1	Consec. No.		.001	.002	.003	.004	.005	.006	.007	.008	.009	.010	.011	.012	.015	.016
2	$\dot{m}$(G)	kg/h	1250												ϕ40	
3	$\dot{m}$(D)	kg/h	0													
4	ψ (D,G)	kg/kg	0.00													
5	x	m	0.0	-0.5	-1.0	-1.5	-2.0	-2.5	-3.0	-3.5	-4.0	-4.5	-5.0	-5.5	-4.5	
6	y	m	0.0												4.5	6.0
7	z	m	5.0												20.8	20.5
8	χ(O2)	%	21.0	20.8	20.8	20.9	20.8	20.3	20.9	20.8	20.6	20.6	19.7	20.3	20.8	20.5
9	χ(CO2)	%	nn	0.1	0.1	0.1	0.1	0.4	0.1	0.1	0.2	0.3	0.8	0.5	0.2	0.3
10	χ(CO)	%	nn	nn	nn	nn	nn	nn	nn	nn	nn	nn	nn	nn	nn	nn
11	χ(CxHy)	ppm	<5	<5	<5	<5	<5	<5	<5	<5	<5	<5	<5	<5	<5	<5
12	χ(NOx)	ppm	nn	1	1	1	2	3	1	2	3	3	5	4	2	3
13	Tp	°C	15.5	15.5	15.5	15.5	15.5	16.0	16.0	16.0	16.0	18.5	25.5	23.5	16.5	20.0
14	T(B)	°C	70	70	70	80	90	140	90	90	105	110	195	155	65	80
15	u(kal)	m/s														

nn: χ(CO) < 0.01%, χ(CO2) < 0.1%, χ(NOx) < 1 ppm

χ(CxHy) shown as methane equivalents

Appendix 1 Sheet 2

Test No. 08

1	Consec. No.		.017	.018	.019	.020	.022	.023	.025	.026	.027	.028	.029	.033	.034	0.35
2	$\dot{m}$(G)	kg/h	940											780		
3	$\dot{m}$(D)	kg/h	0													
4	ψ (D,G)	kg/kg	0.00													
5	x	m	-4.5													
6	y	m	0.0						0.5					1.0		
7	z	m	3.5	3.0	2.5	2.0	1.5	1.0	4.5	4.0	3.5	3.0	2.5	4.5	4.0	3.5
8	χ(O2)	%	19.6	19.4	19.8	20.3	20.7	20.9	20.4	20.5	20.3	19.2	19.6	20.7	19.8	19.4
9	χ(CO2)	%	0.7	0.9	0.7	0.4	0.2	0.2	0.3	0.2	0.4	0.8	0.8	0.2	0.5	0.6
10	χ(CO)	%	nn	nn	nn	nn	nn	nn	nn	nn	nn	nn	nn	nn	nn	nn
11	χ(CxHy)	ppm	<5	<5	<5	<5	<5	<5	<5	<5	<5	<5	<5	8	<5	<5
12	χ(NOx)	ppm	5	6	5	4	3	3	4	3	4	6	6	3	5	6
13	Tp	°C	25.0	27.5	25.0	23.0	/	/	22.0	21.0	22.0	26.5	/	17.0	25.0	25.0
14	T(B)	°C	126	220	196	154	105	90	110	120	150	210	195	105	140	195
15	u(kal)	m/s														

nn: χ(CO) < 0.01%, χ(CO2) < 0.1%, χ(NOx) < 1 ppm

χ(CxHy) shown as methane equivalents

Appendix 1 Sheet 2

Test No.. 08

1	Consec. No.		.036	.037	.038	.039	.040	.041	.042	.043	.044	.045	.046	.047	.058	.05
2	$\dot{m}$(G)	kg/h	780					630							1500	
3	$\dot{m}$(D)	kg/h	0					0							225	
4	ψ (D,G)	kg/kg	0.00					0.00							0.15	
5	x	m	-4.5												-2.5	
6	y	m	1.0					1.5							0.0	
7	z	m	3.0	2.5	2.0	1.5	1.0	4.5	4.0	3.5	3.0	2.5	2.0	1.5	5.0	6.0
8	χ(O2)	%	19.3	19.1	19.8	20.5	20.5	21.0	20.3	20.6	20.3	20.1	19.8	20.5	18.3	18.7
9	χ(CO2)	%	0.7	0.9	0.6	0.3	0.3	0.1	0.2	0.2	0.2	0.2	0.5	0.3	1.3	1.0
10	χ(CO)	%	nn	nn	nn	nn	nn	nn	nn	nn	nn	nn	nn	nn	0.04	0.01
11	χ(CxHy)	ppm	<5	<5	<5	<5	<5	<5	<5	<5	<5	<5	<5	<5	270	85
12	χ(NOx)	ppm	6	7	6	5	4	3	4	4	4	5	5	4	8	6
13	Tp	°C	27.0	27.5	25.5	22.0	20.0	17.0	21.0	21.0	21.0	21.0	25.0	22.0	29.0	27.0
14	T(B)	°C	210	230	195	135	110	70	105	100	100	105	135	100	385	315
15	u(kal)	m/s														

nn: χ(CO) < 0.01%, χ(CO2) < 0.1%, χ(NOx) < 1 ppm

χ (CxHy) shown as methane equivalents

Appendix 1 Sheet 2

Test No. 08

1	Consec. No.		.060	.061	.062	.122	.123	.124	.125	.127	.128	.129	.130	.131	.132	.133
2	$\dot{m}$(G)	kg/h	1500			2200				2200						780
3	$\dot{m}$(D)	kg/h	225			1425				1425	1125	825	525	225	75	0
4	ψ (D,G)	kg/kg	0.15			0.65				0.65	0.51	0.38	0.24	0.10	0.03	0.00
5	x	m	-2.5			0.0				0.0						0.0
6	y	m	0.0			0.0				0.0						0.0
7	z	m	7.0	8.0	4.0	8.0	7.0	6.0	5.0	7.0						5.0
8	χ(O2)	%	19.7	20.1	17.6	17.5	17.1	16.6	13.6	16.4	16.4	16.0	17.1	18.2	18.0	19.8
9	χ(CO2)	%	0.5	0.2	1.9	1.8	2.1	2.3	3.9	2.5	2.5	2.8	2.2	1.4	1.5	0.1
10	χ(CO)	%	nn	nn	0.10	nn	nn	nn	nn	nn	nn	0.02	0.03	0.01	0.01	nn
11	χ(CxHy)	ppm	20	<10	530	<10	<10	<10	<10	<10	<10	40	80	120	100	<10
12	χ(NOx)	ppm	3	1	8	6	7	8	11	8	9	12	9	6	8	3
13	Tp	°C	23.0	20.0	34.0	37.5	38.5	39.0	39.5	39.5	39.5	41.5	43.5	34.0	25.0	23.0
14	T(B)	°C	210	105	490	440	485	560	>700	560	540	615	520	370	370	140
15	u(kal)	m/s								6.7	6.0	5.1	3.9	3.5	4.1	

nn: χ(CO) < 0.01%, χ(CO2) < 0.1%, χ(NOx) < 1 ppm

(CxHy) shown as methane equivalents

Appendix 1 Sheet 2

Test No. 08

1	Consec. No.		.134	.135	.136	.138	.139	.140	.141	.143	.144	.145	.146	.148	.149	.150
2	$\dot{m}$(G)	kg/h	780													
3	$\dot{m}$(D)	kg/h	0			225				450				675		
4	ψ (D,G)	kg/kg	0.00			0.29				0.58				0.87		
5	x	m	0.0													
6	y	m	0.0													
7	z	m	5.0	4.0	3.0	6.0	5.0	4.0	3.0	6.0	5.0	4.0	3.0	6.0	5.0	4.0
8	χ(O2)	%	19.4	19.0	17.9	20.5	19.4	19.0	16.4	19.5	18.8	17.6	16.4	18.7	17.3	16.0
9	χ(CO2)	%	0.7	1.1	1.5	nn	0.6	0.7	2.3	0.7	1.2	1.9	2.3	1.1	1.9	2.5
10	χ(CO)	%	nn	0.01	0.11	nn	nn	nn	0.25	nn	nn	nn	0.03	nn	nn	nn
11	χ(Cxdly)	ppm	20	160	1000	<10	25	50	1000	<10	<10	30	60	< 10	<10	<10
12	χ(NOx)	ppm	4	5	9	2	3	3	9	2	3	5	8	2	5	7
13	Tp	°C	25.0	28.5	32.0	25.0	27.0	27.0	36.0	27.5	32.5	36.5	36.0	33.0	35.0	36.5
14	T(B)	°C	195	285	440	100	210	280	545	230	280	455	560	315	455	575
15	u(kal)	m/s														

nn: χ(CO) < 0.01%, χ(CO2) < 0.1%, χ(NOx) < 1 ppm

χ (Cxdly) shown as methane equivalents

Appendix 1 Sheet 2

Test No. 08

1	Consec. No.		.151	.153	.154	.155	.156	.158	.159	.160	.161	.163	.164	.165	.166	.167
2	$\dot{m}$(G)	kg/h	780													
3	$\dot{m}$(D)	kg/h	675	900				1125				1350				
4	Ψ (D,G)	kg/kg	0.87	1.15				1.44				1.73				
5	x	m	0.0													
6	y	m	0.0													
7	z	m	3.0	6.0	5.0	4.0	3.0	6.0	5.0	4.0	3.0	6.0	5.0	4.0	3.0	4.0
8	χ(O2)	%	15.8	18.9	17.9	17.1	16.2	19.2	18.1	17.3	15.6	19.0	18.1	17.9	16.7	17.9
9	χ(CO2)	%	2.8	1.0	1.5	2.1	2.6	0.7	1.4	2.0	3.0	0.9	1.3	1.5	2.1	1.5
10	χ(CO)	%	nn	nn	nn	nn	nn	nn	nn	nn	nn	0.005	0.01	0.02	0.03	0.03
11	χ(CxHy)	ppm	<10	50	70	80	100	75	75	95	100	130	200	325	390	360
12	χ(NOx)	ppm	8	2	3	4	5	1	2	4	6	1	2	2	4	2
13	Tp	°C	37.0	33.5	34.0	35.0	33.0	31.5	32.5	34.5	37.0	36.5	35.0	35.5	41.0	37.5
14	T(B)	°C	660	315	365	490	630	240	350	470	645	285	345	400	525	420
15	u(kal)	m/s														

nn: χ(CO) < 0.01%, χ(CO2) < 0.1%, χ(NOx) < 1 ppm

χ (CxHy) shown as methane equivalents

Test No. 08

1	Consec. No.		.168	.169	.170	.171	.172
2	$\dot{m}$(G)	kg/h	780				
3	$\dot{m}$(D)	kg/h	1050	750	450	150	0
4	ψ (D,G)	kg/kg	1.35	0.96	0.58	0.19	0.00
5	x	m	0.0			0.5	2.0
6	y	m	0.0			0.0	0.5
7	z	m	4.0				
8	χ(O2)	%	17.5	16.6	15.8	15.2	16.2
9	χ(CO2)	%	1.7	2.2	2.8	2.7	2.3
10	χ(CO)	%	0.01	0.01	0.01	0.28	0.26
11	χ(CxHy)	ppm	90	5	5	100	530
12	χ(NOx)	ppm	3	5	8	5	8
13	Tp	^{o}C	38.0	39.0	42.5	45.0	41.0
14	T(B)	^{o}C	440	520	580	525	490
15	u(kal)	m/s	>7.6	6.2	5.4	2.5	3.1

nn: χ(CO) < 0.01%, χ(CO2) < 0.1%, χ(NOx) < 1 ppm

χ (CxHy) shown as methane equivalents

Appendix 1 Sheet 1

Flare gas analysis

Test No. 11.011-.105

	x in %
H_2	50.6
H_2S	0.2
CH_4	13.8
C_2H_6	6.8
C_2H_4	0.01
C_2H_2	nn
C_3H_8	11.8
C_3H_6	0.04
$i\text{-}C_4H_{10}$	2.2
$n\text{-}C_4H_{10}$	5.0
$1\text{-}C_4H_8$	nn
$i\text{-}C_5H_{12}$	4.7
$n\text{-}C_5H_{12}$	3.2
C_5-Isom.	0.8
C_6H_{14}	nn
C_6H_6	nn
$C_6H_5\text{-}CH_3$	nn
$C_6H_5\text{-}C_2H_5$	nn
N_2	0.6

nn: < 0.01%

$\varrho_G^o = 1.0$ kg/m^3

$M = 22$ g/mol

$\varrho_o^C = 0.75$ $\frac{\text{kg carbon}}{\text{m}^3 \text{ flare gas}}$

$w_C = 0.75$ $\frac{\text{kg carbon}}{\text{kg flare gas}}$

$\varrho_o^H = 0.22$ $\frac{\text{kg hydrogen}}{\text{m}^3 \text{ flare gas}}$

$w_H = 0.22$ $\frac{\text{kg hydrogen}}{\text{kg flare gas}}$

Appendix 1 Sheet. 2

Test No. 11

1	Consec. No.		.001	.002	.003	.004	.006	.007	.008	.009	.012	.014	.015	.016	.017	.018
2	$\dot{m}$(G)	kg/h	1100													
3	$\dot{m}$(D)	kg/h	750													
4	ψ (D,G)	kg/kg	0.68													
5	x	m	0.0	0.5	1.0	-0.5	-1.5	-2.0	-2.5	-1.0						
6	y	m	0.0								0.5	1.0	1.5	2.0	2.5	-0.5
7	z	m	7.0													
8	χ(O2)	%	18.4	20.1	21.0	18.8	18.4	19.7	20.6	17.3	17.8	19.7	20.1	20.4	20.6	18.0
9	χ(CO2)	%	1.5	0.5	0.1	1.4	1.4	0.8	0.3	2.2	2.0	0.9	0.5	0.4	0.3	1.8
10	χ(CO)	%	nn	nn	nn	nn	nn	nn	nn	nn	nn	nn	nn	nn	nn	nn
11	χ(CxHy)	ppm	<10	<10	<10	<10	<10	<10	<10	23	<10	<10	<10	<10	<10	<10
12	χ(NOx)	ppm	6	2	nn	5	6	3	2	9	8	3	2	2	2	6
13	Tp	°C	32.0	30.0	24.0	31.0	31.0	27.0	22.0	29.0	32.0	30.0	29.0	26.0	23.0	31.0
14	T(B)	°C	385	210	40	380	380	245	105	485	455	260	180	140	90	420
15	u(kal)	m/s	4.6	1.9	1.2	4.6	5.8	4.6	3.1	7.1	5.4	2.8	2.0	1.6	2.2	6.2

nn: χ(CO) < 0.01%, χ(CO2) < 0.1%, χ(NOx) < 1 ppm

χ(CxHy) shown as methane equivalents

Appendix 1 Sheet 2

Test No. 11

1	Consec. No.		0.19	.020	.021	.022	.023	.024	.025	.026	.027	.029	.030	.031	.032	.033
2	$\dot{m}$(G)	kg/h	1100													
3	$\dot{m}$(D)	kg/h	750													
4	ψ (D,G)	kg/kg	0.68													
5	x	m	-1.0			-2.5	0.5	0.0	-2.0	-1.5	-0.5	-1.5	-0.5	-2.0	0.0	0.5
6	y	m	-1.0	-1.5	-2.0	-1.5		-1.0		-0.5		0.5		1.0		1.5
7	z	m	7.0													
8	χ(O2)	%	19.1	20.4	21.0	21.0	21.0	20.4	20.9	19.9	19.5	19.7	18.0	20.8	18.6	20.1
9	χ(CO2)	%	1.3	0.4	0.1	0.1	0.1	0.4	0.2	0.6	0.8	0.7	1.7	0.3	1.2	0.
10	χ(CO)	%	nn	nn	nn	nn	nn	nn	nn	nn	nn	nn	nn	nn	nn	n
11	χ(CxHy)	ppm	<10	<10	<10	<10	<10	<10	<10	30	12	26	67	37	30	3
12	χ(NOx)	ppm	5	2	1	1	1	2	1	3	3	3	6	2	5	
13	Tp	°C	29.0	25.0	20.0	18.0	16.0	19.0	20.0	23.0	27.0	28.0	29.0	27.0	25.0	26.
14	T(B)	°C	335	175	70	35	25	140	70	210	245	230	420	160	310	17
15	u(kal)	m/s	5.4	2.7	1.5	1.0	1.0	2.8	2.0	4.6	5.1	4.4	6.2	3.2	5.1	3.

nn: χ(CO) < 0.01%, χ(CO2) < 0.1%, χ(NOx) < 1 ppm

χ (CxHy) . shown as methane equivalents

Appendix 1 Sheet 2

Test No. 11

1	Consec. No.		.034	.035	.066	.067	.068	.069	.070	.072	.074	.075	.076	.077	.078	07
2	$\dot{m}$(G)	kg/h	1100		940											94
3	$\dot{m}$(D)	kg/h	750		300											120
4	ψ (D,G)	kg/kg	0.68		0.32											1.28
5	x	m	-2.5	1.0	3.0	2.5	2.0	1.5	1.0	0.5	0.0	-0.5	-1.0	-1.5	-2.0	0.0
6	y	m	1.5	2.0	0.0											
7	z	m	7.0													5.5
8	χ(O2)	%	21.0	21.0	21.0	21.0	21.0	20.6	20.1	18.4	17.1	18.6	20.6	20.8	21.0	16.9
9	χ(CO2)	%	nn	nn	nn	nn	0.1	0.3	0.5	1.7	2.5	1.5	0.3	0.1	nn	2.4
10	χ(CO)	%	nn	nn	nn	nn	nn	nn	nn	nn	nn	nn	nn	nn	nn	nn
11	χ(CxHy)	ppm	35	<10	<10	<10	<10	<10	<10	<10	55	30	15	<10	<10	<10
12	χ(NOx)	ppm	1	1	nn	1	1	3	3	6	11	10	1	nn	nn	nn
13	Tp	°C	24.0	21.0	13.0	15.0	14.0	23.0	23.0	29.0	29.0	28.0	24.0	20.0	17.0	31.0
14	T(B)	°C	70	45	35	40	50	105	155	315	490	420	210	120	50	545
15	u(kal)	m/s	0,5	1,5	1,4	1,6	1,8	2,2	3,1	4,6	5,1	4,3	1,2	1,0	0,5	7.0

nn: χ(CO) < 0.01%, χ(CO2) < 0.1%, χ(NOx) < 1 ppm
χ(CxHy) shown as methane equivalents

Appendix 1 Sheet 2

Test No. 11

1	Consec. No.		.095	.097	.098	.100	.102	.103	.104	.105	.107	.108	.110	.111	.113	.115
2	$\dot{m}$(G)	kg/h	940								780					
3	$\dot{m}$(D)	kg/h	1200								1300					
4	ψ (D,G)	kg/kg	1.28								1.67					
5	x	m	-0.5	-1.0	-1.5	2.0	2.5	1.5	1.0	0.5	-1.5	-1.0	-0.5	0.0	0.5	1.0
6	y	m	0.0													
7	z	m	5.5								3.5					
8	χ(O2)	%	19.1	20.9	21.0	20.6	21.0	19.9	19.5	17.1	21.0	20.4	17.5	16.7	16.9	19.7
9	χ(CO2)	%	1.0	0.1	nn	0.4	0.1	0.7	0.9	2.0	nn	0.4	0.8	1.8	2.0	0.8
10	χ(CO)	%	nn	nn	nn	nn	nn	nn	nn	nn	nn	nn	0.03	0.05	0.07	0.02
11	χ(CxHy)	ppm	<10	<10	<10	<10	<10	<10	<10	<10	<10	<10	50	125	210	<10
12	χ(NOx)	ppm	2	1	1	2	1	3	3	6	nn	1	4	5	4	2
13	Tp	°C	29.0	23.0	19.0	23.0	27.0	30.0	31.0	35.0	17.0	20.0	27.0	30.0	34.0	31.0
14	T(B)	°C	365	140	70	125	70	155	225	455	80	15	450	520	430	265
15	u(kal)	m/s	4.7	0.7	0.7	2.1	1.9	2.6	4.3	7.6	0.8	2.4	7.8	7.8	6.6	3.7

nn: χ(CO) < 0.01%, χ(CO2) < 0.1%, χ(NOx) < 1 ppm

χ(CxHy) shown as methane equivalents

Test No. 11

1	Consec. No.		.116	.117	.118	.142	.143	.144	.145
2	$\dot{m}$(G)	kg/h	780			1100			
3	$\dot{m}$(D)	kg/h	1300			0			
4	Ψ (D,G)	kg/kg	1.67			0.00			
5	x	m	1.5	2.0	2.5	0.0			
6	y	m	0.0						
7	z	m	3.5			8.0	7.0	6.0	5.0
8	χ(O2)	%	20.4	20.9	21.0	19.6	17.8	16.9	16.2
9	χ(CO2)	%	0.3	0.1	nn	1.0	1.7	2.1	2.5
10	χ(CO)	%	nn	nn	nn	nn	0.10	0.20	0.30
11	χ(CxHy)	ppm	<10	<10	<10	30	300	615	1100
12	χ(NOx)	ppm	1	1	nn	6	5	10	13
13	Tp	°C	29.0	27.0	26.0	30.0	29.0	30.0	35.0
14	T(B)	°C	175	90	50	265	350	490	580
15	u(kal)	m/s	2.5	1.4	0.8				

nn: χ(CO) < 0.01%, χ(CO2) < 0.1%, χ(NOx) < 1 ppm

χ (CxHy) shown as methane equivalents

Volume portions of hydrocarbons and hydrogen in the off-gas

Test No. 11

Measuring object	% in		Sample drawn at consec. No. Coordinates not known		
CH_4	ppm	370	135	740	120
C_2H_6	ppm	5	5	5	nn
C_2H_4	ppm	60	40	150	10
C_2H_2	ppm	180	55	335	35
C_3H_8	ppm	10	5	5	5
C_3H_6	ppm	nn	nn	5	nn
$i\text{-}C_4H_{10}$	ppm	5	nn	nn	nn
$n\text{-}C_4H_{10}$	ppm	15	5	5	nn
$1\text{-}C_4H_8$	ppm	nn	nn	nn	nn
$i\text{-}C_5H_{12}$	ppm	nn	nn	nn	nn
$n\text{-}C_5H_{12}$	ppm	30	15	10	nn
C_5-Isom.	ppm	nn	nn	nn	nn
C_6H_{14}	ppm	nn	nn	nn	nn

nn : < 1 ppm

Appendix 1 Sheet 1

Flare gas analysis — Test No.: 12.030-.034

	x in %
H_2	45.4
H_2S	nn
CH_4	10.3
C_2H_6	4.8
C_2H_4	nn
C_2H_2	nn
C_3H_8	4.2
C_3H_6	nn
$i\text{-}C_4H_{10}$	4.1
$n\text{-}C_4H_{10}$	12.1
$1\text{-}C_4H_8$	nn
$i\text{-}C_5H_{12}$	2.8
$n\text{-}C_5H_{12}$	3.8
C_5-Isom.	3.5
C_6H_{14}	nn
C_6H_6	nn
$C_6H_5\text{-}CH_3$	nn
$C_6H_5\text{-}C_2H_5$	nn
N_2	7.5
H_2O	1.7

nn: < 0.01%

$\varrho_G^o = 1.16$ kg/m³

$M = 26$ g/mol

$\varrho_{oC} = 0.83$ kg carbon / m³ flare gas

$w_C = 0.72$ kg carbon / kg flare gas

$\varrho_{oH} = 0.22$ kg hydrogen / m³ flare gas

$w_H = 0.19$ kg hydrogen / kg flare gas

Appendix 1 Sheet 2

Test No. 12

1	Consec. No.		.030						.032						
2	$\dot{m}$(G)	kg/h	600						750						
3	$\dot{m}$(D)	kg/h	150						180						
4	Ψ (D,G)	kg/kg	0.25						0.24						
5	x	m	2.0						1.0						
6	y	m	0.2						0.2						
7	z	m	6.5						8.0						
8	$\hat{x}$(O2)	%	16.5	17.2	16.6	16.8	17.6	14.9	16.1	16.9	17.2	18.5	19.2	18.2	18.1	19.1
9	$\hat{x}$(CO2)	%	2.1	1.6	1.9	1.8	1.4	2.8	2.3	1.8	1.6	0.9	0.4	0.6	0.9	0.1
10	$\hat{x}$(CO)	%	0.04	nn	0.03	nn	0.05	0.12	0.07	0.05	nn	nn	nn	nn	nn	nn
11	$\hat{x}$(CxHy)	ppm	570	90	205	350	90	735	1000	200	10	10	20	10	200	10
12	x(NOx)	ppm														
13	Tp	°C														
14	$\hat{T}$(D)	°C	330	346	385	406	396	497	406	371	315	266	210	196	217	13
15	u(kal)	m/s														

nn: $\hat{x}$(CO) < 0.01%, $\hat{x}$(CO2) < 0.1%, x(NOx) < 1 ppm

x (CxHy) shown as methane equivalents

Appendix 1 Sheet 2

Test No. 12

1	Consec. No.		.032								.034				
2	$\dot{m}$(G)	kg/h	750												
3	$\dot{m}$(D)	kg/h	180												
4	ψ (D,G)	kg/kg	0.24												
5	x	m	1.0								1.0				
6	y	m	0.2								0.0				
7	z	m	8.0								6.0				
8	$\hat{\chi}$(O2)	%	18.7	18.9	18.5	18.3	18.5	18.5	17.9	17.2	19.6	17.9	18.3	18.5	17.6	17.9
9	$\hat{\chi}$(CO2)	%	0.7	0.5	1.0	1.2	0.9	0.9	1.4	1.1	0.5	1.2	1.1	0.9	1.2	1.2
10	$\hat{\chi}$(CO)	%	nn	nn	nn	nn	nn	nn	nn	nn	nn	nn	nn	nn	nn	nn
11	$\hat{\chi}$(CxHy)	ppm	70	10	10	55	140	100	10	45	50	190	5	100	310	215
12	χ(NOx)	ppm														
13	Tp	°C														
14	$\hat{T}$(D)	°C	147	140	182	217	203	217	245	207	140	287	301	294	315	330
15	u(kal)	m/s														

nn: $\hat{\chi}$(CO) < 0.01%, $\hat{\chi}$(CO2) < 0.1%, χ(NOx) < 1 ppm

$\hat{\chi}$(CxHy) shown as methane equivalents

Appendix 1 Sheet 2

Test No. 12

1	Consec. No.		.034				
2	$\dot{m}(G)$	kg/h	750				
3	$\dot{m}(D)$	kg/h	180				
4	Ψ (D,G)	kg/kg	0.24				
5	x	m	1.0				
6	y	m	0.0				
7	z	m	6.0				
8	$\hat{\chi}(O2)$	%	18.1	18.1	17.8	16.0	19.9
9	$\hat{\chi}(CO2)$	%	1.3	1.2	1.1	2.6	0.3
10	$\hat{\chi}(CO)$	%	nn	nn	nn	0.11	nn
11	$\hat{\chi}(Cx Hy)$	ppm	10	200	120	680	225
12	$\chi(NOx)$	ppm					
13	Tp	^oC					
14	$\hat{T}(D)$	^oC	350	330	330	450	310
15	u(kal)	m/s					

nn: $\hat{\chi}(CO) < 0.01\%$, $\hat{\chi}(CO2) < 0.1\%$, $\hat{\chi}(NOx) < 1$ ppm

$\hat{\chi}(Cx Hy)$ shown as methane equivalents

Appendix 1 Sheet 3

Volume portions of hydrocarbons and hydrogen in the off-gas

Test No. 12

Measuring object	x	Sample drawn at consec. No.	
	in	.032	.034
CH_4	ppm	260	240
C_2H_6	ppm	2	5
C_2H_4	ppm	15	20
C_2H_2	ppm	115	100
C_3H_8	ppm	15	20
C_3H_6	ppm	nn	nn
$i\text{-}C_4H_{10}$	ppm	15	10
$n\text{-}C_4H_{10}$	ppm	45	25
$1\text{-}C_4H_8$	ppm	nn	nn
$i\text{-}C_5H_{12}$	ppm	85	75
$n\text{-}C_5H_{12}$	ppm	65	60
C_5-Isom.	ppm	nn	nn
C_6H_{14}	ppm	nn	nn

nn : 1 ppm

Flare gas analysis

Test No. 13.001-.020

	x in %
H_2	63.0
H_2S	nn
CH_4	13.9
C_2H_6	6.5
C_2H_4	0.02
C_2H_2	nn
C_3H_8	3.5
C_3H_6	0.1
$i\text{-}C_4H_{10}$	1.0
$n\text{-}C_4H_{10}$	2.0
$1\text{-}C_4H_8$	nn
$i\text{-}C_5H_{12}$	5.1
$n\text{-}C_5H_{12}$	3.6
C_5-Isom.	1.5
C_6H_{14}	nn
C_6H_6	nn
$C_6H_5\text{-}CH_3$	nn
$C_6H_5\text{-}C_2H_5$	nn
N_2	nn

nn: < 0.01%

$\varrho_G^o = 0.75$ kg/m^3

$M = 17$ g/mol

$\varrho_o^C = 0.57$ kg carbon / m^3 flare gas

$w_C = 0.76$ kg carbon / kg flare gas

$\varrho_o^H = 0.18$ kg hydrogen / m^3 flare gas

$w_H = 0.24$ kg hydrogen / kg flare gas

Appendix 1 Sheet 2

Test No. 13

1	Consec.No.		.011	.012	.013	.014	.015	.016	.017	.018	.019	.020
2	$\dot{m}$(G)	kg/h	1780									
3	$\dot{m}$(D)	kg/h	0									
4	ψ (D,G)	kg/kg	0.00									
5	x	m	-0.5	-1.0	-1.5	-2.0	-2.5	0.0	0.5	1.0	1.5	2.0
6	y	m	0.0									
7	z	m	8.0									
8	χ(O2)	%	18.4	20.4	20.5	21.0	21.0	13.2	17.0	19.2	19.3	20.6
9	χ(CO2)	%	1.6	0.2	0.1	nn	nn	4.2	2.9	0.8	0.7	0.2
10	χ(CO)	%	0.06	nn	nn	nn	nn	0.67	0.13	nn	nn	nn
11	χ(CxHy)	ppm	370	10	10	10	10	2780	1250	160	40	10
12	χ(NOx)	ppm	7	1	1	1	1	9	9	4	3	1
13	Tp	^oC	30.0	20.0	15.0	14.0	14.0	32.5	30.0	28.0	24.0	20.0
14	T(B)	^oC	530	295	205	190	175	670	560	400	290	105
15	u(kal)	m/s	3.1	1.1	1.0	0.8	0.8	5.0	3.4	1.9	3.3	1.9

nn: χ(CO) < 0.01%, χ(CO2) < 0.1%, χ(NOx) < 1 ppm

χ(CxHy) shown as methane equivalents

Flare gas analysis

Test No. 14.017-.031

	x in %
H_2	63.4
H_2S	nn
CH_4	12.3
C_2H_6	4.8
C_2H_4	nn
C_2H_2	nn
C_3H_8	7.6
C_3H_6	0.01
$i\text{-}C_4H_{10}$	2.0
$n\text{-}C_4H_{10}$	4.0
$1\text{-}C_4H_8$	nn
$i\text{-}C_5H_{12}$	3.9
$n\text{-}C_5H_{12}$	1.4
C_5-Isom.	0.3
C_6H_{14}	nn
C_6H_6	nn
$C_6H_5\text{-}CH_3$	nn
$C_6H_5\text{-}C_2H_5$	nn
N_2	nn

ϱ^o_G = 0.72 kg/m³

M = 16 g/mol

ϱ_{oC} = 0.54 kg carbon / m³ flare gas

w_C = 0.75 kg carbon / kg flare gas

ϱ_{oH} = 0.18 kg hydrogen / m³ flare gas

w_H = 0.25 kg hydrogen / kg flare gas

nn: < 0.01%

Appendix 1 Sheet 2

Test No. 14

1	Consec.No.		.017	.018	.019	.020	.021	.028	.029	.030	.031
2	$\dot{m}$(G)	kg/h	940					940			
3	$\dot{m}$(D)	kg/h	0					315			
4	ψ (D,G)	kg/kg	0.00					0.34			
5	x	m	-2.0	-1.5	-1.0	-0.5	0.0	-2.0	-2.5	-1.5	-0.5
6	y	m	0.0					6.0			
7	z	m	8.0								
8	χ(O2)	%	20.8	20.6	19.8	19.0	20.6	18.7	19.1	18.7	20.1
9	χ(CO2)	%	0.2	0.3	0.6	1.0	0.4	1.3	1.0	1.4	0.4
10	χ(CO)	%	nn	nn	nn	nn	nn	nn	nn	nn	nn
11	χ(CxHy)	ppm	10	10	10	11	7	12	nn	12	nn
12	χ(NOx)	ppm	5	5	5	6	5	5	5	6	5
13	Tp	^{o}C	15.0	17.0	20.0	26.0	17.0	30.0	25.0	38.0	23.0
14	T(B)	^{o}C	65	70	210	315	150	385	315	420	175
15	u(kal)	m/s	1.4	1.2	3.5	4.2	1.6	3.7	3.8	3.3	1.4

nn: χ(CO) < 0.01%, χ(CO2) < 0.1%, χ(NOx) < 1 ppm

χ(CxHy) shown as methane equivalents

Flare gas analysis

Test No. 15 Soot

	x in %
H_2	53.4
H_2S	0.1
CH_4	11.5
C_2H_6	7.3
C_2H_4	nn
C_2H_2	nn
C_3H_8	6.0
C_3H_6	nn
i-C_4H_{10}	4.7
n-C_4H_{10}	8.5
1-C_4H_8	nn
i-C_5H_{12}	6.3
n-C_5H_{12}	1.1
C_5-Isom.	1.4
C_6H_{14}	nn
C_6H_6	nn
C_6H_5-CH_3	nn
C_6H_5-C_2H_5	nn
N_2	nn

nn: <0.01%

ϱ_G^o = 1.0 kg/m³

M = 22 g/mol

ϱ_{oC} = 0.78 kg carbon / m³ flare gas

w_C = 0.78 kg carbon / kg flare gas

ϱ_{oH} = 0.22 kg hydrogen / m³ flare gas

w_H = 0.22 kg hydrogen / kg flare gas

Flare gas analysis

Test No. 16.001-.089

	x in %
H_2	58.8
H_2S	nn
CH_4	6.7
C_2H_6	5.0
C_2H_4	nn
C_2H_2	nn
C_3H_8	4.3
C_3H_6	nn
i-C_4H_{10}	3.1
n-C_4H_{10}	6.8
1-C_4H_8	nn
i-C_5H_{12}	1.8
n-C_5H_{12}	0.6
C_5-Isom.	0.3
C_6H_{14}	nn
C_6H_6	nn
C_6H_5-CH_3	nn
C_6H_5-C_2H_5	nn
N_2	11.4
H_2O	1.8

nn: < 0.01%

ϱ_G^o = 0.77 kg/m³

M = 17 g/mol

ϱ_{oC} = 0.46 kg carbon / m³ flare gas

w_C = 0.60 kg carbon / kg flare gas

ϱ_{oH} = 0.16 kg hydrogen / m³ flare gas

w_H = 0.21 kg hydrogen / kg flare gas

Appendix 1 Sheet 2

Test No. 16

1	Consec.No.		.001	.002	.003	.004	.005	.010	.011	.012	.013	.014	.015	.016	.017	.018
2	$\dot{m}$(G)	kg/h	2200													
3	$\dot{m}$(D)	kg/h	50													
4	ψ (D,G)	kg/kg	0.02													
5	x	m	-6.0											-0.5		
6	y	m	0.0					0.5								
7	z	m	5.0	4.0	3.0	2.0	1.0	5.0	4.0	3.0	2.0	1.0	0.0	5.0	4.0	3.
8	χ(O2)	%	20.1	20.0	20.5	20.4	21.0	19.8	19.5	19.9	20.3	20.9	21.0	21.0	20.1	19.
9	χ(CO2)	%	0.5	0.5	0.4	0.2	0.1	0.7	0.9	0.7	0.4	0.2	0.1	0.6	0.0	0.
10	χ(CO)	%	nn	nn	nn	nn	nn	nn	nn	nn	nn	nn	nn	nn	nn	
11	χ(CxHy)	ppm	10	15	40	20	5	35	75	90	75	10	10	20	40.	
12	χ(NOx)	ppm	3	3	nn	nn	1	4	4	4	2	nn	nn	3	4	
13	Tp	^{o}C	20.9	21.0	19.0	15.0	13.0	23.0	23.0	22.0	19.0	14.0	13.0	20.0	23.0	22
14	T(B)	^{o}C	170	205	140	100	40	50	310	265	175	90	140	190	260	
15	u(kal)	m/s														

nn: χ(CO) < 0.01%, χ(CO2) < 0.1%, χ(NOx) < 1 ppm

χ(CxHy) shown as methane equivalents

Appendix 1 Sheet 2

Test No. 16

1	Consec.No.		.019	.020	.021	.022	.023	.024	.025	.026	.027	.049	.050	.051	.052	.053
2	$\dot{m}$(G)	kg/h	2200									2200				
3	$\dot{m}$(D)	kg/h	50									325				
4	ψ (D,G)	kg/kg	0.02									0.15				
5	x	m	-6.0									-8.5	-8.0	-7.0	-6.6	-5.
6	y	m	-0.5			-1.0						0.0				
7	z	m	2.0	1.0	0.0	5.0	4.0	3.0	2.0	1.0	0.0	5.00				
8	χ(O2)	%	19.9	20.2	20.7	20.8	20.4	20.3	20.0	20.4	20.2	20.2	20.0	19.7	19.5	20.
9	χ(CO2)	%	0.6	0.2	0.2	0.4	0.6	0.6	0.4	0.3	0.2	0.4	0.6	0.7	0.8	0.
10	χ(CO)	%	nn	nn	nn	nn	nn	nn	nn	nn	nn	nn	nn	nn	nn	n
11	χ(CxHy)	ppm	80	10	10	10	15	15	<10	<10	<10	10	10	10	10	1
12	χ(NOx)	ppm	3	2	1	3	4	3	2	2	nn	2	3	4	5	
13	Tp	°C	21.0	17.5	15.0	18.5	21.5	20.0	18.5	17.0	15.5	19.5	21.0	22.0	24.0	20.
14	T(B)	°C	195	125	80	155	210	190	140	115	70	140	175	210	280	16
15	u(kal)	m/s														

nn: χ(CO) < 0.01%, χ(CO2) < 0.1%, χ(NOx) < 1 ppm

χ (CxHy) shown as methane equivalents

Appendix 1 Sheet 2

Test No. 16

1	Consec.No.		.054	.055	.056	.057	.058	.059	.060	.061	.062	.063	.064	.065	.066	.0 7
2	$\dot{m}$(G)	kg/h	2200													
3	$\dot{m}$(D)	kg/h	325													
4	Ψ (D,G)	kg/kg	0.15													
5	x	m	-4.0	-8.5	-8.0	-7.0	-6.0	-5.0	-4.0	-3.0	-2.0	-1.0	0.0	-1.0	-2.0	-3.0
6	y	m	0.0													
7	z	m	5.0	4.0									3.0			
8	χ(O2)	%	20.4	20.5	20.0	19.8	19.2	18.5	18.3	19.3	20.5	21.0	20.7	19.7	16.5	16.1
9	χ(CO2)	%	0.5	0.3	0.4	0.7	0.9	1.2	1.7	1.3	0.5	0.1	0.2	0.5	1.7	2.7
10	χ(CO)	%	nn	nn	nn	nn	nn	0.01	0.04	0.07	0.01	nn	0.05	0.11	0.60	0.40
11	χ(CxHy)	ppm	25	10	10	10	20	50	200	300	90	25	145	800	2125	1110
12	χ(NOx)	ppm	3	2	2	4	5	8	9	8	3	nn	nn	4	10	15
13	Tp	^{o}C	19.0	17.0	18.0	22.5	24.5	29.0	31.0	28.0	20.0	13.5	12.0	21.5	34.0	39.0
14	T(B)	^{o}C	140	105	140	210	280	400	560	525	265	140	80	280	840	840
15	u(kal)	m/s														

nn: χ(CO) < 0.01%, χ(CO2) < 0.1%, χ(NOx) < 1 ppm

χ(CxHy) shown as methane equivalents

Appendix 1 Sheet 2

Test No. 16

1	Consec.No.		.068	.069	.070	.071	.072	.073	.074	.075	.076	.077	.078	.079	.082	.083
2	$\dot{m}$(G)	kg/h	2200													
3	$\dot{m}$(D)	kg/h	325													
4	ψ (D,G)	kg/kg	0.15													
5	x	m	-4.0	-5.0	-6.0	-7.0	-8.0	-8.5		-8.0	-7.0	-6.0	-5.0	-4.0	-3.0	-2.0
6	y	m	0.0						2.0							
7	z	m	3.0													
8	χ(O2)	%	19.0	20.6	21.0	21.0	20.8	20.8	20.8	20.8	20.8	20.8	20.8	20.3	20.6	18.3
9	χ(CO2)	%	1.1	0.5	0.1	0.1	0.1	0.1	0.1	0.1	0.1	0.1	0.1	0.1	0.2	1.3
10	χ(CO)	%	0.03	nn	nn	nn	nn	nn	nn	nn	nn	nn	nn	nn	nn	0.12
11	χ(CxHy)	ppm	240	20	25	30	25	15	20	20	20	25	32	35	40	900
12	χ(NOx)	ppm	7	2	nn	nn	nn	nn	nn	nn	nn	nn	nn	nn	2	6
13	Tp	°C	/	/	12.5	12.5	13.0	13.5	14.0	14.5	14.5	14.5	14.5	14.5	15.5	21.5
14	T(B)	°C	630	525	435	335	245	190	160	125	105	90	90	110	195	590
15	u(kal)	m/s														

nn: χ(CO) < 0.01%, χ(CO2) < 0.1%, χ(NOx) < 1 ppm

χ (CxHy) shown as methane equivalents

Appendix 1 Sheet 2

Test No. 16

1	Consec.No.		.084	.091	.092	.094	0.95	.042a	.033
2	$\dot{m}$(G)	kg/h	2200					2200	2200
3	$\dot{m}$(D)	kg/h	325	0		250		325	50
4	ψ (D,G)	kg/kg	0.15	0.00		0.11		0.15	0.02
5	x	m	-1.0	0.0				-4.0	-4.5
6	y	m	0.0					0.0	0.0
7	z	m	2.0	0.0	1.0	0.0	1.0	4.0	2.5
8	χ(O2)	%	14.0	8.2	12.0	5.3	6.0	17.0	18.5
9	χ(CO2)	%	2.3	2.5	3.2	2.0	4.2	1.3	1.3
10	χ(CO)	%	1.0	1.5	0.5	2.5	5.0	0.03	0.1
11	χ(CxHy)	ppm	5000	>MB	>MB	>MB	>MB	250	535
12	χ(NOx)	ppm	20	40	35	30	25	10	8
13	Tp	^{o}C	46.0	43.0	43.0	54.0	45.0	27.0	27.5
14	T(B)	^{o}C	860	490	840	400	630	405	490
15	u(kal)	m/s							

nn: χ(CO) < 0,01%, χ(CO2) < 0.1%, χ(NOx) < 1 ppm, MB: χ (CxHy) = 1% C_2H_6

χ(CxHy) shown as methane equivalents

Volume portions of hydrocarbons and hydrogen in the off-gas

Test No. 16

Measuring Object	%	Sample taken under Consec.No.		
	in	.042a	.033	.033
H_2	%	0.57	0.49	0.44
CH_4	ppm	915	775	420
C_2H_6	ppm	140	145	155
C_2H_4	ppm	nn	nn	120
C_2H_2	ppm	290	205	100
C_3H_8	ppm	nn	nn	130
C_3H_6	ppm	nn	nn	nn
i-C_4H_{10}	ppm	nn	nn	85
n-C_4H_{10}	ppm	nn	nn	175
1-C_4H_8	ppm	nn	nn	nn
i-C_5H_{12}	ppm	nn	nn	nn
n-C_5H_{12}	ppm	nn	nn	nn
C_5-Isom.	ppm	nn	nn	nn
C_6H_{14}	ppm	nn	nn	nn

nn : < 1 ppm

Volume portions of hydrocarbons and hydrogen in the flame

Test No. 16

Measuring object	x	Sample drawn from consec. No.			
	in	.092	.092	.095	.095
H_2	%	18.82	16.46	16.46	15.9
CH_4	%	1.68	3.96	1.23	1.20
C_2H_6	%	0.81	0.74	0.75	0.73
C_2H_4	%	0.51	2.18	0.13	0.13
C_2H_2	%	0.03	0.07	0.08	0.08
C_3H_8	%	0.57	0.21	0.61	0.60
C_3H_6	%	0.30	0.68	0.04	0.04
$i\text{-}C_4H_{10}$	%	0.02	0.09	0.42	0.42
$n\text{-}C_4H_{10}$	%	0.37	0.16	0.90	0.88
$1\text{-}C_4H_8$	%	0.76	nn	nn	nn
$i\text{-}C_5H_{12}$	%	0.22	nn	0.30	0.29
$n\text{-}C_5H_{12}$	%	0.06	nn	0.12	0.11
C_5-Isom.	%	nn	nn	0.09	0.07

nn : $< 0{,}01$ %

Appendix 1 Sheet 1

Flare gas analysis

Test No. 17.001-.051

	x in %
H_2	64.1
H_2S	0.2
CH_4	7.4
C_2H_6	5.3
C_2H_4	nn
C_2H_2	nn
C_3H_8	4.2
C_3H_6	nn
i-C_4H_{10}	1.7
n-C_4H_{10}	2.8
1-C_4H_8	nn
i-C_5H_{12}	2.2
n-C_5H_{12}	1.1
C_5-Isom.	nn
C_6H_{14}	nn
C_6H_6	nn
C_6H_5-CH_3	nn
C_6H_5-C_2H_5	nn
N_2	11.2
Σ	

nn: < 0.01%

ϱ^o_G = 0.64 kg/m³

M = 14 g/mol

ϱ^o_C = 0.36 kg carbon / m³ flare gas

w_C = 0.60 kg carbon / kg flare gas

ϱ^o_H = 0.14 kg hydrogen / m³ flare gas

w_H = 0.20 kg hydrogen / kg flare gas

Appendix 1 Sheet 2

Test No. 17

1	Consec. No.		.002	.003	.004	.005	.006	.009	.010	.011	.012	.025	.026	.027	.029	.0
2	$\dot{m}$(G)	kg/h	1570									1720				
3	$\dot{m}$(D)	kg/h	600									300				
4	Ψ (D,G)	kg/kg	0.38									0.17				
5	x	m	0.0									0.0				
6	y	m	0.0													
7	z	m	4.50	3.50	2.50	1.50	0.50	-0.50	-0.25	0.00	0.25	-0.75	-0.50	-0.25	0.00	0.2
8	χ(O2)	%	16.6	9.4	7.2	2.2	0.6	nn	nn	nn	0.3	nn	nn	0.6	1.0	1.
9	χ(CO2)	%	2.1	5.3	5.5	6.1	5.5	nn	1.8	3.7	4.0	nn	nn	2.1	1.8	3.
10	χ(CO)	%	0.1	0.4	1.9	4.0	6.5	2.0	4.6	10.0	10.0	nn	0.1	2.0	0.1	2.
11	χ(CxHy)	ppm	300	810	2250	7000	>MB	>MB	>MB	>MB	>MB	>MB	>MB	>MB	>MB	950
12	χ(NOx)	ppm														
13	Tp	°C	29.0	31.0	33.0	34.0	35.0	38.0	52.0	55.0	55.0	45.0	44.0	48.0	55.0	50.
14	T(D)	°C	630	875	930	980	930	30	60	350	665	30	35	50	280	7
15	u(kal)	m/s														

nn: χ(CO) < 0.01%, χ(CO2) < 0.1%, χ(NOx) < 1 ppm, MB: χ (CxHy) = 1% C_2H_6

(CxHy) shown as ethane equivalents

Test No. 17

1	Consec. No.		.032	.033	.034	.035	.036	.037	.038	.039	.040	.041	.042	.043	.044	.045
2	$\dot{m}$(G)	kg/h	1720							1720						
3	$\dot{m}$(D)	kg/h	300							900						
4	ψ (D,G)	kg/kg	0.17							0.52						
5	x	m	0.0							0.0						
6	y	m	0.0							0.0						
7	z	m	0.75	1.25	1.75	2.25	2.75	3.25	4.25	0.00	0.50	1.00	1.50	2.00	2.50	3.00
8	χ(O2)	%	2.5	3.5	7.5	9.0	13.8	16.2	16.9	.0.5	0.7	1.2	1.8	3.0	6.8	10.0
9	χ(CO2)	%	3.7	3.8	3.2	3.5	2.5	1.8	1.7	2.8	3.5	4.9	5.1	5.1	4,7	4.2
10	χ(CO)	%	3.5	4.9	3.6	1.9	0.4	0.3	0.2	3.3	nn	8.0	6.1	4.1	2.1	0.5
11	χ(CxHy)	ppm	> MB	>MB	8550	6200	3400	1000	500	>MB	>MB	>MB	8300	7200	3400	1400
12	χ(NOx)	ppm														
13	Tp	°C	55.0	57.0	57.0	56.0	53.0	50.0	45.0	45.0	45.0	50.0	60.0	61.0	60.0	59.0
14	T(B)	°C	820	890	910	890	820	700	630	425	630	875	980	990	980	945
15	u(kal)	m/s														

nn: χ(CO) < 0.01%, χ(CO2) < 0.1%, χ(NOx) < 1 ppm ; MB: χ(CxHy) = 1% C_2H_6
(CxHy) shown as ethane equivalents

Appendix 1 Sheet 2

Test No. 17

1	Consec. No.		.046	.047	.050	.051
2	$\dot{m}$(G)	kg/h	1720			
3	$\dot{m}$(D)	kg/h	900	0	300	600
4	Ψ (D,G)	kg/kg	0.52	0.00	0.17	0.35
5	x	m	0.0			
6	y	m	0.0			
7	z	m	3.5	0.5		
8	χ(O2)	%	18.0	6.8	3.8	2.4
9	χ(CO2)	%	1.5	1.3	2.8	3.5
10	χ(CO)	%	0.1	1.0	2.4	5.6
11	χ(CxHy)	ppm	120	>MB	>MB	>MB
12	χ(NOx)	ppm				
13	Tp	°C	55.0	46.0	55.0	58.0
14	T(B)	°C	630	630	735	790
15	u(kal)	m/s				

nn: χ(CO) < 0.01%, χ(CO2) < 0.1%, χ(NOx) < 1 ppm, MB: χ (CxHy) = 1% C_2H_6
χ(CxHy) shown as ethane equivalents

Appendix 1 Sheet 3

Volume portions of hydrocarbons and hydrogen in the flame

Test No. 17

Measuring object	%	Sample drawn from consec. No.	
	in	.006	.005
H_2	%	27	4.7
CH_4	%	2.50	0.84
C_2H_6	%	1.40	nn
C_2H_4	%	0.32	0.18
C_2H_2	%	0.14	0.10
C_3H_8	%	0.31	nn
C_3H_6	%	0.14	nn
$i\text{-}C_4H_{10}$	%	0.56	nn
$n\text{-}C_4H_{10}$	%	0.79	nn
$1\text{-}C_4H_8$	%	nn	nn
$i\text{-}C_5H_{12}$	%	0.55	nn
$n\text{-}C_5H_{12}$	%	0.29	nn
C_5-Isom.	%	nn	nn
C_6H_{14}	%	nn	nn

nn : $< 0{,}01$ %

Supplement to Appendix 2

Calculation of the combustion air- and off-gas volume flow and of the oxygen volume flow with the aid of the combustion equation.

given: w_C in kg C/kg Gas

w_H in kg H/kg Gas

$\dot{m}_G$ in kg/h

$\dot{V}_o^{out}$ in m^3/h

$$l_o(O_2) = MV \left[\frac{w_C}{M_C} + \frac{1}{2} \frac{w_H}{M_{H_2}} \right] \qquad [m^3/kg]$$

$$\dot{l}_o = l_o(O_2) \left[1 + \frac{\chi_{N_2}(L)}{\chi_{O_2}(L)} \right] \qquad [m^3/kg]$$

$$\dot{i}_o = l_o \dot{m}_G \qquad [m^3/h]$$

$$v_o = MV \frac{w_C}{M_C} + \chi_{N_2}(L) \cdot l_o \qquad [m^3/kg]$$

$$\dot{v}_o = v_o \dot{m}_G \qquad [m^3/h]$$

$$\lambda = \frac{\dot{V}_o^{out} - \dot{v}_o + \dot{i}_o}{\dot{i}_o} = \frac{\dot{L}_o}{\dot{i}_o}$$

$$\chi_{O_2} = \frac{\chi_{O_2}(L) \cdot \dot{i}_o (\lambda - 1)}{(\lambda - 1)\, \dot{i}_o + \dot{v}_o}$$

Appendix 2 (Supplement to Table 6-1)

Balance sheet data for flare flames burning without wind

1	Test No.		11.001-.035	11.066-.078	11.093-.105	14.017-.021	14.028-.0
2	Flame No.		1	2	3	4	5
3	$\dot{m}_{H2}^{in}$	kg/h	275	235	235	235	235
4	$\dot{m}_{D}^{in}$	kg/h	750	300	1200	0	315
5	T(L)	^{o}C	10	10	8	15	15
6	φ(L)	%	89	90	86	82	82
7	ϱ_{H2O}(L)	g/m^3	8.7	8.8	7.7	11.3	11.3
8	$f = \frac{1}{\delta_C}$		1.476	2.975	1.201	(2.975)	1.846
9	$\dot{m}_G$	kg/h	1100	940	940	940	940
10	w_C	kg/kg	0.75	0.75	0.75	0.75	0.75
11	w_H	kg/kg	0.25	0.25	0.25	0.25	0.25

12	$\dot{V}_o^{out}$	$10^3 m^3/h$	128	189	63	187	99	181	74		74	1
13	$\dot{i}_o^{in}$	$10^3 m^3/h$	14.7		12.5		12.5		12.5		12.5	
14	$\dot{v}_o^{out}$	$10^3 m^3/h$	13.1		11.2		11.2		11.2		11.2	
15	$\dot{L}_o^{in}$	$10^3 m^3/h$	130	190	64	189	100	182	75		75	1
16	$\dot{m}_{H2O}^{in}(H)$	kg/h	2475		2115		2115		2115		2115	
17	$\dot{m}_{H2O}^{in}(D)$	kg/h	750		300		1200		0		315	
18	$\dot{m}_{H2O}^{in}(L)$	kg/h	1110	1660	565	1665	742	1350	850		845	19
19	$\sum \dot{m}_{H2O}^{in}$	kg/h	4335	4885	2980	4080	4055	4665	2965		3275	39
20	$\dot{m}_{H2O}^{out}$	kg/h	3480	5135	1560	4640	2760	5050	1115		2635	48
21	$\delta_{H2O} = \frac{\dot{m}_{H2O}^{out}}{\dot{m}_{H2O}^{in}}$		0.80	1.05	0.52	1.14	0.68	1.08	0.38		0.80	1.
22	λ		8.8	13.0	5.1	15.1	8.0	14.6			6.0	11
23	$\varkappa_{O2}$	%	18.6	19.3	17.1	19.5	18.6	19.7			17.8	19

Appendix 3

Calculation of the mass concentration of organically bound carbon at the end of the flame as a function of the degree of conversion.

given: w_C in kg C/kg Gas

w_H in kg H/kg Gas

χ_{O_2}

$$l_o(U) = \frac{1}{\chi_{O_2}(L)} MV \left[\frac{w_C}{M_C} + \frac{2\, w_H}{2\, M_{H_2}} \right] U = a \cdot U$$

$$v_o(U) = \underbrace{MV \frac{w_C}{M_C}}_{b} + \underbrace{MV \frac{w_H}{M_{H_2}}}_{c} (1-U) + \underbrace{\chi_{N_2}(L)}_{d} \cdot U$$

$$\lambda = 1 + \frac{v_o}{l_o} \frac{\chi_{O_2}}{\underbrace{\chi_{O_2}(L) - \chi_{O_2}}_{e}}$$

$$\lambda = 1 + \frac{b + c(1-U) + d \cdot U}{a \cdot U} \cdot e$$

$$V_o = v_o + (\lambda - 1)\, l_o$$

$$= b + c(1-U) + d \cdot U + \left[b + c(1-U) + d \cdot U \right] e$$

$$\varrho C_u = \frac{w_C(1-U)}{V_o}$$

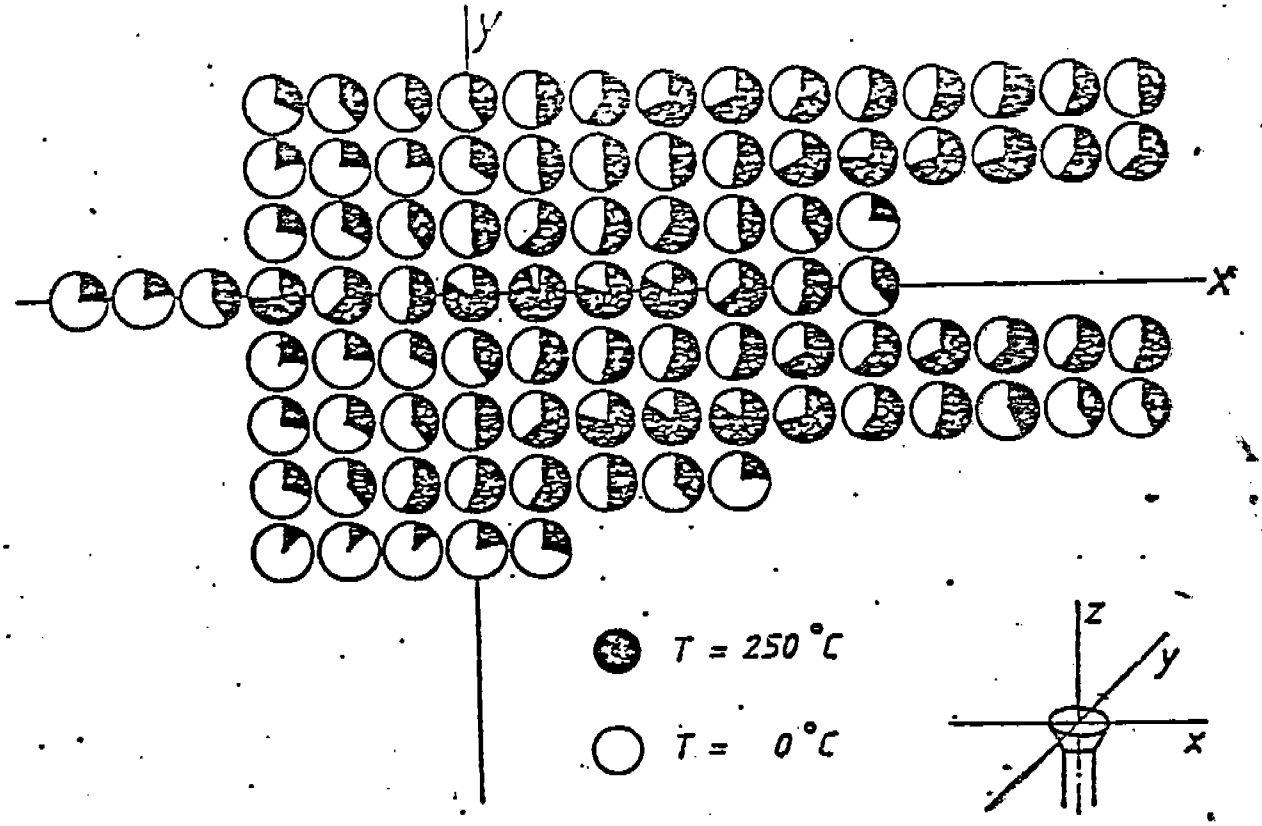

to Fig. 6-7: Distribution of the temperature in a horizontal plane above a flare flame burning in a cross draft.
Test 06.010-.143

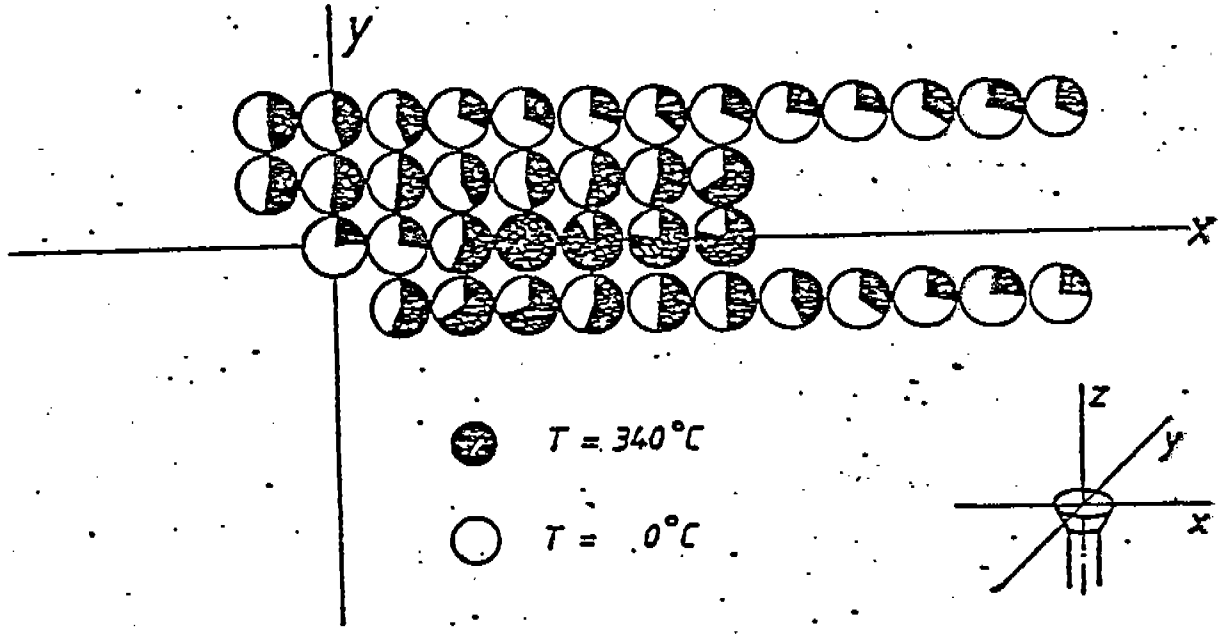

to Fig. 6-8: Distribution of the temperature in a horizontal plane above a flare flame burning in a cross draft.
Test 03.001-.039

Appendix 5

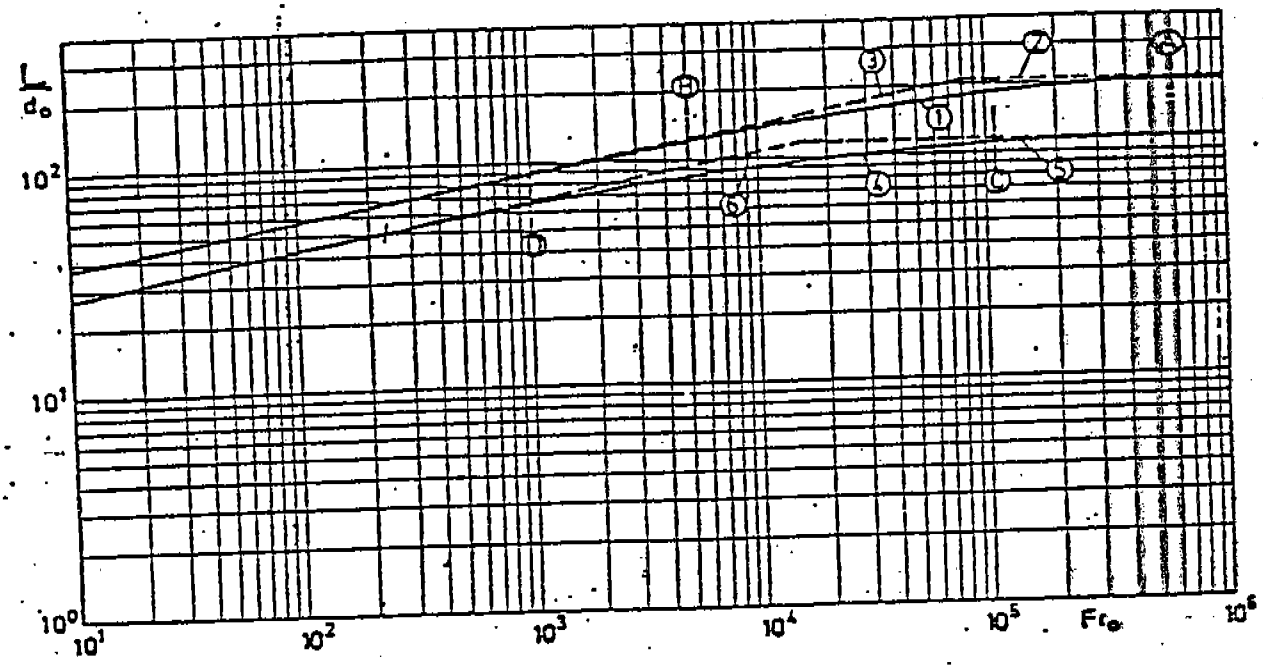

Fig. 7-8. Flame length for city-gas and natural gas, with allowance made for segregation.

A and C: up-draft-free limit for natural and city-gas
B and D: up-draft-affected limit for natural and city-gas
2 and 5: asymptotic equation without up-draft (7.3-1)
3 and 6: asymptotic equation with up-draft (7.3-2)
1 and 4: generally valid equation (7.3-3)

The diagram was taken from:

Y. Lee, "The course of combustion in up-draft-affected flames with and without the effect of wind".

Dissertation, University Karlsruhe, 1977.

Appendix 6

Pressure at the flarejectors (PI 123) as a function of the steam mass flow (FI 121)

FI 121	PI 123	PI 121	TI 121	PI 122
kg D/h	bar	bar	°C	bar
100	1.9	13.2	192	2.0
200	2.3	13.2	191	2.5
375	3.4	13.0	191	3.5
450	4.2	12.9	191	4.5
500	4.5	12.9	191	5.0
600	5.5	12.7	191	6.0
725	6.4	12.4	190	7.0
875	7.3	11.9	189	8.0
1025	8.2	11.5	187	9.0
1225	9.1	10.9	186	10.0

Appendix 7 Analytical Methods

A.7-1. Gas-Chromatographic Determination of the Flare Gas- and Off-Gas Components and Preparation of the External Standards for their Quantification

The gas samples drawn at Q 111 and Q 213 with gas-collecting tubes were worked up gas-chromatographically. The gas-collecting tubes were connected via a ~ 10 cm long teflon line ($\varnothing_i$ = 4 mm) to the gas sample inlet of a gas-chromatograph. The gas loop had a volume of 0.25 ml and could be switched into the carrier gas stream via a 6-way stopcock.

The feeding of the sample is sketched in Fig. 7-1. Via a reservoir mounted higher than the gas-collecting tube, acidulated water was forced from below into the collecting tube and sampling gas was passed into the gas loop. After the elution of approximately 50 ml sample gas, the gas loop was switched into the carrier gas stream.

The operating conditions for the gas-chromatographic analysis are listed in Table A.7-1. For all the analyses, a packed steel column with an i.d. of 2.2 mm was used. The detectors were connected to an electronic integrator with line-recorder.

For the evaluation of the test results, the volume portions of the components were needed which - after the calibration - were calculated from the integrator values.

For the calibration, gas mixtures were prepared in gas-collecting tubes in which the volume portions of the components could be calculated according to Dalton's partial pressure law.

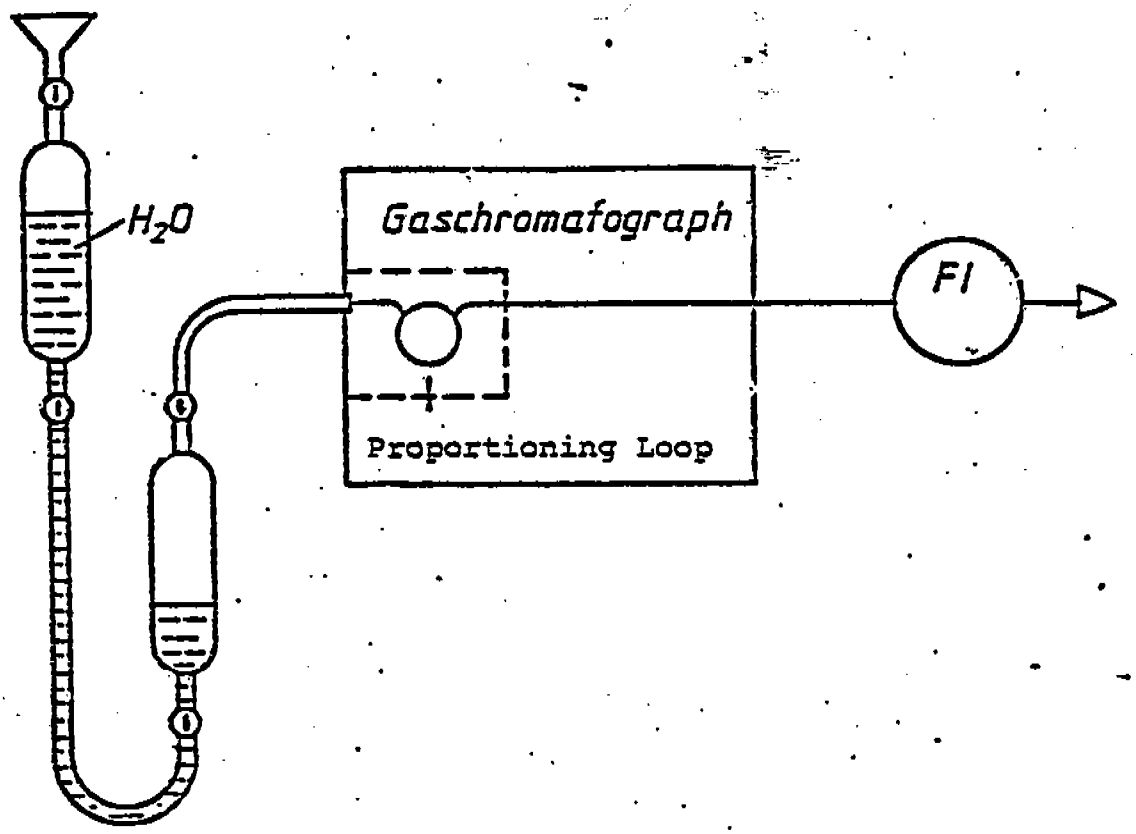

Fi-. A.7-1: Flow diagram for introducing the sample in the gas-chromatographic analysis

Table A.7-1: Operating conditions in the gas-chromatographic analysis

Measuring objects	Aliphatics	Aromatics	H_2 N_2
Separating column	3.5m Spherosil XOB 075	3.5m 10% Carbowax 20M Chrom.W AW-DMCS	2m Carbosieve B
Carrier gas	N_2 20ml/min	N_2 20ml/min	N_2 15ml/min He
Furnace temperature	80°C isothermal	95°C isothermal	50°C isothermal
Detector	FID 120°C	FID 120°C	WLD 90°C

These gas mixtures were worked up like the gas samples drawn in the tests.

The preparation of the gas mixtures is sketched in Fig. A.7-2.

A gas-collecting tube was evacuated with a vacuum pump three times and each time filled with hydrogen in order to remove the air. Then, after the evacuation, the tube was first filled with hydrogen up to about 200 mbar and then with the components in accordance with the desired volume portion. Th. total pressure which was chosen equal to atmospheric pressure was adjusted with hydrogen. The pressure in the gas-collecting tube was read on the manometer and recorded by hand before and after the addition of a component. As the manometer, a precision manometer with a measuring range of 0 to 1.6 bar was used. The reading precision is given by the manufacturer (Wika) as ± 0.1%.

The measuring objects are listed below.

1. methane
2. ethane
3. ethene
4. acetylene
5. propane
6. propene
7. n-butane
8. i-butane
9. n-pentane
10. i-pentane
11. benzene
12. toluene
13. ethyl benzene
14. hydrogen
15. nitrogen

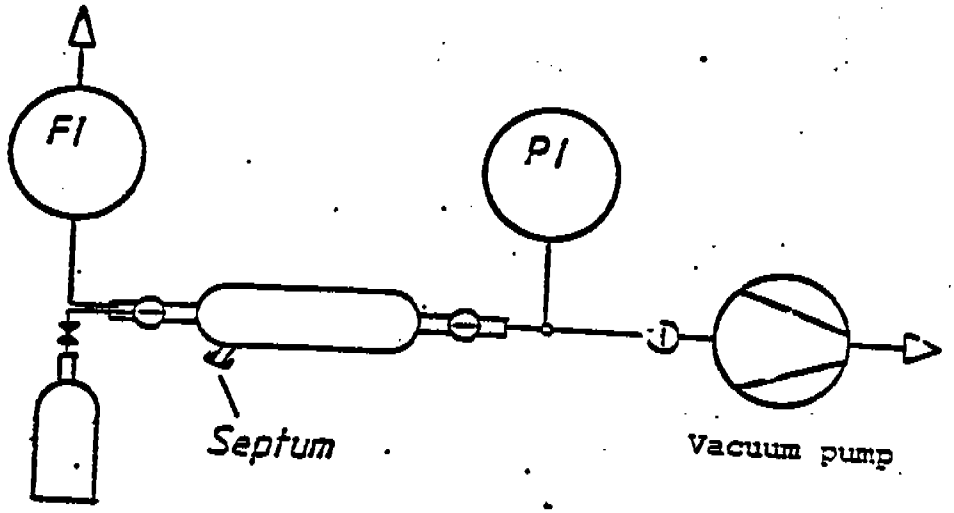

Fig. A.7-2: Flow diagram for the preparation of the external standard

The components 1 to 8 were obtained as laboratory gases from the Merck-Schuchard Co., the components 9 to 13 from the Merck Co. and the components 14 and 15 from the Messer-Griesheim Co. The components 1 to 8 and 14 and 15 were, after flushing the line with the respective component, allowed to flow into the gas-collecting tube. Components 9 to 13 were introduced into the gas-collecting tube with a syringe via the septum.

According to Dalton, the ratio of the partial pressure of a gas to the total pressure is equal to the ratio of the number of its moles to the total number of the moles of all the gases in the mixture.

$$\frac{p_i}{p_{tot}} = \frac{n_i}{\sum n_i} = x_i = \chi_i$$

The volume portion of the component can, therefore, be calculated from the pressure difference.

The process parameters were determined for hydrogen, ethane, propene and n-pentane.

To this end, gas samples were prepared with different volume portions as listed below.

χ in	%	%	%	%	%
H_2	40.2	44.8	50.7	55.3	60.9
C_2H_6	4.9	12.2	15.1	20.4	24.9
C_3H_6	4.8	9.8	14.9	20.1	25.0
C_5H_{12}	3.9	4.1	4.8	6.4	

For each sample, we first determined the standard deviation of the gas-chromatographic analysis from 4 repeat measurements. The standard deviation

$$s = \sqrt{\frac{\sum A_i^2 - n\bar{A}^2}{n - 1}}$$

gave for all the components a value smaller than 0.25%, based on the respective absolute value.

In order to be able to make a statement concerning the degree of the relation between the volume portions calculated from the pressure differences χ_i and the integrator values A_i, we